

**UNIVERSITA' DEGLI STUDI DI NAPOLI**

**“ FEDERICO II “**



**DIPARTIMENTO DI FARMACIA**

**DOTTORATO DI RICERCA IN SCIENZA DEL FARMACO**

**XXVIII CICLO**

***Design and Synthesis of heterocyclic molecules as novel agents for the treatment of chemo-resistant cancers***

Coordinatore

Chiar.ma Prof.ssa Maria Valeria D'Auria

TUTOR:

Prof.ssa Luciana Marinelli

CANDIDATA:

Hilde Cassese

*“Live as if you were to die tomorrow. Learn as if you were to live forever.”*

*Mahatma Gandhi*

*Alla mia Famiglia e a Luca,  
che mi hanno incoraggiata e sostenuta in questo percorso.*

*A mia Nonna e a Tutti i miei Cari,  
che hanno sconfitto il cancro con "la vita eterna".*

## Abstract

The drugs use in human medicine covers the whole range of chemical structure types, but the majority are heterocyclic small molecules or have heterocyclic structural components. In particular, anticancer drugs include rings in their structures. IUPAC gives the following definition of heterocyclic compounds : “cyclic compounds having as ring members atoms of at least two different elements” [1]. Heterocycles ring structures are in essence composed of elements other than carbon, where the most frequent substituents are oxygen, nitrogen and sulfur [2]. The discovery of novel multicomponent reactions enables new methodologies to synthesize known medicinally active compounds. Among all the multicomponent reactions presently known, the MCRs (multicomponent reactions) mediated by isocyanides are the most popular. The peculiar ability of the divalent carbon of isocyanides to react first with electrophiles and subsequently with nucleophiles, is key to the success of the multicomponent process. For this reason, the discovery of new electrophilic partners is a starting point for the development of novel multicomponent transformations. In this context, it is reported the usage of  $\alpha$ -isocyanoacetamides along with (Z)-Aryl chlorides to give substituted 1,3-oxazol-2-oxime. However, since the final product is not stable, it can be hydrolyzed to give  $\alpha$ -ketoamide amides. These molecules constitute useful scaffolds and intermediates for a variety of transformations in organic chemistry. As a continuation of this study, this work demonstrates that an electron deficient phenol could be a good nucleophiles third component in a reaction with (Z)- aryl chlorides and isocyanide to form a library of 41 aryloxyiminoamide derivates. The final product, namely aryloxyiminoamide, is an interesting compound because it can be used as intermediate for further synthetic transformations.

The modern treatment of cancer involves surgery, radiotherapy and chemotherapy. However, the development of chemo-resistance, namely the lack of drugs response, is a persistent problem for the treatment of local and disseminated cancers. In fact, one of the hallmarks of human cancers is the ability to escape cell death, which is a major cause of treatment failures. In particular, the cancer cells block the apoptotic process by increasing the expression of anti-apoptotic BCL-2 members at the mitochondria and inactivate the effector arm of apoptosis, e.g. BAX, through mutations or inhibition. The recent discovery of the first small heterocyclic molecule BAM7 as BAX direct activator represents the starting point for a structure-based lead optimization program aimed at the discovery of new potent BAX activators. My work resulted in the discovery of BTC-8 which resulted 10 fold more potent than the lead BAM7. In vivo experiments have suggested that BAX direct activators may be considered as novel, effective anticancer drugs in a near future.

Furthemore, some compounds ,which were synthesized as BAX direct activators, were included in the library of small molecules selected for acting as pharmacological chaperones on a misfolded mutant of the Frizzled4 (Fz4) receptor [3]. Fz4 is a key component of Wnt- $\beta$ -catenin signalling and misregulation of Fz4 activity is involved in tumor proliferation and cancer stem cell genesis in many typer of malignancies, such as glioblastoma, colorectal and breast cancer. My work reported ,what are to our knowledge, the first small molecules that address the until-now-undruggable Fz4 receptor and inhibit Wnt signalling. This goal is achieved by using the potency of candidate molecules to rescue the misfolding mutant of the Fz4, as a readout in screening campaigns toward the identification of new ligands.

Another key aspect of cancer cells is an increase of aerobic glycolysis and an altered energy metabolism supporting continuous cell growth and proliferation. The epigenetic mechanisms involving covalent modifications of both DNA and histones have recently emerged as important players in the regulation of glucose metabolism. In particular, the sirtuin family of histone deacetylases are important regulators of diverse physiological and pathological events, including cancer metabolism. The most representative example is SIRT6, which is considered a promising pharmaceutical target for chemo-resistance cancers treatment. In this thesis, the identification of one heterocyclic compound which binds and inhibits the function of SIRT6 is reported. The result of this work, although very preliminary, may represent a starting point for the development of SIRT6 inhibitors.

# Contents

Abstract .....	IV
List of Figures.....	- 2 -
List of Schemes .....	- 6 -
List of Table.....	- 8 -
Abbreviations.....	- 9 -
1. Multicomponent reactions .....	- 12 -
1.1 History of MCRs.....	- 13 -
1.2 Chemistry of Isocyanides.....	- 15 -
1.3 Passerini and Ugi reactions .....	- 16 -
1.4 Novel MCRs: A procedure for the synthesis of Aryl $\alpha$ -ketoamide Amides .....	- 18 -
1.5 Novel MCRs: Solution-Phase Parallel Synthesis of Aryloxyimino Amides.....	- 23 -
1.5.1 Result and method .....	- 24 -
2. Structure-Based Lead Optimization and Biological Evaluation of BAX Direct Activators as Novel Potential Anticancer Agents.....	- 27 -
2.1 Programmed Cell Death -Apoptosis.....	- 28 -
2.2 Apoptosis in Cancer Cells .....	- 32 -
2.3 Design Strategy.....	- 33 -
2.4 Chemistry .....	- 35 -
2.5 Biological Results .....	- 38 -
2.6 Pharmacological folding chaperones act as allosteric ligand of Frizzled4 .....	- 51 -
2.6.1 Results .....	- 53 -
2.6.2 FzM1 binding site .....	- 54 -
2.6.3 The effect of FzM1 on tumor cells .....	- 56 -
3. Design and synthesis of Novel SIRT6 inhibitors.....	- 57 -

3.1 The Human Sirtuin Family .....	- 58 -
3.2 Biochemical functions of SIRT6 .....	- 61 -
3.3 Structure of SIRT6.....	- 70 -
3.4 Results and Discussion .....	- 73 -
3.5 Synthesis.....	- 75 -
3.6 SIRT6 Inhibitor in vitro test: HPLC Assay .....	- 77 -
3.7 Future Perspectives.....	- 79 -
4. Experiments .....	- 80 -
4.1 Part I : Synthesis of Aryl- $\alpha$ -ketoamide Amides .....	- 80 -
4.2 Part II: Synthesis of Aryloxyimino Amides .....	- 94 -
4.3 Part III: Synthesis of BAX Direct Activators as Novel Potential Anticancer Agents.....	- 111 -
4.4 Part IV: Synthesis of Sirt6 Inhibitors .....	- 127 -
5. Conclusions .....	- 134 -
Bibliography.....	- 136 -





# List of Figures

Figure 1 Intramolecular trapping of the nascent nitrilium ion.....	- 19 -
Figure 2 Comparison between Zhu's work and the reaction described in this work.....	- 19 -
Figure 3 Structure of (Z)-chlorooximes and $\alpha$ - isocyanoacetamides.....	- 20 -
Figure 4 Synthesized aryl- $\alpha$ -ketoamides .....	- 22 -
Figure 5 Passerini-Smiles Mechanism .....	- 23 -
Figure 6 Building blocks used .....	- 25 -
Figure 7 General scheme of the aryloxyiminoamides synthesized .....	- 25 -
Figure 8 Intrinsic and extrinsic pathways .....	- 28 -
Figure 9 Model of BCL-2 family control over mitochondrial apoptosis.....	- 31 -
Figure 10 The apoptotic blocks used by cancer cells .....	- 32 -
Figure 11 Design strategy. a) Docked structure of BAM-7 (pink) at the BAX rear site (green surface). BIM BH3 helix is colored in transparent blue b) Representation of the re-branching approach. c) Binding mode of 8 (BTC-8) within BAX rear site. ....	- 34 -
Figure 12 Affinity of FITC-BIM for recombinant BCL-2 family targets. FITC-BIM Direct specific binding isotherms are shown for engagement of FITC-BIM by GST-BAX (green curve), BCL-2 (red curve) and BCL-XL (blue curve). Total binding (black lines) are shown for comparison. Fraction of FITC-BIM bound was measured before and after the addition of Acetylated-BIM (50 $\mu$ M). FITC-BIM specific binding was calculated subtracting non specific binding (measured in the presence of Acetylated-BIM) from total binding (measured in the absence of Acetylated-BIM). Mean of three experiments and S.D. are indicated. ...	- 38 -
Figure 13 8 binds BAX at BIM binding site. Competition between 8 (upper panel) or BAM-7 (lower panel) and FITC-BIM for binding to BAX (green curve), BCL-2 (red curve) and BCL-XL (blue curve). Mean of three experiments (SD. are indicated). ....	- 39 -
Figure 14 8 induces apoptosis in a BAX dependent way. Effect of 8 treatment on MEF cells. Apoptotic rate of the indicated MEF clones upon 24 h of treatment with vehicle (0.1% DMSO, gray bars), 1 (15 $\mu$ M, white bars), or 8 (15 $\mu$ M, green bars). The photographs represent appearance of apoptotic cell membrane blebbing upon MEF treatment with 8 and its absence when 8 treatment was done in the presence of the caspase inhibitor Ac-DEVD-CHO (10 $\mu$ M). ....	- 42 -
Figure 15. 8 affects mitochondria in HuH7 cells. (a) Mitochondrial activity of 8 and 1 treated cells visualized by Mitotracker Red fluorescence uptake. Magnification bars are indicated. (b) After lysis of the cells absorbance of the dye was measured at 570 nm and plotted versus 8 or 1 concentration. EC50 were calculated by fitting values by non linear regression analysis of dose response analysis and reported together with their 95% CI (error bars are indicated, n = 3). ....	- 43 -

Figure 16 mitochondrial Effect of 12 (a) and 72 hours (b) of compounds 1-16 treatment on mitochondrial activity of HuH7 cells measured by Mitotracker Red accumulation. After lysis of the cells absorbance of the dye was measured at 570 nm and reported as percentage of that measured in untreated cells (mean of at least 3 experiments, error bars are indicated (S.D.)). ..... - 44 -

Figure 17 8 activates BAX. Lysates of HuH7 cells treated with 8 or with vehicle alone were immunoprecipitated or not with the 6A7 monoclonal anti-BAX antibody. All samples were equally boiled, run on a SDS-PAGE and decorated with a polyclonal antibody anti-BAX. .... - 44 -

Figure 18 8 induces translocation of BAX to mitochondria. a) HuH7 cells were treated with 1 and 8 to be then fixed and processed for immunofluorescence to localize BAX intracellularly. In untreated cells, BAX localizes in the cell cytoplasm with no clear indication of association to any intracellular organelle, while after treatment of the cell with 10  $\mu$ M 1 or 8, BAX localization drastically changes moving to punctuate structures. b) As further proof HuH7 cells were cultured with the indicated amount of 8, or with vehicle alone for 12 hours. After treatment cell were permeabilized and the mitochondrial and cytosolic fractions were isolated as described in the manuscript. Equal amount of proteins were separated by SDS PAGE and processed for Western Blotting. BAX was revealed by decorating the filters with the indicated anti-BAX antibody (fullblots are shown). ..... - 45 -

Figure 19 8 induces cyt-C release from mitochondria. HuH7 cells were treated with BAM-7 (1) and 8, then were fixed and processed for immunofluorescence to localize cyt-C intracellularly. Before the treatment with 8, the cyt-C is localized in mitochondria, as shown by its colocalization with the structures labeled by the Mitotracker Red. After the treatment with 8, its localization changed becoming diffuse thus indicating its exit from the organelle. Boxed area are shown at higher magnification at the corner of each panel. . - 46 -

Figure 20a) 8 induces caspase-3 activation and formation of apoptotic nuclei. b) Quantification of caspase-3 positive cells after treatment with 8 and 1 as described in the manuscript. Mean of 10 random fields (error bars are indicated S.D.)..... - 46 -

Figure 21 8 induces apoptosis in tumor cells but it does not alter apoptotic rate in healthy splenocytes. The indicated tumor cell lines (a) or primary splenocytes (b) were incubated for 72 h with 8 (10  $\mu$ M). Apoptosis rates were detected by counting apoptotic nuclei. Mean values are reported together with their SD (n = 3 in a; n = 4 in b). ..... - 47 -

Figure 22 8 induces growth arrest and cell death. (a) Cells were incubated for 72 h with the indicated concentration of 1 and 8 and then with Mitotracker. Absorbance was measured after lysis of the cell. Values are the mean of at least three experiment. Error bars (SD) are indicated. (b) HuH7 cells were incubated for the indicated time with 10  $\mu$  1 or 8 or vehicle alone. After the treatment cells were counted. Values are expressed as percentage of control (cells at 0 min of treatment) and are representative of at least three experiments. .... - 48 -

Figure 23 In vivo treatment with 8 induces in situ BAX activation. Homogenates of mouse lungs treated or not with 8 were lysed and immunoprecipitated with the 6A7 monoclonal antibody. Samples were boiled, run on a SDS-PAGE, and decorated with a polyclonal antibody anti-BAX (only relevant part of the gel is shown). ..... - 49 -

Figure 24. In vivo activity of 8. (a) Effect of the daily administration of 8 1 mg/kg from day 14 to day 17 on tumor growth (dark violet staining). Microphotographs showing the entire lung sections; the boxed areas in the upper-magnification H&E panels are shown at a higher magnification in the lower panels. (b) Graph showing the effect of 8 on tumor growth. The results are expressed as tumor lesions/lung area ratio.

Individual data points represent average value per mouse; horizontal bars denote mean. $P < 0.01$ vs control group. ....	- 50 -
Figure 25 Schematic cartoon of Fz4-WT (a) and Fz4-FEVR (b) receptors. Through improper interactions with the ER membranes, the Fz4-FEVR tail causes receptor aggregation.....	- 51 -
Figure 26 Chemical structures of compound FzM1, 2 and 3. Their EC <sub>50</sub> for PM rescue of Fz4- FEVR are indicated together with s.e.m. ( n= 3). ....	- 53 -
Figure 27 Chemical structure of FzM1alk. EC <sub>50</sub> values for FzM1alk as a folding chaperone for Fz4-FEVR and as a Wnt inhibitor are indicated. (n=3, means $\pm$ s.e.m.) .....	- 54 -
Figure 28 Solvent accesibility of Fz4 region upon binding to FzM1 measured by the rate of HDX. The color scale reflects the level of deuterium exchange measured as difference in peptide mass in the presence or in the absence of FzM1. The arrows indicate FzM1 binding site and the C-terminal tail movement upon FzM1 binding. Numbers indicate TMDhelices (5–7) and the C-terminal tail helix (8). ICL3 is indicated.....	- 55 -
Figure 29 Enzymatic function of sirtuins. (A) NAD-dependent protein lysine deacylation activity of different sirtuins. (B) Enzymatic reaction mechanism of sirtuins. ....	- 58 -
Figure 30 Structure of a ternary sirtuin-NAD-acetyl peptide complex(PDB ID 2H4F). NAD, acetyl lysine, and the key catalytic His residue are shown in stick representation. Bound zinc is shown as a gray sphere. Protein structure picture is generated using PyMol. ....	- 59 -
Figure 31 Sirtuin 6 (SIRT6) cellular functions and their impact on organismal biology and disease. ....	- 61 -
Figure 32 Three-dimensional structure of sirtuin. The enzyme is shown in cartoon representation without bound ligands. The Rossmann-fold domain is indicated in magenta, the small domain in blue, the loops in green, the cofactor binding loop in black, the Zn ion in red, the N-terminal region in orange, and the C-terminal region in yellow. Disordered regions are indicated with dashed lines.....	- 65 -
Figure 33 Sirtuin active site binding cleft. . The Hst2 protein is shown in tan surface representation. The catalytic residues H135 and N116 are shown in red stick representation in the close-up view. The peptide substrate backbone is shown in green cartoon representation, the acetyl-lysine side chain is shown in green cpk stick representation, and the NAD <sup>+</sup> substrate molecule is shown in cyan cpk stick representation...	- 66 -
Figure 34 . Conformational changes of the cofactor binding loop upon substrate and product binding. The Hst2 protein is shown in tan cartoon representation, the C-terminus is shown in yellow, and the cofactor binding loop is shown in magenta. The peptide substrate is shown in green cartoon representation, while the acetyl-lysine residue is shown in green cpk stick representation. (A) The apo Hst2 enzyme, the cofactor binding loop is disordered (dashed lines). (B) Hst2 with bound peptide substrate and carba-NAD <sup>+</sup> , the cofactor binding loop is in an open conformation. (C) Hst2 with bound peptide substrate and 2"-O-acetyl-ADP-ribose, the cofactor binding loop is in a closed conformation.....	- 66 -
Figure 35 Productive NAD <sup>+</sup> binding interactions in several sirtuin proteins. ....	- 67 -
Figure 36 Acetyl-lysine peptide binding to the sirtuin active site.(A) A peptide containing an acetyl-lysine residue (green) is shown bound to the Sir2-Af2 sirtuin enzyme (tan, cartoon representation) active site forming the $\beta$ staple with flanking $\beta$ strands of the enzyme (cyan). (B) The acetyl-lysine containing peptide (green) makes main chain $\beta$ strand hydrogen bonds (red dashes) with main chain atoms of the enzyme	

(cyan). (C) The acetyl-lysine residue (green) binds in a hydrophobic tunnel of the enzyme (tan, surface representation), making several van der Waals interactions with enzyme residues (orange) and one hydrogen bond (red dashes) with an enzyme residue. .... - 68 -

Figure 37 Structure of human SIRT6 in complex with ADP-ribose. A, overall structural features of SIRT6 monomer. B, superimposition of the six molecules in the asymmetric unit. Red, chain A; green, chain B; dark blue, chain C; orange, chain D; cyan, chain E; yellow, chain F. C, schematic illustration of the hydrogen bonding network surrounding ADPr; hydrogen bonds are indicated as dashed lines, and water molecules are shown as spheres. .... - 70 -

Figure 38 Chemical structure of the compound 1..... - 73 -

Figure 39 Compounds synthesized as SIRT6 inhibitors ..... - 74 -

Figure 40 Possible conformation of the compound 1 in SIRT6 ..... - 78 -

Figure 41 Changes in the chemical structure of compound 1..... - 79 -

# List of Schemes

Schema 1 Strecker synthesis of $\alpha$ -amino acids. ....	- 13 -
Schema 2 Hantzsch multicomponent synthesis of dihydropyridines .....	- 13 -
Schema 3 Hantzsch multicomponent synthesis of pyrroles.....	- 13 -
Schema 4 Biginelli multicomponent synthesis of dihydropyrimidines .....	- 13 -
Schema 5 Mannich reaction .....	- 14 -
Schema 6 The Passerini three component reaction (P-3CR).....	- 14 -
Schema 7 The Ugi four component reaction (U-4CR). ....	- 14 -
Schema 8 The Hofman reaction .....	- 15 -
Schema 9 Suggested mechanism of P-3CR.....	- 16 -
Schema 10 Simplified mechanism of the U-4CR .....	- 17 -
Schema 11 Proposed scheme for the formation of Novel MCRs via Nitrile N-oxide species .....	- 18 -
Schema 12 The reported reaction between nitrile-N-oxides and isocyanides .....	- 18 -
Schema 13 Proposed mechanism for the formation of isocyanates and cyanides starting from nitrile N-oxides and isocyanides. ....	- 19 -
Schema 14 Acid Hydrolysis and Deoximation of 1,3-Oxazol-2-oximino Derivates. ....	- 21 -
Schema 15 Three-Component Synthesis of Aryloxyimino Amide .....	- 24 -
Schema 16 Synthesis of Benzo[d]isoxazole-3-carboxamides .....	- 26 -
Schema 17 Synthesis of Compounds 1-7. <sup>a</sup> Reagents and reaction conditions: (a) ethyl acetoacetate, acetic acid, reflux temperature, 3 h, 62%; (b) appropriate benzaldehyde, piperidine, anhydrous ethanol, reflux temperature, 3 h, 28–61%; (c) (i) potassium tert-butoxide, anhydrous tetrahydrofuran, –40 °C, 1 h, (ii) 2-(2-ethoxyphenyl)acetyl chloride, 25 °C, 1 h, 74%; (d) potassium permanganate, catalytic sulfuric acid, acetone, reflux temperature, 5%. ....	- 36 -
Schema 18 Synthesis of Compounds 8, 9, 11-13 and 15a <sup>a</sup> Reagents and reaction conditions: (a) tin(II) chloride dihydrate, ethyl acetate, reflux, 3 h; (b) (i) sodium nitrite, 37% hydrogen chloride, 0 °C, 20 min, (ii) tin(II) chloride dihydrate, 0 °C, 20 min, crude product; (c) ethyl acetoacetate, acetic acid, 80 °C, 3 h, 13%; (d) 2-ethoxybenzenediazonium chloride or naphthalene-2-diazonium chloride, sodium acetate, 96° ethanol, 0 °C, 2 h, 3–48%; (e) appropriate boronic acid, 2 M sodium carbonate, dichloro[1,1'-bis(diphenylphosphino)ferrocene]-palladium(II) dichloromethane complex (1:1), tetrahydrofuran, reflux temperature, 90 min, Ar stream, 13–66%. ....	- 36 -
Schema 19 Synthesis of Compounds 10 and 14a <sup>a</sup> Reagents and reaction conditions: (a) appropriate boronic acid, 2 M sodium carbonate, dichloro[1,1' bis(diphenylphosphino)ferrocene]-palladium(II) dichloromethane	

complex (1:1), reflux temperature, 90 min, Ar stream, 14–25%; (b) tin(II) chloride dihydrate, ethyl acetate, reflux, 3 h; (c) (i) sodium nitrite, 37% hydrogen chloride, 0 °C, 20 min, (ii) tin(II) chloride dihydrate, 0 °C, 20 min, crude product; (d) ethyl acetoacetate, acetic acid, 80 °C, 3 h, 12–13%; (e) 2-ethoxybenzenediazonium chloride, sodium acetate, 96° ethanol, 0 °C, 2 h, 36–47%..... - 37 -

## *List of Table*

Table 1. $K_i$ ( $\mu\text{M}$ ) of Compounds 1-15 for BAX, BCL-2, and BCL-XL (FPA, FITC-BIM Displacement). .....	- 39 -
Table 2 $EC_{50}$ ( $\mu\text{M}$ ) Values of Apoptosis Induction of Compound 8 or 1 Treatment on the Indicated MEF Knockout Clones .....	- 41 -
Table 3 Sensitivity of the indicated MEF clones to 24 hours of treatment with the candidate compounds (15 $\mu\text{M}$ ). – (less than 5% of apoptotic cells); + (5-30% of apoptotic cells); ++ (30-60% of apoptotic cells); +++ (more than 60% of apoptotic cells). .....	- 41 -

# *Abbreviations*

**MCR:** Multicomponent reaction

**MOMP:** Mitochondrial outer membrane permeabilization

**BCL-2:** B-cell lymphoma 2

**BH3-only :** BCL-2 homology domain 3

**SIRT:** Sirtuin protein

**HDAC:** Histone Deacetylases

**NAD:** Nicotinamide adenine dinucleotide

**TNF- $\alpha$ :** tumor necrosis factor alpha

**U-4CR:** Ugi four-component reaction

**P-3CR:** Passerini three component-reaction

**TEA:** Triethylamine

**DCM:** Dichlorometane

**DBU:** 1,8-Diazabicyclo[5.4.0]undec-7-ene

**TNFR1:** Tumor necrosis factor receptor 1

**FasL:** Fatty acid synthetase ligand Fas ligand

**FasR:** Fatty acid synthetase receptor Fas receptor

**Apo3L:** Apo3 ligand

**DR3:** Death receptor 3

**Apo2L:** Apo2 ligand

**DR4:** Death receptor 4

**DR5:** Death receptor 5

**FADD:** Fas-associated death domain

**TRADD:** TNF receptor-associated death domain

**RIP:** Receptor-interacting protein

**DISC:** death-inducing signaling complex



**Caspase-8:** CysteinyI aspartic acid-protease 8

**c-FLIP:** FLICE-inhibitory protein

**cyt-c:** cytochrome complex

**Smac/DIABLO:** Second mitochondria-derived activator of caspase/direct inhibitor of apoptosis-binding protein with low pI

**HtrA2/OMI:** HtrA, high temperature requirement A serine peptidase 2

**Apaf 1:** apoptotic protease activating factor-1

**IAP:** Inhibitors of apoptosis proteins

**AIF:** Apoptosis inducing factor

**CAD:** Caspase-Activated DNase

**OM:** outer mitochondria membrane

**ANT:** adenine nucleotide translocase

**VDAC:** voltage dependent anion channel

**COX:** cytochrome c oxidase

**PTPC:** permeability transition pore complex

**MMP:** mitochondria membrane permeabilization

**MOMP:** mitochondrial outer membrane permeabilization

**SAR:** structure-activity relationship

**FITC-BIM:** fluorescein-5-isothiocyanate-BIM

**FPA:** Fluorescence polarization assay

**NMR:** Nuclear magnetic resonance

**MEF:** Mouse Embryo Fibroblast

**K:** Lys    **E:** Glu    **F:** Phe    **Y:** Tyr    **L:** Leu    **I:** Ile    **D:** Asp

**Ac-DEVD-CHO caspase inhibitor:** (peptide inhibitor) N-Ac-Asp-Glu-Val-Asp-CHO

**HuH7:** human hepatoma cells

**Jurkat:** T-cell lymphoma

**NB4:** leukemic cells ( promyelocytic)

**LLC1:** Lewis lung carcinoma

**SHSY-5Y:** human neuroblastoma cells

**DMSO:** dimethylsulfoxide

**H&E:** hematoxylin and eosin

**MS:** Mass spectra

**IR:** Infrared spectra

**Fz4:** Frizzled-4

**GPCRs:** G protein–coupled receptors

**TM:** Seven-transmembrane

**TMD:** TM bundle

**ICL:** intracellular loops

**ECD:** extracellular domain

**PM:** plasma membrane

**FEVR:** familial exudative vitreoretinopathy

**HA-Fz4-WT:** hemagglutinin (HA)-tagged WT Fz4

**U87MG:** glioblastoma cells

**2-O-Ac-ADPr:** 2-O-Acetyl- Adenosine diphosphate -ribose

**TCF/LEF:** T-cell factor/lymphoid enhancer factor

**HDX:** hydrogen-to-deuterium exchange

**Dsh:** Dishevelled protein

**Sir2:** silent information regulator 2

## *Chapter 1 – Multicomponent reactions*

The expectation in terms of the number and quality of compounds for drug discovery has increased enormously with the introduction of molecular biology and high-throughput biological screening. Multicomponent reactions have naturally become a rapidly evolving field of research due to their inherent convergence and high productivity, together with their exploratory and complexity-generating power and they have attracted the attention of both academic and industrial scientists. Multicomponent reactions (MCRs) are defined as a one-pot process that involves the reaction of at least three components to form a single product that incorporates essentially all the atoms of the starting materials. These reactions are atom economic, step efficient, and have high exploratory power with regard to chemical space and are therefore ideally suited for the generation of libraries of compounds [4]. MCRs constitute an especially attractive synthetic strategy since they provide easy and rapid access to large libraries of organic compounds with diverse substitution patterns. Very large libraries can be built up from a small set of starting materials within a short time, which can be used then for research on medicinal substances.

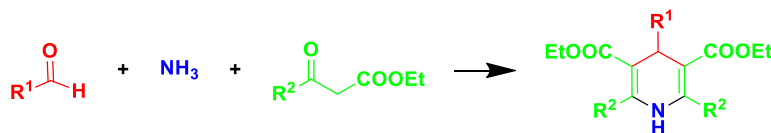
## 1.1 History of MCRs

The first modern contribution to the development of multicomponent chemistry was made in 1850 by Strecker. In this reaction an aldehyde is condensed with ammonium chloride in the presence of potassium cyanide to form an  $\alpha$ -aminonitrile, which is subsequently hydrolyzed to give the desired  $\alpha$ - amino acid (**Scheme 1**) [5].



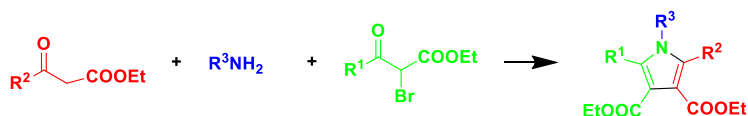
**Scheme 1** Strecker synthesis of  $\alpha$ -amino acids.

Many important heterocycle synthesis are MCRs. 1,4-Dihydropyridines were first synthesized in a four component reaction by Hantzsch in 1882 from ammonia, aldehydes and 2 equivalent of  $\beta$ -ketoesters. (**Scheme 2**) [6]



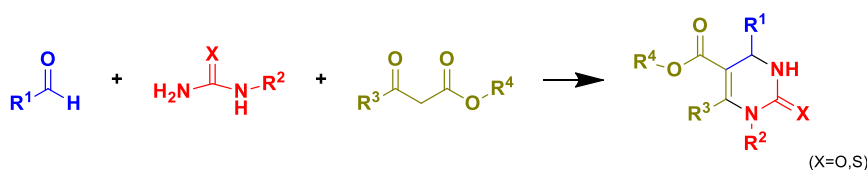
**Scheme 2** Hantzsch multicomponent synthesis of dihydropyridines

Another contribution made by Hantzsch in 1890 to MCRs was the synthesis of pyrroles by reacting primary amines,  $\beta$ -ketoesters and  $\alpha$ - halogenated  $\beta$ -ketoesters. (**Scheme 3**). [7]



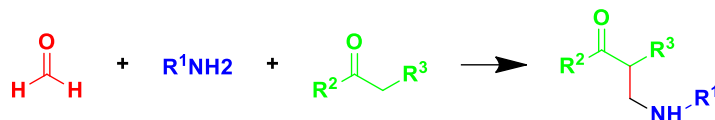
**Scheme 3** Hantzsch multicomponent synthesis of pyrroles

The Biginelli reaction, discovered in 1891, involves the synthesis of 3,4-dihydropyrimidin-2(1H)-ones from aldehydes, (thio)ureas and  $\beta$ -ketoesters (**Scheme 4**). [8]



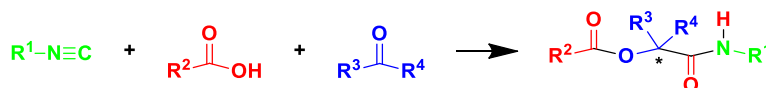
**Scheme 4** Biginelli multicomponent synthesis of dihydropyrimidines

The Mannich reaction (1912) consists of an amino alkylation of an acidic proton placed next to a carbonyl functional group with formaldehyde and ammonia or any primary or secondary amine; the final product is a  $\beta$ -aminocarbonyl compound also known as a Mannich base. **(Scheme 5)**



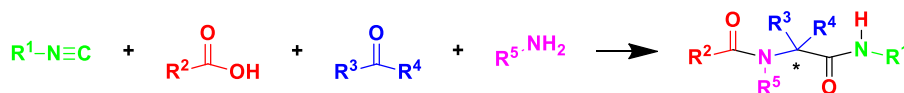
**Scheme 5** Mannich reaction

The first famous isocyanide-based MCRs, was described in 1921, was the Passerini reaction. This is a reaction between isocyanides, carboxylic acids, and aldehydes or ketones to afford  $\alpha$ -acyl carboxamides in a single step [9] **(Scheme 6)**.



**Scheme 6** The Passerini three component reaction (P-3CR).

The second and arguably the most important isocyanide-based MCR is the Ugi four component reaction **(Scheme 7)**. This elegant four-component reaction, discovered in 1959, is a reaction between isocyanides, carboxylic acids, ketones or (usually) aldehydes and primary amines to afford dipeptide-like structures. [10]

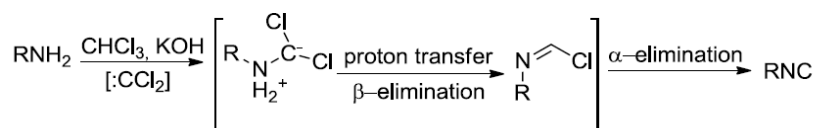


**Scheme 7** The Ugi four component reaction (U-4CR).

Owing to their flexibility, MCRs have found application in many fields of chemistry and in medicinal chemistry in particular.

## 1.2 Chemistry of Isocyanides

A large and important class of MCRs are the Isocyanide Multicomponent reactions. Isocyanides, formerly known as isonitriles, represented for a long time the only class of stable organic compounds with a formally divalent carbon. Moreover, in exothermic reactions C<sup>II</sup> is oxidized to C<sup>IV</sup>. The isocyanides are also well-known for their strange odour. Almost all commercially available isocyanides are volatile and carry this repulsive odour “ which is reminiscent of artichokes and phosphorus at the same time” [11]. Prolonged inhalation of isocyanides is believed to increase the intensity of dreams at night. Isocyanides were first synthesized in 1859 by Lieke, who did not recognize them and believed them to be nitriles [12]. It was Gautier the first to understand the isomeric relationship between isocyanides and nitriles in 1869 [13]. At the same time Hofmann [14] found a new approach to isocyanides with the reaction of primary amines with potash and chloroform (**Scheme 8**). Anyway, all methods known at that time were complicated, poorly generalizable and low yields affected, with difficult separation of isocyanides from their isomeric accompanying nitriles. The method of choice regarding cost, yield and execution remains however the dehydration of the corresponding *N*-formamides with inorganic dehydratants and organic matching bases, such as POCl<sub>3</sub> or Phosgene, and Triethylamine [15].

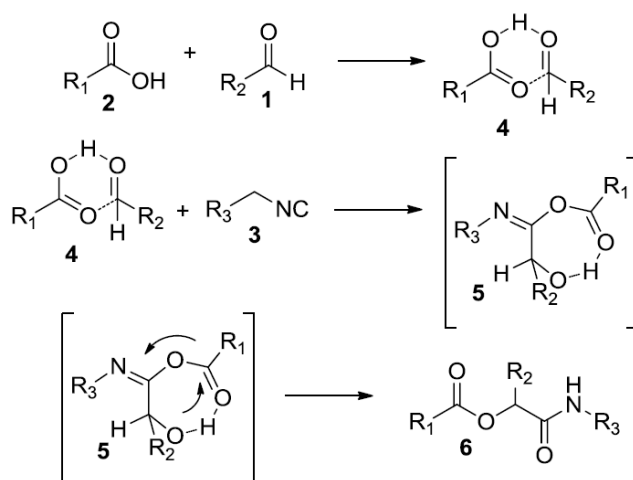


**Scheme 8** The Hofman reaction

The chemistry of isocyanides is characterized by three properties: the  $\alpha$ -acidity, the  $\alpha$ - addition, an intrinsic high affinity toward metallorganic reagents and their subsequent reactions, and the easy formation of radicals. Especially phenyl-isocyanides are substrates for radical-induced cyclizations. The  $\alpha$ -acidity is increased by further electron-withdrawing substituents in the  $\alpha$ -position such as carboxylic esters, nitriles, phosphonic esters, or sulfonyl groups. Isocyanides polymerize under Lewis acid catalysis to polyiminomethylenes. The most important property of isocyanides is the reaction with nucleophiles and electrophiles at the isocyanide carbon atom. The  $\alpha$ -addition of nucleophiles and electrophiles leads to the  $\alpha$ -adduct. Only carbenes and carbon monoxide share this property with the isocyanides [16]. The great potential of isocyanides for the development of MCRs lies in the diversity of bond forming processes available, their functional group tolerance, and the high level of chemo- and regio-selectivity often observed.

## 1.3 Passerini and Ugi reactions

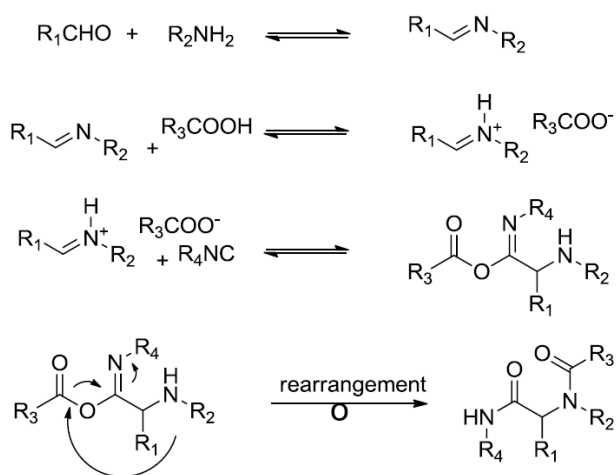
The Passerini reaction, described in 1921, involves an oxo-component (an aldehyde or ketone), an isocyanide and a nucleophile (typically carboxylic acids) to afford  $\alpha$ -acyloxycarboxamides in one step. A plausible mechanism provides the formation of a loosely hydrogen-bonded adduct **4** from a carbonyl compound **1** and a carboxylic acid **2**, followed by the  $\alpha$ -addition of the electrophilic carbonyl carbon and the nucleophilic oxygen atom of the carboxylic acid to the isocyanide carbon of **3** (**Scheme 9**) under formation of a cyclic transition state with all three parent compounds. The  $\alpha$ -adduct **5**, which cannot be isolated, rearranges in an intramolecular trans-acylation to the stable  $\alpha$ -acyloxycarboxamide **6**.



**Scheme 9** Suggested mechanism of P-3CR

The Passerini reaction is carried out at high concentrations of the starting materials and in inert solvents at or below room temperature. On the other hand, Ugi reaction (**Scheme 10**) could be seen as the aza-version of the Passerini 3-CR, as it involves an amine as additional fourth component: it is indeed the reaction of a Schiff base or an enamine with a nucleophile and an isocyanide affording  $\alpha$ -acylaminoamides. The Ugi 4-CR is much more versatile than the Passerini in terms of library size and scaffold. First of all the U-4CR is favoured in a polar solvent (MeOH being the most common) in contrast the P-3CR, which is accelerated by aprotic solvents. In the first step the oxo component and the amine condense to the imine, the Schiff base, via a hydroxyl aminal. It is also possible that the hydroxyl aminal can be transformed directly in the course of the reaction without formation of a Schiff base under certain circumstances. Imines can be seen as carbonyl analogues. Like most imine reactions, the U-4CR runs better upon activation of the Schiff base. For this, the acid component protonates the nitrogen atom of the Schiff base, thus increasing the electrophilicity of the C=N bond. Depending on the solvent, the ions can be present as a salt pair or separately. The electrophilic iminium ion and the nucleophilic acid anion add to the isocyanide carbon atom. The  $\alpha$ -adduct thus formed can be seen as a hetero analogue of an acid anhydride in which an *exo*-oxygen atom has been substituted by an NR group. After an intramolecular acylation, the stable Ugi linear, peptide-like adduct is obtained. This type of intramolecular acylation was first described in 1910 by Mumm and was subsequently called the Mumm rearrangement [17]. All elementary steps of this reaction are equilibria; however, the last step, the rearrangement to the stable  $\alpha$ -acylaminoamide, lied exclusively on

the product side. The driving force of the total reaction sequence is the oxidation of the isocyanide C<sup>II</sup> atom to the amide C<sup>IV</sup> atom.

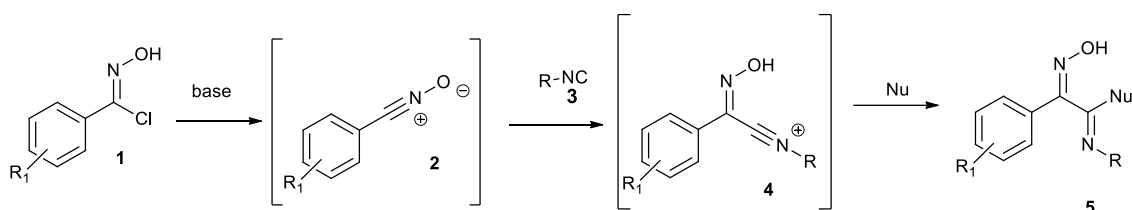


**Scheme 10** Simplified mechanism of the U-4CR



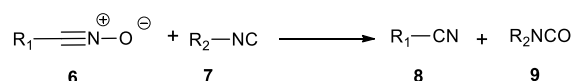
## 1.4 Novel MCRs: A procedure for the synthesis of Aryl $\alpha$ -ketoamide Amides

The discovery of novel multicomponent reactions can afford the development of innovative ways to synthesize known or unknown molecular scaffolds. The most of MCRs are mediated by isocyanides, which are the only class of stable organic compounds with a divalent carbon. This property is very important because the divalent carbon reacts first with electrophiles and subsequently with nucleophiles. The identification of novel electrophilic partners constitutes a starting point for the discovery of new MCRs. The recent discovery that nitrile N-oxide species **2**, which generated by base dehydrochlorination of (Z)-chlorooximes **1** [18], are good electrophilic partners for isocyanides **3** to give a nitrilium ion **4**, that can be intercepted by a third nucleophile [19], has led to the development of novel multicomponent reactions. (Scheme 11)



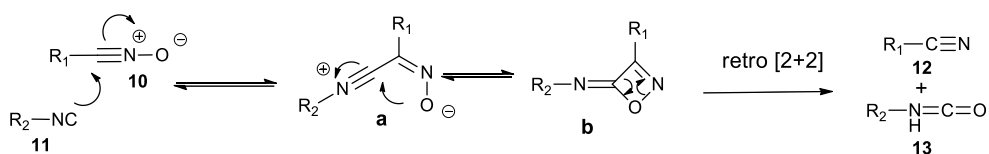
**Scheme 11** Proposed scheme for the formation of Novel MCRs via Nitrile N-oxide species

A possible explanation of this missed opportunity might be found in a 1965 paper [20] where it was documented that nitrile N-oxides **6** and isocyanides **7** react to give isocyanates **8** and nitriles **9** according to the reaction reported in **Scheme 12**.



**Scheme 12** The reported reaction between nitrile-N-oxides and isocyanides

It was proposed the following mechanism: the isocyanide **11** attacks, in a stereospecific way [21], the electrophilic carbon of the nitrile N-oxide **10** to give the intermediate **a**. This intermediate is then intramolecularly intercepted by the oxygen of the nitrile N-oxide, to give the highly unstable 4H-1,2-oxazet-4-imine derivative **b** [22], which, by a retro [2+2] cycloaddition, provides the corresponding cyanide **12** and isocyanate **13** (**Scheme 13**).



**Scheme 13** Proposed mechanism for the formation of isocyanates and cyanides starting from nitrile N-oxides and isocyanides.

The presence of a third nucleophile in the reaction mixture can preclude the formation of the high energy content 4H-1,2-oxazet-4-imine derivative **b** driving the reaction toward another synthetic pathway as reported in this work. On the other hand, an isocyanide containing an internal nucleophile can intramolecularly intercept the nitrilium ion species generating a novel molecular framework. (**Figure 1**)

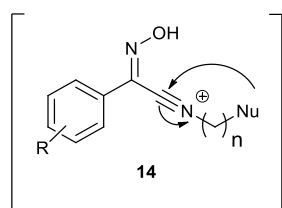


**Figure 1** Intramolecular trapping of the nascent nitrilium ion

As a starting point for this study, it was inspired by pioneering work by Professor Jeping Zhu reported in a paper 2001 [23]. He demonstrated a three-component reaction of aldehydes, primary or secondary amines and  $\alpha$ -isocyanoacetamides to provide 5-aminoxazoles through interception of the nitrilium ion by the oxygen atom of the amide. For this reason the  $\alpha$ -isocyanoacetamides could react with the nitrile N-oxides and then intermolecularly intercept the nascent nitrilium species. In this work [24] it was explored the reaction between (Z)-arylchlorooximes **5** and  $\alpha$ -isocyanoacetamides **2** to produce 1,3-oxazol-2-oxime derivatives **18** in good yields. (**Figure 2**)

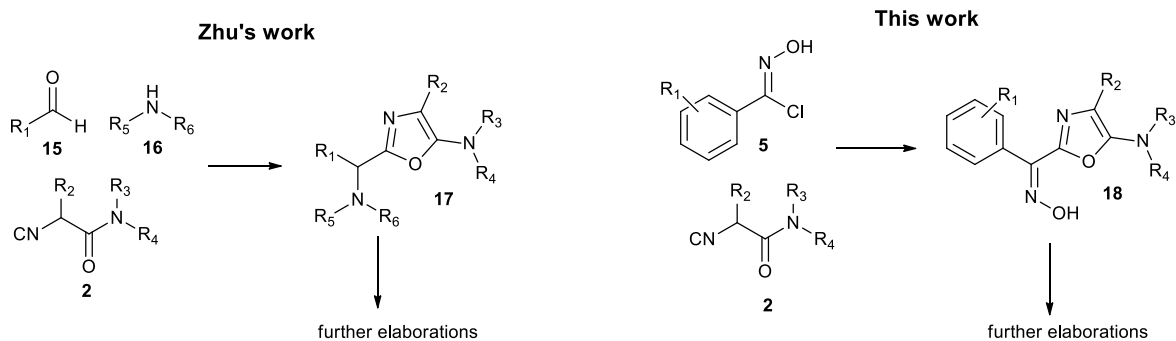


**Figure 2** Comparison between Zhu's work and the reaction described in this work

The reaction was carried out without TEA and with 1 equiv of TEA in dichlorometane at room temperature. The results were that the reaction with TEA was complete after 2h giving the desired product in good yields after column chromatography. On the other hand, the reaction without TEA didn't formed the desired product and starting material, syn-chlorooxime was recovered after column chromatography. The reaction was explored using these already optimized conditions ( 1 equiv of TEA, room temperature , DCM) and (Z)-phenylchloroximes bearing electron-withdrawing (**22,26,27,28,29**) or electron-donating (methyl **23** or methoxy **24**) substituents on the *para* position, as well as one (Z)-heteroarylchloroxime with thiophene ring(**25**).  $\alpha$ -Isocyanoacetamides contain two points of diversity: the amide function derived from cyclic secondary amines (**20,30-32,36,37**) or noncyclic secondary amines (**35**) and  $\alpha$ -substitution (methyl **30** or benzyl **31,32**). (Figure 3)

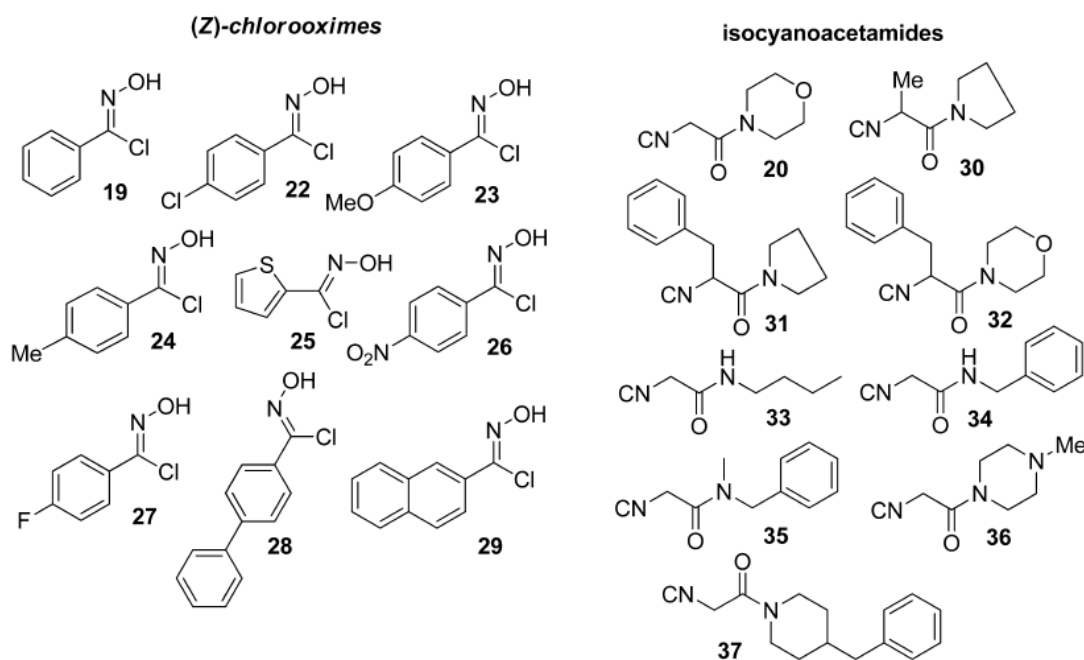
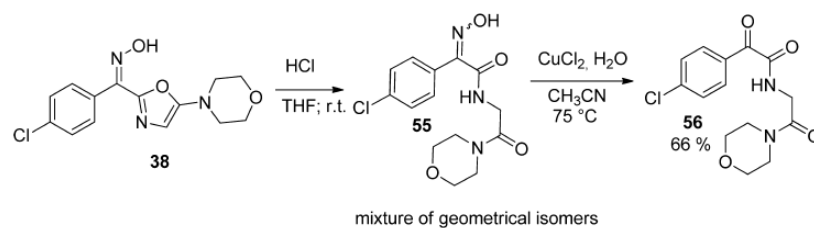


Figure 3 Structure of (Z)-chlorooximes and  $\alpha$ - isocyanoacetamides.

Arylchloroximes were synthesized by chlorination of the corresponding oximes with N-chlorosuccinimide [25], while  $\alpha$ -isocyanoacetamides were accessible by amidation of the corresponding  $\alpha$ -isocyanomethyl ester using The Dömling procedure [26]( $\alpha$ -Isocyanoacetic acid methyl ester was added to amine and stirred overnight at room temperature); to obtain the  $\alpha$ -substituted  $\alpha$ -isocyanoacetamides the alkylation was carried out in the presence of cesium hydroxide in acetonitrile at 0°C. [27] The different (Z)-arylchloroximes reacted with the isocyanoacetamides giving the corresponding 1,3-oxazol-2-oxime derivatives in a range of yields from 32% to 88%. Moreover, when isocyanoacetamide **36** was used, the base TEA was not necessary because the basic nitrogen of piperazine was able to trigger the formation of the nitrile N-oxide species. The reaction failed when a secondary amide was present such as in the isocyanoacetamides (**33** e **34**).

1,3-Oxazol-2-oximes were not stable molecules with isomerization of the oxime, especially when the oxazole ring was substituted at the 4-position, and formation of decomposition products. Although we have fully characterized them, they cannot be stored for long time (even at 0 °C). At the beginning, we attempted a one-pot procedure for the conversion of 1,3-oxazol-2-oximes into aryl- $\alpha$ -ketoamides. Hydrolysis of these intermediates in the presence of HCl, at room temperature, afforded the oxime-dipeptide analogue **55**, favoring, at the same time, the partial isomerization of the oxime. When the reaction was heated, we did observe the hydrolysis of the oxime and also the formation of several byproducts, which decrease the yield and make difficult the chromatographic purification. For these reasons, we opted to use milder catalysts as a Lewis acid, and we identified the copper(II) chloride [28] as the reagent of choice. After the aminooxazole ring was opened with HCl, the deoxygenation reaction in the presence of copper(II) chloride was carried out. Both reactions proceeded well and only a purification step was required (**Scheme 14**).



**Scheme 14** Acid Hydrolysis and Deoxygenation of 1,3-Oxazol-2-oximino Derivates.

By using this protocol, we prepared different aryl- $\alpha$ - ketoamide amides (**57–73**) in good yields (**Figure 4**)

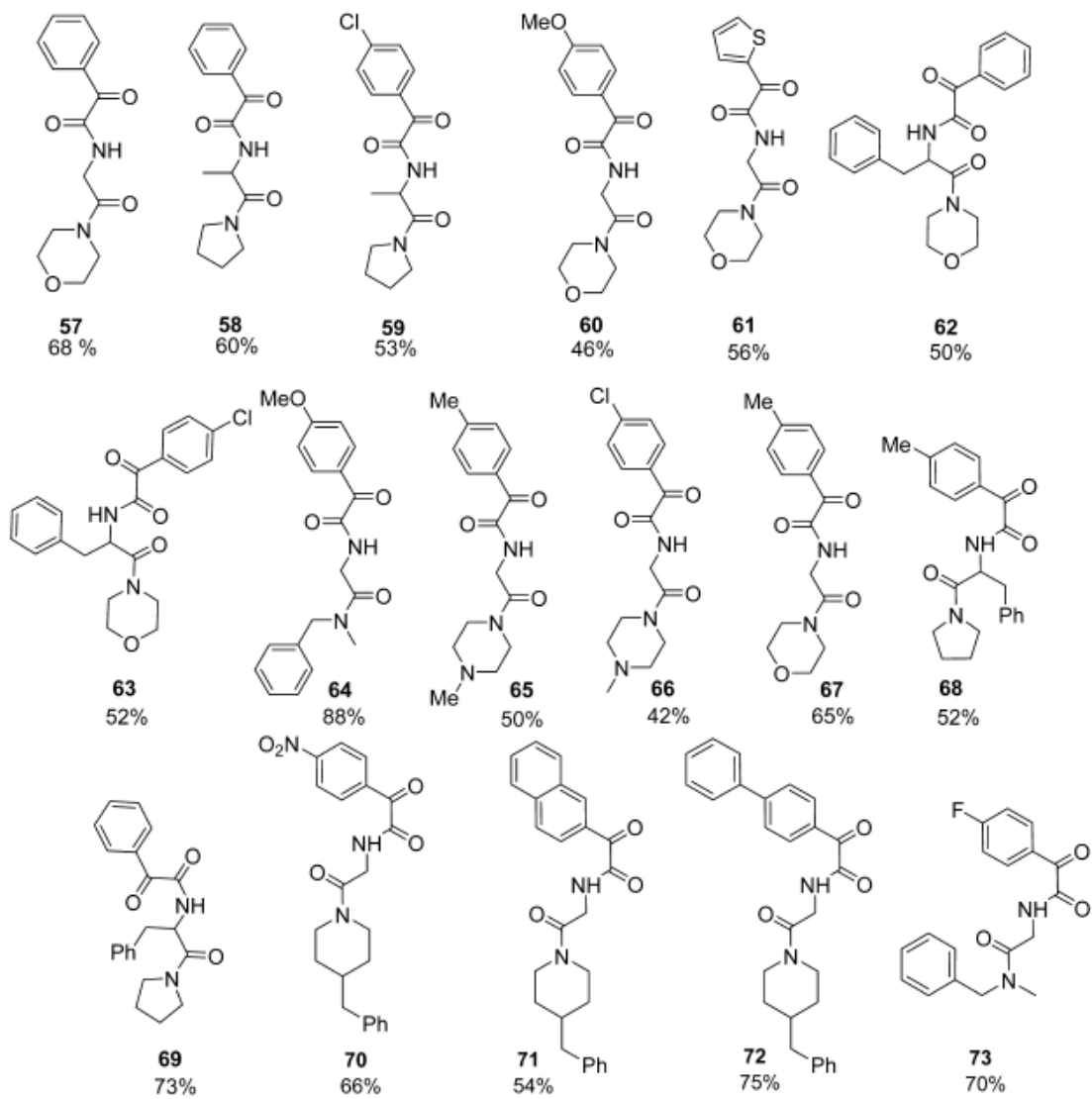


Figure 4 Synthesized aryl- $\alpha$ -ketoamides

## 1.5 Novel MCRs: Solution-Phase Parallel Synthesis of Aryloxyimino Amides

As a continuation of previous studies, an electron deficient phenol could be a good nucleophile third component to intercept the nitrilium ion giving aryloxyiminoamides. The mechanism of this reaction remember the Passerini-Smiles reaction developed by Prof El Kaim [29] [30]. The Passerini coupling involves an aldehyde, an acid carboxylic and an isocyanide and the mechanism consists in the activation of the aldehyde by the carboxylic acid followed the addition of the nucleophilic isocyanide and trapping of the resulting nitrilium by the carboxylate. All of these reversible reactions are finally displaced by a Mumm type rearrangement to form  $\alpha$ -hydroxyamide derivates.

An interesting strategy for discovery the new reactions and reactivity is to use surrogates of the carboxylic or the carbonyl partners. The o-nitrophenol is a good group because it is acidic ( $pK_a=7.2$ ) enough to activate carbonyl compound and induce isocyanide addition. The phenoxide is a good nucleophilic to trap the resulting nitrilium, forming imidate **2**. The latter undergoes a Smiles rearrangement (consisting of the transfer of an aromatic ring from one heteroatom to another located in the same chain) to give the more stable  $\alpha$ -aryloxi amide **3** [31]. (Figure 5)

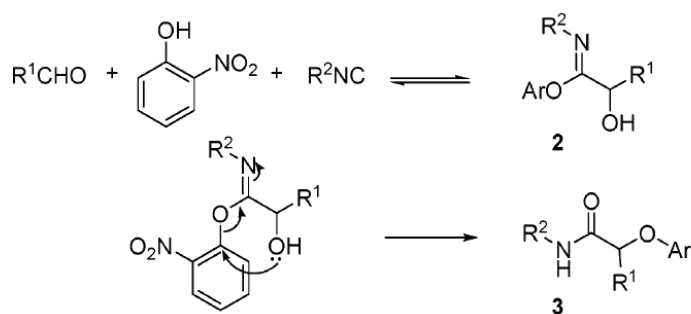
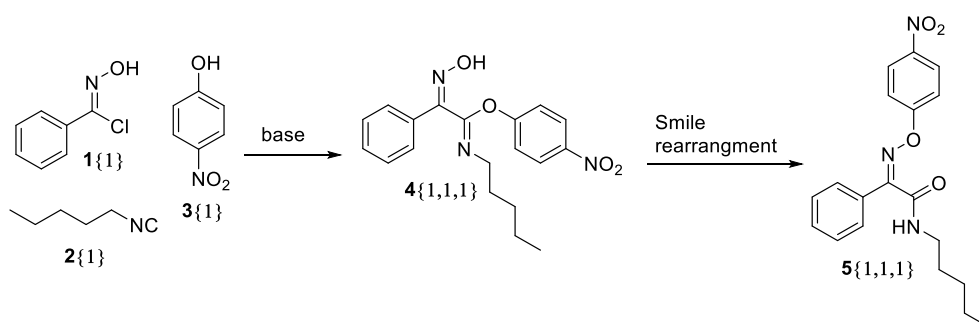


Figure 5 Passerini-Smiles Mechanism

## 1.5.1 Results and method

In this work a library of 41 aryloxyimino amides was prepared via solution phase parallel synthesis using (Z)-chlorooximes, isocyanides and electron-deficient phenols. This is a simil Passerini-Smiles reaction when is changed the carbonyl species with syn-chlorooximes; an phenol could be attack the nitrilium ion and after the formation of the imidate , the hydroxyl group of the oxime, which is properly positioned, thanks to the stereoselective addition of isocyanide to the nitrile N-oxide, should trigger a Smiles rearrangement. In this case, a six membered transition state should occur [32], contrary to the typical Smiles rearrangement which forms a five-membered transition state.



**Scheme 15** Three-Component Synthesis of Aryloxyimino Amide

To analyse this reaction, it is used (Z)-phenylchlorooxime (1), pentylisocyanide(2), and p-nitrophenol(3). **(Scheme 15)**. The last component has been shown to be less reactive in Ugi-Smiles [33] and completely non reactive in the Passerini-Smiles rearrangement [29]. Moreover it is more problematic than o-nitrophenol in favouring the Smiles rearrangement, and so presented a good challenge for reaction development and optimization. The reaction was carried out in the presence of 2 equiv of TEA , in dichlorometane at room temperature (2h), it was obtained a mixture of the desired product 5 and the imidate 4 , with yields of 14% and 20%, respectively. The result did not change when the reaction was heated at reflux in toluene (6h). The difficulty in triggering the Smile rearrangement could be due to the inability of TEA ( $pK_a=10.65$ ) to fully deprotonate the oxime ( $pK_a=10.78$ ). The use of 2 equiv of potassium tert-butoxide ( $pK_a=18$ ) did not improve the result. Under such conditions the reaction was not clean and the desired compound (5) {1,1,1} was isolated only in very low yield (less than 10%). For this reason , it is possible to search for a base stronger than TEA but weaker than *t*-BuOK, such as using 2 equiv of DBU ( $pK_a=12$ ) which the desired product 5 was obtained in 20% yield and the imidate 4 was not observed. In this case, as with TEA, heating the reaction at 80°C in toluene(6h) did not change the yield. To put it simply, the formation of the nitrile N-oxide species required an equimolar amount of base, while the Smiles rearrangement ,occurring after the addition of p-nitrophenol to the nitrilium ion, could proceed in the presence of a catalytic amount of base. In this way, reducing amount of DBU to 1.2 equiv in dichlorometane at room temperature overnight, the product was be isolated in 37% yield without the imidate.

The aryloxyimino amide is stable in particular with respect to a potential Beckmann rearrangement due to the presence of a nitrophenol leaving group. After refluxing in toluene for several hours no signal of Beckmann product could be detected. In this work three aryl-(Z)- chlorooximes 1 {1-3} bearing electron

donor substituents, three isocyanides **2** {1-3} and five electron-deficient arenes **3** {1-5} were involved in the combinatorial parallel synthesis of a library of **45** compounds (**Figure 6**).

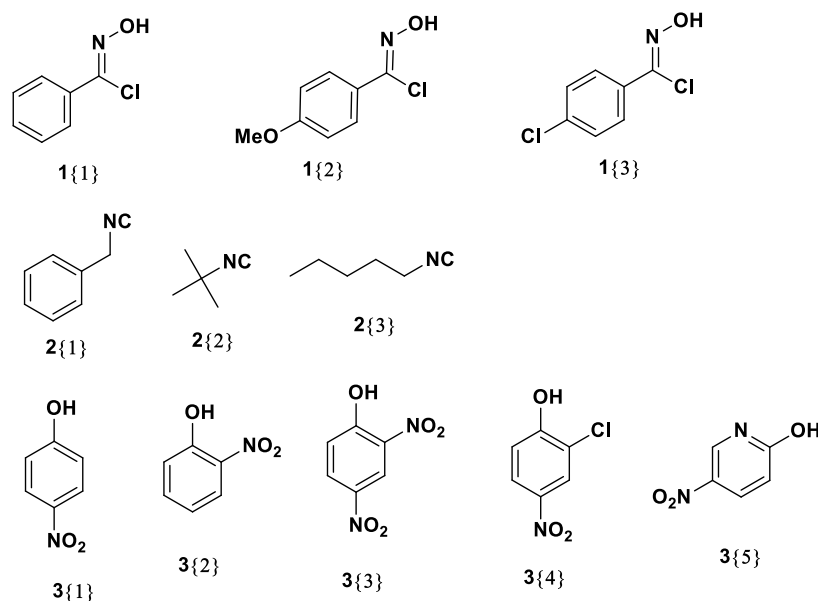


**Figure 6** Building blocks used

To optimize the management of such a large number of reactions and minimize the chances of trival operator errors (such as miscalculations which could compromise the outcome of some of the reactions), the computer program MCRcombiS was used, able to manage large amounts of data and quickly output the correct quantities/concentrations of reagents (mmol, mg/mL, etc.) to be used in each reaction. This program is now freely available for non-commercial use [34]. The results obtained are shown in **Figure 7**.

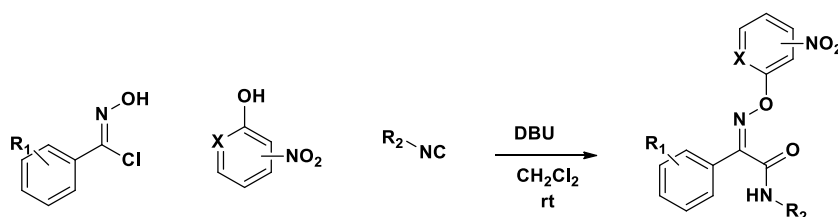
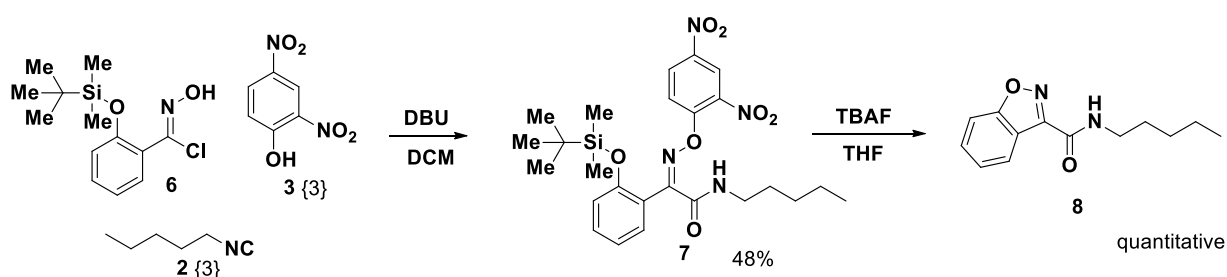


**Figure 7** General scheme of the aryloxyiminoamides synthesized

The reactions proceeded efficiently and only in four cases the desired aryloxyimino amide was not isolate . The reaction does not seem to be very sensitive to steric or electronic factors. The purity of the final compounds were analyzed by HPLC-UV-MS after a simple silica gel filtration. Four compound **5** {1,3,5}, **5** {2,3,5}, **5** {2,3,1}, **5** {3,3,5} were found to be mixture of Z and E isomers of the oxime, detected by both  $^1\text{H}$



NMR and HPLC, while six compounds [5 {1,1,1}, 5 {1,2,1}, 5 {1,1,2}, 5 {2,2,1}, 5 {2,1,2}, and 5 {2,2,2}] showed the presence of less than 5% of the E isomer visible only by HPLC. In this case, the E-isomer was easily removed by crystallization. Aryloxyimino amides are interesting compounds per se, but it was also intrigued by their potential use as intermediates for further synthetic transformations. As an example, the synthesis of benzo[d]isoxazole-3-carboxamides was explored, a well-known scaffold in medicinal chemistry, which usually requires a long and tedious synthesis (8 steps) [35]. As it has been demonstrated that  $S_N2$  reactions can occur at the  $sp^2$  nitrogen of oximes [36], so the aryloxyimino amide **7**, derived from the (Z)-chlorooxime of salicylaldehyde (**6**) may, after hydroxyl deprotection, trigger an intramolecular  $S_N2$  type reaction affording benzo[d]isoxazole-3-carboxamides (**8**) (**Scheme 16**). It was pleased to find that, when TBAF was used to cleave the silyl protecting group, the desired transformation occurred in quantitative yield.



**Scheme 16** Synthesis of Benzo[d]isoxazole-3-carboxamides

The discovery of these multicomponent reactions lead to development of new synthetic methodologies, which can be apply in medicinal chemistry.

*Chapter 2 – Structure-Based Lead Optimization and Biological Evaluation of BAX Direct Activators as Novel Potential Anticancer Agents*

## 2.1 Programmed Cell Death -Apoptosis

Apoptosis is a genetically programme leading to cell death that is involved in normal development and homeostasis to maintain cell populations in tissues. Apoptosis also occurs as a defence mechanism such as in immune reactions or when cells are damaged by disease or noxious agents. In vertebrate cells, the process of apoptosis can occur in two different pathways , namely the extrinsic and the mitochondria-mediated pathway.

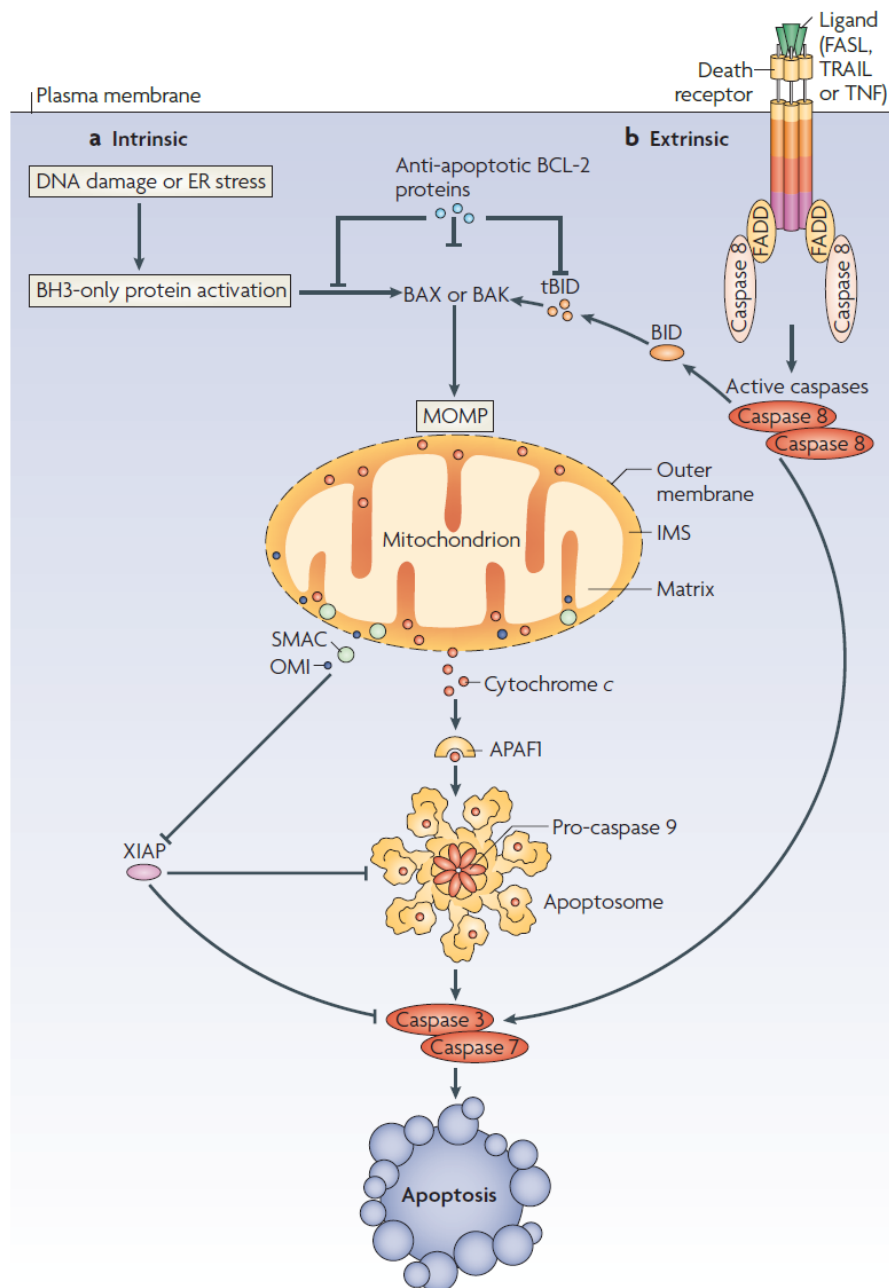
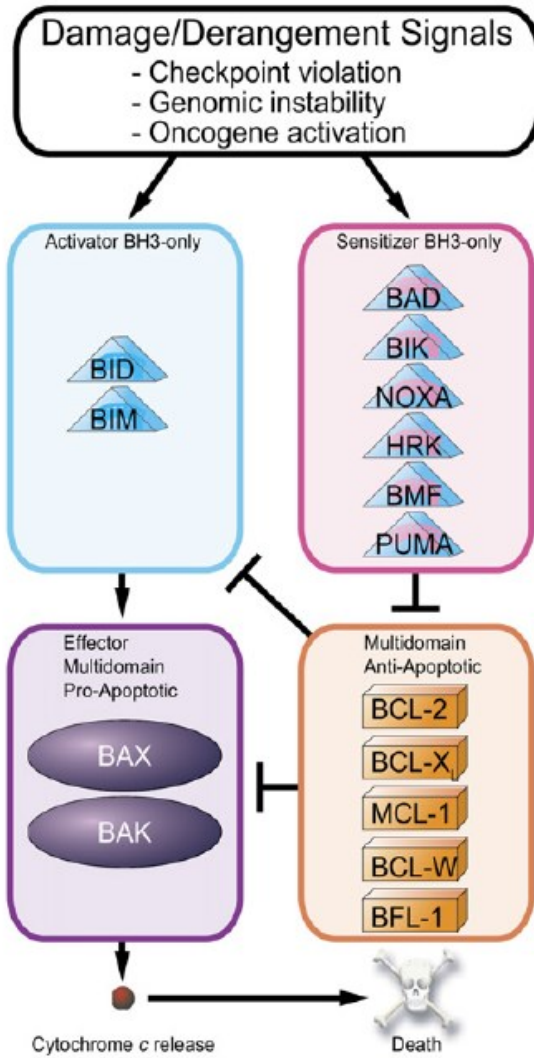


Figure 8 Intrinsic and extrinsic pathways

In the extrinsic signalling pathways (**Figure 8**) that initiate apoptosis, involve transmembrane death receptors, that are members of the tumor necrosis factor (TNF) receptor gene superfamily . Members of the TNF receptor family share similar cysteine-rich extracellular domains and have a cytoplasmic domain of about 80 amino acids called the “death domain” . This death domain plays a critical role in transmitting the death signal from the cell surface to the intracellular signalling pathways. To date, the best-characterized ligands and corresponding death receptors include FasL/FasR, TNF- $\alpha$ /TNFR1, Apo3L/DR3, Apo2L/DR4 and Apo2L/DR5. The sequence of events that define the extrinsic phase of apoptosis are best characterized with the FasL (Fatty acid synthetase ligand )/FasR (Fatty acid synthetase receptor) and TNF- $\alpha$  (Tumor necrosis factor alpha )/TNFR1 (Tumor necrosis factor receptor 1) models. In these models, there are clustering of receptors and binding with the homologous trimeric ligand. Upon ligand binding, cytoplasmic adapter proteins are recruited which exhibit corresponding death domains that bind with the receptors. The binding of Fas ligand to Fas receptor results in the binding of the adapter protein FADD (Fas-associated death domain) and the binding of TNF ligand to TNF receptor results in the binding of the adapter protein TRADD (TNF receptor-associated death domain) with recruitment of FADD and RIP (Receptor-interacting protein). FADD then associates with procaspase-8 via dimerization of the death effector domain. At this point, a death-inducing signaling complex (DISC) is formed, resulting in the auto-catalytic activation of procaspase-8. Once caspase-8 is activated, the execution phase of apoptosis is triggered. Death receptor-mediated apoptosis can be inhibited by a protein called c-FLIP (FLICE-inhibitory protein) which will bind to FADD and caspase-8, rendering them ineffective. Another point of potential apoptosis regulation involves a protein called Toso, which has been shown to block Fas-induced apoptosis in T cells via inhibition of caspase-8 processing [37] .

The mitochondria pathway of cell death (**Figure 8**) can be activated by a variety of receptor-independent stimuli such as radiation, toxins, hypoxia, hyperthermia, viral infections, and free radicals. All of these stimuli cause changes in the inner mitochondrial membrane that results in an opening of the mitochondrial permeability transition (MPT) pore. The major consequences of this change of permeability are the loss of the mitochondrial transmembrane potential ( $\Delta\Psi_m$ ), the release of pro-apoptotic proteins and the arrest of the bioenergetics function of the organelle. The proteins that are released can be broadly classified into two categories. The first group consists of cytochrome *c* (*cyt c*) , Smac/DIABLO(second mitochondria-derived activator of caspases), and the serine protease HtrA2/Omi. These proteins activate the caspase-dependent mitochondrial pathway. Cytochrome *c* binds and activates Apaf-1 as well as procaspase-9, forming an “apoptosome” . The clustering of procaspase-9 in this manner leads to caspase-9 activation and then activates the executioner caspases 3 and 7 resulting in the dismantling of the cell through nuclear fragmentation [38]. Smac/DIABLO and HtrA2/Omi are reported to promote apoptosis by inhibiting IAP (inhibitors of apoptosis proteins) activity [39]. The second group of pro-apoptotic proteins, AIF, endonuclease G and CAD, are released from the mitochondria during apoptosis, but this is a late event that occurs after the cell has committed to die. AIF translocates to the nucleus and causes DNA fragmentation into ~ 50–300 kb pieces and condensation of peripheral nuclear chromatin [40] . This early form of nuclear condensation is referred to as “stage I” condensation [41] . Endonuclease G also translocates to the nucleus where it cleaves nuclear chromatin to produce oligonucleosomal DNA fragments [42] . AIF and endonuclease G both function in a caspase-independent manner. CAD is subsequently released from the mitochondria and translocates to the nucleus where, after cleavage by caspase-3, it leads to oligonucleosomal DNA fragmentation and a more pronounced and advanced chromatin condensation [43] . This later and more pronounced chromatin condensation is referred to as “stage II” condensation [41]. The control and regulation of these apoptotic mitochondrial events occurs through members of the BCL-2 family of proteins. The founding member of BCL-2 family of proteins, *bcl-2*, was first cloned in neoplastic B cells with the t (14; 18) chromosome translocation [44] . Apoptotic events are highly regulated by this family of proteins, which shares homology in any of the four conserved “ Bcl-2 homology (BH) domains”, all

of which include  $\alpha$ -helical segments. The BCL-2 family of proteins has been divided into three main groups based on sequence homology and function [45]. The anti-apoptotic proteins, BCL-2, BCL-X<sub>L</sub>, MCL-1, BCL-w and BFL-1 possess all the four domains (BH1-4). These proteins also contain a hydrophobic carboxy-terminal domain that enables them to dock onto the outer mitochondria membrane (OM), the nucleus and ER. It has been shown that BCL-2 and Bcl-X<sub>L</sub> can protect the cells by interacting with mitochondrial proteins such as the adenine nucleotide translocase (ANT) or the voltage dependent anion channel (VDAC), thus preventing them from forming mitochondrial pores, protecting membrane integrity, and inhibiting the release of apoptogenic factors such as cyt c [46]. More recent evidence has highlighted novel functional biology of the anti-apoptotic protein BCL-2 [47]. Overexpression of BCL-2 was associated with a slight increase in steady state intracellular superoxide (O<sub>2</sub><sup>-</sup>) production, which was linked to increases in mitochondrial oxygen consumption and the activity of the rate limiting enzyme in the electron transport chain, cytochrome c oxidase (COX). Interestingly, pharmacological or molecular inhibition of the NADPH oxidase restored apoptosis sensitivity of BCL-2 overexpressing cells, thus implicating the pro-oxidant activity of BCL-2 in its anti-apoptotic function [48]. The second category of BCL-2 family, also known as multidomain pro-apoptotic proteins or “effectors”, share homology in the BH domains 1, 2 and 3. These proteins would include BAX and BAK. BAX is a pro-apoptotic protein that resides in the cytosol under physiological conditions. An apoptotic trigger, however, can lead to its translocation to the mitochondria and its subsequent insertion into the OMM. At the mitochondria, BAX can homodimerize or heterodimerize with other pro-apoptotic members such as BAK or truncated BID, thus disrupting the integrity of the OMM by forming mitochondrial pores and increasing its permeability. These pores can then lead to the release of apoptogenic factors such as cyt c [49]. Some reports have also suggested that BAX engages in a close molecular cooperation with proteins from the PTPC, such as ANT and/or VDAC, to induce mitochondria membrane permeabilization (MMP) [50]. BCL-2 and BCL-X<sub>L</sub> have been shown to antagonize the apoptotic cascade by a direct interaction and sequestration of these pro-apoptotic proteins [51]. Similarly BAK, which is normally inhibited by its interaction with VDAC, can also homodimerize and result in pore formation at the mitochondria when freed. The third group of BCL-2 family of proteins is the BH3-only proteins. They are so named because they share homology only in the BH3 domain, which is essential for pro-death function. Certain of the BH3- only proteins, including BIM and BID, are called “activators” and induce activation by causing an allosteric change in BAX and BAK. A second class of proapoptotic BH3-only proteins, called “sensitizer”, include BAD, BIK, NOXA, HRX, BMF and PUMA, are unable to induce activation of BAX and BAK directly. They act by neutralizing the anti-apoptotic proteins, binding the anti-apoptotic BCL-2 proteins causing a release of pro-apoptotic proteins. Sensitizers may be considered inhibitors of the inhibitors of apoptosis. [52]. Interactions between members of the sensitizer BH3-only class and the antiapoptotic class are selective. For instance, while BCL-2 is bound and antagonized by the BAD BH3 domain, NOXA BH3 binds BCL-2 very poorly. **(Figure 9)**



**Figure 9** Model of BCL-2 family control over mitochondrial apoptosis.

## 2.2 Apoptosis in Cancer Cells

Cancer cells block the apoptotic process by increasing the expression of anti-apoptotic BCL-2 members at the mitochondria. There are many mechanisms known by which BCL-2 is expressed at high levels in cancer cells. BCL-2 was originally cloned from the breakpoint of the chromosomal translocation t(14; 18) in patients with follicular lymphoma [44]. The translocation placed BCL-2 next to enhancer elements of the immunoglobulin promoter causing an increased expression of BCL-2. The BCL-2 translocation occurs in approximately 90% of follicular lymphomas and in about one-third of diffuse large B cell lymphomas [53]. On the other hand, BCL-2 overexpression has also been linked to gene amplification [54], hypermethylation of the BCL-2 gene [55], or chromosomal deletions causing the loss of micro-RNAs involved in the silencing of BCL-2 [56]. Reciprocally, cancer cells can evade death through mutations that inactivate the effector arm of apoptosis, such as the mutations of BAX observed in some solid tumors and hematopoietic malignancies [57]. For example, single nucleotide substitution or frameshift mutations of the BAX gene can occur in mismatch repair-deficient colon cancer or hematopoietic malignancies [58]. An especially common defect of cancers is a mutation in the tumor suppressor gene p53 [59], which in turn has a negative effect on the activation of apoptosis, as the BH3-only proteins NOXA and PUMA are transcriptional targets of p53.

A recent paper [60] segregated each of these blocks in apoptosis into three classes. In a Class A block, there is a loss of activator BH3-only proteins. A Class B block is caused by a failure to activate the effector arm of apoptosis through loss or inactivation of BAX or BAK. Finally, increased expression of an inhibitor protein such as BCL-2/MCL-1 causes a class C block (**Figure 10**).

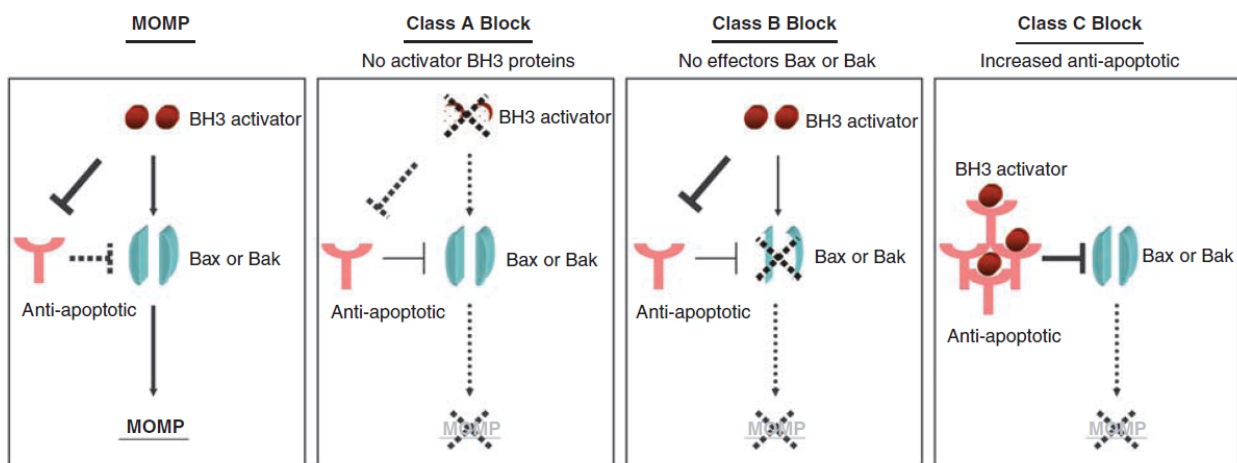


**Figure 10** The apoptotic blocks used by cancer cells .

A new technique called BH3 profiling can detect the class of apoptotic block a cancer cell has evolved to evade apoptosis. BH3 profiling exploits the binding pattern of sensitizer BH3 proteins to the anti-apoptotic proteins. BH3 profiling has been used to categorize diffuse large cell lymphoma cell lines into each of the three classes of apoptotic blocks, and it has shown that membership in the class C block correlates with increased drug sensitivity. From the results generated by overexpression studies in cell lines, it is easy to envision that increased expression of BCL-2 would provide additional opposition against chemotherapy [61].

## 2.3 Design Strategy

The three-dimensional superimposition of BAX, alone (inactive state) [62] and with BIM–BH3 helix (active state) bound in the “rear site” [63] clearly revealed that, upon BIM binding, significant changes took place in the  $\alpha$ 1– $\alpha$ 2 loop, which moves from a closed to an open conformation. Similar changes were observed upon **1** (BAM7) binding [64]. As the first step of this lead optimization protocol, docking experiments were performed, by means of Glide, [65] [66] in order to reproduce the **1** binding mode, [64] which was then overlapped onto that of BIM peptide. As shown in **Figure 11a**, the strongest interaction was observed between the carbonyl group of **1** pyrazolone core and the BAX K21, a key residue which interacts with BIM as well (see **Figure 11a**, charge–charge interaction with BIM E158). Notably, the ethoxyphenyl group of **1** lays adjacent to a presumed hinge site for loop opening upon initiation of BAX activation and well overlaps onto BIM F159. However, as shown in **Figure 11a**, the BIM–BH3 helix is much longer if, compared to **1**, holding five further amino acids next to F159, (e.g., Y162 and Y163). On the opposite side, the phenylthiazole portion of **1** well fitted on BIM L152 and I155, although lacking the terminal amino group, that as in the case of BIM, engages charge reinforced hydrogen bonds with BAX D142 and E146, respectively. On the basis of these premises, it was planned lead optimization studies of **1** aimed at understanding the BAX requirements and hopefully at improving the binding affinity. Given the importance of the pyrazolone core, it was retained while a rebranching approach was accomplished in the attempt to better mimic the essential features of the physiological activator (BIM BH3 only protein). Thus, as shown in **Figure 11b**, a number of different moieties were considered. Basically, in the replacement of the 2-ethoxyphenyl-hydrazono group, two considerations were taken into account: (i) substitution of hydrazone bridge with other spacer groups, for synthetic reasons, and (ii) substitution of the ethoxyphenyl with bulkier aromatic moieties (see compounds **2–7**, and **15–16**), in the attempt to approach the region occupied by BIM Tyr residues, which abut the hinge site for  $\alpha$ 1– $\alpha$ 2 loop opening. Analogously, for the replacement of the phenylthiazole group, the substitutions were planned based on the following considerations: (i) neither the N nor the S of the thiazole ring engaged interactions with BAX, so that the thiazole ring could, in principle, be replaceable by other aromatic systems such as phenyl ring, which can be easily substituted with the aim to establish further interactions with other BAX residues (e.g., E17), (ii) the *para* position of the biphenyl moiety is in proximity of D142 that together with E146 seizes the BIM amino terminal group (**Figure 11a**). Thus, it was inserted an exocyclic or endocyclic basic group at the terminal phenyl ring (**8**, **12**, and **10**, respectively). Compounds **9** and **13** were synthesized as negative control to test the importance of the *N,N*-dimethylamino group. Compound **14** was synthesized as negative control to test the importance of the hydroxyl group on the biphenyl moiety. Finally, **11** was conceived as a replacement of the 5–6 thiazole-phenyl system with a 6–5-phenyl-thiazole one.



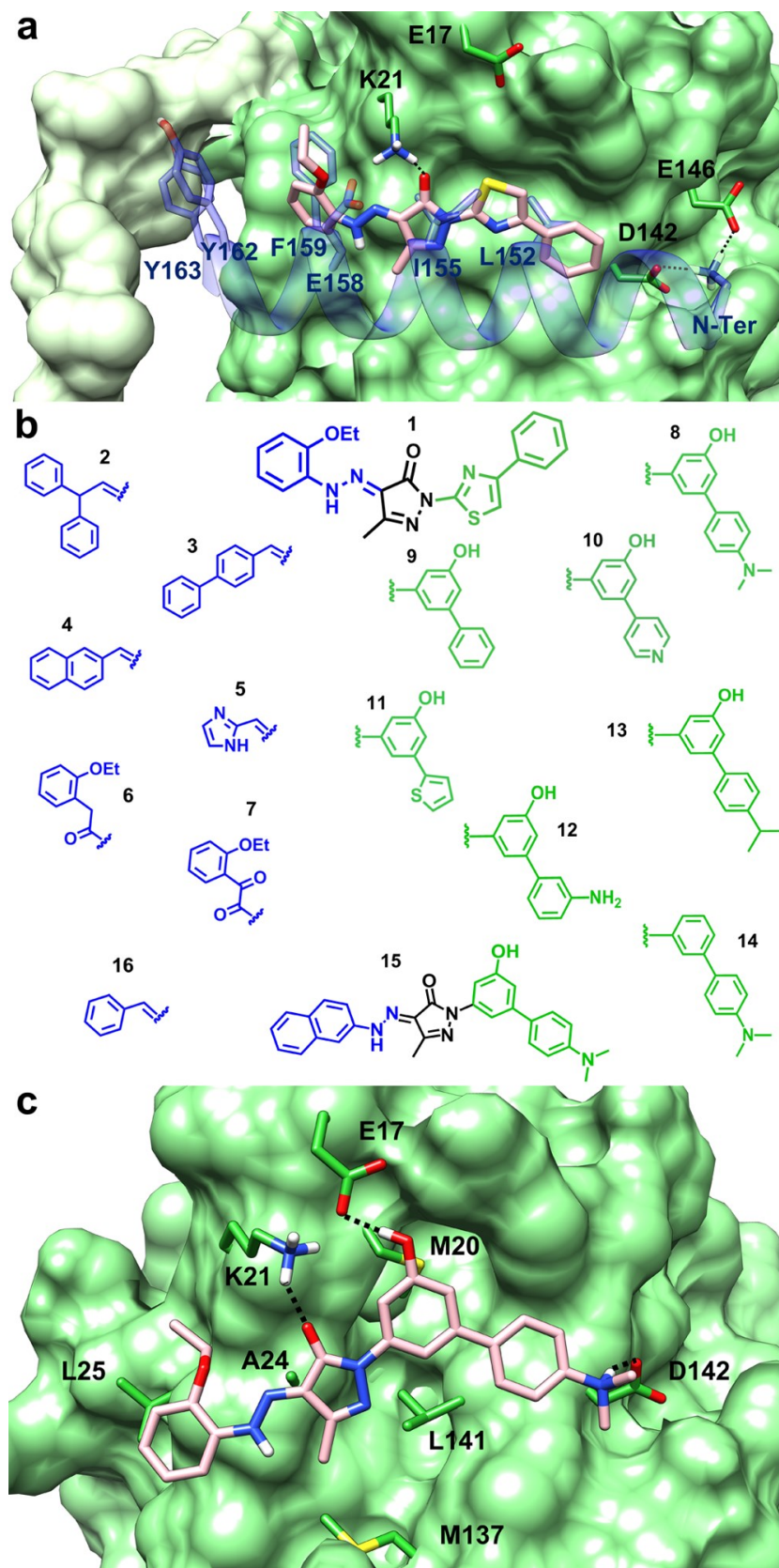
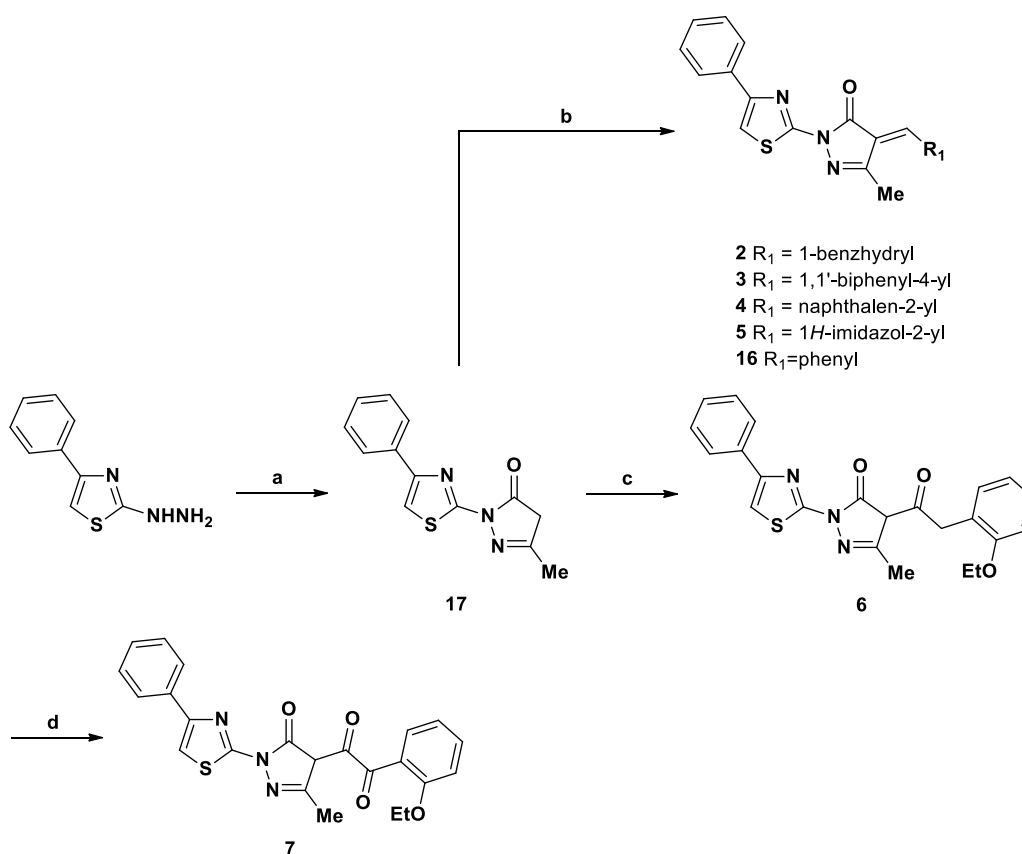


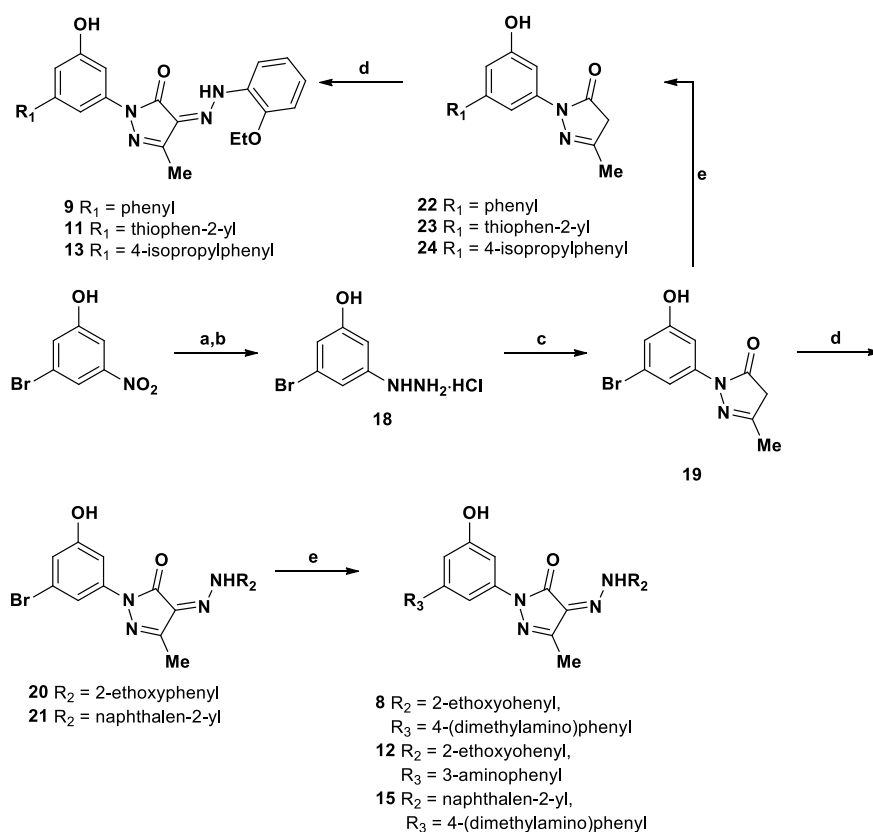
**Figure 11** Design strategy. a) Docked structure of BAM-7 (pink) at the BAX rear site (green surface). BIM BH3 helix is colored in transparent blue) Representation of the re-branching approach. c) Binding mode of 8 (BTC-8) within BAX rear site.

## 2.4 Chemistry

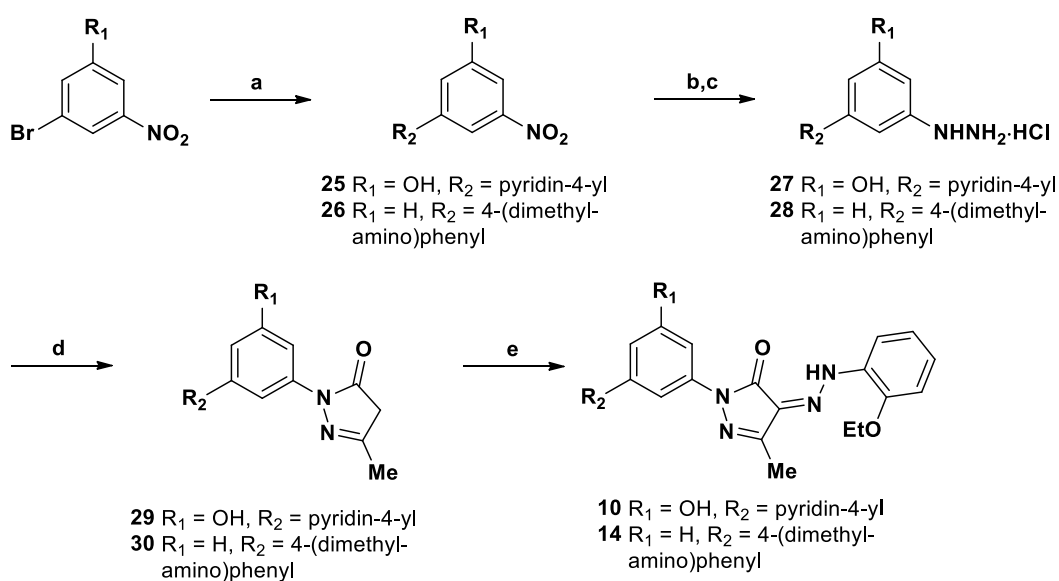
Synthesis of compounds **2–16** are depicted in **Scheme 17–Scheme 19**. Compounds **2–5** and **16** were prepared by reacting the 5- methyl-2-(4-phenylthiazol-2-yl)-2,4-dihydro-3H-pyrazol-3-one (**17**), obtained by treatment of 2-hydrazinyl-4-phenylthiazole with ethyl acetoacetate in acetic acid at reflux temperature for 3 h, with the appropriate benzaldehyde in the presence of piperidine in boiling ethanol for 4 h (**Scheme 17**). Reaction of compound **17** with 2-(2-ethoxyphenyl)acetyl chloride in the presence of potassium *tert*-butoxide in anhydrous tetrahydrofuran at 0 °C for 1 h furnished the derivative **6**, which was converted into the corresponding dione **7** by oxidation with potassium permanganate in the presence of a catalytic amount of sulfuric acid in acetone at reflux temperature for 12 h. Compounds **8**, **12**, and **15** were synthesized starting from the 2- (3-bromo-5-hydroxyphenyl)-5-methyl-2,4-dihydro-3H-pyrazol- 3-one (**19**), which was treated with 2-ethoxybenzenediazonium chloride or naphthalene-2-diazonium chloride in the presence of sodium acetate in ethanol at 0 °C for 2 h and then coupled with the appropriate boronic acid in the presence of sodium carbonate and Pd catalyst in tetrahydrofuran at reflux temperature for 90 min under Ar stream (**Scheme 18**). Analogously, treatment of compound **19** with the appropriate boronic acid and subsequent reaction with 2-ethoxybenzenediazonium chloride gave derivatives **9**, **11**, and **13**. Compounds **22–24** were prepared as above-reported, starting from the 3- bromo-5-hydrazinylphenol hydrochloride (**18**), obtained by reaction of 3-bromo-5-nitrophenol with tin(II) chloride dihydrate in boiling ethyl acetate for 3 h, treatment with sodium nitrite and 37% HCl at 0 °C for 20 min, and final reduction with tin(II) chloride dihydrate at 0 °C for 20 min. Derivatives **10** and **14** were obtained similarly to **8**, starting from pyrazolones **29** and **30**, respectively (**Scheme 19**). Derivatives **29** and **30** were prepared as above-reported, by treatment of 3-bromo-5-nitrophenol with the appropriate boronic acid, conversion into the corresponding phenylhydrazine derivative, and final cyclization with ethyl acetoacetate.



**Scheme 17** Synthesis of Compounds 1-7. a) Reagents and reaction conditions: (a) ethyl acetoacetate, acetic acid, reflux temperature, 3 h, 62%; (b) appropriate benzaldehyde, piperidine, anhydrous ethanol, reflux temperature, 3 h, 28–61%; (c) (i) potassium tert-butoxide, anhydrous tetrahydrofuran,  $-40\text{ }^{\circ}\text{C}$ , 1 h, (ii) 2-(2-ethoxyphenyl)acetyl chloride,  $25\text{ }^{\circ}\text{C}$ , 1 h, 74%; (d) potassium permanganate, catalytic sulfuric acid, acetone, reflux temperature, 5%.



**Scheme 18** Synthesis of Compounds 8, 9, 11-13 and 15a<sup>a</sup>. Reagents and reaction conditions: (a) tin(II) chloride dihydrate, ethyl acetate, reflux, 3 h; (b) (i) sodium nitrite, 37% hydrogen chloride,  $0\text{ }^{\circ}\text{C}$ , 20 min, (ii) tin(II) chloride dihydrate,  $0\text{ }^{\circ}\text{C}$ , 20 min, crude product; (c) ethyl acetoacetate, acetic acid,  $80\text{ }^{\circ}\text{C}$ , 3 h, 13%; (d) 2-ethoxybenzenediazonium chloride or naphthalene-2-diazonium chloride, sodium acetate, 96% ethanol,  $0\text{ }^{\circ}\text{C}$ , 2 h, 3–48%; (e) appropriate boronic acid, 2 M sodium carbonate, dichloro[1,1'-bis(diphenylphosphino)ferrocene]-palladium(II) dichloromethane complex (1:1), tetrahydrofuran, reflux temperature, 90 min, Ar stream, 13–66%.



**Schema 19** Synthesis of Compounds 10 and 14. Reagents and reaction conditions: (a) appropriate boronic acid, 2 M sodium carbonate, dichloro[1,1 bis(diphenylphosphino)ferrocene]-palladium(II) dichloromethane complex (1:1), reflux temperature, 90 min, Ar stream, 14–25%; (b) tin(II) chloride dihydrate, ethyl acetate, reflux, 3 h; (c) (i) sodium nitrite, 37% hydrogen chloride, 0 °C, 20 min, (ii) tin(II) chloride dihydrate, 0 °C, 20 min, crude product; (d) ethyl acetoacetate, acetic acid, 80 °C, 3 h, 12–13%; (e) 2-ethoxybenzenediazonium chloride, sodium acetate, 96° ethanol, 0 °C, 2 h, 36–47%.

## 2.5 Biological Results

*In Vitro BAX Affinity, Selectivity Profile, and SAR Rationalization.* Affinities of candidate compounds for recombinant BCL-2 family members were measured in vitro by fluorescence polarization assay (FPA). GST tagged full length BAX, untagged BCL-2, and BCL-XL show nanomolar affinity for FITC-BIM ( $K_i$  values of 200, 132, and 794 nM, respectively) ( **Figure 12**) in line with data previously reported. [63] [64].

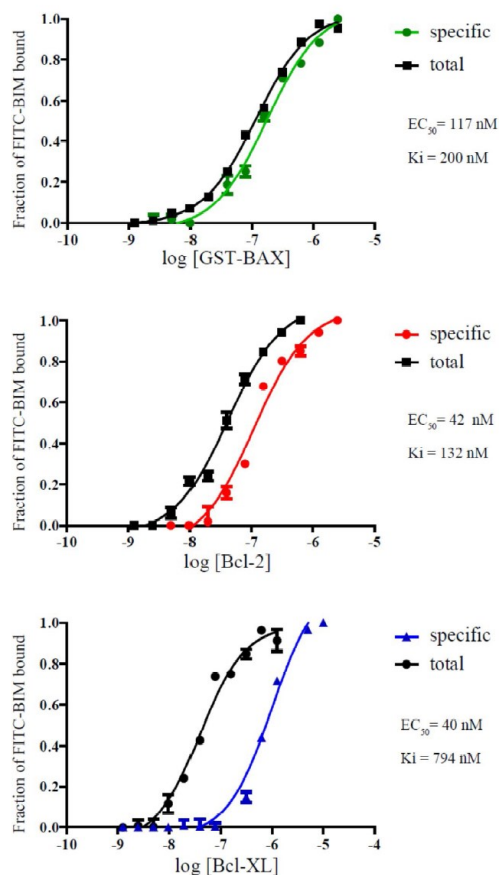


**Figure 12** Affinity of FITC-BIM for recombinant BCL-2 family targets. FITC-BIM Direct specific binding isotherms are shown for engagement of FITC-BIM by GST-BAX (green curve), BCL-2 (red curve) and BCL-XL (blue curve). Total binding (black lines) are shown for comparison. Fraction of FITC-BIM bound was measured before and after the addition of Acetylated-BIM (50 $\mu$ M). FITC-BIM specific binding was calculated subtracting non specific binding (measured in the presence of Acetylated-BIM) from total binding (measured in the absence of Acetylated-BIM). Mean of three experiments and S.D. are indicated.

The ability of **1–15** to displace bound FITC-BIM was used to calculate their  $K_i$  for each of the three proteins (**Figure 13** and **Table 1**).

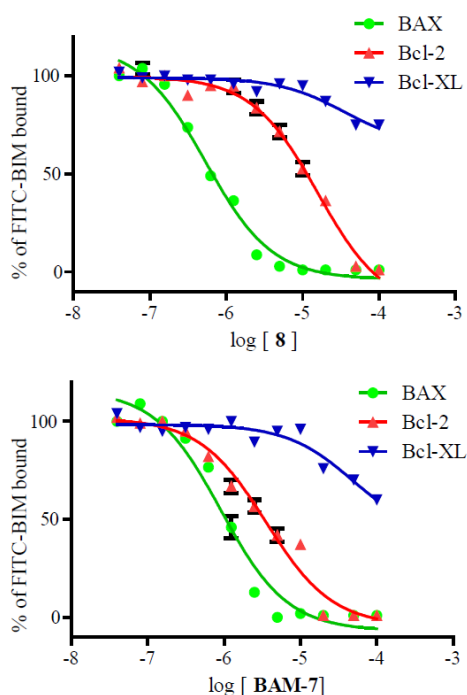


**Figure 13** **8** binds BAX at BIM binding site. Competition between **8** (upper panel) or BAM-7 (lower panel) and FITC-BIM for binding to BAX (green curve), BCL-2 (red curve) and BCL-XL (blue curve). Mean of three experiments (SD. are indicated).

As previously reported, **1** is selective on BAX over BCL-X<sub>L</sub> (**Figure 13** and **Table 1**). It displays, however, affinity for BCL-2 despite this being somehow slightly lower than the one for BAX ( $K_i$  values of 3.0 and 1.1  $\mu$ M, respectively). In the range of concentration tested, the new compounds show either higher affinity for BCL-2 over BAX and BCL-X<sub>L</sub> (compounds **2** and **5**), higher affinity for both BCL-2 and BCLX<sub>L</sub> over BAX (compounds **3–5**), and similar affinities for the three proteins (compounds **16**) or for none of them (compounds **6–7**) (**Table 1**).

compd	BAX	BCL-2	BCL-X <sub>L</sub>
1	1.1	3.0	>100
2	13.5	1.6	>100
3	12.9	1.6	3.1
4	12.6	2.0	3.4
5	15.8	2.0	6.8
6	63.1	>100	>100
7	85.1	>100	>100
8	0.8	12.0	>100
9	9.1	>100	>100
10	1.7	>100	30.9
11	30.9	>100	>100
12	1.3	>100	>100
13	1.2	1.9	15.5
14	1.3	4.2	>100
15	1	33.9	3.4
16	2.5	1.9	2.4

**Table 1.**  $K_i$  ( $\mu\text{M}$ ) of Compounds 1-15 for BAX, BCL-2, and BCL-XL (FPA, FITC-BIM Displacement).

Compounds **8–10** show higher affinity for BAX over BCL-2 and BCL-X<sub>L</sub>. Among them, **8** displays higher affinity for BAX ( $K_i = 0.8 \mu\text{M}$ ) than **1** ( $K_i = 1.1 \mu\text{M}$ , **Figure 13**). **9** and **11** are selective for BAX, but they are somehow weaker binders than **8**. **12** is specific for BAX, but its BAX affinity is lower than **8** and comparable to that of **1**. **13–15** display high affinity for BAX but less specificity (**Table 1**) over the other two proteins. SAR toward BAX were rationalized on the basis of the complex between **1** and BAX, which was previously obtained by a combined approach of docking and NMR experiments [64] and on the basis of docking of its analogue **8**. Molecular docking of **8** within the BAX rear site resulted in a binding mode highly superimposable to that of **1** (**Figure 11a,c**). However, in line with the lower  $K_i$  of **8**, compared to that of **1**, **8** reinforces its binding to BAX surface through an H-bond with E17 by the ligand hydroxyl group and through a charge reinforced hydrogen bond with D142 coupled with hydrophobic interactions between the methyl groups and D142 carbon chain. According to then observed interactions, **9** (unsubstituted on the terminal phenyl ring) is less active than **8**, **13**, and **14**. The importance of an amino group on the terminal phenyl ring is also proved by the affinity of **12** compared to that of **9** and by the reduced specificity of **13** compared to **8** and **12**. All in all, SAR where the phenylthiazole group is replaced by other moieties clearly demonstrate that such a branch is replaceable by other aromatic systems, that if adequately decorated bring an improvement of BAX affinity. Regarding the 2-ethoxyphenylhydrazono group of **1**, SAR were designed to explore: (i) bridges different from the hydrazono one and (ii) possible, fruitful hydrophobic interactions established by different aromatic moieties. Among the different bridges synthesized, just the ene one (**16**) seems to be well tolerated. The higher  $K_i$  of **6** and **7** seemed to be ascribable to the different geometries of ketomethylen- and diketo bridges with respect to hydrazono group, which would bring the 2-ethoxyphenyl farther from L25, with which an hydrophobic interaction was observed (**Figure 11a**). Although no H-bond between the ethoxy group of **1** and K21 was observed with a semiflexible docking approach, their proximity would suggest a possible interaction, which can be also the reason for the slightly lower  $K_i$  of **16** with respect to that of **1**. Analogues of **1**, where the phenyl moiety were replaced by a benzhydryl (**2**), biphenyl

(3), and naphthalene (4) group, were all less active than the lead. Rationalization of the lower  $K_i$  of 2–4 is somehow difficult, as the benzhydryl, biphenyl, and naphthalene group would occupy the hinge site for loop opening, a region that undergoes to profound change upon ligand binding and activation.

*Cell Viability and Apoptosis Assays.* Affinities and selectivity of 1–15 measured by FPA well correlate with their potency on inducing apoptosis in MEF knock out cells. At the  $EC_{50}$  of 1, all the compounds but 6, 7, and 1 induced apoptosis in MEF wt cells (Table 2 and Table 3), while they were ineffective on MEF BAK<sup>-/-</sup> BAK<sup>-/-</sup> double knockout cells, indicating that they ultimately lead to pro-apoptotic protein activation.

compd	wt	Bcl2 <sup>-/-</sup>	Bad <sup>-/-</sup>	Bid <sup>-/-</sup>	Bak <sup>-/-</sup>	Bax <sup>-/-</sup>	Bax <sup>-/-</sup> Bak <sup>-/-</sup>
1	7.7	3.2	3.5	4.0	6.0	>50	>50
8	1.1	0.6	0.8	0.7	1.3	>50	>50

**Table 2**  $EC_{50}$  ( $\mu$ M) Values of Apoptosis Induction of Compound 8 or 1 Treatment on the Indicated MEF Knockout Clones

1, 8–10, and 12–15 are the most effective at the concentration of 10  $\mu$ M. 2–5 potencies are overall lower and partially affected by the absence of BCL-2 as well as of BID, BAD, BAK, or BAX, suggesting that, at least in MEF cells, BAX direct activation is not their main mechanism of action (Table 3).

Compound	MEF wt	MEF Bak <sup>-/-</sup> Bak <sup>-/-</sup>	MEF Bcl2 <sup>-/-</sup>	MEF Bid <sup>-/-</sup>	MEF Bad <sup>-/-</sup>	MEF Bax <sup>-/-</sup>	MEF Bak <sup>-/-</sup>
1	+++	-	++	++	++	-	++
2	++	-	+	+	+	+	+
3	++	-	+	+	+	+	+
4	++	-	+	+	+	+	+
5	++	-	+	+	+	+	+
6	-	-	-	-	-	-	-
7	-	-	-	-	-	-	-
8	+++	-	++	++	++	-	++
9	+++	-	++	++	++	-	++
10	+++	-	++	++	++	-	++
11	-	-	-	-	-	-	-
12	+++	-	++	++	++	-	++
13	+++	-	++	++	++	++	++
14	+++	-	++	++	++	++	++
15	+++	-	++	++	++	-	++
16	++	-	++	++	++	-	-

**Table 3** Sensitivity of the indicated MEF clones to 24 hours of treatment with the candidate compounds (15  $\mu$ M). – (less than 5% of apoptotic cells); + (5-30% of apoptotic cells); ++ (30-60% of apoptotic cells); +++ (more than 60% of apoptotic cells).



On the contrary, **1**, **8–10**, and **12–16** induce apoptosis independently by the absence of BCL-2, BID, and BAD, pointing to their target being located downstream in the apoptotic pathway (**Figure 14**, and **Table 3**).

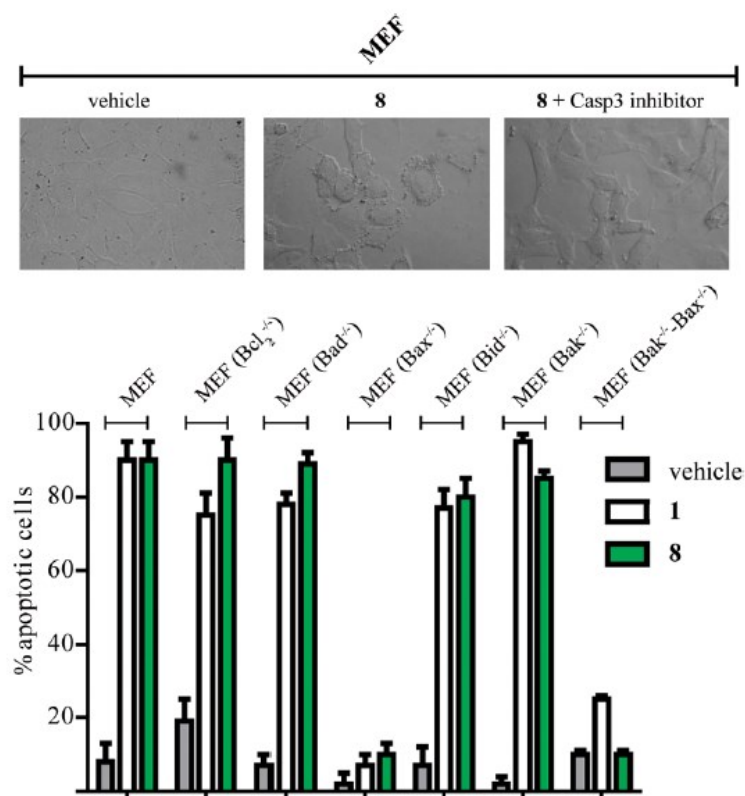


**Figure 14** 8 induces apoptosis in a BAX dependent way. Effect of 8 treatment on MEF cells. Apoptotic rate of the indicated MEF clones upon 24 h of treatment with vehicle (0.1% DMSO, gray bars), 1 (15  $\mu$ M, white bars), or 8 (15  $\mu$ M, green bars). The photographs represent appearance of apoptotic cell membrane blebbing upon MEF treatment with 8 and its absence when 8 treatment was done in the presence of the caspase inhibitor Ac-DEVD-CHO (10  $\mu$ M).

**12**, **13**, **14**, and **16** affected MEF BAX<sup>-/-</sup> as well as MEF BAK<sup>-/-</sup>, indicating that they can trigger apoptosis either by BAK or by BAX. **8–10** and **15** similarly to **1** induced apoptosis in BAK<sup>-/-</sup> but not in BAX<sup>-/-</sup> knockout cells and represent, among the tested ones, the candidate compounds with the best features of selective BAX activators (**Figure 14**, **Table 3**). MEF cells treated with **8**, the most potent compound of our series (EC<sub>50</sub> of **8** on MEF-wt of 1.1  $\mu$ M, EC<sub>50</sub> of **1** on MEF-wt of 7.7  $\mu$ M) undergo apoptotic processes, as shown by the appearance of fragmented nuclei and cell membrane blebbing. Moreover, its potency is reduced by the presence of the caspase inhibitor Ac-DEVD-CHO [67] (**Figure 14**), indicating that its mechanism of action involve apoptotic effectors. Differently from MEF cells, tumor cells overcome pro-apoptotic stimuli by overexpressing anti-apoptotic proteins or by downregulating pro-apoptotic ones. It was thus decided to challenge these compounds in inducing apoptosis in in vitro cultured tumor cells. Apoptosis was followed in human hepatoma HuH7 cells, which express wt BAX, a high level of BCL-2 but a low level of caspase 3, [68] the final effector of the apoptotic cascade. Under apoptotic stimuli, they survive for longer time than other tumor cells and, thus, they represent an ideal platform to look exclusively at the early events of the apoptotic process. Apoptosis was followed in HuH7 by measuring MOMP, which inhibits

mitochondrial accumulation of the fluorescent probe Mitotracker Red. Among the tested compounds, **8** was the most potent in affecting probe accumulation (**Figure 15** and **Figure 16**).

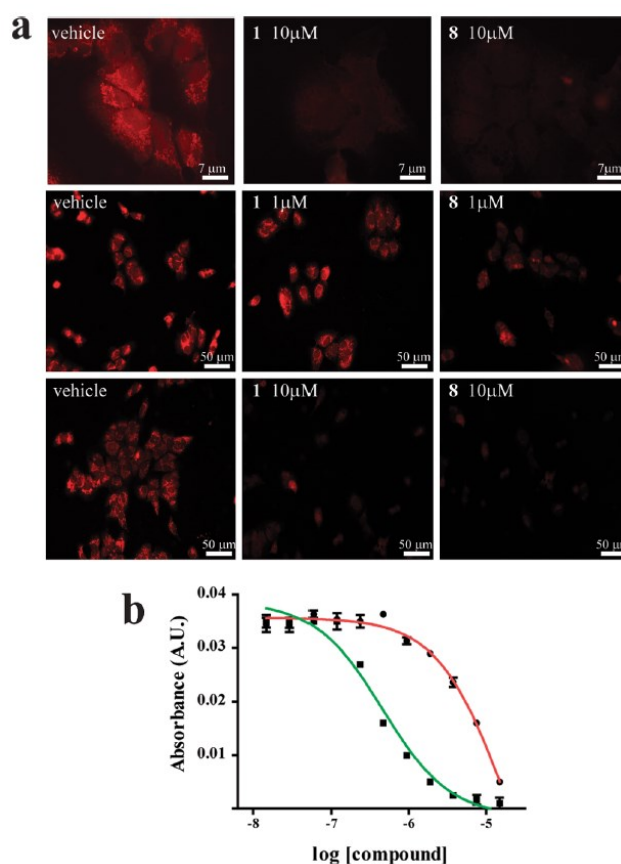


**Figure 15.** **8** affects mitochondria in HuH7 cells. (a) Mitochondrial activity of **8** and **1** treated cells visualized by Mitotracker Red fluorescence uptake. Magnification bars are indicated. (b) After lysis of the cells absorbance of the dye was measured at 570 nm and plotted versus **8** or **1** concentration. EC50 were calculated by fitting values by non linear regression analysis of dose response analysis and reported together with their 95% CI (error bars are indicated, n = 3).

Other compounds of the series (e.g., **2** and **3**) affected mitochondrial potential only after 72 h of treatment, in line with a reduced affinity for BAX but an increased affinity for BCL-2 or BCL-X<sub>L</sub> or both (**Table 1** and **Figure 16**).

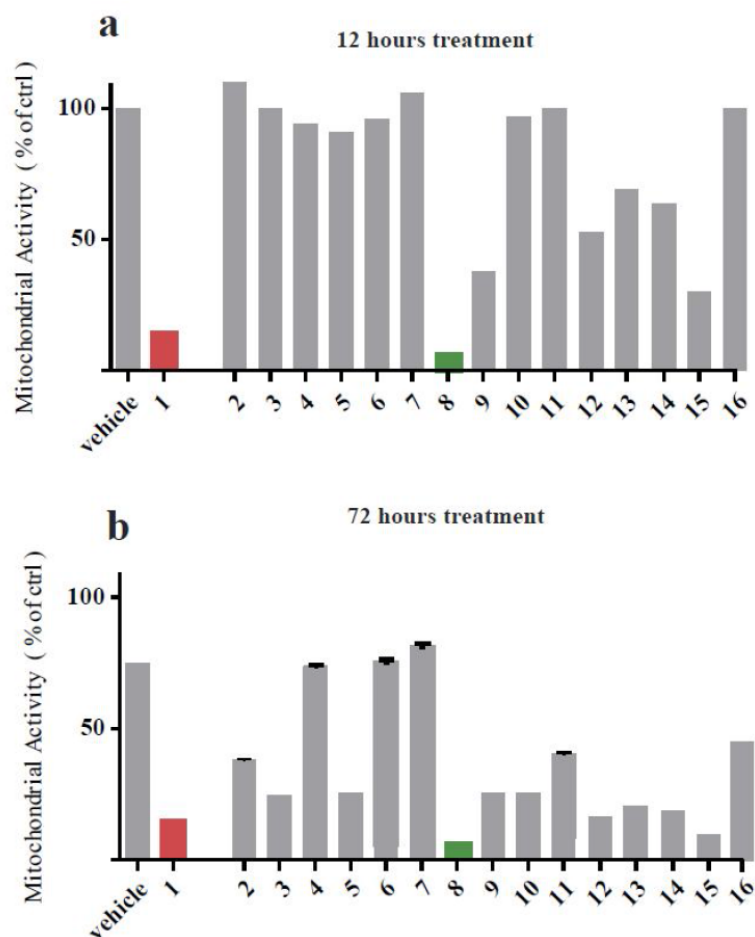


**Figure 16** mitochondrial Effect of 12 (a) and 72 hours (b) of compounds **1-16** treatment on mitochondrial activity of HuH7 cells measured by Mitotracker Red accumulation. After lysis of the cells absorbance of the dye was measured at 570 nm and reported as percentage of that measured in untreated cells (mean of at least 3 experiments, error bars are indicated (S.D.)).

While **1** and **8** affected the cultures similarly at 10  $\mu\text{M}$ , **8** induced a stronger reduction in probe accumulation at 1  $\mu\text{M}$  (**Figure 15a**). The higher potency of **8** over **1** was quantified by a dose response curve revealing the  $\text{EC}_{50}$  of **1** and **8** in cultured HuH7 cells to be 8.2  $\mu\text{M}$  and 700 nM, respectively (**Figure 15b** and **Table 3**). Similarly to **1**, **8** induces a conformational change in BAX that exposes an epitope recognized by the anti-BAX 6A7 antibody [64], specific for the activated form of the protein (**Figure 17**).

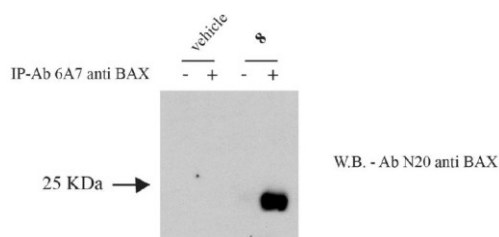


**Figure 17** **8** activates BAX. Lysates of HuH7 cells treated with **8** or with vehicle alone were immunoprecipitated or not with the 6A7 monoclonal anti-BAX antibody. All samples were equally boiled, run on a SDS-PAGE and decorated with a polyclonal antibody anti-BAX.

As expected from a BAX direct activator, **8** was able to induce the translocation of BAX to mitochondria, the cyt-C release from these organelles (**Figure 18** and **Figure 19**), the activation of caspase 3, and the formation of apoptotic nuclei (**Figure 18** and **Figure 20**).

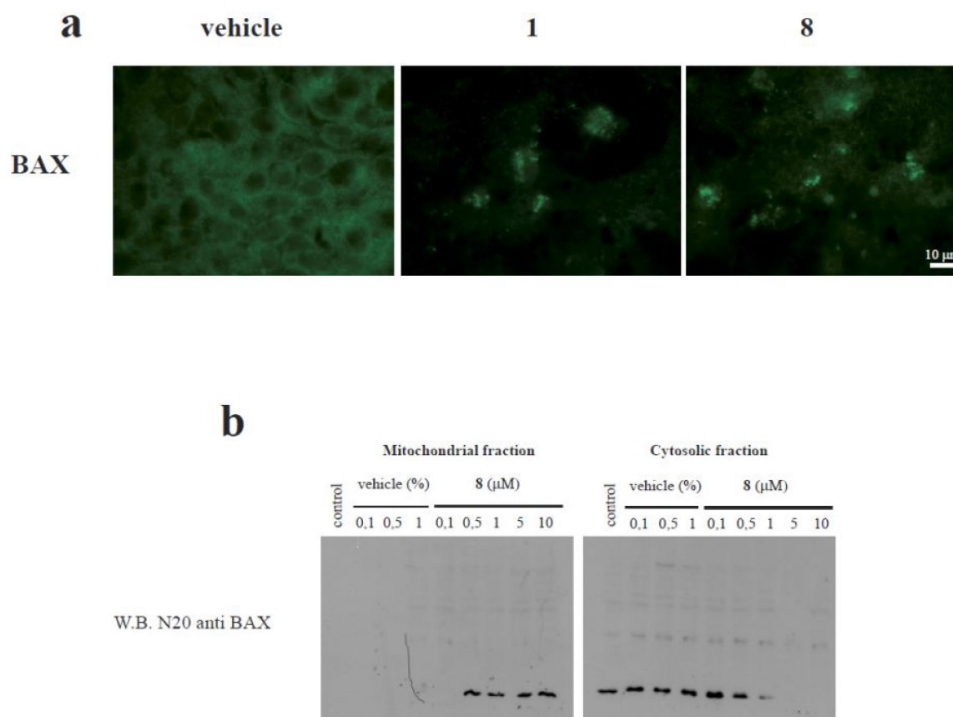


**Figure 18** **8** induces translocation of BAX to mitochondria. **a)** HuH7 cells were treated with **1** and **8** to be then fixed and processed for immunofluorescence to localize BAX intracellularly. In untreated cells, BAX localizes in the cell cytoplasm with no clear indication of association to any intracellular organelle, while after treatment of the cell with 10 μM **1** or **8**, BAX localization drastically changes moving to punctuate structures. **b)** As further proof HuH7 cells were cultured with the indicated amount of **8**, or with vehicle alone for 12 hours. After treatment cell were permeabilized and the mitochondrial and cytosolic fractions were isolated as described in the manuscript. Equal amount of proteins were separated by SDS PAGE and processed for Western Blotting. BAX was revealed by decorating the filters with the indicated anti-BAX antibody (fullblots are shown).

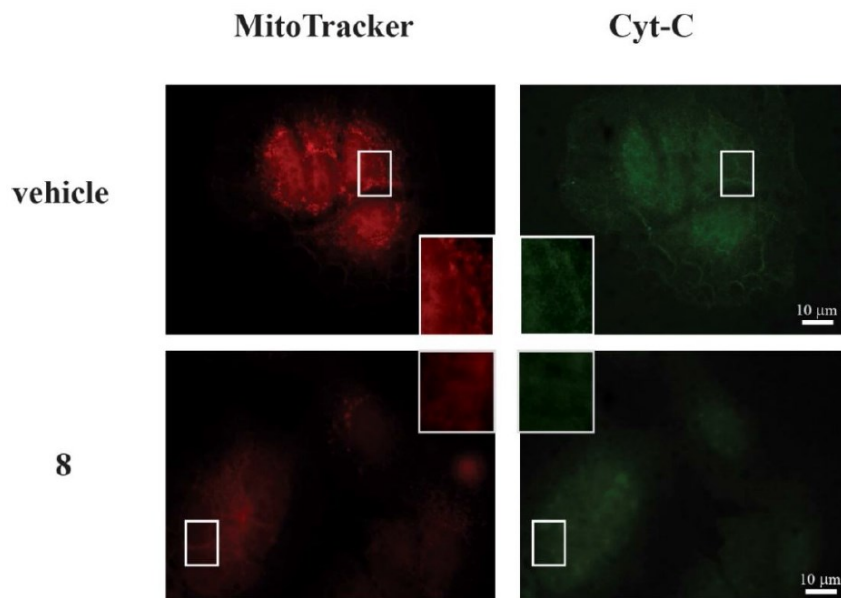


**Figure 19** 8 induces cyt-C release from mitochondria. Hu7 cells were treated with BAM-7 (1) and 8, then were fixed and processed for immunofluorescence to localize cyt-C intracellularly. Before the treatment with 8, the cyt-C is localized in mitochondria, as shown by its colocalization with the structures labeled by the Mitotracker Red. After the treatment with 8, its localization changed becoming diffuse thus indicating its exit from the organelle. Boxed area are shown at higher magnification at the corner of each panel.

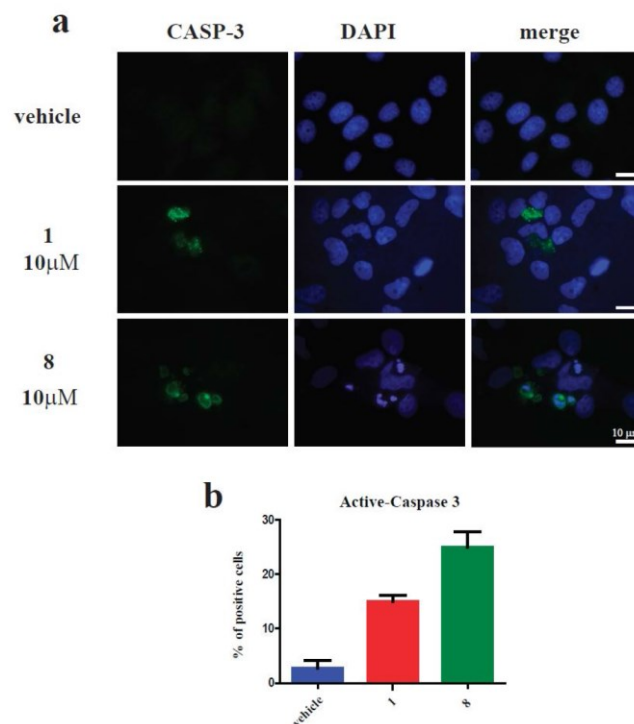


**Figure 20a)** 8 induces caspase-3 activation and formation of apoptotic nuclei. **b)** Quantification of caspase-3 positive cells after treatment with 8 and 1 as described in the manuscript. Mean of 10 random fields (error bars are indicated S.D.)

Similarly to what we have already shown in MEF BAX<sup>-/-</sup> cells, **8** treatment had no effects on the leukemic Jurkat (T-cell lymphoma) cell line. Jurkat cells express a mutated form of BAX and rely only on BAK to induce MOMP [69]. Jurkat cells resulted insensitive to **8** treatment, confirming that our compound activates selectively BAX (**Figure 20**). Differently leukemic NB4 cells (promyelocytic), which express wt BAX [70], showed hallmarks of apoptosis already after 12 h of treatment with **8**. Then, to have indication about the toxicity of **8** on healthy cells, we tested the effect of the compound on primary healthy splenocytes. At concentration of 10  $\mu$ M, **8** did not alter the apoptosis rate in primary cells, indicating that could selectively affect tumoral cells (**Figure 20**). This observation could be explained by the fact that, as seen for many other cancer drugs, **8** could affect predominantly highly proliferating cells rather than resting ones.

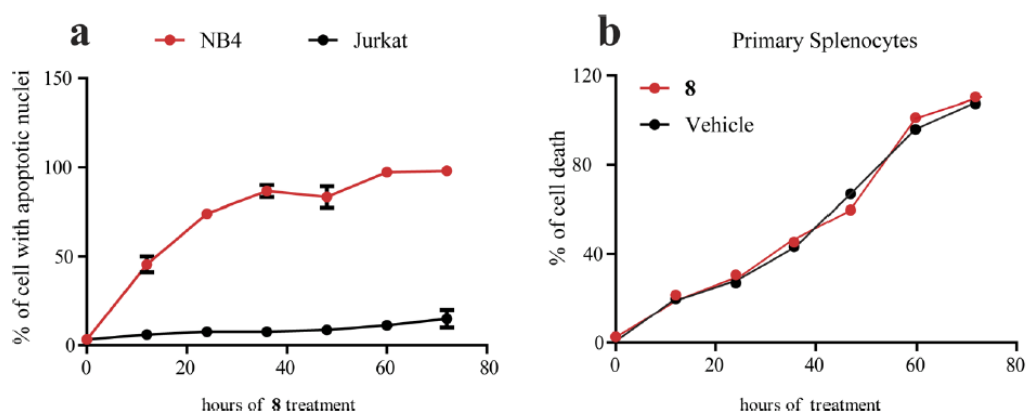


**Figure 21** **8** induces apoptosis in tumor cells but it does not alter apoptotic rate in healthy splenocytes. The indicated tumor cell lines (a) or primary splenocytes (b) were incubated for 72 h with **8** (10  $\mu$ M). Apoptosis rates were detected by counting apoptotic nuclei. Mean values are reported together with their SD (n = 3 in a; n = 4 in b).

Compound **8** is able to affect mitochondrial membrane potential in all the tumor cell lines tested (**Figure 22**). Like HuH7, Lewis lung carcinoma (LLC1) and human neuroblastoma (SHSY-5Y) cells were reported to be highly resistant to conventional pro-apoptotic drugs. Like for HuH7, after treatment with **8**, these cells did not show sign of death (visible in only the 20% of cell (data not shown)), but they stop duplicating to undergo in a process of growth arrest. This effect likely suggests that even in those tumor cell lines that have developed strategies to block the initiation of the apoptotic process or its completion, BAX direct activation can hamper mitochondrial activity, reduce intracellular energy content, and ultimately affects cell growth.

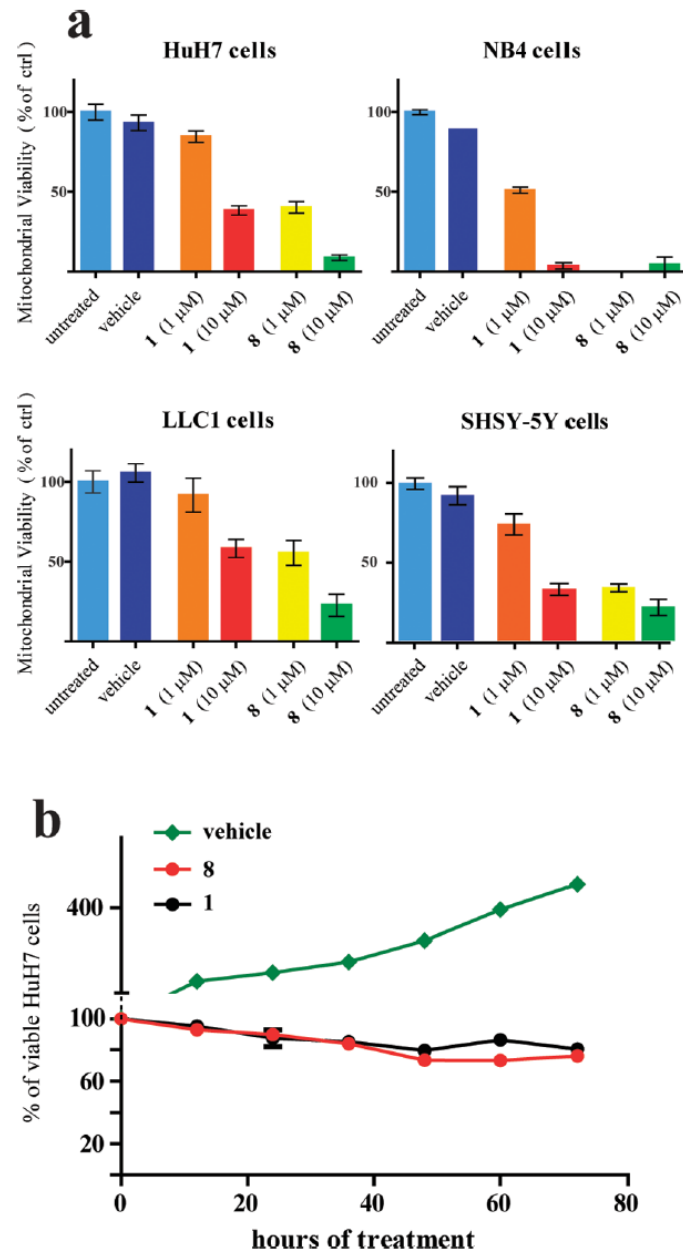


**Figure 22** **8** induces growth arrest and cell death. (a) Cells were incubated for 72 h with the indicated concentration of **1** and **8** and then with Mitotracker. Absorbance was measured after lysis of the cell. Values are the mean of at least three experiment. Error bars (SD) are indicated. (b) HuH7 cells were incubated for the indicated time with 10  $\mu$  **1** or **8** or vehicle alone. After the treatment cells were counted. Values are expressed as percentage of control (cells at 0 min of treatment) and are representative of at least three experiments.

*In Situ BAX Activation and in Vivo Tests.* LLC1 cells resulted sensitive to **8** (Figure 22). These cells well represent lung carcinoma, the primary cause of adult mortality. To establish whether **8** would be efficacious in vivo, it was used them in a murine Lewis lung carcinoma model that reliably recapitulates human lung cancer in pathology, disease progression, clinical outcome, and response to therapies [71]. LLC1 cells have a high tropism for the lung and are able to form tumor lesions [72] that after 14 days are in exponential growth, making the drug treatment clinically relevant. On day 0, tumor cells were injected into

mice via the tail vein. From day 14 to day 17, one group of mice were treated once a day with an intraperitoneal injection of **8** (1 mg/kg) or of vehicle (1% DMSO). On day 17, animals were euthanized. The compound ability to induce an in vivo activation of BAX was confirmed through immunoprecipitation of lung lysates with 6A7 antibody (**Figure 23**).

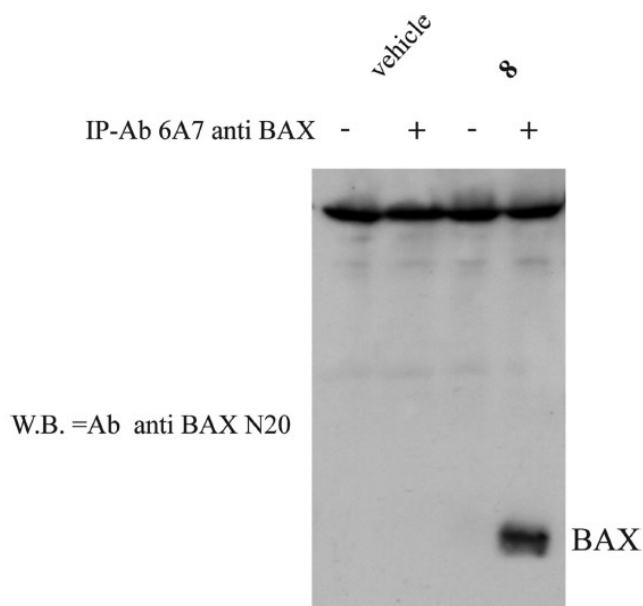


**Figure 23** In vivo treatment with **8** induces in situ BAX activation. Homogenates of mouse lungs treated or not with **8** were lysed and immunoprecipitated with the 6A7 monoclonal antibody. Samples were boiled, run on a SDS-PAGE, and decorated with a polyclonal antibody anti-BAX (only relevant part of the gel is shown).

A visual inspection of the exposed lung of control mice showed very large tumor lesions covering the lung surface, whereas the lungs of mice treated with **8** showed highly size-reduced tumor lesions. Histological analysis using hematoxylin and eosin (H&E) staining of lung sections demonstrated that after only 4 days of treatment the ratio between tumor burden and lung area in mice treated with **8** compared with control was significantly ( $P < 0.01$ ) decreased by 50% (**Figure 24**).



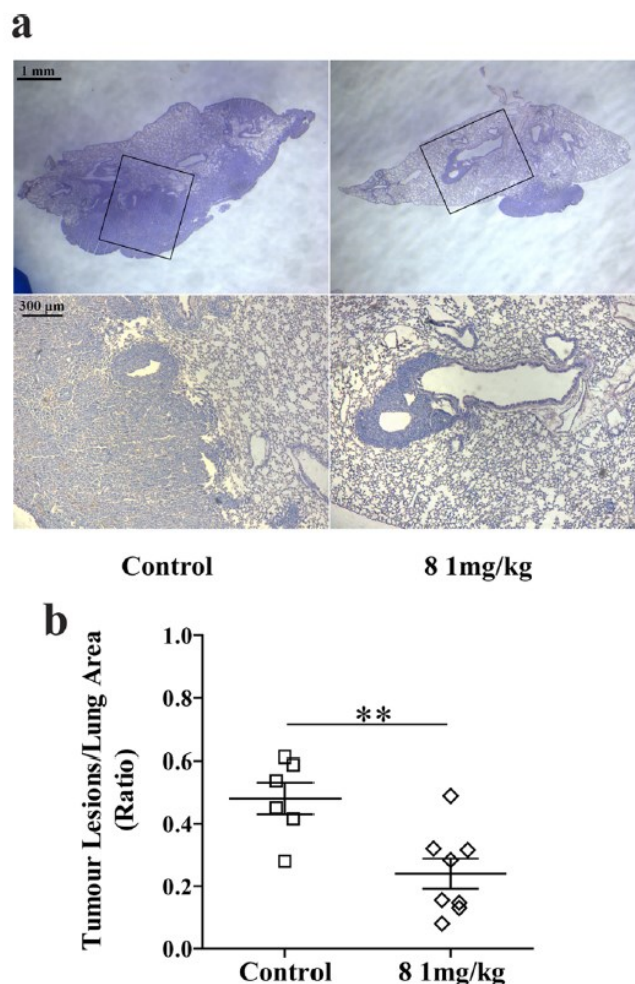


**Figure 24.** In vivo activity of **8**. (a) Effect of the daily administration of **8** 1 mg/kg from day 14 to day 17 on tumor growth (dark violet staining). Microphotographs showing the entire lung sections; the boxed areas in the upper-magnification H&E panels are shown at a higher magnification in the lower panels. (b) Graph showing the effect of **8** on tumor growth. The results are expressed as tumor lesions/lung area ratio. Individual data points represent average value per mouse; horizontal bars denote mean.  $P < 0.01$  vs control group.

It is noteworthy that **8** seemed to be well tolerated because no mortalities, evidence of gross toxicity, behavioral side effects, or body weight changes were observed in the four days of treatments. A microscopic examination of heart, femoral muscle, and healthy lung did not reveal any pathologic change (data not shown). The in vivo efficiency of **8** in tumor mass reduction was of relevance especially if a rough comparison with marketed anticancer drugs on similar tumor models is done. In fact, cyclophosphamide (60 mg/kg) or adriamycin (1.25 mg/kg) gave a reduction of 40% even in the case of prolonged treatments. [73] [74].

## 2.6 Pharmacological folding chaperones act as allosteric ligand of Frizzled4

Upon binding, ligands can chaperone their protein targets by preventing them from misfolding and aggregating. Thus, an organic molecule that works as folding chaperone for a protein might be its specific ligand, and, similarly, the chaperone potential could represent an alternative readout in a molecular screening campaign toward the identification of new hits. The aim of this work is to demonstrate that small molecules selected for acting as pharmacological chaperones on a misfolded mutant of the Frizzled4 (Fz4) receptor bind and modulate wild-type Fz4, representing what are to our knowledge the first organic ligands of this until-now-undruggable GPCR. The novelty and the advantages of the screening platform, the allosteric binding site addressed by these new ligands and the mechanism they use to modulate Fz4 suggest new avenues for development of inhibitors of the Wnt–b-catenin pathway and for drug discovery. The compounds **2,3,4,5,16** (**Figure 11b**), which were synthesized as BAX direct activators, were included in this library of small molecules selected for acting as pharmacological chaperones on a misfolded mutant of the Frizzled4 (Fz4) receptor [3]. Fz4 is a member of the Frizzled cell surface receptors, which belong to the GPCR class F family [75]. Seven-transmembrane (TM) segments arrange in the canonical GPCR TM bundle (TMD) and interconnect via three intracellular loops (ICL) and extracellular loops [75] (**Figure 25**). A large extracellular domain (ECD) binds the receptor's ligands, the lipoproteins WNTs [75] and Norrin [76]. Finally, a short cytosolic C-terminal tail helps the ICLs orchestrate the downstream intracellular signal [77]. Several mutations in the coding region of the Fz4 gene have been described in different organisms. In humans, despite being rare, they lead to the development of familial exudative vitreoretinopathy (FEVR), a pathology resulting in aberrant vascularization of the retina during embryo development [78]. Among the mutations, the frameshift L501fsX533 of Fz4 shows autosomal dominant inheritance and causes a conformational defect by generating a different and shorter C-terminal cytosolic tail that hampers signaling of the mutant receptor (henceforth referred as Fz4-FEVR) and its correct folding and transport to the cell plasma membrane (PM) [78] (**Figure 25**).

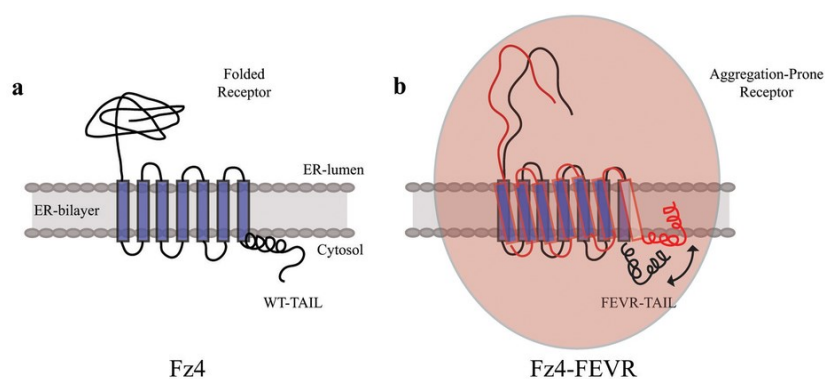


**Figure 25** Schematic cartoon of Fz4-WT (a) and Fz4-FEVR (b) receptors. Through improper interactions with the ER membranes, the Fz4-FEVR tail causes receptor aggregation.

The search for organic modulators of Fz4 was recently intensified owing to evidence of its involvement in malignancy. Fz4 is indeed a key component of Wnt- $\beta$ -catenin signaling that regulates stemness during cellular development and in adult life [79]. Misregulation of Fz4 activity is involved in tumor proliferation and cancer stem cell genesis in many types of malignancies, such as glioblastoma, colorectal and breast cancer [80]. In this work it was attempted a molecular screening campaign toward pharmacological chaperones rescuing Fz4-FEVR folding with the ultimate goal to identify small organic wild-type (WT) Fz4 (Fz4-WT) modulators. It was selected molecules able to work as folding chaperones by measuring their potency in restoring Fz4-FEVR folding and localization at the PM. It was identified three pharmacological chaperones of Fz4-FEVR that are indeed Fz4-WT ligands and act as Wnt- $\beta$ -catenin inhibitors, proving the validity of the new screening strategy. One of our hits, namely FzM1, exerts its modulatory activity by inducing conformational changes in Fz4-WT that ultimately allow it to inhibit  $\beta$ -catenin nuclear transport and antagonize the Wnt pathway. The Fz4 modulators here described represent what are to our knowledge the first organic molecules addressing this still-undruggable receptor. Here, the novelty of the screening approach, the step of the Wnt- $\beta$ -catenin cascade targeted by our new compounds together with their mechanism of action are discussed in terms of future development of Wnt pathway inhibitors.

## 2.6.1 Results

Among the Fz4 mutations described, the one resulting in Fz4-FEVR shows the most clearly identifiable phenotype, trapping the mutant receptor in the endoplasmic reticulum (ER) and hampering its transport to the PM of the cells [78]. The mutated C-terminal tail of Fz4-FEVR improperly interacts with the ER lipid bilayer, disturbing receptor stability and inducing its aggregation and retention in the ER [81] (**Figure 25b**). Notwithstanding, Fz4-FEVR localization at the PM can be rescued by overexpressing the protein chaperone  $\alpha$ -B crystallin [82]. Fz4-FEVR can be thus included among the proteins that are responsible for conformational diseases whose phenotype can be rescued by strategies aiming to improve folding. The marked difference in localization between the WT and mutant receptor makes Fz4-FEVR an ideal platform to screen for folding chaperones by offering an unambiguous readout. Two cell lines stably expressing hemagglutinin (HA)-tagged WT Fz4 (HA-Fz4-WT) or Fz4-FEVR (HA-Fz4-FEVR) were generated. As previously shown [82], HA-Fz4-WT was localized in the Golgi complex and at the PM, whereas HA-Fz4-FEVR appeared to be trapped intracellularly, mainly in the ER [78]. HA-Fz4-FEVR HEK293 cells were treated with a library of small molecules for 48 h. Chaperone activity was then assayed by measuring the recovery of HA-Fz4-FEVR localization at the PM. Among others, the library contained folding chaperones (radicolol, geldanamycin and 17AAG) and correctors (acridine derivatives, DMSO and glycerol) with known rescuing activity on the cystic fibrosis transmembrane conductance regulator (CFTR) mutant CFTR $\Delta$ F508 [83]. Those folding chaperones that were already known failed in rescuing Fz4-FEVR localization, whereas the compound FzM1 rescued Fz4-FEVR localization at the PM in 15% of the cell population. FzM1 pharmacological activity was confirmed after resynthesis. A further pool of molecules that were structurally similar to FzM1 was added to the screen (**Figure 11b** compounds **2-3-4-5-16**). Among the tested candidates, FzM1, **2** and **3** rescued HA-Fz4-FEVR PM localization with an efficiency higher than 10% and with a half-maximum effective concentration ( $EC_{50}$ ) in the micromolar range (**Figure 26**) In untreated cells, Fz4-FEVR forms covalent aggregate [81].

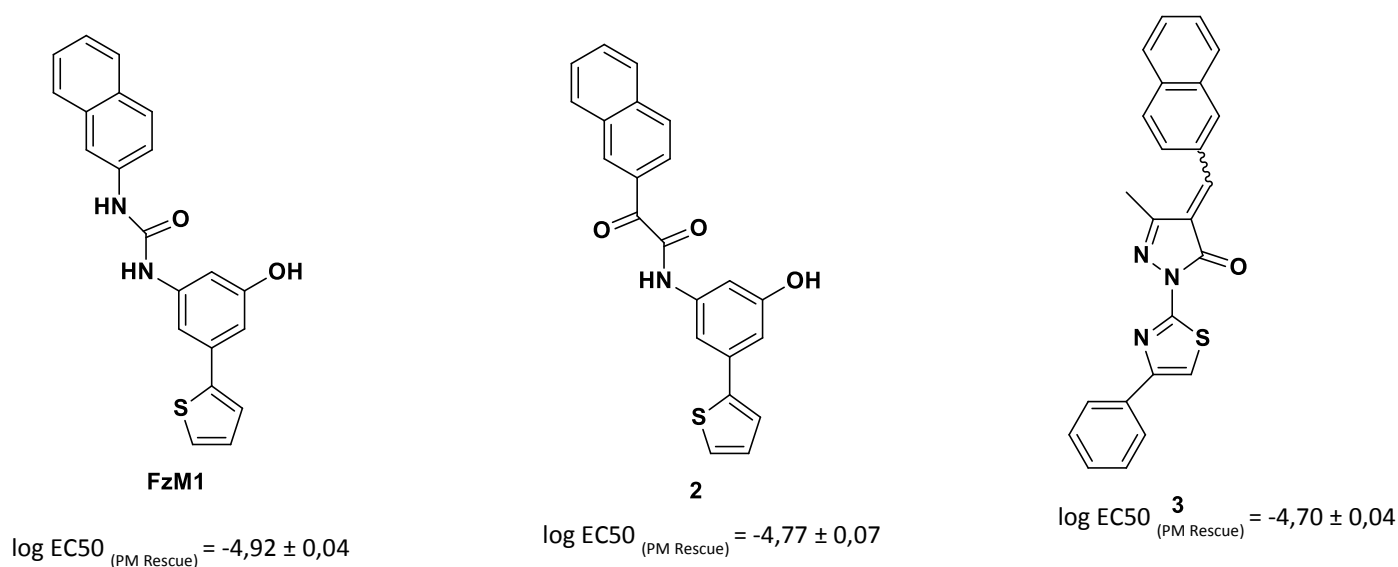


**Figure 26** Chemical structures of compound **FzM1**, **2** and **3**. Their  $EC_{50}$  for PM rescue of Fz4-FEVR are indicated together with s.e.m. (n=3).

## 2.6.2 FzM1 binding site

To further confirm that the new screening platform indeed selected molecules addressing our target, it was identified the FzM1 binding site on Fz4-WT. Attempting to transform FzM1 in a molecular probe, it was derivatized with an alkyne moiety (FzM1alk). Despite being extremely unreactive, alkynes can receive nucleophilic attacks from sulfhydryl or hydroxyl group of amino acids to generate covalent adducts. This extremely rare event has been shown to happen at catalytic sites of enzymes as well as in ligand binding pockets [84]. FzM1alk is still a pharmacological chaperone of Fz4-FEVR, and it is also able to inhibit Wnt- $\beta$ -catenin pathway in Fz4-WT-expressing cells (log EC<sub>50</sub> as pharmacological chaperones and as Wnt antagonist of -4.8 and -4.9, respectively; **Figure 27**).

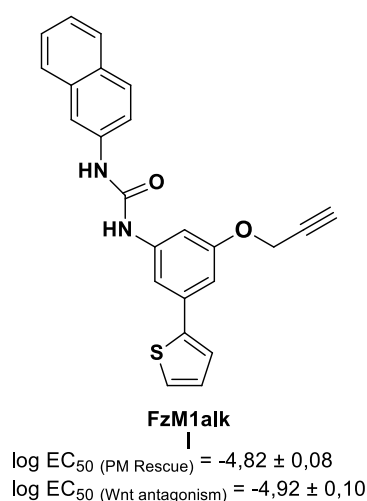


**Figure 27** Chemical structure of FzM1alk. EC<sub>50</sub> values for FzM1alk as a folding chaperone for Fz4-FEVR and as a Wnt inhibitor are indicated. (n=3, means ± s.e.m.)

HA-Fz4-WT HEK293 cells were cultured in the presence of FzM1alk. Fz4 was immunopurified, digested with trypsin and analyzed by LC/MS. HPLC profiles of samples from FzM1alk-treated cells and untreated cells were compared. These almost totally overlapped, with the exception of a fraction eluting with a retention time of 17.2 min and present only in samples obtained from FzM1alk-treated cells. Among the peptides eluting in this fraction, the one with an m/z of 1,386.9 Da corresponded, with a deviation ( $\Delta$ mass) of 1.6 Da from the theoretical mass, to amino acids 418–426 of Fz4 ICL3 (theoretical mass of 990 Da) carrying FzM1alk (molecular weight 398.5 Da) covalently linked either to S418 or to T425; theoretical mass [M-H-FzM1alk]<sup>+</sup> of 1,388.5 Da). Thus, the spectra indicated that FzM1alk interacted with Fz4 ICL3 by contacting at least S418 or T425. Together with the C-terminal tail, this loop forms the binding region for Dsh [85]. Binding of FzM1alk or FzM1 to Fz4 ICL3 should cause a change in solvent accessibility in this region of the receptor. These changes can be highlighted by measuring the rate of hydrogen-to-deuterium exchange (HDX) at this site (**Figure 28**). In the absence of FzM1, almost the entire receptor exchanged its hydrogen atoms with deuterium (with the exception of a helix of the ECD domain, amino acids 154–164). As expected, the C-terminal tail and the ECD of the receptor showed the higher rate of exchange compared to the TMD. Upon FzM1 binding, solvent accessibility of ICL3, TM5–7 and the C-terminal tail of the receptor was reduced, whereas the rest of the protein became more solvent accessible (**Figure 28**). The buried ICL is part of the Dsh binding region [85]. Its burial from solvent upon ligand binding appears compatible with

ICL3 being contacted by FzM1 and with a change in the conformation of this loop. A burial of the C-terminal tail can be also hypothesized from the HDX data. The latter could be due to a tighter interaction of the tail with ICL3 or, more likely, as seen for many other GPCRs<sup>41</sup>, with the tail interacting with the detergent micelles. It was envisaged that the diminished solvent accessibility of ICL3 upon FzM1 binding could have been the mechanism behind the folding chaperone effect of the molecule on Fz4-FEVR.

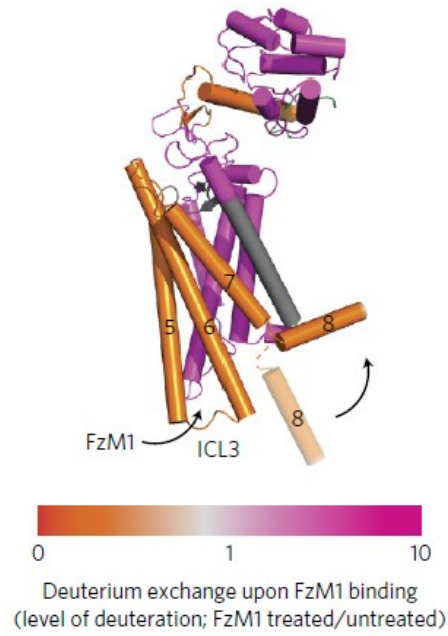


**Figure 28** Solvent accessibility of Fz4 region upon binding to FzM1 measured by the rate of HDX. The color scale reflects the level of deuterium exchange measured as difference in peptide mass in the presence or in the absence of FzM1. The arrows indicate FzM1 binding site and the C-terminal tail movement upon FzM1 binding. Numbers indicate TMDhelices (5–7) and the C-terminal tail helix (8). ICL3 is indicated.

### *2.6.3 The effect of FzM1 on tumor cells*

FzM1 acts as inhibitor of Wnt- $\beta$ -catenin signaling by inhibiting transcription of TCF/LEF-regulated genes (T-cell factor/lymphoid enhancer factor). The prerequisite for TCF/LEF transcription is the nuclear accumulation of  $\beta$ -catenin [86]. However, for this to happen,  $\beta$ -catenin must be first dislodged from the PM, where it forms a stable complex with E-cadherin. This complex keeps  $\beta$ -catenin in a resting state by protecting it both from the APC destruction complex (Axin, APC and GSK3- $\beta$ ) [86], which is responsible for its degradation, and from its nuclear transport, which is necessary for TCF/LEF activation. Fz4 controls several events leading to  $\beta$ -catenin nuclear accumulation. It recruits Dsh, which is protected by proteasomal degradation [87], and, in complex with Fz4, recruits the intracellular kinases [88] responsible for  $\beta$ -catenin C-terminal phosphorylation and its dislodgment from the PM [89]. Furthermore, the Dsh-Fz4 complex destabilizes the APC complex, protecting  $\beta$ -catenin from degradation and ultimately allowing its nuclear translocation. By blocking TCF/LEF-dependent gene transcription, FzM1 might have potential as an inhibitor of tumor cell growth. Some of the TCF/LEF genes are, indeed, related to tumor cell survival, differentiation and invasiveness [86]. It was thus looked at the effects of FzM1 treatment on growth, differentiation and migration of U87MG glioblastoma cells. Fz4 expression in these cells has already been shown to relate to invasiveness and the differentiation state of the cells [80]. The treatment with FzM1 reduced cell viability and affected their morphology, causing them to acquire a more elongated or neuronal appearance.

The Wnt inhibition exerted by FzM1 affects the growth, migration and differentiation of U87MG glioblastoma cells, which well represent this frequent and highly malignant type of brain tumor [80], suggesting the future applicability of these Fz4 allosteric modulators as antitumor drugs [90]. FzM1 is to our knowledge the first example of a compound able to hit the same protein-protein complex by contacting, in contrast, the Dsh binding site on Fz4. Owing to its properties, FzM1 represents what is to our knowledge the first template on which Fz4 modulators with improved potency and efficacy can be designed and suggests new avenues for developing Wnt- $\beta$ -catenin pathway modulators [3].

*Chapter 3 – Design and synthesis of Novel SIRT6  
inhibitors*



### 3.1 The Human Sirtuin Family

The founding member of the sirtuin family, yeast Sir2 (silent information regulator 2), was originally isolated in a screen for silencing the mating-type information loci in yeast [91]. Sir 2-4 are also required for gene silencing at telomeres [92]. Sir 2 also mediates gene silencing at the rDNA loci, which was shown to be independent of other Sir proteins. It was demonstrated that the silencing genetic loci have low histone acetylation levels compared to loci that are not silenced. Mutation in Sir2-4 increase histone acetylation levels and overexpression of Sir2 but not other Sir proteins led to decreases in histone H4, H2B and H3 acetylation [93].

Sirtuins are evolutionarily conserved in all domains of life. On the basis of sequence similarity, sirtuins from different species are classified into at least four classes, classes I–IV [94]. Mammalian SIRT1–3 and all yeast sirtuins belong to class I. Mammalian SIRT4 is in class II, SIRT5 is in class III, while SIRT6 and SIRT7 are both in class IV. Sirtuins compose the class III family of histone deacetylase enzymes (HDACs) that, unlike the class I and II HDACs, require the cofactor  $\text{NAD}^+$  as a substrate. Sirtuins catalyze the removal of an acetyl moiety from the  $\epsilon$ -amino group of lysine residues within protein targets [95] to yield the deacetylated protein product, nicotinamide, and 2'-O-acetyl-ADP-ribose. The enzymatic reaction mechanism for sirtuin-catalyzed NAD-dependent protein lysine deacetylation is reported in **Figure 29**.

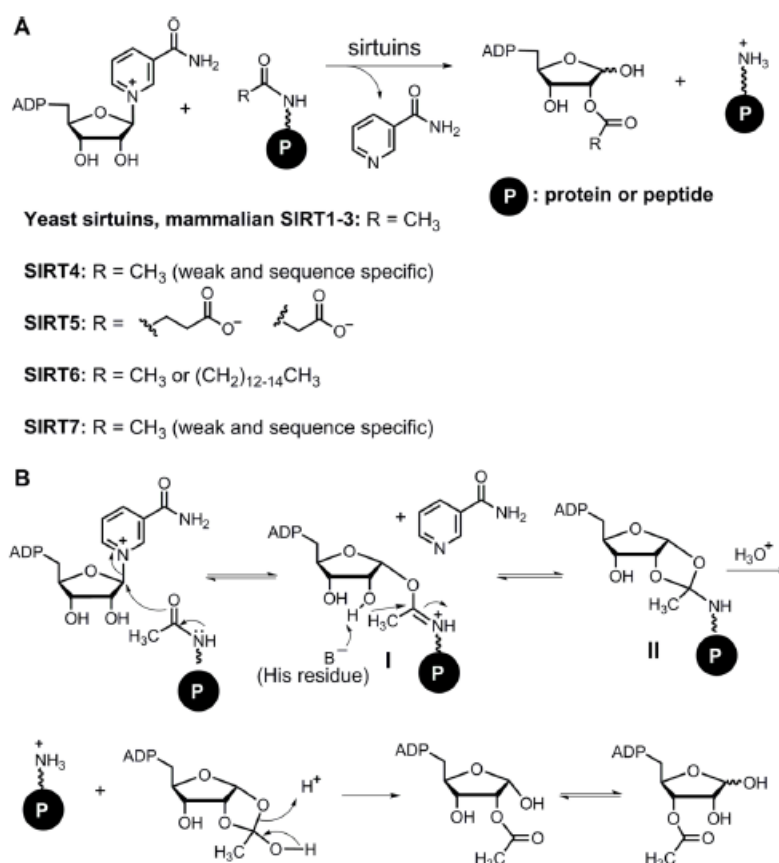


**Figure 29** Enzymatic function of sirtuins. (A) NAD-dependent protein lysine deacetylation activity of different sirtuins. (B) Enzymatic reaction mechanism of sirtuins.

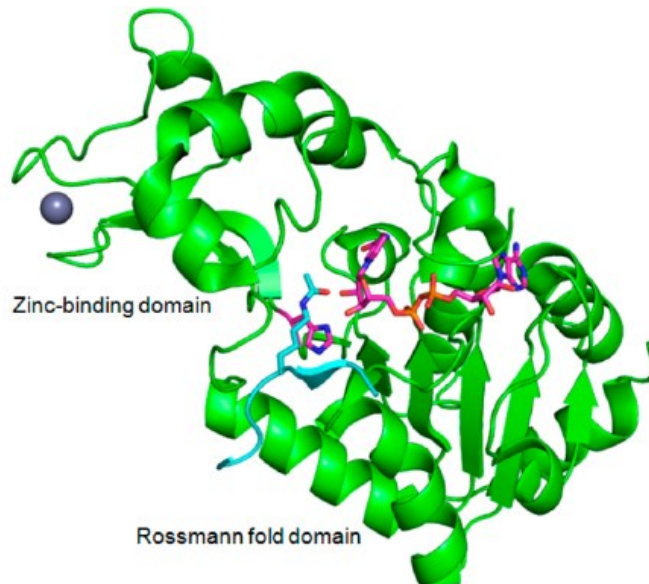


**Figure 30** Structure of a ternary sirtuin-NAD-acetyl peptide complex(PDB ID 2H4F). NAD, acetyl lysine, and the key catalytic His residue are shown in stick representation. Bound zinc is shown as a gray sphere. Protein structure picture is generated using PyMol.

The conserved catalytic core of sirtuins consists of a zinc-binding domain and a Rossmann fold domain (**Figure 30**) [96]. The active site lies at the interface of the two domains. It was thought that the acetyl lysine peptide binds first, followed by the binding of  $\text{NAD}^+$ . Once the tertiary complex is formed, the carbonyl oxygen of the acetyl group attacks the C1-position of the nicotinamide ribose, displacing nicotinamide and forming the alkylamidate intermediate (intermediate I, **Figure 29B**) [97]. A conserved histidine residue then serves as a general base to deprotonate the ribose 2-OH, which then attacks intermediate I at the carbonyl carbon, generating the 1,2-cyclic intermediate (intermediate II, **Figure 29B**). Intermediate II is then hydrolyzed to produce 2-O-acetyl-ADP-ribose (2-O-Ac-ADPr), which can be non-enzymatically isomerized to 3-O-Ac-ADPr. [97]. Sirtuins regulate many aspects of chromatin biology, such as transcription, recombination, and genome stability, by modifying histones, transcription factors, and epigenetic enzymes. Sirtuins also regulate metabolism by modifying a diverse set of metabolic enzymes, both in the cytosol and in the mitochondria. The defatty-acylation activity of SIRT6 on TNF also revealed that sirtuins can regulate protein secretion and membrane trafficking. The diverse substrate proteins of sirtuins also dictate that sirtuins may be involved in various human diseases, such as cancer, neurodegeneration, diabetes, and other metabolic disorders [98]. Humans have seven proteins of the sirtuin family (SIRT1 through 7) that share the catalytic domain with Sir2 [99].

**SIRT1** is by far the most understood mammalian sirtuin and has the greatest homology to yeast SIR2. SIRT1 is predominantly present in the nucleus, yet it shuttles between the nucleus and the cytoplasm in a context-dependent manner. SIRT1 deacetylates lysine residues in both histones and non-histone proteins, thereby regulating transcription, protein stabilities, and activities. SIRT1 controls various cellular processes, such as chromatin organization, metabolism, cell survival, differentiation, and development, as well as stress responses. Although the role of SIRT1 is far more expansive, the majority of its functions are intimately connected to epigenetic regulation. The role of SIRT1 in epigenetics is achieved via several different mechanisms, such as regulating chromatin structure by histone deacetylation, regulating the activity of

transcription factors by deacetylation, and regulating the activity of other epigenetic enzymes by deacetylation. **SIRT2** is connected with multiple cellular processes, including mitosis, cell cycle, cell death, metabolism, and aging. SIRT2 was initially reported to be mainly in the cytoplasm, co-localizes with microtubules, and deacetylates  $\alpha$ -tubulin at Lys40 [100]. It was recently reported to regulate many other cytosolic proteins, including LDH-A (lactate dehydrogenase A), PEPCK1 (phosphoenolpyruvate carboxykinase 1), ACLY (ATP-citrate lyase), and G6PD (glucose-6-phosphate dehydrogenase). It was later found that SIRT2 can translocate to the nucleus and has important epigenetic roles. **SIRT3–5** are considered to localize mainly in the mitochondria, where they regulate numerous mitochondrial proteins. Therefore, the roles of SIRT3–5 are mainly in metabolic regulation. Consistently, SIRT3 regulates substrates involved, for example, in ATP production, fatty acid oxidation, and the citric acid cycle but also in mitochondrial integrity, oxidative stress responses, and apoptosis [101]. SIRT4 influences fatty acid metabolism through deacetylation of malonyl-CoA decarboxylase [102], and strong evidence links this isoform to insulin secretion [103]. SIRT5 was recently described to more efficiently demalonylate or desuccinylate its substrates [104] and it was reported to regulate the urea cycle through its target carbamoyl phosphate synthetase 1 [105].

Similar to SIRT6, **SIRT7** is also a class IV sirtuin that is mainly localized in the nucleus. SIRT7 specifically mediates deacetylation of histone H3 at 'Lys-18' (H3K18Ac). In contrast to other histone deacetylases, displays selectivity for a single histone mark, H3K18Ac, directly linked to control of gene expression. H3K18Ac is mainly present around the transcription start site of genes and has been linked to activation of nuclear hormone receptors. SIRT7 thereby acts as a transcription repressor. Moreover, H3K18 hypoacetylation has been reported as a marker of malignancy in various cancers and seems to maintain the transformed phenotype of cancer cells [106]. These data suggest that SIRT7 may play a key role in oncogenic transformation by suppresses expression of tumor suppressor genes by locus-specific deacetylation of H3K18Ac at promoter regions. Also required to restore the transcription of ribosomal RNA (rRNA) at the exit from mitosis: promotes the association of RNA polymerase I with the rDNA promoter region and coding region. Stimulates transcription activity of the RNA polymerase I complex. May also deacetylate p53/TP53 and promotes cell survival, however such data need additional confirmation.

## 3.2 Biochemical functions of SIRT6

**SIRT6** is a nuclear sirtuin that possess diverse enzymatic activities, including: 1) deacetylation of histone H3 at lysine 9 (H3K9ac) and 56 (H3K56ac) as well as the acetyltransferase GCN5 and the C-terminal binding protein interacting protein (CtIP); 2) mono ADP-ribosylation of itself and poly[adenosine diphosphate (ADP)-ribose] polymerase 1 (PARP1); and 3) hydrolysis of long-chain fatty acyl groups (deacetylation) from lysine residues in tumor necrosis factor- $\alpha$ (TNF-  $\alpha$ ) [107] . **Figure 31** summarizes all the catalytic functions of SIRT6, as mentioned above.

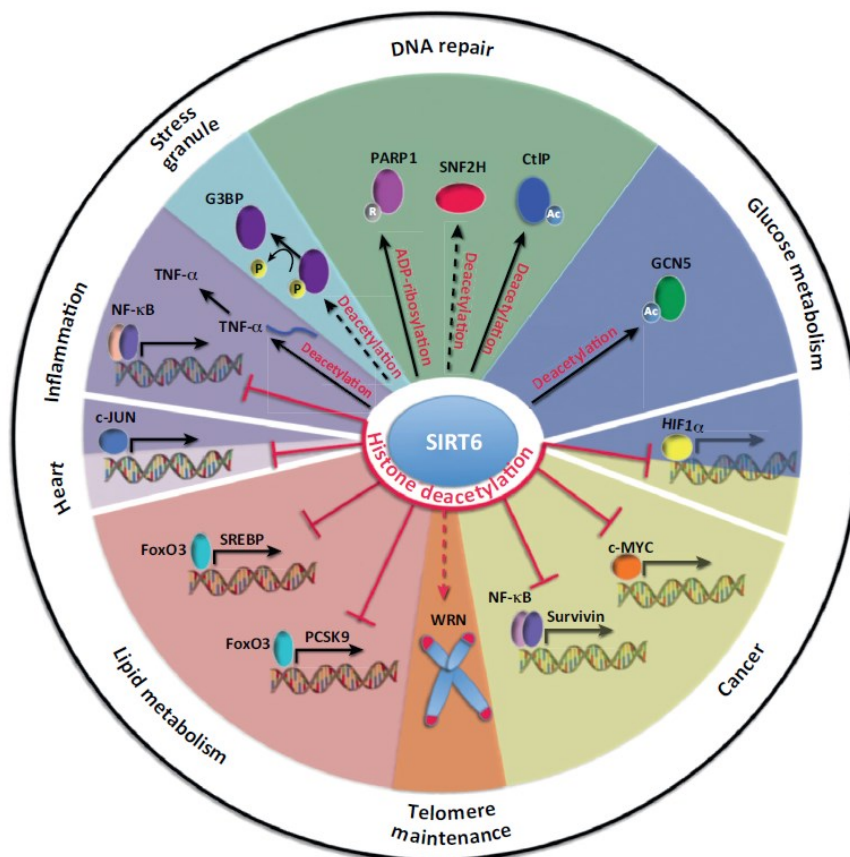


**Figure 31** Sirtuin 6 (SIRT6) cellular functions and their impact on organismal biology and disease.

SIRT6 is tightly bound to chromatin [108] and is best characterized as a  $\text{NAD}^+$ -dependent deacetylase of histone H3 lysine 9 (H3K9) [109] and H3 lysine 56 (H3K56) [110]. Histone deacetylation is associated with a closed chromatin conformation and decreased chromatin accessibility [111]. Thus, the discovery of this enzymatic activity instigated a series of studies that demonstrated roles for SIRT6 in regulating telomeric chromatin, the dynamic binding of DNA repair factors to chromatin, and gene expression. SIRT6-mediated deacetylation of telomeric H3K9 [109] and H3K56 residues [112] during S-phase is required for efficient association of the Werner syndrome (WRN) protein with telomeric chromatin [109]. ( Figure 31).

The WRN protein is a RecQ-like helicase that plays a major role in genome stability, particularly during DNA replication and telomere metabolism [113]. WRN may be required for proper capping of telomeres by the telosome/shelterin complex, as well as for replication of lagging telomeric DNA [114]; therefore, the genomic instability observed when SIRT6 is lost could partly be explained by a loss of association between WRN and chromatin. Both deacetylation and mono-ADP-ribosylation activities of SIRT6 are required to stimulate DSB repair (Double-strand break). More specifically, SIRT6 was found to interact and ADP-ribosylate PARP1 and stimulate its poly-ADP-ribosylation activity [115]. The effect of SIRT6 on PARP1 may only play a role during DNA damage caused by oxidative stress. Because PARP1 is involved in both BER (base excision repair) and DSB repair, the role of SIRT6 as an activator of PARP1 may also explain the BER defects observed in SIRT6-deficient cells. Moreover, SIRT6 interacts and deacetylates CtIP [C-terminal binding protein (CtBP) interacting protein [116] ( **Figure 31**) CtIP [117] and BRCA1 (breast cancer 1) [118] are responsible for DSB end resection, which results in single-stranded DNA (ssDNA). This ssDNA is bound by replication protein A (RPA), leading to the formation of a ssDNA–RAD51 nucleoprotein filament that mediates HR (homologous recombination) [119]. SIRT6 thus promotes end resection and HR, thereby improving genome stability. SIRT6 also interacts with the DNA-dependent protein kinase (DNA-PKc) holoenzyme macromolecular complex, which comprises repair factors such as DNA-PKc and Ku70/80. This complex is known to promote DNA DSB repair in mammalian cells [120]. Finally, recent studies indicate that SIRT6 deacetylation of H3K56 and its interaction with the ATP-dependent chromatin remodeler SNF2H (SWI/SNF-related matrix-associated actin-dependent regulator of chromatin; also known as SMARCA5) accelerate the localization of SNF2H to sites of DSB damage, and both of these events are required for efficient DSB repair [121] ( **Figure 31**).

#### *Glucose metabolism*

SIRT6 is a central regulator of glucose homeostasis, and SIRT6 function impacts upon both glycolysis and gluconeogenesis. SIRT6 was found to suppress directly the expression of multiple glucose-metabolic genes [pyruvate dehydrogenase kinase-1 (PDK1), lactate dehydrogenase (LDH), phosphofructokinase-1 (PFK1), and GLUT1] by interacting with hypoxia inducible factor-1a (HIF1a) and deacetylating H3K9 at the promoter of HIF1a target genes ( **Figure 31**). HIF1a is known to modulate multiple genes to activate glycolysis and repress simultaneously mitochondrial respiration in a coordinated fashion [122]. In addition, SIRT6 controls gluconeogenesis through by modulating the activity of peroxisome proliferator-activated receptor- $\alpha$  coactivator 1a (PGC-1a), the main regulator of gluconeogenesis that stimulates hepatic gluconeogenesis in part by increasing the expression of gluconeogenic enzymes [123]. SIRT6 does this through its interaction with GCN5 (general control non-repressed protein 5) ( **Figure 31**) which enhances its activity. GCN5, in turn, is an acetyltransferase that catalyzes acetylation of PGC-1a. Acetylation of PGC-1a coincides with its relocalization away from the promoters of its gluconeogenic enzyme target genes, thus SIRT6 suppresses hepatic glucose production.

#### *Lipid metabolism*

SIRT6 serves as a negative regulator of triglycerides (TG) synthesis [124]. ( **Figure 31**) SIRT6 was also recently described as a crucial histone deacetylase in the regulation of expression of the proprotein convertase subtilisin/kexin type 9 (PCSK9) gene and low-density lipoprotein (LDL)–cholesterol homeostasis [125]. PCSK9 binds to the LDL receptor, the receptor is broken down and can no longer remove LDL cholesterol from the blood so to increase LDL-cholesterol levels. FoxO3 works to recruit SIRT6 to the Pcsk9 gene promoter to suppress its gene expression through H3K9 and H3K56 deacetylation.

SIRT6 was found to repress the sterol-regulatory element binding protein (SREBP), a key regulator of cholesterol biosynthesis, by three mechanisms. First, SIRT6 is recruited by FoxO3 to the Srebp gene promoter where it represses the transcription levels of Srebp and that of its target genes by deacetylating H3K9 and H3K56 [126] at Srebp promoter regions. Second, SIRT6 inhibits the cleavage of SREBP1/SREBP2 into their active forms by decreasing the transcription of the SREBP1/SREBP2 pro- tease complex (SCAP, S1P, and S2P) [127]. Third, SIRT6 activates AMPK by increasing the AMP/ATP ratio; AMPK phosphorylates SREBP1 on Ser372, thus inactivating SREBP1 by suppressing its cleavage and nuclear translocation. In addition, SIRT6 was also found to hydrolytically remove long-chain fatty-acyl groups, including myristoyl and palmitoyl groups, a process known as lysine deacylation [128]. In fact, long-chain deacylase activity was found to be an intrinsic activity of most sirtuins. Acyl lysine modifications such as formylation, propionylation, butyrylation, crotonylation, malonylation, succinylation, and myristoylation are post-translational modifications that may occur on histones or other cellular proteins for which their removal could modify enzyme activity or chromatin regulation.

### *Inflammation*

SIRT6 can catalyze the hydrolysis of myristoylated lysine 19 and 20 of tumor necrosis factor- $\alpha$  (TNF- $\alpha$ ), which allows TNF- $\alpha$  secretion from the cell [128]. (**Figure 31**) TNF- $\alpha$  is a key proinflammatory cytokine that is known to play a major part in numerous inflammatory diseases. On the other hand, SIRT6 could also play an anti-inflammatory role by inhibiting TNF- $\alpha$  function downstream. TNF- $\alpha$  is known to activate nuclear factor  $\kappa$ B (NF- $\kappa$ B), a potent proinflammatory cytokine. It was demonstrated that SIRT6 is recruited to promoters of a subset of NF- $\kappa$ B target genes through a physical interaction with the NF- $\kappa$ B subunit RELA (v-rel avian reticuloendotheliosis viral oncogene homolog A) and functions as a corepressor of NF- $\kappa$ B, silencing NF- $\kappa$ B target genes through deacetylation of H3K9 at target gene promoters and decreasing NF- $\kappa$ B-dependent apoptosis and senescence [129]. Mechanistically, SIRT6 interacts with c-JUN and deacetylates H3K9 at the promoter of proinflammatory genes including those encoding monocyte chemoattractant protein-1 (MCP-1), interleukin 6 (IL-6), and TNF- $\alpha$ . SIRT6 acts as a negative regulator of cardiac hypertrophy. At the cellular level, SIRT6 blocks IGF signaling by interacting with c-JUN and deacetylating H3K9 at IGF downstream targets. Inhibition of c-JUN or IGF signaling blocks hypertrophy of SIRT6-deficient hearts [130].

### *Cancer*

Proliferating tumor cells have unique metabolic requirements, characterized by enhanced cell-autonomous nutrient uptake and reorganization of metabolic pathways supporting the biosynthesis of macromolecules needed for cell growth and division [131]. Enhanced glycolysis under aerobic conditions is the best-known example of metabolic reprogramming observed in cancer cells, as described decades ago by Otto Warburg (the Warburg Effect) [132]. SIRT6 is a critical regulator of glucose homeostasis by controlling the HIF1 $\alpha$ -dependent transcriptional activation of glycolytic gene [133]. (**Figure 31**) Consequently, the expression of glycolytic genes is elevated in SIRT6 depleted cells, which leads to lower levels of oxygen consumption along with high production of lactate, a phenotype that is reminiscent of the Warburg effect. In addition, SIRT6 also plays a critical role in maintaining genomic stability, another hallmark in transformed cells, since accumulation of genomic abnormalities are associated with the tumorigenic capacity of cancer cell [134]. Indeed, SIRT6 was recently described to function as a tumor suppressor by regulating the metabolic defects associated with cancer [135]. These studies showed that SIRT6 suppresses aerobic glycolysis, in addition to repressing MYC-dependent ribosome biosynthesis [135]. MYC-mediated regulation of ribosome biogenesis is associated with tumorigenesis. Additionally, the expression of SIRT6 was shown to decrease in human colorectal and pancreatic cancers [135]. An additional enzymatic activity of SIRT6 is the hydrolysis of long-chain fatty acyl modifications (myristoyl groups) from lysine residues in TNF- $\alpha$  [107]. SIRT6-dependent

hydrolysis of myristoyl groups triggers the secretion of TNF- $\alpha$ . TNF- $\alpha$  is a pro-inflammatory cytokine having a pleiotropic function in cell physiology, whose release can signal either cell survival and proliferation, or cell death [136]. Binding of TNF- $\alpha$  to its receptor TNF-R1 was shown to promote apoptosis through the caspase-8-activating complex [137]. This pro-apoptotic effect mediated by TNF- $\alpha$  was shown to be antagonized upon NF- $\kappa$ B-dependent suppression of reactive oxygen species [138]. More specifically, the pro-apoptotic effect induced by TNF- $\alpha$  is dependent on the balance between NF- $\kappa$ B-dependent cell survival and the JNK signaling promoting cell death pathway [139]. Since SIRT6 was also shown to attenuate NF- $\kappa$ B signaling [112], it is plausible that TNF- $\alpha$ -dependent tumor cell death might be regulated upon SIRT6-mediated removal of myristoyl groups to trigger the secretion of TNF- $\alpha$ , a hypothesis that remains to be tested. This could add to the molecular mechanisms by which SIRT6 functions as a tumor suppressor. The expression of SIRT6 has been recently shown to be downregulated by the microRNA-34a (miR-34a) in human keratinocytes (HKCs). In contrast to normal keratinocytes, miR-34a is suppressed in skin cancers such as squamous cell carcinomas (SCCs) leading to an increment in SIRT6 expression. Thus, in contrast to other cancers such as hepatocellular carcinomas and colon adenocarcinomas, the expression of SIRT6 seems to be upregulated in SCCs due to a miR-34a downregulation.

### 3.3 Structure of Sirtuins

The sirtuin proteins contain an approximately 275 amino acid conserved catalytic core region. Additionally, the sirtuin proteins have N- and C-terminal flanking regions that are variable in length and sequence [140]. The catalytic core region adopts an elongated shape containing a large and structurally homologous Rossmann-fold domain, characteristic of NAD<sup>+</sup>/NADH binding proteins; a more structurally diverse, smaller, zinc-binding domain; and several loops connecting the two domains (**Figure 32**).

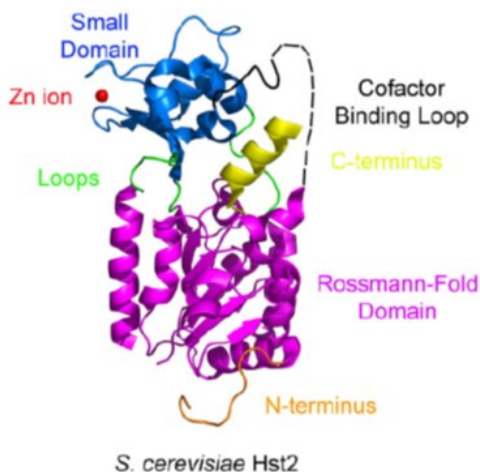


**Figure 32** Three-dimensional structure of sirtuin. The enzyme is shown in cartoon representation without bound ligands. The Rossmann-fold domain is indicated in magenta, the small domain in blue, the loops in green, the cofactor binding loop in black, the Zn ion in red, the N-terminal region in orange, and the C-terminal region in yellow. Disordered regions are indicated with dashed lines.

These loops form an pronounced, extended cleft between the large and small domains where the NAD<sup>+</sup> and acetyl-lysine containing peptide substrates enter from opposite sides and bind to the enzyme (**Figure 33**). The amino acids involved in catalysis and the reactive groups of both bound substrate molecules are buried within a protein tunnel in the cleft between the two domains (**Figure 33**), the region of the enzyme that contains the highest sequence conservation within the sirtuin enzymes.

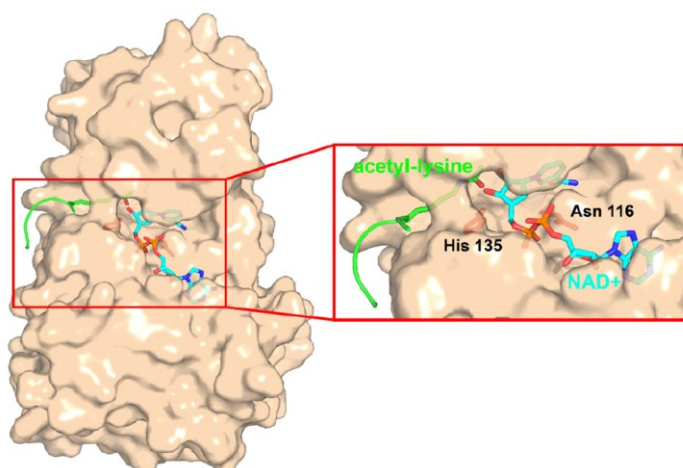




**Figure 33** Sirtuin active site binding cleft. . The Hst2 protein is shown in tan surface representation. The catalytic residues H135 and N116 are shown in red stick representation in the close-up view. The peptide substrate backbone is shown in green cartoon representation, the acetyl-lysine side chain is shown in green cpk stick representation, and the NAD<sup>+</sup> substrate molecule is shown in cyan cpk stick representation.

The Rossmann-fold domain contains many of the hallmarks of a typical NAD<sup>+</sup>-binding site such as a conserved Gly-X-Gly sequence important for phosphate binding, a pocket to accommodate an NAD<sup>+</sup> molecule, and charged residues responsible for ribose group binding [141]. The small, structural Zn<sup>2+</sup> binding domain results from two insertions in the Rossmann-fold domain and is the most diverse region between sirtuins for which structures have been determined in terms of primary sequence, three-dimensional structure, and position relative to the large domain ( **Figure 32**). A Zn<sup>2+</sup> molecule is bound by the sulphhydryl groups of two pairs of strictly conserved cysteine residues in the  $\beta$  sheet module in a tetrahedral conformation [142]. The small domain contains the conserved sequence motif Cys-X<sub>2-4</sub>-Cys-X<sub>15-40</sub>-Cys-X<sub>2-4</sub>-Cys, a characteristic Zn-binding motif. The role of the zinc ion seems to be structural, as it is postulated to be required for holding together the  $\beta$  strands in the small domain. One of the most interesting characteristics of the small domain is a conserved salt bridge (between R/K178 and E186, Hst2 numbering, unless otherwise indicated) [142], which seems to be important for positioning the small domain with respect to the large domain. The position of the small domain relative to the Rossmann-fold domain is also dependent on the conformation of bound NAD<sup>+</sup> or the presence of acetyl-lysine in the enzyme active site . The diversity in the small domain may have a potential role in regulating protein-protein interactions, which may be important for substrate specificity, enzyme localization, and potentially for modulation of enzyme activity. Indeed, structural differences between sirtuin proteins within the small domain might be exploited as binding sites for sirtuin-selective small molecule inhibitors.

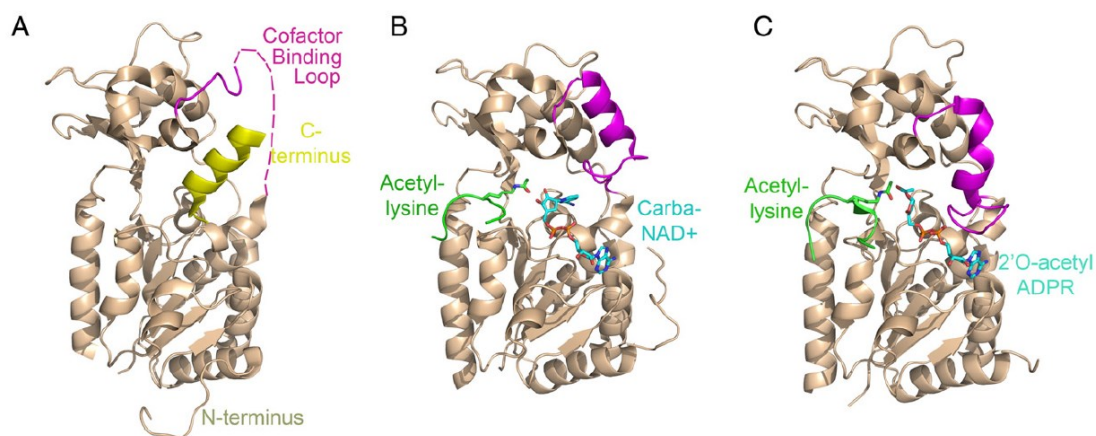


**Figure 34** . Conformational changes of the cofactor binding loop upon substrate and product binding. The Hst2 protein is shown in tan cartoon representation, the C-terminus is shown in yellow, and the cofactor binding loop is shown in magenta. The peptide substrate is shown in green cartoon representation, while the acetyl-lysine residue is shown in green cpk stick representation. (A) The apo Hst2 enzyme, the cofactor binding loop is disordered (dashed lines). (B) Hst2 with bound peptide substrate and carbamoyl-NAD<sup>+</sup>, the cofactor binding loop is in an open conformation. (C) Hst2 with bound peptide substrate and 2''-O-acetyl-ADP-ribose, the cofactor binding loop is in a closed conformation.

The four loops that connect the small and large domains form the cleft that acts as the enzyme active site. Both the NAD<sup>+</sup> and acetyl lysine substrates bind in this cleft ( **Figure 33**). This region has the most sequence homology among the protein family, and mutation of several residues in this region disrupts histone deacetylase activity, underscoring the importance of this region in sirtuin catalysis. Generally the largest of these four loops (the  $\beta$ 1- $\alpha$ 2 loop in Hst2) is one of the most conformationally dynamic regions of the sirtuin enzymes ( **Figure 34**). Since this loop forms part of the cofactor NAD<sup>+</sup> binding site and its conformation is largely dependent on the conformation and identity of the bound NAD<sup>+</sup> molecule or intermediate, it was called as the cofactor binding loop [142] . The cofactor binding loop appears to be disordered or highly flexible when NAD<sup>+</sup> is not bound ( **Figure 34A**), and becomes ordered upon NAD<sup>+</sup> binding into a relatively open conformation with residues of the loop (D43-Y52) about 7 Å away from the NAD<sup>+</sup> binding site ( **Figure 34B**) [143] . Residues (A33, G34, T37, F44, and D43) of the cofactor binding loop form part of the so-called C pocket, the region of the enzyme where the nicotinamide moiety of NAD<sup>+</sup> binds, and they mediate almost half of the enzyme contacts to NAD<sup>+</sup> [143], which implies that this cofactor binding loop plays an important role in NAD<sup>+</sup> binding. When the sirtuin reaction product 2'-O-acetyl-ADP-ribose is bound to the enzyme active site, the cofactor binding loop adopts a more closed conformation bringing residues (D43-Y52) of the loop ~5.5 Å closer to the nicotinamide-binding pocket, partially occluding the site ( **Figure 34C**) [144] , suggesting that the loop may also play a role in nicotinamide release. The switch between the open and closed conformations of the cofactor binding loop seems to be dependent upon the presence of the bound alkylamidate intermediate directly after nucleophilic attack of acetyl-lysine on an NAD<sup>+</sup> -derived intermediate and not upon nicotinamide cleavage or complete reaction product formation, as the closed conformation of the loop is also seen when an analog of the O-alkylamidate intermediate, S-alkylamidate, is bound to the enzyme [145] . When the reaction product nicotinamide is bound in the C pocket either in complex with acetyl-lysine, NAD<sup>+</sup> , or ADP-ribose, the cofactor binding loop adopts slightly different conformations which facilitate slightly different interactions between nicotinamide and the C pocket residues, although it is not clear whether the binding of different ligands of the ternary complex or the different nicotinamide conformations cause the differences in conformation of the cofactor binding loop [146] .

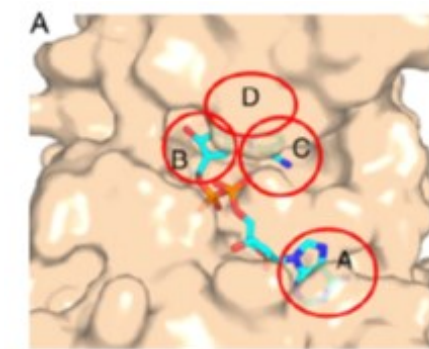


**Figure 35** Productive NAD<sup>+</sup> binding interactions in several sirtuin proteins.

The NAD<sup>+</sup> binding site, consisting in the large domain and in the loop region which is mainly represented by the cofactor binding loop, can be divided into three regions: site A, the adenine-ribose binding site; site B, the nicotinamide ribose binding site; and site C, the nicotinamide moiety binding site [142] ( **Figure 35**). The conformation of the nicotinamide ribose is variable depending on the NAD<sup>+</sup> analog bound (ADP-ribose, non productive NAD<sup>+</sup>, productive NAD<sup>+</sup>, or carba-NAD<sup>+</sup>), which other substrates are also bound to the enzyme, or even the particular sirtuin homologue. In fact, crystallographic structures available in the Protein Data Bank show that the nicotinamide moiety of NAD<sup>+</sup> is often bound outside of the C pocket in a conformation

that is not compatible with acetyl-lysine binding and deacetylation reaction, the so-called non-productive conformation. Vice versa, a productive conformation of  $\text{NAD}^+$  requires the presence of an acetyl-lysine containing peptide. Moreover, the hydrophobic tunnel which acts as the acetyl-lysine binding site and not simply the peptide binding site must be occupied to facilitate the productive binding of  $\text{NAD}^+$  [146]. In this productive conformation, the bound  $\text{NAD}^+$  is compatible with both acetyl-lysine binding and enzyme catalysis.

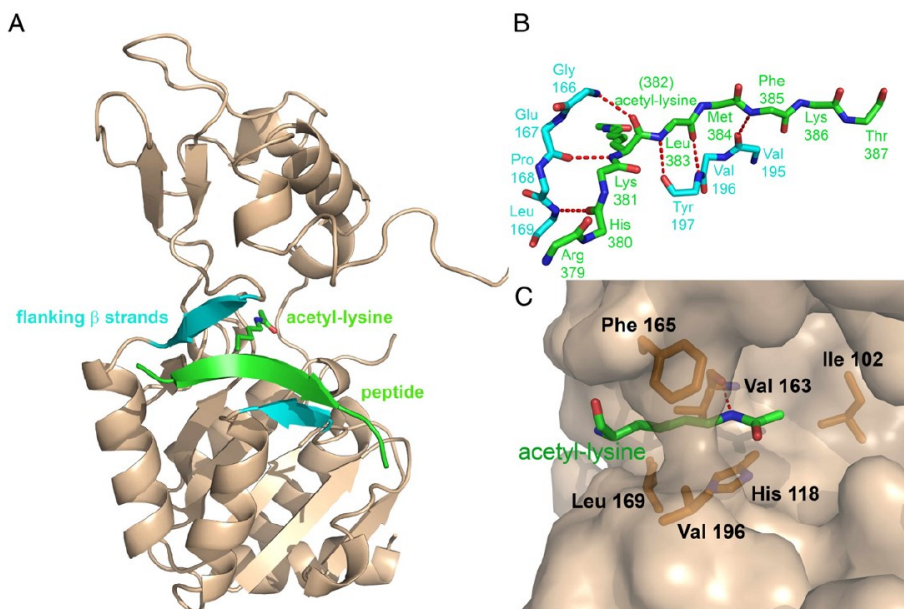


**Figure 36** Acetyl-lysine peptide binding to the sirtuin active site. (A) A peptide containing an acetyl-lysine residue (green) is shown bound to the Sir2-Af2 sirtuin enzyme (tan, cartoon representation) active site forming the  $\beta$  staple with flanking  $\beta$  strands of the enzyme (cyan). (B) The acetyl-lysine containing peptide (green) makes main chain  $\beta$  strand hydrogen bonds (red dashes) with main chain atoms of the enzyme (cyan). (C) The acetyl-lysine residue (green) binds in a hydrophobic tunnel of the enzyme (tan, surface representation), making several van der Waals interactions with enzyme residues (orange) and one hydrogen bond (red dashes) with an enzyme residue.

The peptide itself binds to the cleft between the small and large domains with the acetyl-lysine side chain inserting into a hydrophobic tunnel located within the cleft. The peptide backbone containing the acetyl-lysine side chain forms  $\beta$  sheet-like interactions with two flanking strands in the enzyme (**Figure 36A**) [147]. This staggered, antiparallel three-stranded  $\beta$  sheet is referred to as the  $\beta$  staple. Main chain atoms of the peptide make several hydrogen bonds with main chain atoms of catalytic residues from the flanking strands of the  $\beta$  staple (**Figure 36B**). A comparison of sirtuin enzymes with and without bound acetyl-lysine containing peptide suggests that peptide binding induces a significant shift in the position of the small domain relative to the large domain, bringing the two domains together to form the  $\beta$  staple motif and resulting in the correct positioning of conserved residues for formation of the acetyl-lysine binding tunnel [148]. It has been hypothesized that  $\text{NAD}^+$  and peptide binding may be cooperative, as the region surrounding the peptide binding site adopts the more closed conformation seen in the peptide bound structure when  $\text{NAD}^+$  is bound but not in the absence of  $\text{NAD}^+$  [147]. The aliphatic region of the acetyl-lysine side chain makes several van der Waals interactions with conserved hydrophobic residues (H135, V228, F184, and L188). The acetyl group appears to be positioned by a single hydrogen bond between the Ne atom of the lysine side chain and the main chain of a valine residue (182) and van der Waals interactions between the acetyl methyl group and other highly conserved residues (I117 and H135), which position the

unliganded carbonyl oxygen toward the NAD<sup>+</sup> binding B site (**Figure 36C**) [147] . When the peptide is bound in a ternary complex with the intermediate-like molecule ADP ribose, or the reaction product 2'-O-acetyl-ADP-ribose, the acetyl-lysine carbonyl oxygen hydrogen bonds to the 1'-OH of the nicotinamide ribose ring [143] . The  $\beta$  staple binding motif and the residues involved in peptide binding seem to be conserved features of acetyl-lysine peptide binding.

### 3.3 Structure of SIRT6

SIRT6 displays low deacetylase activity (~ 1000-fold lower) compared with other sirtuins. Human SIRT6 has 355 amino acids and consists of a putative catalytic sirtuin core with N- and C-terminal flanking extensions.

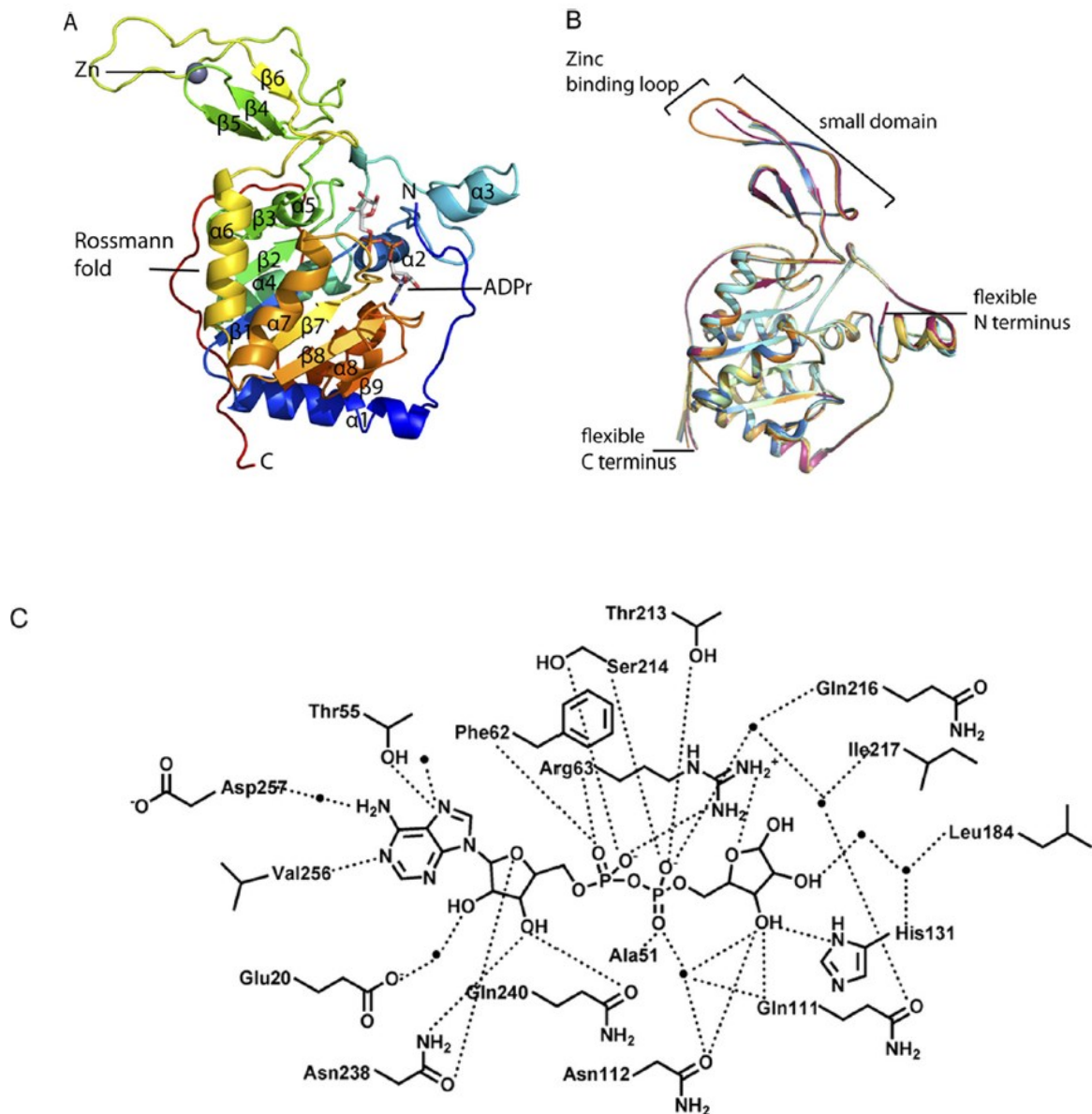


**Figure 37** Structure of human SIRT6 in complex with ADP-ribose. A, overall structural features of SIRT6 monomer. B, superimposition of the six molecules in the asymmetric unit. Red, chain A; green, chain B; dark blue, chain C; orange, chain D; cyan, chain E; yellow, chain F. C, schematic illustration of the hydrogen bonding network surrounding ADPr; hydrogen bonds are indicated as dashed lines, and water molecules are shown as spheres.

As mentioned for other solved sirtuin structures, SIRT6 contains two globular domains composed of eight  $\alpha$ -helices and nine  $\beta$ -strands: a large Rossmann fold for NAD<sup>+</sup> binding (residues 25–128 and 191–266) and a smaller domain, which contains a zinc-binding motif (residues 129–190) (**Figure 37A**). The large Rossmann fold domain is formed by a six-stranded ( $\beta$ 1, $\beta$ 2,  $\beta$ 3,  $\beta$ 7,  $\beta$ 8, and  $\beta$ 9) parallel  $\beta$ -sheet sandwiched between two helices ( $\alpha$ 6 and  $\alpha$ 7) on one side and four helices ( $\alpha$ 1, $\alpha$ 4, $\alpha$ 5, and  $\alpha$ 8) on the other side. The small domain is formed by two extending loops (connecting  $\beta$ 3 and  $\alpha$ 6) from the large domain and consists of a three stranded antiparallel  $\beta$ -sheet ( $\beta$ 4,  $\beta$ 5, and  $\beta$ 6). Interestingly, although most sirtuins contain a Cys-XX-Cys-X15–20-Cys-X-X-Cys sequence motif for Zn<sup>2+</sup> - binding, SIRT6 contains a 10-residue insertion between the second set of cysteines, resulting in an extended flexible long loop . The NAD<sup>+</sup>- binding pocket of sirtuins has been divided into three regions: sites A, B, and C [142]. Similar to all other solved sirtuin structures, the adenosine moiety of ADPr is bound in the A site of SIRT6, and the nicotinamide ribose moiety is bound in the B site. Many of the residues involved in ADPr binding are conserved between SIRT6 and the other sirtuins . The ADPr interactions in the SIRT6 active site are shown in **Figure 37C** . For all six molecules in the asymmetric unit, the ribose moiety of ADPr assumes the C2' exo conformation in its  $\alpha$ -form. Although SIRT6 shares the overall domain architecture with SIRT2, SIRT3 , and SIRT5 , there are several differences on the surface of the protein. In all previously solved sirtuin structures, a conserved “cofactor binding loop” [142] is involved in NAD<sup>+</sup> binding; this loop adopts several different conformations depending on the ligand(s) bound in the active site . SIRT6 lacks the cofactor-binding loop, which is replaced by a single helix ( $\alpha$ 3) containing several NAD<sup>+</sup>-binding residues, which appears to be ordered in the SIRT6.ADPr and SIRT6.NAADPr structures. This is an indication that the SIRT6 substrate-binding pocket may be less flexible and does not significantly vary its conformation when different ligands are bound. In addition, helix  $\alpha$ 1 in SIRT6 is much longer, and the N-terminal unstructured coil folds back toward and may structurally stabilize the NAD<sup>+</sup> binding site ,although there is no direct interaction between the random coil and ADPr. In contrast to class I, II, and III human sirtuins, class IV sirtuins contain a deletion in the sequence immediately following the  $\alpha$ 3 helix .The result is that SIRT6 does not have a helix bundle in its small domain. The helix bundle is replaced by a short loop, which interacts with the loop between  $\alpha$ 2 and  $\alpha$ 3 and contacts a small region on the zinc binding module. The lack of a helix bundle to form extensive interactions with the  $\beta$ -sheets in the zinc-binding module provides one explanation for why SIRT6 has a splayed small domain. This unique structural feature is likely to be adopted by SIRT7, another class IV sirtuin that also contains a deletion in this region but that has not yet been structurally and functionally characterized. This unique feature may be responsible for the observed lower activity (1000 times) of SIRT6. To date, there are no reports of detectable deacetylase activity for SIRT7. In addition to the missing helical bundle, another reason for the splayed small domain in SIRT6 is the loss of a conserved salt bridge, which has been reported to contribute to the positioning of the zinc-binding motif with respect to the Rossmann fold domain and substrate-binding site [142] . Based on precedent from other sirtuins, a salt bridge should be formed between Arg<sup>180</sup> and Asp<sup>188</sup> in SIRT6. However, this interaction is not observed. The side chain of Arg<sup>180</sup> is directed toward the surface of the protein rather than toward the Asp<sup>188</sup> residue. Instead, Arg<sup>124</sup> on the loop connecting  $\alpha$ 5 and  $\beta$ 3 and Gln<sup>145</sup> on  $\beta$ 5 form a hydrogen bond to tether the zinc-binding motif and the large domain together .The loss of the previously described salt bridge removes the constraint on the two loops, which would otherwise result in a more closed conformation. The new Arg<sup>124</sup>–Gln<sup>145</sup> hydrogen bond in SIRT6 pulls the two domains together on the opposite side, and therefore, the small domain is not directly above the Rossmann fold but rather in an open conformation tilted in a 45° angle. It is generally observed that peptide substrates interact with sirtuins via nonspecific backbone interactions [149] . There is a conserved FGEXL ( Phe, Gly, Glu, Lys, Leu) loop that forms hydrogen bonds with the substrate peptide [147]. However, in the case of SIRT6, the sequence is WEDSL ( Trp, Glu, Asp, Ser, Leu) .The amide nitrogen of Trp<sup>186</sup> appears to be flipped, whereas its analog in other sirtuins is involved in a hydrogen bond with a carbonyl group from the peptide substrate backbone.

Sirtuins catalyze deacetylation through a sequential mechanism in which the substrate peptide binds first to form an ordered NAD<sup>+</sup>-binding pocket for the subsequent co-substrate binding. SIRT1, SIRT2, and SIRT3 were all found to require a substrate/ligand binding prior to NAD<sup>+</sup> binding [149]. The unique SIRT6 structural features suggest that SIRT6 utilizes a different binding mechanism, which does not require peptide substrate binding prior to NAD<sup>+</sup> binding. These features include an ordered helix regardless of substrate binding, a large open channel in the substrate and NAD<sup>+</sup> binding site due to the missing helix bundle, and a NAD<sup>+</sup> site potentially reinforced by the N-terminal loop. In a paper 2011 [150] it was monitored by isothermal titration calorimetry ITC, the binding of NAD<sup>+</sup> in the absence of an acetyl lysine substrate. SIRT1 to -3, and SIRT5 did not bind NAD<sup>+</sup> in the absence of the acetyl lysine substrate, while SIRT6 can bind NAD<sup>+</sup> efficiently in the absence of an acetylated substrate. Moreover there was no binding when NADH was titrated into SIRT6 suggesting that SIRT6 cannot accommodate the puckered conformation of the nicotinamide ring of NADH. The binding pocket of SIRT6 distinguishes structural differences between NAD<sup>+</sup> and ADPr. Interestingly, unlike NAD<sup>+</sup> and ADPr, 2'-NAADPr bound to SIRT6 with a negative  $-T\Delta S$ , suggesting that there is more disorder when 2'-NAADPr binds. This result is consistent with the crystal structure, which showed a high degree of variability and poor electron density for the 2'-N-acetyl-ribose moiety of 2'-NAADPr.

### 3.4 Results and Discussion

To the author's knowledge, no study has ever been published in the literature concerning SIRT6 inhibition by small molecules. Hence, structure-activity relationship (SAR) analyses have never been carried out really. This thesis constitutes a starting point for the development and SAR analysis of small molecules inhibitors of SIRT6. In the absence of any literature guidance, this work focuses on the potent pan SIRT1/SIRT2/SIRT3 inhibitor (compound **1**) [151] trying to assess its potential capability to bind to SIRT6 (**Figure 38**). The authors in [151] have demonstrated that the compound **1** is a potent pan SIRT1/2/3 inhibitor and exhibits a low nanomolar value of  $IC_{50}$ . However, compound **1** had never been tested on SIRT6 before this work.

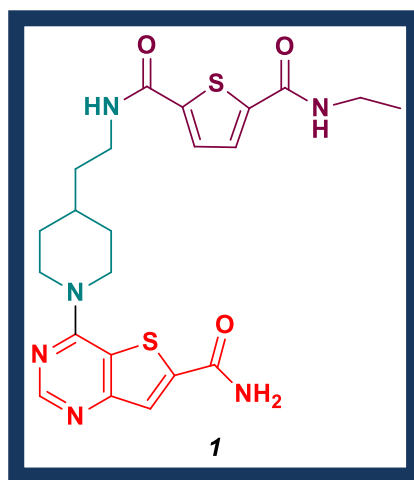
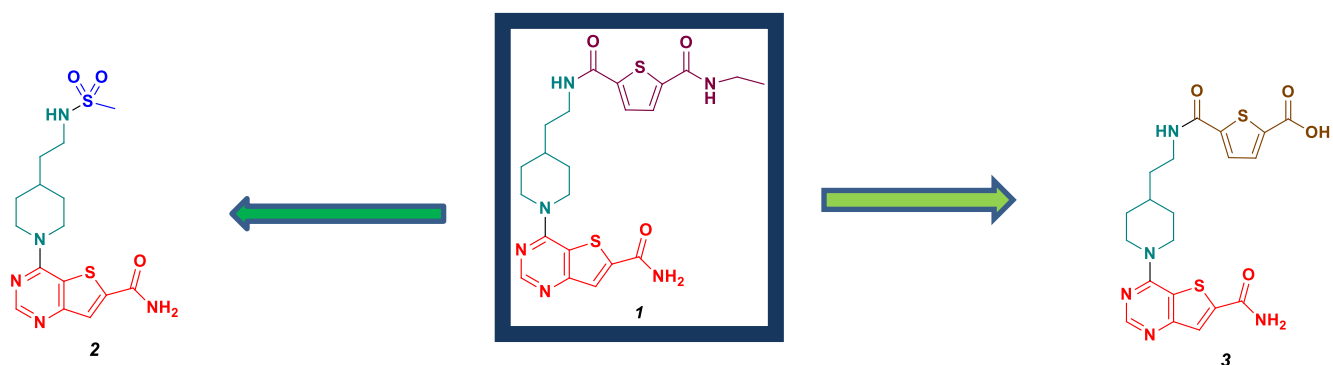


**Figure 38** Chemical structure of the compound **1**.

As the first step, the structure-activity study has been done, yielding compounds **2** and **3** which are obtained by introducing modifications in the side chain of compound **1**. Specifically, the thiophene in the side chain of compound **1** is replaced by the polar sulfonamide group in compound **2**, whereas the ethylamide substituent on the thiophene of compound **1** is substituted with carboxylic acid in compound **3**. In addition, the intermediate compounds **4** and **5**, are analysed. In particular, compound **4** is the intermediate Boc-protected on the amine, and compound **5** is the amine-free derivate. Compounds **6** and **7**, instead, are truncated analogues in which the linker length is changed, more specifically the ethyl linker is replaced by the methyl linker (**Figure 39**).





*J. Med. Chem.* 2013, 56, 3666–3679

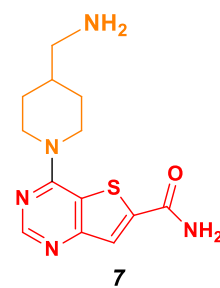
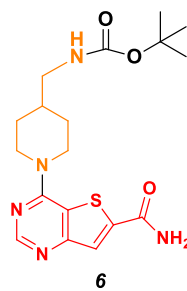
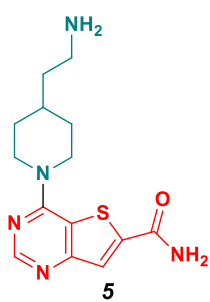
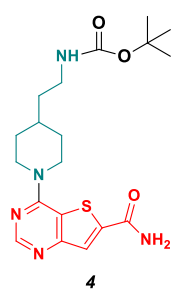
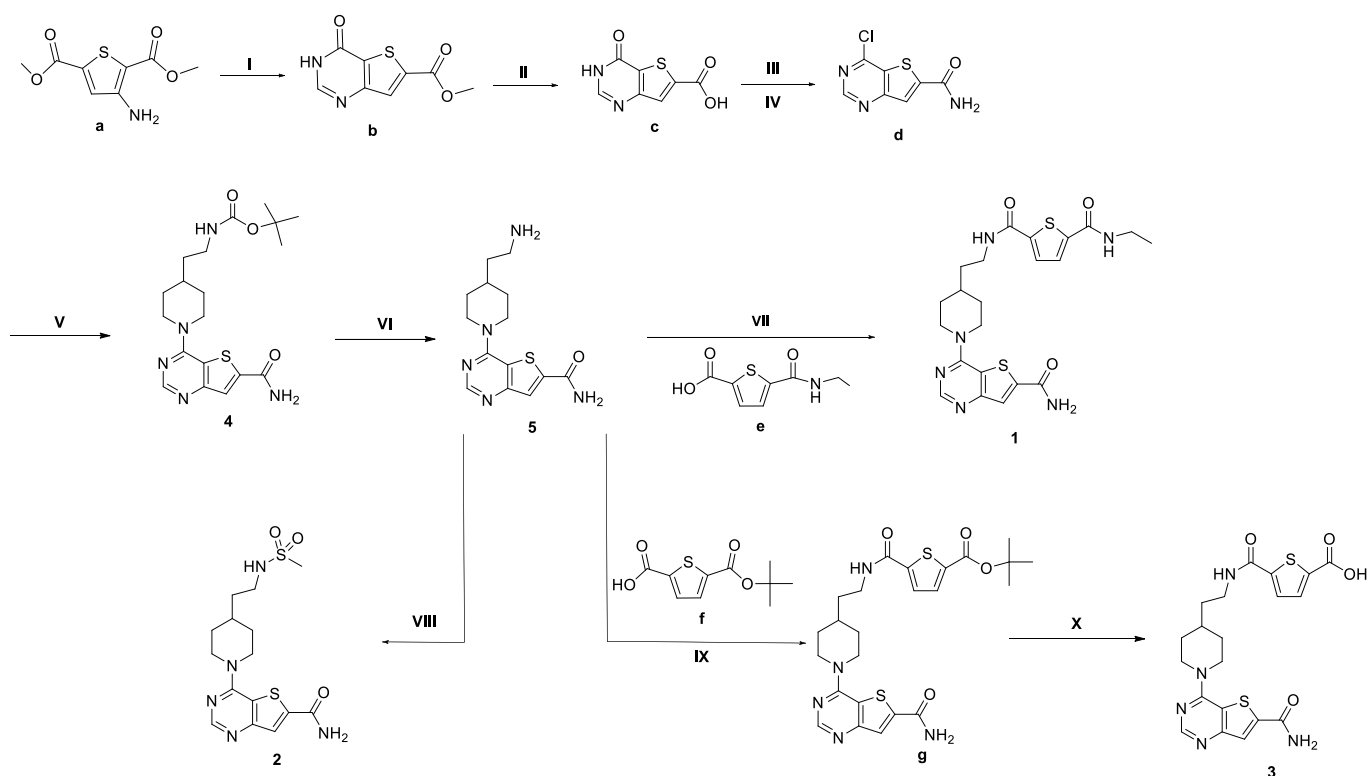


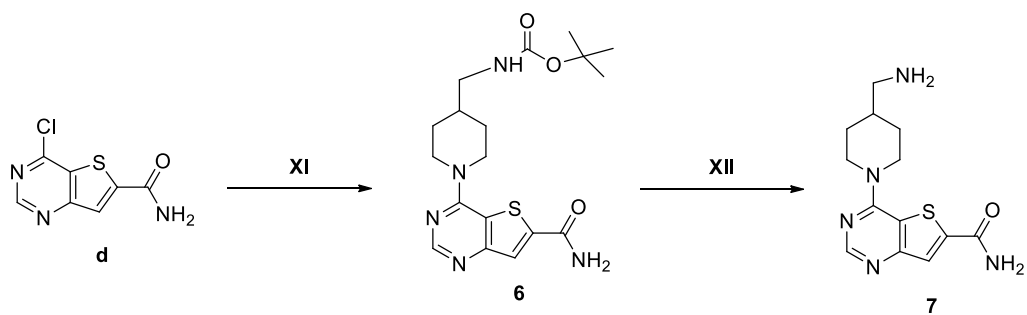
**Figure 39** Compounds synthesized as SIRT6 inhibitors

## 3.5 Synthesis

Synthesis of compounds 1-5 are showed in **Scheme 20** and compounds 6-7 in **Scheme 21**. Compounds were prepared by treatment of dimethyl-3-aminothiophene-2,5-dicarboxylate **a** with formamidine acetate salt in 2-methoxyethanol dry at 130°C for overnight to obtain the methyl-3H thieno[3,2-d]pyrimidin-4-one-6-carboxylate **b**. Then the ester of **b** was hydrolyzed through the solution of lithium hydroxide monohydrate in 2-propanol at 75°C for 1h. Treating **b** with oxalyl chloride in DMF dry and quenching the intermediate acid chloride with ammonia hydroxide solution in EtOAc at rt for 2h afforded the versatile 4-chloro-thieno[3,2-d]pyrimidine-6-carboxamide intermediate **d**. The chloride on **d** was subsequently displaced with 4-(2-Boc-aminoethyl)piperidine or 4-(Boc-aminomethyl)piperidine in CH<sub>3</sub>CN in presence of DIEA at reflux for 2h to afford Boc-protected precursors **4** and **6** (**Scheme 21**). The Boc group were removed by treatment with trifluoroacetic acid in CH<sub>2</sub>Cl<sub>2</sub>, and the resulting amines **5** and **7** were reacted under amide coupling conditions (HATU, DIEA, DMF) with 5-(ethylcarbamoyl)thiophene-2-carboxylic acid **e** and 5-(tert-butoxycarbonyl)thiophene-2-carboxylic acid **f** to afford **1** and **3** after chromatography column. Treatment of compound **5** with methansulfonyl chloride in presence of TEA and pyridine at rt overnight gave the compound **2**.



**Scheme 20** Synthesis of Compounds 1-5. Reagents and reaction conditions: I) formamidine acetate salt, 2-methoxyethanol dry, 130°C, overnight. II) LiOH.H<sub>2</sub>O, 2-propanol, H<sub>2</sub>O, 75°C, 1h. III) SO<sub>2</sub>Cl<sub>2</sub>, DMF, 80°C, 2h, crude product. IV) NH<sub>4</sub>OH 28-30% basis, in EtOAc, rt, 2h. V) 4-(2-Boc-aminoethyl)piperidine, DIEA, CH<sub>3</sub>CN, reflux, 2h. VI) TFA, CH<sub>2</sub>Cl<sub>2</sub>, rt, overnight. VII) 5-(ethylcarbamoyl)thiophene-2-carboxylic acid **e**, HATU, DIEA, DMF, rt, overnight. VIII) TEA, Pyridine, CH<sub>3</sub>SO<sub>2</sub>Cl, 0°C-rt, overnight. IX) 5-(tert-butoxycarbonyl)thiophene-2-carboxylic acid **f**, HATU, DIEA, DMF, rt, overnight. X) TFA, CH<sub>2</sub>Cl<sub>2</sub>, rt, overnight.



**Scheme 21** Synthesis of compounds 6-7. Reagents and reaction conditions: **XI**) 4-(Boc-aminomethyl)piperidine, DIEA, CH<sub>3</sub>CN, reflux, 2h. **XII**) TFA, CH<sub>2</sub>Cl<sub>2</sub>, rt, overnight.

### 3.6 SIRT6 Inhibitor *in vitro* test: HPLC Assay

The compounds affinity with SIRT6 is measured using a SIRT6 Inhibitor *in vitro* test, specifically a HPLC assay. The HPLC-based Deacetylase Assay relies on the separation of substrates and products of the deacetylase reaction by a reversed-phase HPLC. Quenched reaction mixtures are injected onto a C18 column and, using a gradient of increased levels of organic solvent, substrates, products, and enzyme can be resolved. 25  $\mu\text{M}$  of inhibitors and 3 $\mu\text{M}$  of SIRT6 are mixed and pre-incubated in a 37°C water bath for 15 min, then 25 $\mu\text{M}$  of Myr-H3K9 is added and the reaction can finally take place. After 1 hour, the reaction is quenched by the addition of a quantity of TFA to the final concentration of 1%. Quenched samples are kept on ice or stored at the temperature of -20°C if they are not immediately injected onto the HPLC column. Next, samples are injected onto a reversed-phase HPLC column (e.g., a Vydac C18 column) to resolve substrates and products. A 100- $\mu\text{l}$  loop is typically used for the injections and the flow rate is set to 1 ml/min. After injection, the system is run isocratically with solvent A (0.05% TFA/H<sub>2</sub>O) for 1 minute followed by increasing levels of solvent B (0.02% TFA in acetonitrile). The gradient used for each assay may vary depending on the type of peptide substrate used. Following each run, the column is washed with 100% B for 3–5 column volumes followed by reequilibration with solvent A for 3–5 column volumes. Elution of substrates and products is monitored by measuring the absorbance at 214 nm (to monitor all substrates and products) or at 260 nm (to specifically monitor nicotinamide, NAD<sup>+</sup>, and O-AADPr). The areas of the peaks are integrated for quantification. To calculate the percentage of deacetylation, the area of the deacetylated peptide peak is compared to the combined areas of the acetylated and deacetylated peptide peaks. Because a known amount of acetylated peptide is used, the percentage of the deacetylation is then used to determine the amount of deacetylated product formed over the particular time of the assay, to obtain an initial rate. The results of this first test are shown in the graphs depicted in **Table 4**, which report the percentage of NAD<sup>+</sup>, consumed by the SIRT6 defatty-acylation activity, against the synthesized compounds. Compound **1** is the only product showing a low percentage of consumed NAD<sup>+</sup> and consequently able to bind and reduce the SIRT6 activity. On the other hand, nearly all the other compounds appear to increase SIRT6 activity, possibly due to the absence of a side chain (in the case of compounds **4-5-6-7**) as can be noticed in **Figure 39**. Focusing on compound **2**, it has the polar sulfonamide group which is substantially different from the thiophene of compound **1**. Finally, concerning compound **3**, it has the carboxyl acid as substituent of the thiophene, and as a consequence it generates different interactions. Beyond the synthesized compounds, the graphs plot a positive control (Ctrl), chosen ad-hoc to yield 100% NAD<sup>+</sup> consume, and the Thiomyristoyl peptide (TM3) which reduces SIRT6 activity by a 50% factor [152]. The main reason why TM3 has such a positive effect is because it acts using a fundamentally different mechanism, in that it forms a stalled covalent intermediate with NAD<sup>+</sup> in the sirtuin active sites and inhibits SIRT6 as a direct effect [152].

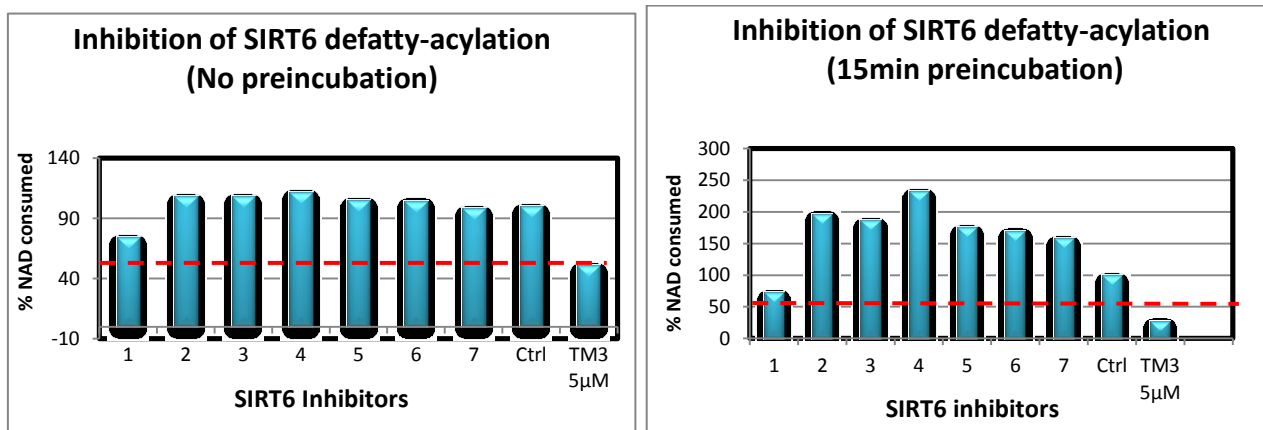


**Table 4** Test in vitro HPLC

In the light of the above results, the docking experiments have been performed in order to reproduce the binding mode of compound **1** to SIRT6, demonstrating, for the first time, the activity of compound **1** on SIRT6. As a result, it has been observed that compound **1** is able to take on many different isoenergetic poses in the binding sites of SIRT6, which are the nicotinamide C and substrate binding pockets. In order to identify one “favourite” (in terms of thermodynamics) pose (**Figure 40**), molecular dynamic studies have been carried out. As shown in **Figure 40**, compound **1** sits in the substrate binding pocket where it is involved in the formation of hydrogen bonds with the aminoacid residues left in the pocket.

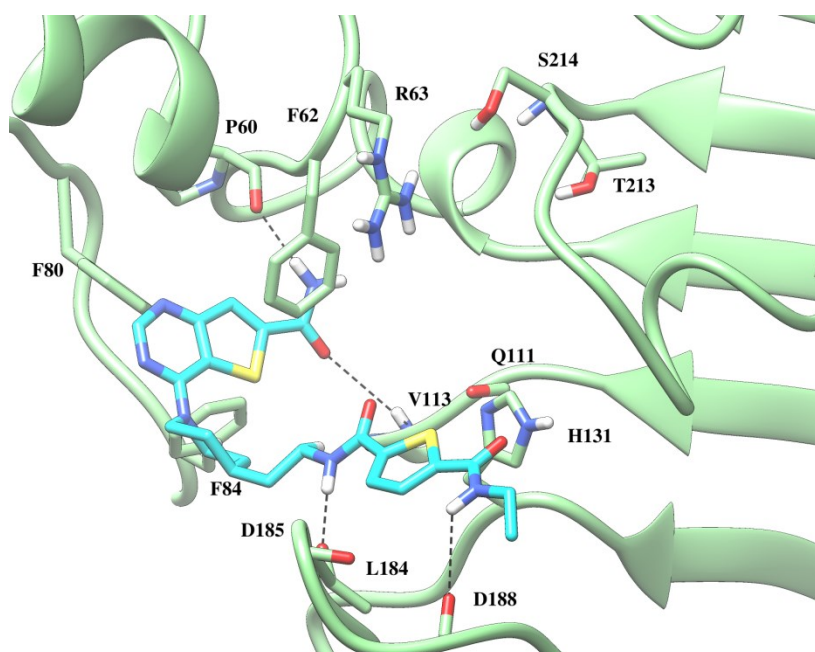


**Figure 40** Possible conformation of the compound **1** in SIRT6

### 3.7 Future Perspectives

Based on the lack of small molecule inhibitors of SIRT6 in the literature, the main contribution of this work has been to synthesize and test the pan inhibitor **1** on SIRT6 and to identify, for the first time, its ability to bind it and reduce its deacetylation activity. The identification of the compound **1** as one of the first small molecule SIRT6 inhibitors, may represent the starting point for future structure-activity relationship and lead optimization studies. As future developments, more docking experiments may be performed in order to explore possible changes in the chemical structure of compound **1**. As an example, changing the ethylamide substituent on the thiophene present in compound **1** to chains of different lengths, or to different groups with similar physicochemical properties could be a meaningful way to proceed. In addition, the spacer ethylpiperidine and the core thieno[3,2-d]pyrimidine-6-carboxamide could be replaced with other groups. In any case molecular studies could be an important tool to identify novel SIRT6 small molecule inhibitors which could find significant applications in cancer treatment by targeting several aspects of cancer pathophysiology and contributing to enhance the efficacy of currently available therapeutics.

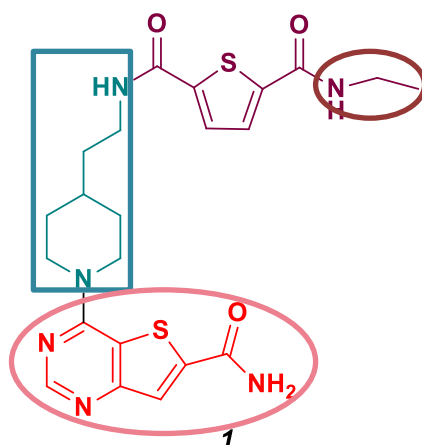


**Figure 41** Changes in the chemical structure of compound **1**

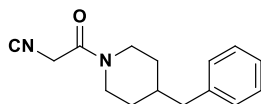
## Chapter 4 – Experiments

### 4.1 Part I : Synthesis of Aryl- $\alpha$ -ketoamide Amides

#### General information

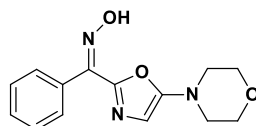
Commercially available reagents and solvents were used without further purification. Dichloromethane was dried by distillation from P2O5 and stored over activated molecular sieves (4 Å). When necessary, the reactions were performed in oven-dried glassware under a positive pressure of dry nitrogen. Melting points were determined in open glass capillaries and are uncorrected. All the compounds were characterized by IR, <sup>1</sup>H and <sup>13</sup>C APT NMR were recorded on a 300 MHz. Mass spectrometry was equipped with an ESI source and an ion trap detector. HRMS were recorded on ORBITRAP mass spectrometer equipped with an ESI source. Chemical shifts ( $\delta$ ) are reported in part per million (ppm) relative to the residual solvent peak. Column chromatography was performed on silica gel (Merck Kieselgel 70-230 mesh ASTM) using the reported eluents. Thin layer chromatography (TLC) was carried out on 5 x 20 cm plates with a layer thickness of 0.25 mm (Silica gel 60 F254). When necessary, they were developed with KMnO4. Elemental analysis (C, H, N) of all the new compounds were within  $\pm$  0.4% of the calculated values. Chloroximes **19** and **22-29** are not new, and they were prepared following literature procedure [25]. Isocyanoacetamides **20** and **33-36** were prepared following Domling's procedure [26], while isocyanoacetamides 30-32 were prepared following Zhu's procedure [27].

*Synthesis of 4-Benzyl-1-(isocyanoacetyl)piperidine (37)* Methyl isocyanate (1 equiv) was reacted with 4-benzylpiperidine (1 equiv) overnight under neat conditions. The solution was evaporated and the crude was purified by column chromatography Hex/EtOAc 7:3 to give 37 as amorphous solid ( yield 75%): <sup>1</sup>H NMR (400 MHz, CDCl3)  $\delta$  7.26-7.09 (m, 5H), 4.45 (br d, 1H), 4.24 (br d, 2H), 3.45 (br d, 1H), 2.93 (br t, 1H), 2.51-2.49 (m, 3H), 1.73-1.64 (m, 3H), 1.17-1.10 (m, 2H); <sup>13</sup>C NMR (75 MHz, CDCl3)  $\delta$  160.7, 160.4, 139.7, 129.1, 128.3, 126.1, 45.6, 44.6, 42.8, 42.6, 37.7, 32.0, 31.3; HRMS (ESI) m/z (M+H)<sup>+</sup> calcd for C<sub>15</sub>H<sub>18</sub>N<sub>2</sub>O 242.1419, found 242.1422

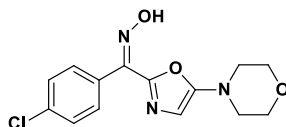


*General Preparation of 1,3-Oxazol-2-oximes (21, 38-54).* The chlorooxime (1 equiv) was dissolved in dry dichloromethane, and  $\alpha$ -isocyanoacetamide (1 equiv) was added dropwise or portionwise at room temperature. Finally, TEA (1 equiv) was added dropwise (the reaction is slightly exothermic and on a large scale the addition shouldn't be done at 0 °C), and the reaction was stirred at room temperature under a nitrogen atmosphere until all the chlorooxime was consumed (typically 2-3 h as judged by TLC). The reaction mixture was concentrated under reduced pressure, and the crude material was purified by column chromatography.

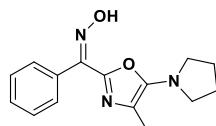
*(Z)*-(5-Morpholinooxazol-2-yl)phenylmethanone Oxime (**21**). Starting material: chlorooxime 150 mg (0.96 mmol), isocyanoacetamide 148 mg (0.96 mmol). The crude material was purified by column chromatography (PE/EtOAc 7:3) to give 195 mg of product as yellow solid (yield 74%): <sup>1</sup>H NMR (300 MHz, CDCl<sub>3</sub>) δH 7.66–7.62 (m, 2H), 7.44–7.40 (m, 3H), 6.26 (br s, 1H), 3.78 (br t, 4H), 3.16 (br t, 4H); <sup>13</sup>C NMR (75 MHz, CDCl<sub>3</sub>) δC 156.2, 146.9, 141.9, 133.0, 129.5, 128.4 (2C), 101.5, 65.8, 47.3; HRMS (ESI) m/z (M + Na)<sup>+</sup> calcd for C<sub>14</sub>H<sub>15</sub>N<sub>3</sub>NaO<sub>3</sub> 296.1011, found 296.1012.



*(Z)*-(4-Chlorophenyl)(5-morpholinooxazol-2-yl)methanone Oxime (**38**). Starting material: chlorooxime 150 mg (0.79 mmol), isocyanoacetamide 122 mg (0.79 mmol). The crude material was purified by column chromatography (PE/EtOAc 6:4) to give 187 mg of product as a yellow solid (yield 78%): <sup>1</sup>H NMR (300 MHz, CDCl<sub>3</sub>) δH 7.60–7.56 (m, 2 H, AA' XX' ), 7.44–7.36 (m, 2 H, AA' XX' ), 6.26 (br s, 1H), 3.80–3.77 (m, 4H), 3.18–3.15 (m, 4H); <sup>13</sup>C NMR (75 MHz, CDCl<sub>3</sub>) δC 156.2, 146.5, 141.0, 135.6, 131.5, 129.7, 128.7, 101.6, 65.7, 47.2; HRMS (ESI) m/z (M + H)<sup>+</sup> calcd for C<sub>14</sub>H<sub>14</sub>ClN<sub>3</sub>O<sub>3</sub> 307.0724, found 307.0727.



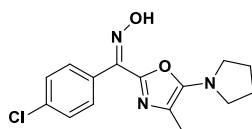
*(Z)*-(4-Methyl-5-(pyrrolidin-1-yl)oxazol-2-yl)phenylmethanone Oxime (**39**). Starting material: chlorooxime 150 mg (0.96 mmol), isocyanoacetamide 147 mg (0.96 mmol). The crude material was purified by column chromatography (PE/EtOAc 7:3) to give 180 mg of product as yellow solid (yield 69%): <sup>1</sup>H NMR (300 MHz, CDCl<sub>3</sub>) δH 7.69–7.66 (m, 2H), 7.40–7.38 (m, 3H), 3.42–3.38 (m, 4H), 2.27 (s, 3H), 1.95–1.91 (m, 4H); <sup>13</sup>C NMR (75 MHz, CDCl<sub>3</sub>) δC 150.2, 143.9, 141.4, 133.3, 129.2, 128.4, 128.3, 108.4, 48.8, 25.4, 11.7; HRMS (ESI) m/z (M + H)<sup>+</sup> calcd for C<sub>15</sub>H<sub>17</sub>N<sub>3</sub>O<sub>2</sub> 271.1321, found 271.1321.



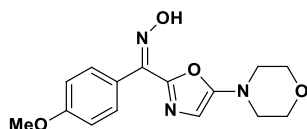
*(Z)*-(4-Chlorophenyl)(4-methyl-5-(pyrrolidin-1-yl)oxazol-2-yl)- methanone Oxime (**40**). Starting material: chlorooxime 150 mg (0.79 mmol), isocyanoacetamide 120 mg (0.79 mmol). The crude material was purified by column chromatography (PE/EtOAc 6:4) to give 190 mg of product as orange solid (yield 79%): <sup>1</sup>H NMR (300 MHz, bCDCl<sub>3</sub>) δH 7.65–7.62 (m, 2H, AA' XX' ), 7.40–7.37 (m, 2H, AA' XX' ), 3.45–3.43 (m, 4H), 2.29



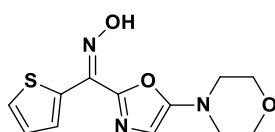
(s, 3H), 1.98–1.92 (m, 4H);  $^{13}\text{C}$  NMR (75 MHz,  $\text{CDCl}_3$ )  $\delta\text{C}$  150.3, 143.7, 140.5, 135.3, 131.9, 129.8, 128.6, 108.5, 48.9, 25.5, 11.7; HRMS (ESI)  $m/z$  ( $\text{M} + \text{H}$ ) $^+$  calcd for  $\text{C}_{15}\text{H}_{16}\text{ClN}_3\text{O}_2$  305.0931, found 305.0933.



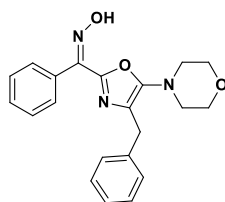
*(Z)*-(4-Methoxyphenyl)(5-morpholinooxazol-2-yl)methanone Oxime (**41**). Starting material: chlorooxime 150 mg (0.81 mmol), isocyanoacetamide 125 mg (0.81 mmol). The crude material was purified by column chromatography (PE/EtOAc 5:5) to give 196 mg of product as yellow solid (yield 80%):  $^1\text{H}$  NMR (300 MHz,  $\text{CDCl}_3$ )  $\delta\text{H}$  7.60–7.56 (m, 2H, AA' XX' ), 6.97–6.91 (m, 2H, AA' XX' ), 6.25 (br s, 1H), 3.81–3.78 (m, 7H), 3.17–3.15 (m, 4H);  $^{13}\text{C}$  NMR (75 MHz,  $\text{CDCl}_3$ )  $\delta\text{C}$  160.6, 156.1, 147.1, 141.5, 129.7, 125.5, 113.8, 101.5, 65.8, 55.4, 47.3; HRMS (ESI)  $m/z$  ( $\text{M} + \text{Na}$ ) $^+$  calcd for  $\text{C}_{15}\text{H}_{17}\text{N}_3\text{NaO}_4$  326.1117, found 326.1120.



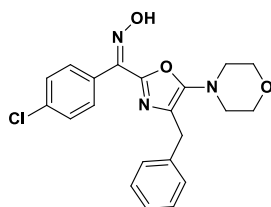
*(E)*-(5-Morpholinooxazol-2-yl)(thiophene-2-yl)methanone Oxime (**42**). Starting material: chlorooxime 150 mg (0.93 mmol), isocyanoacetamide 143 mg (0.93 mmol). The crude material was purified by column chromatography (PE/EtOAc 6:4) to give 108 mg of product as brown solid (yield 42%):  $^1\text{H}$  NMR (300 MHz,  $\text{CDCl}_3$ )  $\delta\text{H}$  7.60–7.58 (m, 1H), 7.36–7.34 (m, 1H), 7.10–7.06 (m, 1H), 6.26 (br s, 1H), 3.87–3.83 (m, 4H), 3.28–3.26 (m, 4H);  $^{13}\text{C}$  NMR (75 MHz,  $\text{CDCl}_3$ )  $\delta\text{C}$  156.2, 146.1, 137.1, 135.6, 127.6, 127.3, 127.2, 101.4, 65.8, 47.3; HRMS (ESI)  $m/z$  ( $\text{M} + \text{H}$ ) $^+$  calcd for  $\text{C}_{12}\text{H}_{13}\text{N}_3\text{O}_3\text{S}$  279.0678, found 279.0677.



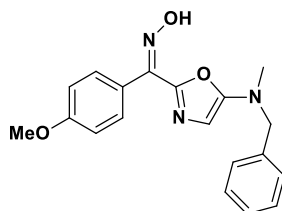
*(Z)*-(4-Benzyl-5-morpholinooxazol-2-yl)phenylmethanone Oxime (**43**). Starting material: chlorooxime 150 mg (0.96 mmol), isocyanoacetamide 236 mg (0.96 mmol). The crude material was purified by column chromatography (PE/EtOAc 7:3) to give 169 mg of product as yellow oil (yield 55%). Mixture of E/Z isomers; signals are referred to the main isomer:  $^1\text{H}$  NMR (300 MHz,  $\text{CDCl}_3$ )  $\delta\text{H}$  7.69–7.66 (m, 2H), 7.45–7.39 (m, 3H), 7.35–7.21 (m, 5H), 3.94 (s, 2H), 3.75–3.71 (m, 4H), 3.10–3.06 (m, 4H);  $^{13}\text{C}$  NMR (75 MHz,  $\text{CDCl}_3$ )  $\delta\text{C}$  151.2, 148.3, 141.9, 138.3, 132.8, 129.5, 128.7, 128.4, 128.3, 128.0, 126.7, 121.4, 66.5, 49.9, 31.80; HRMS (ESI)  $m/z$  ( $\text{M} + \text{H}$ ) $^+$  calcd for  $\text{C}_{21}\text{H}_{21}\text{N}_3\text{O}_3$  363.1583, found 363.1583.



*(Z)*-(4-Benzyl-5-morpholinooxazol-2-yl)(4-chlorophenyl)-methanone Oxime (**44**). Starting material: chlorooxime 150 mg (0.79 mmol), isocyanoacetamide 193 mg (0.79 mmol). The crude material was purified by column chromatography (PE/EtOAc 7:3) to give 200 mg of product as white solid (yield 64%). Mixture of E/Z isomers, signals are referred to the main isomer:  $^1\text{H}$  NMR (300 MHz,  $\text{CDCl}_3$ )  $\delta$ H 7.65–7.58 (m, 2H), 7.43–7.36 (m, 2H), 7.32–7.18 (m, 5H), 3.96 (s, 2H), 3.75–3.67 (m, 4H), 3.09–3.06 (m, 4H);  $^{13}\text{C}$  NMR (75 MHz,  $\text{CDCl}_3$ )  $\delta$ C 151.3, 147.7, 141.2, 138.3, 135.5, 131.4, 129.6, 128.8, 128.59, 128.32, 126.65, 121.3, 66.6, 49.8, 31.81; HRMS (ESI)  $m/z$  (M + H)<sup>+</sup>calcd for  $\text{C}_{21}\text{H}_{20}\text{ClN}_3\text{O}_3$  397.1193, found 397.1197.

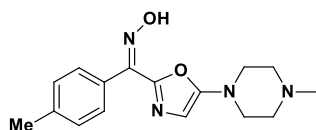


*(Z)*-(5-(Benzylmethylamino)oxazol-2-yl)(4-methoxyphenyl)-methanone Oxime (**45**). Starting material: chlorooxime 150 mg (0.81 mmol), isocyanoacetamide 152 mg (0.81 mmol). The crude material was purified by column chromatography (PE/EtOAc 7:3) to give 210 mg product as yellow solid (yield 77%):  $^1\text{H}$  NMR (300 MHz,  $\text{CDCl}_3$ )  $\delta$ H 7.61–7.56 (m, 2H, AA' XX'), 7.37–7.27 (m, 3H), 7.25–7.19 (m 2H), 6.94–6.90 (m, 2H, AA'XX'), 6.15 (br s, 1H), 4.37 (s, 2H), 3.85, (s, 3H);  $^{13}\text{C}$  NMR (75 MHz,  $\text{CDCl}_3$ )  $\delta$ C 160.5, 156.1, 145.8, 141.3, 136.1, 129.7, 128.8, 127.9, 127.7, 125.6, 113.7, 55.5, 55.3, 36.6; HRMS (ESI)  $m/z$  (M + H)<sup>+</sup> calcd for  $\text{C}_{19}\text{H}_{19}\text{N}_3\text{O}_3$  337.1426, found 337.1426.

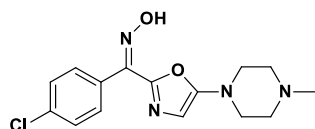


*(Z)*-(5-(4-Methylpiperazin-1-yl)oxazol-2-yl)(p-tolyl)methanone Oxime (**46**). Starting materials: chlorooxime 150 mg (0.88 mmol), isocyanoacetamide 147 mg (0.88 mmol). The crude material was purified by column chromatography (DCM/MeOH 95:5) to give 232 mg product as yellow solid (88% yield):  $^1\text{H}$  NMR (400 MHz,  $\text{CDCl}_3$ )  $\delta$ H 7.56 (d, J = 7.8 Hz, 2H), 7.23 (m, 2H) partially overlapped to the solvent, 6.23 (s, 1H), 3.22 (br t,

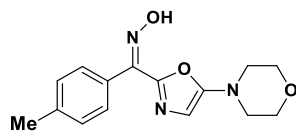
4H), 2.50 (br t, 4H), 2.39 (s, 3H), 2.33 (s, 3H);  $^{13}\text{C}$  NMR (100 MHz,  $\text{CDCl}_3$ )  $\delta\text{C}$  156.2, 146.7, 142.0, 139.3, 130.4, 128.9, 128.1, 101.4, 53.6, 46.9, 46.0, 21.3; HRMS (ESI)  $m/z$  ( $\text{M} + \text{H}$ ) $^+$  calcd for  $\text{C}_{16}\text{H}_{20}\text{N}_4\text{O}_2$  300.1586, found 300.1590.



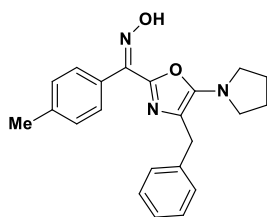
*(Z)*-(4-Chlorophenyl)-(5-(4-methylpiperazin-1-yl)oxazol-2-yl)-methanone Oxime (**47**). Starting materials: chlorooxime 150 mg (0.79 mmol), isocyanoacetamide 132 mg (0.79 mmol). The crude material was purified by column chromatography ( $\text{DCM}/\text{MeOH}$  97:3) to give the product as yellow solid (195 mg, 77% yield):  $^1\text{H}$  NMR (400 MHz,  $\text{CDCl}_3$ )  $\delta\text{H}$  7.57–7.55 (m, 2H, AA'XX'), 7.36–7.34 (m, 2H, AA'XX'), 6.23 (s, 1H), 3.23 (br t, 4H), 2.52 (br t, 4H), 2.33 (s, 3H);  $^{13}\text{C}$  NMR (100 MHz,  $\text{CDCl}_3$ )  $\delta\text{C}$  156.3, 146.2, 141.2, 135.3, 131.9, 129.5, 128.5, 101.7, 53.6, 46.9, 46.0; HRMS (ESI)  $m/z$  ( $\text{M} + \text{H}$ ) $^+$  calcd for  $\text{C}_{15}\text{H}_{17}\text{ClN}_4\text{O}_2$  320.1040, found 320.1042.



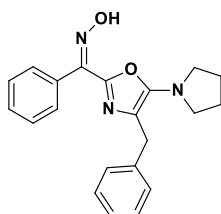
*(Z)*-(5-Morpholinooxazol-2-yl)-p-tolylmethanone Oxime (**48**). Starting materials: chlorooxime 150 mg (0.88 mmol), isocyanoacetamide 136 mg (0.88 mmol). The crude material was purified by column chromatography ( $n\text{-hexane}/\text{AcOEt}$  7:3) to give the product as yellow solid (197 mg, 78% yield):  $^1\text{H}$  NMR (400 MHz,  $\text{CDCl}_3$ )  $\delta\text{H}$  7.54 (m, 2H, AA'XX'), 7.23 (m, 2H, AA'XX'), 6.26 (s, 1H), 3.80 (m, 4H), 3.17 (m, 4H), 2.39 (s, 3H);  $^{13}\text{C}$  NMR (100 MHz,  $\text{CDCl}_3$ )  $\delta\text{C}$  156.0, 147.0, 141.7, 139.4, 130.0, 129.0, 128.2, 101.3, 65.7, 47.2, 21.3; HRMS (ESI)  $m/z$  ( $\text{M} + \text{H}$ ) $^+$  calcd for  $\text{C}_{15}\text{H}_{17}\text{N}_3\text{O}_3$  287.1270, found 287.1268.



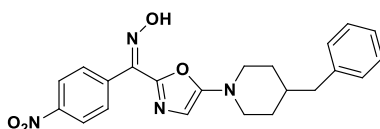
*(4-Benzyl-5-(pyrrolidin-1-yl)oxazol-2-yl)-p-tolylmethanone Oxime* (**49**). Starting materials: chlorooxime 150 mg (0.88 mmol), isocyanoacetamide 202 mg (0.88 mmol). The crude material was purified by column chromatography ( $n\text{-hexane}/\text{AcOEt}$  7:3) to give the product as yellow solid (168 mg, 53% yield). Mixture of E/Z isomers, signals are referred to the main isomer:  $^1\text{H}$  NMR (400 MHz,  $\text{CDCl}_3$ )  $\delta\text{H}$  7.61 (m, 2H, AA'XX'), 7.31–7.22 (m, 7H) partially overlapped to the solvent, 3.99 (s, 2H), 3.42 (br t, 4H), 2.40 (s, 3H), 1.93 (br t, 4H);  $^{13}\text{C}$  NMR (100 MHz,  $\text{CDCl}_3$ )  $\delta\text{C}$  150.3, 144.3, 141.3, 140.0, 139.1, 130.3, 128.9, 128.6, 128.2, 128.1, 126.3, 110.7, 48.8, 31.8, 25.3, 21.3; HRMS (ESI)  $m/z$  ( $\text{M} + \text{H}$ ) $^+$  calcd for  $\text{C}_{22}\text{H}_{23}\text{N}_3\text{O}_2$  361.1790, found 361.1793.



*(Z)*-(4-Benzyl-5-(pyrrolidin-1-yl)oxazol-2-yl)phenylmethanone Oxime (**50**). Starting materials: chlorooxime 150 mg (0.96 mmol), isocynoacetamide 219 mg (0.96 mmol). The crude material was purified by column chromatography (n-hexane/AcOEt 7:3) to give the product as yellow solid (233 mg, 70% yield). Mixture of E/Z isomers, signals are referred to the main isomer:  $^1\text{H}$  NMR (400 MHz,  $\text{CDCl}_3$ )  $\delta$  7.71 (br d, 2H), 7.63–7.57 (m, 1H), 7.43–7.41 (m, 3H), 7.33–7.20 (m, 4H) partially overlapped to the solvent, 4.00 (s, 2H), 3.41 (br t, 4H), 1.92 (br t, 4H);  $^{13}\text{C}$  NMR (100 MHz,  $\text{CDCl}_3$ )  $\delta$  150.3, 144.1, 141.4, 140.0, 133.2, 129.1, 128.6, 128.3, 128.2, 128.1, 126.3, 110.7, 48.7, 31.8, 25.3; HRMS (ESI)  $m/z$  (M + H)<sup>+</sup> calcd for  $\text{C}_{21}\text{H}_{21}\text{N}_3\text{O}_2$  347.1634, found 347.1637.

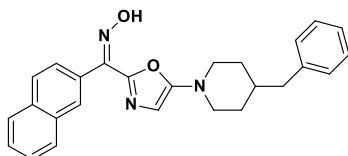


*(Z)*-(5-(4-Benzylpiperidin-1-yl)oxazol-2-yl)(4-nitrophenyl)-methanone Oxime (**51**). Starting materials: chlorooxime 150 mg (0.75 mmol), isocynoacetamide 182 mg (0.75 mmol). The crude material was purified by column chromatography (n-hexane/AcOEt 9:1) to give the product as bright yellow solid (97 mg, 32% yield).  $^1\text{H}$  NMR (400 MHz,  $\text{CDCl}_3$ )  $\delta$  8.28 (d,  $J = 8.7$  Hz, 2H), 7.89 (d,  $J = 8.6$  Hz, 2H), 7.29–7.12 (m, 6H), 6.23 (s, 1H), 3.54 (br d, 2H), 2.83 (br t, 2H), 2.58 (br d, 2H), 1.77–1.73 (m, 3H), 1.39–1.33 (m, 2H);  $^{13}\text{C}$  NMR (100 MHz,  $\text{CDCl}_3$ )  $\delta$  156.5, 148.2, 145.2, 139.9, 139.5, 139.2, 129.1, 129.0, 128.3, 126.1, 123.5, 100.7, 47.5, 42.8, 37.3, 30.7; HRMS (ESI)  $m/z$  (M + H)<sup>+</sup> calcd for  $\text{C}_{22}\text{H}_{22}\text{N}_4\text{O}_4$  406.1641, found 406.1646.

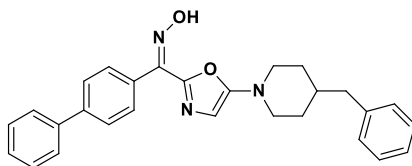


*(Z)*-(5-(4-Benzylpiperidin-1-yl)oxazol-2-yl)(naphthalen-2-yl)-methanone Oxime (**52**). Starting materials: chlorooxime 150 mg (0.73 mmol), isocynoacetamide 178 mg (0.73 mmol). The crude material was purified by column chromatography (n-hexane/AcOEt 9:1) to give the product as yellow solid (177 mg, 59% yield):  $^1\text{H}$  NMR (400 MHz,  $\text{CDCl}_3$ )  $\delta$  8.18 (s, 1H), 7.89–7.85 (m, 3H), 7.79 (br d, 1H), 7.52–7.50 (m, 2H), 7.30–7.25

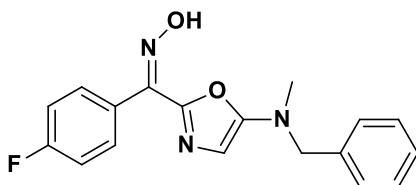
(m, 3H), 7.21 (br d, 1H), 7.13 (br d, 2H), 6.23 (s, 1H), 3.54 (br d, 2H), 2.79 (br t, 2H), 2.56 (br d, 2H), 1.72–1.70 (m, 3H), 1.38–1.29 (m, 2H);  $^{13}\text{C}$  NMR (100 MHz,  $\text{CDCl}_3$ )  $\delta\text{C}$  156.5, 146.2, 141.7, 139.7, 133.6, 133.0, 130.5, 129.1, 128.5, 128.3, 128.2, 127.9, 127.6, 126.8, 126.4, 126.1, 125.6, 100.6, 47.5, 42.8, 37.3, 30.7; HRMS (ESI)  $m/z$  ( $\text{M} + \text{H}$ ) $^+$  calcd for  $\text{C}_{26}\text{H}_{25}\text{N}_3\text{O}_2$  411.1947, found 411.1950.



*(Z)*-[1,1'-Biphenyl]-4-yl(5-(4-benzylpiperidin-1-yl)oxazol-2-yl)-methanone Oxime (**53**). Starting materials: chlorooxime 150 mg (0.65 mmol), isocyanoacetamide 158 mg (0.73 mmol). The crude material was purified by column chromatography (n-hexane/AcOEt 9:1) to give the product as yellowish solid (142 mg, 50% yield):  $^1\text{H}$  NMR (400 MHz,  $\text{CDCl}_3$ )  $\delta\text{H}$  7.76 (br d, 2H), 7.67–7.63 (m, 4H), 7.47–7.44 (m, 3H), 7.38 (br d, 1H), 7.31–7.27 (m, 2H), 7.22 (br d, 1H), 7.14 (br d, 2H), 6.22 (s, 1H), 3.56 (br d, 2H), 2.81 (br t, 2H), 2.58 (br d, 2H), 1.75–1.72 (m, 3H), 1.41–1.32 (m, 2H);  $^{13}\text{C}$  NMR (100 MHz,  $\text{CDCl}_3$ )  $\delta\text{C}$  156.5, 146.2, 142.0, 141.4, 140.3, 139.7, 132.0, 129.1, 128.8, 128.7, 128.3, 127.6, 127.1, 127.0, 126.1, 100.6, 47.6, 42.9, 37.4, 30.7; HRMS (ESI)  $m/z$  ( $\text{M} + \text{H}$ ) $^+$  calcd for  $\text{C}_{26}\text{H}_{25}\text{N}_3\text{O}_2$  411.1947, found 411.1948.

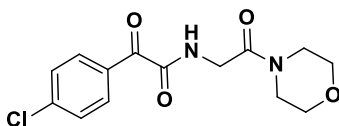


*(Z)*-(5-(Benzylmethylamino)oxazol-2-yl)(4-fluorophenyl)-methanone Oxime (**54**). Starting material: chlorooxime 150 mg (0.87 mmol), isocyanoacetamide 163 mg (0.81 mmol). The crude material was purified by column chromatography (PE/EtOAc 7:3) to give 198 mg product as yellow solid (yield 70%). Mixture of E/Z isomers, signals are referred to the main isomer:  $^1\text{H}$  NMR (300 MHz,  $\text{CDCl}_3$ )  $\delta\text{H}$  7.65–7.53 (m, 3H), 7.37–7.19 (m, 3H), 7.10–7.02 (m, 3H), 6.18 (br s, 1H), 4.38 (s, 2H), 2.90 (s, 3H);  $^{13}\text{C}$  NMR (75 MHz,  $\text{CDCl}_3$ )  $\delta\text{C}$  164.9, 161.7, 156.2, 140.8, 136.0, 131.8, 130.3, 128.7, 128.6, 127.8, 115.4, 99.5, 55.3, 36.6; HRMS (ESI)  $m/z$  ( $\text{M} + \text{H}$ ) $^+$  calcd for  $\text{C}_{18}\text{H}_{16}\text{FN}_3\text{O}_2$  325.1227, found 325.1229.

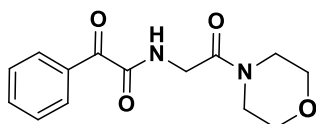


*General Preparation of Aryl- $\alpha$ -ketoamide Amides 56–73.* The 1,3-oxazol-2-oxime was dissolved in THF (0.8 M), concentrated HCl (1 equiv; 2 equiv for oxazoles 46 and 47) was added, and the reaction was stirred at room temperature for 30 min. The reaction mixture was diluted with water and extracted with EtOAc ( $\times 3$ ). The organic phase was washed with NaHCO<sub>3</sub> standard solution ( $\times 1$ ) and brine ( $\times 1$ ), dried over sodium sulfate, filtered, and concentrated under reduced pressure. The crude was dissolved in acetonitrile (0.25 M), and water (55 equiv) and copper(II) chloride (2 equiv) were added. The solution was stirred for 1 h at 75 °C. The reaction mixture was diluted with water and extracted with EtOAc ( $\times 2$ ). The organic phase was washed with brine ( $\times 1$ ), dried over sodium sulfate, filtered, and concentrated under reduced pressure, and the crude material was purified by column chromatography.

*2-(4-Chlorophenyl)-N-(2-morpholino-2-oxoethyl)-2-oxoacetamide (56).* Starting material: 1,3-oxazol-2-oxime 38 150 mg (0.49 mmol). The crude material was purified by column chromatography (PE/ EtOAc 2:8) to give 100 mg of product as white solid (yield 66%): <sup>1</sup>H NMR (300 MHz, CDCl<sub>3</sub>)  $\delta$ H 8.21–8.18 (m, 2H, AA' XX' ), 8.03 (br s, NH), 7.41–7.38 (m, 2H, AA' XX' ), 4.12 (d, J = 4.6 Hz, 2H), 3.65– 3.59 (m, 6H), 3.44.3.41 (m, 2H); <sup>13</sup>C NMR (75 MHz, CDCl<sub>3</sub>)  $\delta$ C 185.8, 165.8, 161.9, 141.1, 132.4, 131.6, 128.9, 66.6, 66.3, 44.9, 42.4, 40.9; m/z 311 (M + H)<sup>+</sup>; IR  $\nu_{\text{max}}$ /cm<sup>-1</sup> (KBr) 3239, 3096, 1670, 1652, 1533, 1465, 1246, 855; mp 122–123 °C. Anal. Calcd for C<sub>14</sub>H<sub>15</sub>ClN<sub>2</sub>O<sub>4</sub>: C, 54.12; H, 4.87; N, 9.02. Found: C, 53.95; H, 4.80; N, 9.31.

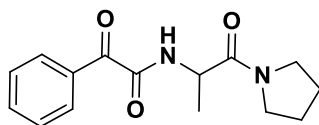


*N-(2-Morpholino-2-oxoethyl)-2-oxo-2-phenylacetamide (57).* Starting materials: 1,3-oxazol-2-oxime 21 150 mg (0.55 mmol). The crude material was purified by column chromatography (n-hexane/ EtOAc 5:5) to give the product as yellowish solid (103 mg, 68% yield): <sup>1</sup>H NMR (400 MHz, CDCl<sub>3</sub>)  $\delta$ H 8.28 (br d, 2H), 7.93 (br s, NH), 7.62 (br t, 1H), 7.47 (br t, 2H), 4.18 (d, J = 4.0 Hz, 2H), 3.72– 3.66 (m, 6H), 3.47–3.45 (m, 2H); <sup>13</sup>C NMR (100 MHz, CDCl<sub>3</sub>)  $\delta$ C 187.1, 165.8, 162.2, 134.4, 133.1, 130.9, 128.5, 66.6, 66.3, 44.9, 42.3, 40.8; MS m/z 277 (M + H)<sup>+</sup>; IR  $\nu_{\text{max}}$ /cm<sup>-1</sup> (KBr) 3380, 1687, 1667, 1642, 1505, 1474, 1275, 745; mp 164–165 °C. Anal. Calcd for C<sub>14</sub>H<sub>16</sub>N<sub>2</sub>O<sub>4</sub>: C, 60.86; H, 5.84; N, 10.14. Found: C, 60.95; H, 5.97; N, 10.01.

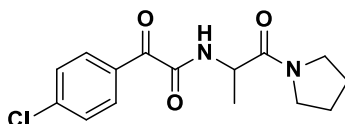


*N-(1-Morpholino-1-oxopropan-2-yl)-2-oxo-2-phenylacetamide (58).* Starting material: 1,3-oxazol-2-oxime 39 150 mg (0.55 mmol). The crude material was purified by column chromatography (PE/EtOAc 3:7) to give 92 mg of product as yellow oil (yield 60%). Mixture of rotamers, signals are referred to the main rotamer: <sup>1</sup>H NMR (300 MHz, CDCl<sub>3</sub>)  $\delta$ H 8.20–8.17 (m, 2H), 8.03 (br d, NH), 7.56–7.38 (m, 3H), 4.80–4.72 (m, 1H), 3.64–3.35 (m, 4H), 1.98–1.78 (m, 4H), 1.39 (d, J = 6.9 Hz, 3H); <sup>13</sup>C NMR (75 MHz, CDCl<sub>3</sub>)  $\delta$ C 187.5, 169.9, 161.6, 134.2, 133.23, 130.9, 128.4, 46.9, 46.4, 46.2, 26.0, 24.1, 17.9; MS m/z 275 (M + H)<sup>+</sup>; IR  $\nu_{\text{max}}$ /cm<sup>-1</sup>

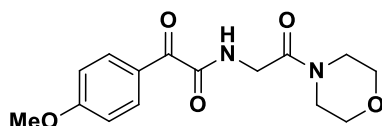
(KBr) 3253, 3062, 1638, 1667, 1510, 1449, 1264, 715. Anal. Calcd for C<sub>15</sub>H<sub>18</sub>N<sub>2</sub>O<sub>3</sub>: C, 65.68; H, 6.61; N, 10.21. Found: C, 65.66; H, 6.65; N, 10.25.



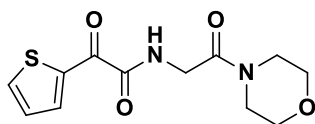
**2-(4-Chlorophenyl)-N-(1-morpholino-1-oxopropan-2-yl)-2-oxoacetamide (59).** Starting material: 1,3-oxazol-2-oxime 40 150 mg (0.49 mmol). The crude material was purified by column chromatography (PE/EtOAc 4:6) to give 80 mg of product as colorless oil (yield 53%): <sup>1</sup>H NMR (300 MHz, CDCl<sub>3</sub>) δH 8.25–8.23 (m, 2H, AA' XX'), 7.97 (br d, NH), 7.43–7.40 (m, 2H, AA' XX'), 4.77–4.72 (m, 1H), 3.66–3.39 (m, 4H), 2.03–1.83 (m, 4H), 1.42 (d, J = 7.0 Hz, 3H); <sup>13</sup>C NMR (75 MHz, CDCl<sub>3</sub>) δC 186.1, 169.9, 161.0, 141.1, 132.6, 131.8, 129.0, 47.1, 46.5, 46.3, 26.2, 24.2, 18.1; MS m/z 309 (M + H)<sup>+</sup>; IR ν<sub>max</sub>/cm<sup>-1</sup> (KBr) 3239, 3062, 1670, 1668, 1586, 1455, 856. Anal. Calcd for C<sub>15</sub>H<sub>17</sub>ClN<sub>2</sub>O<sub>3</sub>: C, 58.35; H, 5.55; N, 9.07. Found: C, 58.23; H, 5.21; N, 9.2.



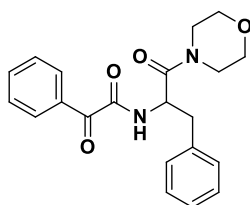
**2-(4-Methoxyphenyl)-N-(2-morpholino-2-oxoethyl)-2-oxoacetamide (60).** Starting material: 1,3-oxazol-2-oxime 41 150 mg (0.49 mmol). The crude material was purified by column chromatography (PE/EtOAc 2:8) to give 70 mg of product as white solid (yield 46%). <sup>1</sup>H NMR (300 MHz, CDCl<sub>3</sub>) δH 8.33–8.8.30 (m, 2H, AA' XX'), 7.97 (br s, NH), 6.94–6.91 (m, 2H, AA' XX'), 4.16 (br d, 2H), 3.87 (s, 3H), 3.71–3.65 (m, 6H), 3.46–4.3 (m, 2H); <sup>13</sup>C NMR (75 MHz, CDCl<sub>3</sub>) δC 185.3, 165.9, 164.8, 162.8, 133.8, 126.3, 114.0, 66.8, 66.4, 55.7, 45.0, 42.4, 41.0; MS m/z 307 (M + H)<sup>+</sup>; IR ν<sub>max</sub>/cm<sup>-1</sup> (KBr) 3349, 3078, 1682, 1647, 1594, 1474, 1257, 861; mp 169–169.5 °C. Anal. Calcd for C<sub>15</sub>H<sub>18</sub>N<sub>2</sub>O<sub>5</sub>: C, 58.82; H, 5.92; N, 9.15. Found: C, 58.93; H, 6.24; N, 9.36.



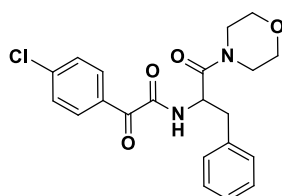
**N-(2-Morpholino-2-oxoethyl)-2-oxo-2-(thiophene-2-yl)acetamide (61).** Starting material: 1,3-oxazol-2-oxime **42** 150 mg (0.54 mmol). The crude material was purified by column chromatography (PE/EtOAc 2:8) to give 85 mg of product as white solid (yield 56%): <sup>1</sup>H NMR (300 MHz, CDCl<sub>3</sub>) δH 8.36 (d, J = 4.0 Hz, 1H), 8.19 (br s, NH), 7.80 (d, J = 4.8 Hz, 1H), 7.18–7.15 (m, 1H), 4.15 (d, J = 4.5 Hz, 2H), 3.71–3.66 (m, 6H), 3.53–3.42 (m, 2H); <sup>13</sup>C NMR (75 MHz, CDCl<sub>3</sub>) δC 177.6, 165.7, 161.0, 138.5, 138.0, 136.9, 128.4, 66.6, 66.40, 42.5, 41.1, 40.7; MS m/z 283 (M + H)<sup>+</sup>; IR ν<sub>max</sub>/cm<sup>-1</sup> (KBr) 3371, 3071, 1691, 1658, 1495, 1359, 1275, 737; mp 193–194 °C. Anal. Calcd for C<sub>12</sub>H<sub>14</sub>N<sub>2</sub>O<sub>4</sub>S: C, 51.05; H, 5.00; N, 9.92. Found: C, 51.34; H, 5.36; N, 10.10.



*N*-(1-Morpholino-1-oxo-3-phenylpropan-2-yl)-2-oxo-2-phenylacetamide (**62**). Starting material: 1,3-oxazol-2-oxime **43** 150 mg (0.41 mmol). The crude material was purified by column chromatography (PE/EtOAc 4:6) to give 76 mg of product as white solid (yield 50%). Mixture of rotamers, signals are referred to the main rotamer:  $^1\text{H}$  NMR (300 MHz,  $\text{CDCl}_3$ )  $\delta$ H 8.21 (d,  $J = 8.2$  Hz, 2H), 7.87 (br d, NH), 7.64–7.59 (br t, 1H), 7.52–7.38 (br t, 2H), 7.34–7.23 (m, 5H), 5.18 (br q, 1H), 3.62–3.44 (m, 6H), 3.16–2.94 (m, 4H);  $^{13}\text{C}$  NMR (75 MHz,  $\text{CDCl}_3$ )  $\delta$ C 187.4, 169.0, 161.6, 135.8, 134.5, 131.0, 129.7, 129.6, 128.8, 128.6, 127.4, 66.4, 66.0, 49.7, 46.1, 42.4, 39.8; MS  $m/z$  367 (M + H)<sup>+</sup>; IR  $\nu_{\text{max}}/\text{cm}^{-1}$  (KBr) 3277, 3027, 1665, 1642, 1524, 1486, 1211; mp 151.5–152 °C. Anal. Calcd for  $\text{C}_{21}\text{H}_{22}\text{N}_2\text{O}_4$ : C, 68.84; H, 6.05; N, 7.65. Found: C, 68.95; H, 6.40; N, 7.34.



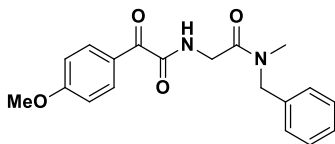
2-(3-Chlorophenyl)-*N*-(1-morpholino-1-oxo-3-phenylpropan-2-yl)-2-oxoacetamide (**63**). Starting material: 1,3-oxazol-2-oxime **44** 150 mg (0.38 mmol). The crude material was purified by column chromatography (PE/EtOAc 5:5) to give 78 mg of product as white solid (yield 52%):  $^1\text{H}$  NMR (300 MHz,  $\text{CDCl}_3$ )  $\delta$ H 8.19 (d,  $J = 8.1$  Hz, 2H), 7.93 (br d, NH), 7.42 (br d, 2H), 7.34–7.22 (m, 5H), 5.16 (br q, 1H), 3.64–3.58 (m, 2H), 3.55–3.25 (m, 4H), 3.14–2.87 (m, 4H);  $^{13}\text{C}$  NMR (75 MHz,  $\text{CDCl}_3$ )  $\delta$ C 185.8, 169.0, 160.9, 141.3, 135.7, 132.6, 131.6, 129.7, 129.0, 128.9, 127.5, 66.5, 66.1, 49.8, 46.1, 42.4, 39.9; MS  $m/z$  401 (M + H)<sup>+</sup>; IR  $\nu_{\text{max}}/\text{cm}^{-1}$  (KBr) 3246, 3064, 1665, 1617, 1586, 1476, 1218, 858; mp 128–129 °C. Anal. Calcd for  $\text{C}_{21}\text{H}_{21}\text{ClN}_2\text{O}_4$ : C, 62.92; H, 5.28; N, 6.99. Found: C, 63.04; H, 5.46; N, 6.74.



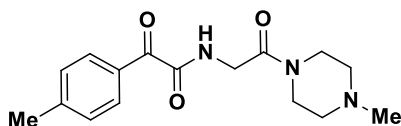
*N*-Benzyl-2-(2-(4-methoxyphenyl)-2-oxoacetamido)-*N*-methylacetamide (**64**). Starting material: 1,3-oxazol-2-oxime **45** 150 mg (0.44 mmol). The crude material was purified by column chromatography (PE/EtOAc



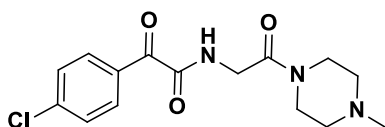
5:5) to give 133 mg of product as colorless oil (yield 88%). Mixture of rotamers, signals are referred to the main rotamer:  $^1\text{H}$  NMR (300 MHz,  $\text{CDCl}_3$ )  $\delta$ H 8.35–8.31 (m, 2H), 8.05 (br s, NH), 7.38–7.14 (m, 5H), 6.94–6.89 (m, 2H), 4.61 (s, 2H), 4.24–4.20 (br t, 2H), 3.85 (s, 3H), 2.92 (s, 3H);  $^{13}\text{C}$  NMR (75 MHz,  $\text{CDCl}_3$ )  $\delta$ C 185.4, 167.4, 164.7, 162.8, 136.4, 133.7, 129.2, 128.8, 127.8, 126.3, 113.9, 55.6, 51.3, 41.3, 33.7; MS  $m/z$  341 ( $\text{M} + \text{H}$ )+; IR  $\nu_{\text{max}}/\text{cm}^{-1}$  (KBr) 3387, 3300, 1646, 1653, 1511, 1453, 1263, 1028. Anal. Calcd for  $\text{C}_{19}\text{H}_{20}\text{N}_2\text{O}_4$ : C, 67.05; H, 5.92; N, 8.23. Found: C, 67.14; H, 6.12; N, 8.46.



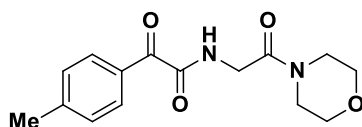
*N*-(2-(4-Methylpiperazin-1-yl)-2-oxoethyl)-2-oxo-2-*p*-tolylacetamide (**65**). Starting material: 1,3-oxazol-2-oxime **46** 150 mg (0.50 mmol). The crude material was purified by column chromatography (DCM/ MeOH 97:3) to give the product as yellow solid (75 mg, 50% yield):  $^1\text{H}$  NMR (400 MHz,  $\text{CDCl}_3$ )  $\delta$ H 8.19 (br d, 2H, AA' XX'), 7.92 (br s, NH), 7.27–7.25 (m, 2H, AA' XX') partially overlapped to the solvent, 4.17 (d,  $J = 4.2$  Hz, 2H), 3.68 (br t, 2H), 3.47 (br t, 2H), 2.44 (br s, 7H), 2.32 (s, 3H);  $^{13}\text{C}$  NMR (100 MHz,  $\text{CDCl}_3$ )  $\delta$ C 186.8, 165.5, 162.5, 145.5, 131.0, 130.7, 129.2, 54.6, 54.3, 45.8, 44.3, 41.9, 40.9, 21.8; MS  $m/z$  304 ( $\text{M} + \text{H}$ )+; IR  $\nu_{\text{max}}/\text{cm}^{-1}$  (KBr) 3351, 3000, 1669, 1642, 1504, 1475, 1276, 789; mp 97–98°C. Anal. Calcd for  $\text{C}_{16}\text{H}_{21}\text{N}_3\text{O}_3$ : C, 63.35; H, 6.98; N, 13.85. Found: C, 63.67; H, 7.12; N, 14.12.



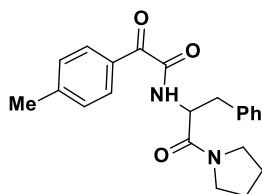
2-(4-Chlorophenyl)-*N*-(2-(4-methylpiperazin-1-yl)-2-oxoethyl)-2-oxoacetamide (**66**). Starting material: 1,3-oxazol-2-oxime **47** 150 mg (0.47 mmol). The crude material was purified by column chromatography (DCM/MeOH 97:3) to give the product as yellowish solid (64 mg, 42% yield):  $^1\text{H}$  NMR (400 MHz,  $\text{CDCl}_3$ )  $\delta$ H 8.23 (d,  $J = 8.4$  Hz, 2H, AA' XX'), 7.98 (br s, NH), 7.41 (d,  $J = 8.4$  Hz, 2H, AA' XX'), 4.12 (d,  $J = 4.0$  Hz, 2H), 3.63 (br t, 2H), 3.43 (br t, 2H), 2.40–2.37 (m, 4H), 2.28 (s, 3H);  $^{13}\text{C}$  NMR (100 MHz,  $\text{CDCl}_3$ )  $\delta$ C 185.7, 165.3, 161.7, 141.0, 132.4, 131.5, 128.8, 54.7, 54.4, 46.0, 44.4, 42.0, 40.9; MS  $m/z$  324 ( $\text{M} + \text{H}$ )+; IR  $\nu_{\text{max}}/\text{cm}^{-1}$  (KBr) 3344, 1673, 1645, 1586, 1443, 1273, 857; mp 127–128 °C. Anal. Calcd for  $\text{C}_{15}\text{H}_{18}\text{ClN}_3\text{O}_3$ : C, 55.64; H, 5.60; N, 12.98. Found: C, 55.54; H, 5.42; N, 12.78.



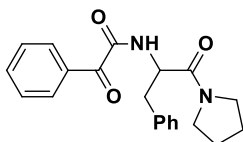
*N*-(2-Morpholino-2-oxoethyl)-2-oxo-2-*p*-tolylacetamide (**67**). Starting material: 1,3-oxazol-2-oxime **48** 150 mg (0.52 mmol). The crude material was purified by column chromatography (DCM/MeOH 97:3) to give the product as yellow solid (98 mg, 65% yield): <sup>1</sup>H NMR (400 MHz, CDCl<sub>3</sub>) δH 8.20 (d, J = 8.2 Hz, 2H), 7.92 (br s, NH), 7.28–7.25 (m, 2H) partially overlapped to the solvent, 4.17 (d, J = 4.0 Hz, 2H), 3.71–3.67 (m, 6H), 3.47–3.46 (m, 2H), 2.42 (s, 3H); <sup>13</sup>C NMR (100 MHz, CDCl<sub>3</sub>) δC 186.6, 165.8, 162.4, 145.6, 131.1, 130.7, 129.2, 66.6, 66.3, 44.9, 42.3, 40.8, 21.8; MS m/z 291 (M + H)<sup>+</sup>; IR ν<sub>max</sub>/cm<sup>-1</sup> (KBr) 3430, 3423, 1695, 1660, 1494, 1276, 785; mp 83–84 °C. Anal. Calcd for C<sub>15</sub>H<sub>18</sub>N<sub>2</sub>O<sub>4</sub>: C, 62.06; H, 6.25; N, 9.65. Found: C, 62.34; H, 6.43; N, 9.78.



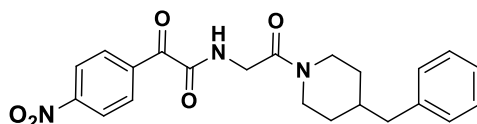
2-Oxo-*N*-(1-oxo-3-phenyl-1-(pyrrolidin-1-yl)propan-2-yl)-2-*p*-tolylacetamide(**68**). Starting material: 1,3-oxazol-2-oxime **49** 150 mg (0.41 mmol). The crude material was purified by column chromatography (n-hexane/AcOEt 7:3) to give the product as a light yellow solid (78 mg, 52% yield): <sup>1</sup>H NMR (400 MHz, CDCl<sub>3</sub>) δH 8.12 (d, J = 8.0 Hz, 2H), 7.79 (br d, NH), 7.28–7.23 (m, 7H), 4.95 (br q, 1H), 3.47–3.30 (m, 3H), 3.09 (d, J = 7.4 Hz, 2H), 2.69–2.63 (m, 1H), 2.40 (s, 3H), 1.80–1.55 (m, 4H); <sup>13</sup>C NMR (100 MHz, CDCl<sub>3</sub>) mixture of rotamers: δC 186.8, 168.6, 161.7, 145.5, 136.1, 132.0, 131.1, 130.7, 129.5, 128.5, 127.1, 52.4, 46.3, 45.8, 39.5, 25.8, 23.9, 21.8; MS m/z 365 (M + H)<sup>+</sup>; IR ν<sub>max</sub>/cm<sup>-1</sup> (KBr) 3239, 3062, 1680, 1662, 1624, 1454, 1228, 763; mp 88–89 °C. Anal. Calcd for C<sub>22</sub>H<sub>24</sub>N<sub>2</sub>O<sub>3</sub>: C, 72.51; H, 6.64; N, 7.69. Found: C, 72.52; H, 6.65; N, 7.65.



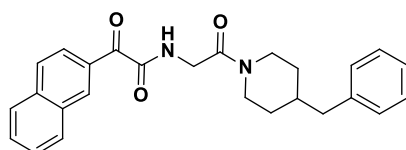
2-Oxo-*N*-(1-oxo-3-phenyl-1-(pyrrolidin-1-yl)propan-2-yl)-2-phenylacetamide(**69**). Starting material: 1,3-oxazol-2-oxime **50** 150 mg (0.43 mmol). The crude material was purified by column chromatography (n-hexane/AcOEt 7:3) to give the product as a yellowish solid (110 mg, 73% yield): <sup>1</sup>H NMR (400 MHz, CDCl<sub>3</sub>) δ 8.21 (d, J = 7.8 Hz, 2H), 7.76 (br d, NH), 7.60 (t, J = 7.4 Hz, 1H), 7.45 (t, J = 7.7 Hz, 2H), 7.31–7.25 (m, 6H), 4.96 (br q, 1H), 3.49–3.36 (m, 3H), 3.10 (d, J = 7.4 Hz, 2H), 2.70–2.64 (m, 1H), 1.81–1.56 (m, 4H); <sup>13</sup>C NMR (100 MHz, CDCl<sub>3</sub>) mixture of rotamers δC 187.4, 168.6, 161.6, 136.0, 134.2, 133.2, 130.8, 129.4, 128.8, 128.5, 128.4, 128.4, 127.0, 52.4, 46.3, 45.8, 39.4, 25.7, 23.9; MS m/z 351 (M + H)<sup>+</sup>; IR ν<sub>max</sub>/cm<sup>-1</sup> (KBr) 3240, 3062, 1682, 1664, 1621, 1555, 1454, 1222; mp 118–119 °C. Anal. Calcd for C<sub>21</sub>H<sub>22</sub>N<sub>2</sub>O<sub>3</sub>: C, 71.98; H, 6.33; N, 7.99. Found: C, 72.21; H, 6.12; N, 8.21.



*N*-(2-(4-Benzylpiperidin-1-yl)-2-oxoethyl)-2-(4-nitrophenyl)-2-oxoacetamide (**70**). Starting material: 1,3-oxazol-2-oxime **51** 150 mg (0.37 mmol). The crude material was purified by column chromatography (n-hexane/AcOEt 5:5) give the product as a yellowish solid (100mg, 66% yield):  $^1\text{H}$  NMR (400 MHz,  $\text{CDCl}_3$ )  $\delta$ H 8.48 (d,  $J = 8.6$  Hz, 2H), 8.31 (d,  $J = 8.8$  Hz, 2H), 8.08 (br s, NH), 7.31–7.12 (m, 5H), 4.59 (br d, 1H), 4.17–4.14 (m, 2H), 3.72 (br d, 1H), 3.02 (br t, 1H), 2.58–2.55 (m, 2H), 1.83–1.76 (m, 3H), 1.21–1.15 (m, 3H);  $^{13}\text{C}$  NMR (100 MHz,  $\text{CDCl}_3$ )  $\delta$ C 185.5, 164.8, 160.8, 150.8, 139.6, 137.9, 132.1, 129.0, 128.4, 126.2, 123.4, 44.8, 42.8, 42.6, 41.0, 38.0, 32.2, 31.5; MS  $m/z$  410 ( $M + H$ )+; IR  $\nu_{\text{max}}/\text{cm}^{-1}$  (KBr) 3280, 1665, 1651, 1602, 1519; mp 78–79 °C. Anal. Calcd for  $\text{C}_{22}\text{H}_{23}\text{N}_3\text{O}_5$ : C, 64.54; H, 5.66; N, 10.26. Found: C, 64.78; H, 5.84; N, 10.02.

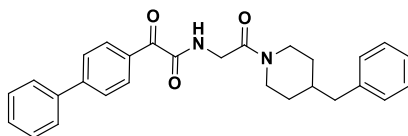


*N*-(2-(4-Benzylpiperidin-1-yl)-2-oxoethyl)-2-(naphthalen-2-yl)-2-oxoacetamide (**71**). Starting material: 1,3-oxazol-2-oxime **52** 150 mg (0.36 mmol). The crude material was purified by column chromatography (n-hexane/AcOEt 5:5) to give the product as a sticky solid (81 mg, 54% yield):  $^1\text{H}$  NMR (400 MHz,  $\text{CDCl}_3$ )  $\delta$ H 9.06 (s, 1H), 8.18 (br d, AA' XX', 1H), 8.06 (br s, NH), 7.98 (d,  $J = 8.1$  Hz, 1H), 7.90–7.85 (m, 2H), 7.64–7.60 (m, 1H), 7.56–7.53 (m, 1H), 7.31–7.19 (m, 3H), 7.13 (br d, 2H), 4.60 (br d, 1H), 4.22–4.19 (m, 2H), 3.75 (br d, 1H), 3.01 (br t, 1H), 2.61–2.55 (m, 2H), 1.82–1.72 (m, 3H), 1.25–1.14 (m, 3H);  $^{13}\text{C}$  NMR (100 MHz,  $\text{CDCl}_3$ )  $\delta$ C 186.9, 165.1, 162.3, 139.6, 136.1, 134.5, 132.3, 130.5, 130.2, 129.2, 129.0, 128.3, 128.3, 127.7, 126.7, 126.1, 125.1, 44.8, 42.8, 42.6, 41.0, 38.0, 32.2, 31.5; MS  $m/z$  415 ( $M + H$ )+; IR  $\nu_{\text{max}}/\text{cm}^{-1}$  (KBr) 3280, 1665, 1651, 1602, 1519. Anal. Calcd for  $\text{C}_{26}\text{H}_{26}\text{N}_2\text{O}_3$ : C, 75.34; H, 6.32; N, 6.76. Found: C, 75.36; H, 6.46; N, 6.73.

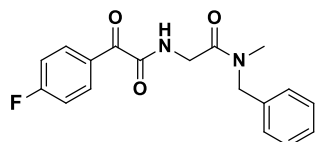


2-([1,1'-Biphenyl]-4-yl)-*N*-(2-(4-benzylpiperidin-1-yl)-2-oxoethyl)-2-oxoacetamide (**72**). Starting material: 1,3-oxazol-2-oxime **53** 150 mg (0.34 mmol). The crude material was purified by column chromatography (n-hexane/AcOEt 5:5) to give the product as a white solid (112 mg, 75% yield):  $^1\text{H}$  NMR (400 MHz,  $\text{CDCl}_3$ )  $\delta$ H 8.38 (br d, AA' XX', 2H), 8.01 (br s, NH), 7.70 (br d, AA' XX', 2H), 7.64 (br d, AA' XX', 2H), 7.49–7.38 (m, 3H), 7.31–7.19 (m, 3H), 7.13 (br d, AA' XX', 2H), 4.60 (br d, 1H), 4.24–4.12 (m, 2H), 3.74 (br d, 1H), 3.01 (br t, 1H), 2.64–2.55 (m, 3H), 1.82–1.75 (m, 3H), 1.25–1.14 (m, 2H);  $^{13}\text{C}$  NMR (100 MHz,  $\text{CDCl}_3$ )  $\delta$ C 186.7, 165.16, 162.3, 146.9, 139.7, 139.6, 132.0, 131.6, 129.0, 128.9, 128.4, 128.3, 127.3, 127.1, 126.1, 44.8,

42.8, 42.6, 41.0, 38.0, 32.2, 31.5; MS m/z 441 (M + H)<sup>+</sup>; IR  $\nu_{\text{max}}/\text{cm}^{-1}$  (KBr) 3364, 2919, 1682, 1628, 1475; mp 140–141 °C. Anal. Calcd for C<sub>28</sub>H<sub>28</sub>N<sub>2</sub>O<sub>3</sub>: C, 76.34; H, 6.41; N, 6.36. Found: C, 76.29; H, 6.42; N, 6.78.



*N*-Benzyl-2-(2-(4-fluorophenyl)-2-oxoacetamido)-*N*-methylacetamide (**73**). Starting material: 1,3-oxazol-2-oxime **54** 150 mg (0.46 mmol). The crude material was purified by column chromatography (PE/EtOAc 5:5) to give 106 mg of product as yellow oil (yield 70%). Mixture of rotamers, signals are referred to the main rotamer: <sup>1</sup>H NMR (300 MHz, CDCl<sub>3</sub>)  $\delta$  8.37–8.29 (m, 2H), 8.11 (br s, NH), 7.34–7.21 (m, 4H), 7.19–7.05 (m, 3H), 4.59 (s, 2H), 4.20 (d, J = 4 Hz, 2H), 2.91 (s, 3H); <sup>13</sup>C NMR (75 MHz, CDCl<sub>3</sub>)  $\delta$  185.4, 167.2, 164.8, 162.1, 136.4, 134.1, 129.7, 128.7, 128.1, 127.7, 115.9, 51.3, 41.2, 33.6; MS m/z 329 (M + H)<sup>+</sup>; IR  $\nu_{\text{max}}/\text{cm}^{-1}$  (KBr) 3377, 2926, 1647, 1595, 1230, 1089. Anal. Calcd for C<sub>18</sub>H<sub>17</sub>FN<sub>2</sub>O<sub>3</sub>: C, 65.84; H, 5.22; N, 8.53. Found C, 65.52; H, 4.98; N, 8.76.



## 4.2 Part II: Synthesis of Aryloxyimino Amides

**Solvents and Reagents.** Commercially available solvents and reagents were used without further purification. Dichloromethane was dried by distillation over P<sub>2</sub>O<sub>5</sub> and stored over activated molecular sieves (4 Å). When needed, the reactions were performed in oven-dried glassware under a positive pressure of dry nitrogen. **Chromatography.** Column chromatography was performed on silica gel 60 (Kieselgel 230–400 mesh ASTM) using the indicated eluents. Thin layer chromatography (TLC) was carried out on 5 × 20 cm plates with a layer thickness of 0.25 mm (Silica gel 60 F254). When needed they were visualized using KMnO<sub>4</sub> reagent. **Spectra.** Infrared spectra were recorded on a FT-IR with absorption maxima ( $\nu_{\text{max}}$ ) recorded in wavenumbers ( $\text{cm}^{-1}$ ). NMR spectra were recorded using a 300 or 400 MHz spectrometer. Chemical shifts ( $\delta$ ) are quoted in parts per million and referenced to the residual solvent peak. The multiplicity of each signal is designated using the following abbreviations: s, singlet; d, doublet; t, triplet; q, quartet; quint, quintet; sext, sextet; hept, heptet; m, multiplet; br, broad singlet. Coupling constants ( $J$ ) are reported in Hertz (Hz). HRMS were recorded on ORBITRAP mass spectrometer equipped with an ESI source. Melting points were determined and remain uncorrected. Chloroximes 1{1}, 1{2}, and 1{3} are not new, and they were prepared following literature procedure [153].

*General Preparation of Aryloxyimino Amides.* The chlorooxime (1 equiv) was dissolved in dry dichloromethane and isocyanide (1 equiv), phenol (1.1 equiv), and DBU (1.2 equiv) were added. The reaction was stirred at room temperature under a nitrogen atmosphere until all the chlorooxime was consumed (typically overnight as judged by TLC). The reaction mixture was concentrated under reduced pressure, and the crude material was purified by column chromatography.

*(Z)-4-nitrophenyl 2-(hydroxyimino)-N-pentyl-2-phenylacetimidate 4{1,3,1}.* The crude material was purified by column chromatography (PE/EtOAc 95:5, 9:1) to give the product as white solid. <sup>1</sup>H-NMR (300 MHz, CDCl<sub>3</sub>, CD<sub>3</sub>OD)  $\delta$  8.16 (d,  $J$  = 7.35 Hz, 2H), 7.58 (d, 2H), 7.37 (m, 5H), 7.08 (br s, NH), 3.12 (br s, 2H), 1.45–1.33 (m, 2H), 1.15 (m, 4H), 0.57 (m, 3H); <sup>13</sup>C-NMR (75 MHz, CDCl<sub>3</sub>)  $\delta$  158.3, 153.4, 148.9, 144.4, 131.2, 130.2, 129.0, 128.6, 125.9, 125.1, 122.4, 50.1, 30.2, 29.5, 22.3, 13.9.

*(Z)-N-benzyl-2-((4-nitrophenoxy)imino)-2-phenylacetamide.5{1,1,1}* The crude material was purified by column chromatography (PE/EtOAc 9:1, 8:2) to give the product as yellow solid (yield 33%). <sup>1</sup>H-NMR (300 MHz, CDCl<sub>3</sub>)  $\delta$  8.23–8.13 (m, 2H), 7.81–7.69 (m, 2H), 7.55–7.18 (m, 10H), 6.52 (br t, NH), 4.67 (d,  $J$  = 5.8 Hz, 2H); <sup>13</sup>C-NMR (75 MHz, CDCl<sub>3</sub>)  $\delta$  163.4, 162.2, 157.6, 142.9, 137.4, 131.8, 129.6, 129.1 (2C), 128.9, 128.0, 127.4, 125.8, 114.5, 43.6;  $\nu_{\text{max}}/\text{cm}^{-1}$  (KBr) 3412, 3258, 1646, 1591, 1342, 919; mp 151–152 °C; HRMS (EI<sup>+</sup>):  $m/z$ : calcd for C<sub>21</sub>H<sub>17</sub>N<sub>3</sub>O<sub>4</sub>: 375.1219, Found: 375.1220.

*(Z)-N-(tert-butyl)-2-((4-nitrophenoxy)imino)-2-phenylacetamide.5{1,2,1}* The crude material was purified by column chromatography (PE/EtOAc 9:1, 8:2) to give the product as white solid (yield 41%). <sup>1</sup>H-NMR (300 MHz, CDCl<sub>3</sub>)  $\delta$  8.13–8.09 (m, 2H), 7.70–7.67 (m, 2H), 7.44–7.34 (m, 3H), 7.23–7.20 (m, 2H), 6.21 (br s, NH), 1.45 (s, 9H); <sup>13</sup>C-NMR (75 MHz, CDCl<sub>3</sub>)  $\delta$  136.5, 161.5, 157.7, 142.5, 131.5, 129.7, 128.9, 127.3, 125.7, 114.3, 52.9, 28.7;  $\nu_{\text{max}}/\text{cm}^{-1}$  (KBr) 3280, 2969, 1646, 1589, 1519, 1341, 918; mp 154.3–155 °C; HRMS (EI<sup>+</sup>):  $m/z$ : calcd for C<sub>18</sub>H<sub>19</sub>N<sub>3</sub>O<sub>4</sub>: 341.1376, Found: 341.1376.

*(Z)*-2-((4-nitrophenoxy)imino)-*N*-pentyl-2-phenylacetamide.5{1,3,1} The crude material was purified by column chromatography (PE/EtOAc 9:1, 8:2) to give the product as yellow solid (yield 37%). <sup>1</sup>H-NMR (300 MHz, CDCl<sub>3</sub>) δ 8.26-8.19 (m, 2H), 7.81-7.76 (m, 2H), 7.53-7.26 (m, 5H), 5.97 (br s, NH), 3.56-3.49 (m, 2H), 1.69-1.64 (m, 2H), 1.42-1.38 (m, 4H), 0.95-0.90 (m, 3H); <sup>13</sup>C-NMR (75 MHz, CDCl<sub>3</sub>) δ 163.5, 162.1, 157.9, 142.9, 131.7, 129.8, 129.1, 127.4, 125.8, 114.5, 39.7, 29.2, 29.1, 22.4, 14.1; ν<sub>max</sub>/cm<sup>-1</sup> (KBr) 3233, 2932, 1650, 1589, 1517, 1338, 921; mp 124-129.9 °C; HRMS (EI<sup>+</sup>): *m/z*: calcd for C<sub>19</sub>H<sub>21</sub>N<sub>3</sub>O<sub>4</sub>: 355.1532, Found: 355.1539.

*(Z)*-*N*-benzyl-2-((2-nitrophenoxy)imino)-2-phenylacetamide.5{1,1,2} The crude material was purified by column chromatography (PE/EtOAc 9:1, 8:2) to give the product as brown solid (yield 25%). <sup>1</sup>H-NMR (300 MHz, CDCl<sub>3</sub>) δ 8.01-7.98 (m, 1H), 7.80-7.77 (m, 3H), 7.64-7.15 (m, 10H), 6.70 (br t, NH), 4.75 (d, *J* = 5.5 Hz, 2H); <sup>13</sup>C-NMR (75 MHz, CDCl<sub>3</sub>) δ 161.6, 157.9, 152.5, 138.0, 137.3, 135.0, 131.6, 129.3, 129.0, 128.9, 128.4, 127.9, 127.8, 125.9, 123.1, 118.1, 44.1; ν<sub>max</sub>/cm<sup>-1</sup> (KBr) 3418, 3235, 1636, 1616, 1523, 918; mp 137.2-138 °C; HRMS (EI<sup>+</sup>): *m/z*: calcd for C<sub>21</sub>H<sub>17</sub>N<sub>3</sub>O<sub>4</sub>: 375.1219, Found: 375.1221.

*(Z)*-*N*-(*tert*-butyl)-2-((2-nitrophenoxy)imino)-2-phenylacetamide.5{1,2,2} The crude material was purified by column chromatography (PE/EtOAc 9:1, 8:2) to give the product as yellow solid (yield 42%). <sup>1</sup>H-NMR (300 MHz, CDCl<sub>3</sub>) δ 7.92 (dd, *J* = 8.26, 1.5 Hz, 1H), 7.78-7.72 (m, 3H), 7.58 (td, *J* = 7.8, 1.5 Hz, 1H), 7.46-7.37 (m, 3H), 7.14 (td, *J* = 7.8, 1.23 Hz, 1H), 6.12 (br s, NH), 1.52 (s, 9H); <sup>13</sup>C-NMR (75 MHz, CDCl<sub>3</sub>) δ 160.9, 157.7, 152.5, 137.9, 134.7, 131.4, 130.2, 128.9, 127.5, 125.5, 122.8, 118.2, 53.2, 28.7; ν<sub>max</sub>/cm<sup>-1</sup> (KBr) 3270, 2964, 1647, 1519, 1563, 1354, 923; mp 139.5-139.9 °C; HRMS (EI<sup>+</sup>): *m/z*: calcd for C<sub>18</sub>H<sub>19</sub>N<sub>3</sub>O<sub>4</sub>: 341.1376, Found: 341.1379.

*(Z)*-2-((2-nitrophenoxy)imino)-*N*-pentyl-2-phenylacetamide.5{1,3,2} The crude material was purified by column chromatography (PE/EtOAc 9:1, 8:2) to give the product as yellow amorphous solid (yield 51%). <sup>1</sup>H-NMR (300 MHz, CDCl<sub>3</sub>) δ 7.96 (dd, *J* = 8.25, 1.8 Hz, 1H), 7.81-7.74 (m, 3H), 7.59 (td, *J* = 7.9, 1.5 Hz, 1H), 7.49-7.35 (m, 3H), 7.16 (td, *J* = 7.16, 1.23 Hz, 1H), 6.50 (br s, NH), 3.56-3.49 (m, 2H), 1.69-1.65 (m, 2H), 1.37-1.35 (m, 4H), 0.92-0.88 (m, 3H); <sup>13</sup>C-NMR (75 MHz, CDCl<sub>3</sub>) δ 161.6, 157.9, 152.4, 137.6, 134.8, 131.3, 130.0, 128.8, 127.6, 125.6, 122.7, 117.8, 39.8, 29.1, 28.8, 22.3, 14.0; ν<sub>max</sub>/cm<sup>-1</sup> (KBr) 3266, 2953, 1668, 1523, 1344, 915; HRMS (EI<sup>+</sup>): *m/z*: calcd for C<sub>19</sub>H<sub>21</sub>N<sub>3</sub>O<sub>4</sub>: 355.1532, Found: 355.1532.

*(Z)*-*N*-benzyl-2-((2,4-dinitrophenoxy)imino)-2-phenylacetamide.5{1,1,3} The crude material was purified by column chromatography (PE/EtOAc 9:1, 8:2) to give the product as white solid (yield 30%). <sup>1</sup>H-NMR (300 MHz, CDCl<sub>3</sub> + 1 gtt CD<sub>3</sub>OD) δ 8.85 (d, *J* = 2.7 Hz, 1H), 8.44 (dd, *J* = 9.18, 2.7 Hz, 1H), 8.01 (d, *J* = 9.18 Hz, 1H), 7.79-7.72 (m, 2H), 7.50-7.24 (m, 9H), 4.64 (s, 2H); <sup>13</sup>C-NMR (75 MHz, CDCl<sub>3</sub> + 1 gtt CD<sub>3</sub>OD) δ 161.8, 160.4, 156.6, 141.3, 137.0, 136.3, 132.2, 129.8, 129.3, 129.0, 128.6, 128.0, 127.6, 127.5, 121.9, 117.4, 43.5; ν<sub>max</sub>/cm<sup>-1</sup> (KBr) 3332, 3116, 1660, 1527, 1345, 927, 902; mp 155-156 °C; HRMS (EI<sup>+</sup>): *m/z*: calcd for C<sub>21</sub>H<sub>16</sub>N<sub>4</sub>O<sub>6</sub>: 420.1070, Found: 420.1075.

*(Z)*-*N*-(*tert*-butyl)-2-((2,4-dinitrophenoxy)imino)-2-phenylacetamide.5{1,2,3} The crude material was purified by column chromatography (PE/EtOAc 9:1, 8:2) to give the product as yellow solid (yield 38%). <sup>1</sup>H-NMR (300 MHz, CDCl<sub>3</sub>) δ 8.83 (d, *J* = 2.7 Hz, 1H), 8.43 (dd, *J* = 9.18, 2.7 Hz, 1H), 7.98 (d, *J* = 9.18 Hz, 1H), 7.76 (dd, *J* = 8.5, 1.5 Hz, 2H), 7.52-7.41 (m, 3H), 5.98 (br s, NH), 1.55 (s, 9H); <sup>13</sup>C-NMR (75 MHz, CDCl<sub>3</sub>) δ 160.3, 159.6, 156.6, 141.3, 136.3, 132.1, 129.3, 129.2, 129.1, 127.7, 121.8, 117.7, 53.4, 28.6; ν<sub>max</sub>/cm<sup>-1</sup> (KBr) 3398, 2975, 1685, 1519, 1344, 929, 901; mp 156.5-157 °C; HRMS (EI<sup>+</sup>): *m/z*: calcd for C<sub>18</sub>H<sub>18</sub>N<sub>4</sub>O<sub>6</sub>: 386.1226, Found: 386.1228.

*(Z)*-2-((2,4-dinitrophenoxy)imino)-*N*-pentyl-2-phenylacetamide.5{1,3,3} The crude material was purified by column chromatography (PE/EtOAc 9:1, 8:2) to give the product as yellow solid (yield 32%). <sup>1</sup>H-NMR (300

MHz, CDCl<sub>3</sub>) δ 8.72-8.70 (m, 1H), 8.36-8.31 (m, 1H), 7.90-7.85 (m, 1H), 7.64-7.63 (m, 2H), 7.45-7.27 (m, 3H), 6.67 (br d, NH), 3.46-3.38 (m, 2H), 1.58 (br s, 2H), 1.31-1.29 (m, 4H), 0.88-0.74 (m, 3H); <sup>13</sup>C-NMR (75 MHz, CDCl<sub>3</sub>) δ 161.2, 160.1, 156.5, 141.3, 136.1, 132.2, 129.4, 129.1, 128.9, 127.8, 122.0, 117.4, 40.0, 29.1, 28.8, 22.3, 14.0; ν<sub>max</sub>/cm<sup>-1</sup> (KBr) 3267, 2952, 1648, 1526, 1344, 929, 904; mp 139.7-141.3 °C; HRMS (EI<sup>+</sup>): *m/z*: calcd for C<sub>19</sub>H<sub>20</sub>N<sub>4</sub>O<sub>6</sub>: 400.1383, Found: 400.1389.

*(Z)*-*N*-benzyl-2-((2-chloro-4-nitrophenoxy)imino)-2-phenylacetamide.5{1,1,4} The crude material was purified by column chromatography (PE/EtOAc 9:1, 8:2) to give the product as white solid (yield 43%). <sup>1</sup>H-NMR (300 MHz, CDCl<sub>3</sub>) δ 8.17 (d, *J* = 2.8 Hz, 1H), 8.06 (dd, *J* = 9.18, 2.1 Hz, 1H), 7.77-7.61 (m, 3H), 7.45-7.26 (m, 9H), 4.59 (br s, 2H); <sup>13</sup>C-NMR (75 MHz, CDCl<sub>3</sub>) δ 161.8, 159.1, 158.8, 142.5, 137.0, 131.9, 129.4, 129.0, 128.8, 128.2, 127.8, 127.5, 125.9, 123.7, 120.8, 115.0, 43.6; ν<sub>max</sub>/cm<sup>-1</sup> (KBr) 3249, 3084, 1653, 1584, 1351, 919, 743; mp 152.8-153 °C; HRMS (EI<sup>+</sup>): *m/z*: calcd for C<sub>21</sub>H<sub>16</sub>ClN<sub>3</sub>O<sub>4</sub>: 409.0829, Found: 409.0832.

*(Z)*-*N*-(*tert*-butyl)-2-((2-chloro-4-nitrophenoxy)imino)-2-phenylacetamide.5{1,2,4} The crude material was purified by column chromatography (PE/EtOAc 9:1, 8:2) to give the product as white solid (yield 45%). <sup>1</sup>H-NMR (300 MHz, CDCl<sub>3</sub>) δ 8.26 (br d, 1H), 8.13 (dd, *J* = 9.2, 1.2 Hz, 1H), 7.78-7.70 (m, 3H), 7.52-7.41 (m, 3H), 5.98 (br s, NH), 1.52 (s, 9H); <sup>13</sup>C-NMR (75 MHz, CDCl<sub>3</sub>) δ 161.4, 159.3, 158.7, 142.2, 131.6, 129.6, 128.8, 127.2, 125.8, 123.7, 120.5, 114.8, 52.7, 28.4; ν<sub>max</sub>/cm<sup>-1</sup> (KBr) 3263, 3085, 1654, 1583, 1365, 922, 742; mp 143-144 °C; HRMS (EI<sup>+</sup>): *m/z*: calcd for C<sub>18</sub>H<sub>18</sub>ClN<sub>3</sub>O<sub>4</sub>: 375.0986, Found: 375.0983.

*(Z)*-2-((2-chloro-4-nitrophenoxy)imino)-*N*-pentyl-2-phenylacetamide.5{1,3,4} The crude material was purified by column chromatography (PE/EtOAc 9:1, 8:2) to give the product as white solid (yield 53%). <sup>1</sup>H-NMR (300 MHz, CDCl<sub>3</sub>) δ 8.15 (d, *J* = 2.8 Hz, 1H), 8.05 (dd, *J* = 9.1, 2.4 Hz, 1H), 7.71-7.68 (m, 2H), 7.61 (dd, *J* = 9.1, 1H), 7.48-7.35 (m, 3H), 6.54 (br t, NH), 3.42 (br q, 2H), 1.62 (br quintetto, 2H), 1.38-1.31 (m, 4H), 0.90-0.86 (m, 3H); <sup>13</sup>C-NMR (75 MHz, CDCl<sub>3</sub>) δ 161.7, 159.1, 158.9, 142.4, 131.8, 129.5, 129.0, 127.6, 125.9, 123.8, 120.7, 114.9, 39.9, 29.2 (2), 22.4, 14.0; ν<sub>max</sub>/cm<sup>-1</sup> (KBr) 3261, 2963, 1653, 1589, 1352, 927, 742; mp 121-122 °C; HRMS (EI<sup>+</sup>): *m/z*: calcd for C<sub>19</sub>H<sub>20</sub>ClN<sub>3</sub>O<sub>4</sub>: 389.1142, Found: 389.1144.

*(Z)*-*N*-(*tert*-butyl)-2-(((5-nitropyridin-2-yl)oxy)imino)-2-phenylacetamide.5{1,2,5} The crude material was purified by column chromatography (PE/EtOAc 9:1, 8:2) to give the product as white solid (yield 20%). <sup>1</sup>H-NMR (300 MHz, CDCl<sub>3</sub>) δ 9.13 (d, *J* = 2.46 Hz, 1H), 8.49 (dd, *J* = 9.18, 2.7 Hz, 1H), 7.79 (dd, *J* = 8.28, 1.26 Hz, 2H), 7.56-7.36 (m, 4H), 5.88 (br s, NH), 1.53 (s, 9H); <sup>13</sup>C-NMR (75 MHz, CDCl<sub>3</sub>) δ 167.7, 161.4, 159.6, 145.0, 140.7, 135.1, 131.9, 130.1, 129.1, 127.5, 109.2, 52.9, 28.7; ν<sub>max</sub>/cm<sup>-1</sup> (KBr) 3290, 2970, 1674, 1516, 1347, 929; mp 169-171.2 °C; HRMS (EI<sup>+</sup>): *m/z*: calcd for C<sub>17</sub>H<sub>18</sub>N<sub>4</sub>O<sub>4</sub>: 342.1328, Found: 342.1327.

*(Z)*-2-(((5-nitropyridin-2-yl)oxy)imino)-*N*-pentyl-2-phenylacetamide.5{1,3,5} The crude material was purified by column chromatography (PE/EtOAc 9:1, 8:2) to give the product as brown amorphous solid (yield 33%). Mixture of *E/Z* isomers, signals are referred to the main isomer: <sup>1</sup>H-NMR (300 MHz, CDCl<sub>3</sub>) δ 8.96 (d, *J* = 2.8 Hz, 1H), 8.45 (dd, *J* = 9.1, 2.8 Hz, 1H), 7.73-7.70 (m, 3H), 7.55-7.47 (m, 4H), 6.69 (br t, NH), 3.51 (br q, 2H), 1.69-1.59 (m, 2H), 1.43-1.33 (m, 4H), 0.92-0.82 (m, 3H); <sup>13</sup>C-NMR (75 MHz, CDCl<sub>3</sub>) δ 167.7, 161.7, 159.4, 148.2, 144.9, 135.2, 133.8, 130.1, 129.3, 127.6, 109.0, 39.8, 29.5, 29.1, 22.4, 14.1; ν<sub>max</sub>/cm<sup>-1</sup> (KBr) 3549, 3417, 1636, 1579, 1345, 937; HRMS (EI<sup>+</sup>): *m/z*: calcd for C<sub>18</sub>H<sub>20</sub>N<sub>4</sub>O<sub>4</sub>: 356.1485, Found: 356.1485.

*(Z)*-*N*-(*tert*-butyl)-2-(4-methoxyphenyl)-2-((4-nitrophenoxy)imino)acetamide.5{2,2,1} The crude material was purified by column chromatography (PE/EtOAc 95:5, 9:1) to give the product as yellow solid (yield 33%). <sup>1</sup>H-NMR (300 MHz, CDCl<sub>3</sub>) δ 8.06 (d, *J* = 9.18 Hz, 2H), 7.57 (d, *J* = 8.7 Hz, 2H), 7.16 (d, *J* = 9.18 Hz, 2H), 6.81 (d, *J* = 8.7 Hz, 2H), 6.32 (br s, NH), 3.76 (s, 3H), 1.42 (s, 9H); <sup>13</sup>C-NMR (75 MHz, CDCl<sub>3</sub>) δ 163.6, 162.0, 161.7, 157.3, 142.2, 128.8, 125.5, 121.9, 114.2, 114.0, 55.3, 52.7, 28.6; ν<sub>max</sub>/cm<sup>-1</sup> (KBr) 3277, 2968, 1646, 1511, 1335, 1239, 914; mp 133.2-134 °C; HRMS (EI<sup>+</sup>): *m/z*: calcd for C<sub>19</sub>H<sub>21</sub>N<sub>3</sub>O<sub>5</sub>: 371.1481, Found: 371.1483.

(Z)-2-(4-methoxyphenyl)-2-((4-nitrophenoxy)imino)-N-pentylacetamide.5{2,3,1} The crude material was purified by column chromatography (PE/EtOAc 9:1, 8:2) to give the product as yellow solid (yield 39%). Mixture of E/Z isomers, signals are referred to the main isomer: <sup>1</sup>H-NMR (300 MHz, CDCl<sub>3</sub>) δ 8.13-8.09 (m, 2H), 7.63-7.59 (m, 2H), 7.22-7.19 (m, 2H), 6.87-6.82 (m, 2H), 6.53 (br t, NH), 3.80 (s, 3H), 3.47-3.42 (m, 2H), 1.60-1.57 (m, 2H), 1.34-1.32 (m, 4H), 0.90-0.87 (m, 3H); <sup>13</sup>C-NMR (75 MHz, CDCl<sub>3</sub>) δ 163.6, 162.6, 162.4, 157.5, 142.6, 129.0, 125.7, 121.9, 114.4, 114.3, 55.5, 39.7, 29.1, 29.0, 22.3, 14.0; ν<sub>max</sub>/cm<sup>-1</sup> (KBr) 3266, 2930, 1650, 1515, 1337, 1180, 931; mp 116.8-117 °C; HRMS (EI<sup>+</sup>): m/z: calcd for C<sub>20</sub>H<sub>23</sub>N<sub>3</sub>O<sub>5</sub>: 385.1638, Found: 385.1640.

(Z)-N-benzyl-2-(4-methoxyphenyl)-2-((2-nitrophenoxy)imino)acetamide.5{2,1,2} The crude material was purified by column chromatography (PE/EtOAc 9:1, 8:2) to give the product as yellow solid (yield 26%). <sup>1</sup>H-NMR (300 MHz, CDCl<sub>3</sub>) δ 7.98 (dd, J = 7.9, 1.5 Hz, 1H), 7.79-7.71 (m, 3H), 7.60 (td, J = 7.8, 1.5 Hz, 1H), 7.43-7.27 (m, 5H), 7.16 (td, J = 7.9, 1.2 Hz, 1H), 6.97-6.91 (m, 2H), 6.60 (br t, NH), 4.75 (d, J = 5.8 Hz, 2H), 3.85 (s, 3H); <sup>13</sup>C-NMR (75 MHz, CDCl<sub>3</sub>) δ 162.4, 162.0, 157.6, 152.6, 137.3, 134.9, 129.5, 129.2, 128.9, 128.3, 127.9, 125.8, 122.7, 122.2, 117.9, 114.5, 55.6, 44.0; ν<sub>max</sub>/cm<sup>-1</sup> (KBr) 3411, 3285, 1646, 1522, 1352, 1176, 924; mp 130.8-131.6 °C; HRMS (EI<sup>+</sup>): m/z: calcd for C<sub>22</sub>H<sub>19</sub>N<sub>3</sub>O: 405.1325, Found: 405.1326.

(Z)-N-(tert-butyl)-2-(4-methoxyphenyl)-2-((2-nitrophenoxy)imino)acetamide.5{2,2,2} The crude material was purified by column chromatography (PE/EtOAc 9:1, 8:2) to give the product as yellow solid (yield 49%). <sup>1</sup>H-NMR (300 MHz, CDCl<sub>3</sub>) δ 7.89 (dd, J = 8.3, 1.5 Hz, 1H), 7.73-7.68 (m, 3H), 7.58-7.53 (m, 1H), 7.14-7.09 (m, 1H), 6.90 (dd, J = 8.8, 1.8 Hz, 2H), 6.07 (br s, NH), 3.82 (s, 3H), 1.51 (s, 9H); <sup>13</sup>C-NMR (75 MHz, CDCl<sub>3</sub>) δ 162.2, 161.2, 157.6, 152.7, 138.0, 134.6, 129.2, 125.4 (2C), 122.5, 118.2, 114.4, 55.5, 53.1, 28.7; ν<sub>max</sub>/cm<sup>-1</sup> (KBr) 3262, 2968, 1646, 1522, 1473, 1230, 918; mp 115.8-116.3 °C; HRMS (EI<sup>+</sup>): m/z: calcd for C<sub>19</sub>H<sub>21</sub>N<sub>3</sub>O<sub>5</sub>: 371.1481, Found: 371.1478.

(Z)-2-(4-methoxyphenyl)-2-((2-nitrophenoxy)imino)-N-pentylacetamide.5{2,3,2} The crude material was purified by column chromatography (PE/EtOAc 9:1, 8:2) to give the product as brown solid (yield 45%). <sup>1</sup>H-NMR (300 MHz, CDCl<sub>3</sub>) δ 7.96-7.89 (m, 1H), 7.77-7.65 (m, 3H), 7.57-7.51 (m, 1H), 7.12-7.06 (m, 1H), 6.89-6.86 (m, 2H), 6.51 (br s, NH), 3.81 (s, 3H), 3.48-3.44 (m, 2H), 1.65-1.61 (m, 2H), 1.34-1.32 (m, 4H), 0.90-0.85 (m, 3H); <sup>13</sup>C-NMR (75 MHz, CDCl<sub>3</sub>) δ 162.2, 161.9, 157.7, 152.6, 137.7, 134.7, 129.3, 125.6, 122.5, 122.3, 117.8, 114.3, 55.4, 39.9, 29.1, 28.9, 22.3, 14.0; ν<sub>max</sub>/cm<sup>-1</sup> (KBr) 3244, 2936, 1645, 1558, 1344, 1179, 916; mp 105-106 °C; HRMS (EI<sup>+</sup>): m/z: calcd for C<sub>20</sub>H<sub>23</sub>N<sub>3</sub>O<sub>5</sub>: 385.1638 Found: 385.1641.

(Z)-N-benzyl-2-((2,4-dinitrophenoxy)imino)-2-(4-methoxyphenyl)acetamide.5{2,1,3} The crude material was purified by column chromatography (PE/EtOAc 8:2, 7:3) to give the product as white solid (yield 40%). <sup>1</sup>H-NMR (300 MHz, CDCl<sub>3</sub> + 1 gtt DMSO-d<sub>6</sub>) δ 8.74 (d, J = 2.46 Hz, 1H), 8.33 (dd, J = 9.5, 2.76 Hz, 1H), 7.88 (dd, J = 9.5, 3.96 Hz, 1H), 7.59 (d, J = 8.6 Hz, 2H), 7.27-7.18 (m, 5H), 6.83 (d, J = 8.6 Hz, 2H), 4.56 (s, 2H), 3.77 (s, 3H); <sup>13</sup>C-NMR (75 MHz, CDCl<sub>3</sub> + 1 gtt DMSO-d<sub>6</sub>) δ 163.0, 160.3, 156.9 (2C), 141.5, 137.1, 136.4, 129.7, 129.5, 128.9, 128.3, 128.0, 122.2, 121.1, 117.6, 114.8, 55.6, 43.9; ν<sub>max</sub>/cm<sup>-1</sup> (KBr) 3269, 1643, 1535, 1340, 1255, 927; mp 163.3-164 °C; HRMS (EI<sup>+</sup>): m/z: calcd for C<sub>22</sub>H<sub>18</sub>N<sub>4</sub>O<sub>7</sub>: 450.1175, Found: 450.1177.

(Z)-N-(tert-butyl)-2-((2,4-dinitrophenoxy)imino)-2-(4-methoxyphenyl)acetamide.5{2,2,3} The crude material was purified by column chromatography (n-hexane/EtOAc 9:1) to give the product as yellow solid (yield 33%). <sup>1</sup>H-NMR (400 MHz, CDCl<sub>3</sub>) δ 8.86 (s, 1H), 8.45 (d, J = 9.00 Hz, 1H), 7.99 (d, J = 9.28 Hz, 1H), 7.75 (d, J = 7.56 Hz, 2H), 6.97 (d, J = 7.64 Hz, 2H), 5.80 (br s, NH), 3.87 (s, 3H), 1.54 (s, 9H); <sup>13</sup>C-NMR (100 MHz, CDCl<sub>3</sub>) δ 162.6, 160.5, 159.2, 156.7, 141.1, 136.2, 129.4, 129.1, 121.7, 121.3, 117.6, 114.5, 55.4, 53.3, 28.5; ν<sub>max</sub>/cm<sup>-1</sup> (KBr) 3295, 2971, 1666, 1526, 1340, 833; mp 148-149 °C; HRMS (EI<sup>+</sup>): m/z: calcd for C<sub>19</sub>H<sub>20</sub>N<sub>4</sub>O<sub>7</sub>: 416.1332, Found: 416.1332.



(Z)-2-((2,4-dinitrophenoxy)imino)-2-(4-methoxyphenyl)-N-pentylacetamide. 5{2,3,3} The crude material was purified by column chromatography (*n*-hexane/EtOAc 9:1) to give the product as pale yellow solid (yield 40%). <sup>1</sup>H-NMR (400 MHz, CDCl<sub>3</sub>) δ 8.82 (br s, 1H), 8.40 (br d, AA'XX', 1H), 7.95 (d, *J* = 9.32 Hz, 1H), 7.68 (d, *J* = 8.56 Hz, 2H), 6.91 (d, *J* = 8.56 Hz, 2H), 6.24 (br t, NH), 3.84 (s, 3H), 3.53-3.48 (m, 2H), 1.67-1.63 (m, 2H), 1.37-1.35 (m, 4H), 0.92-0.89 (m, 3H); <sup>13</sup>C-NMR (100 MHz, CDCl<sub>3</sub>) δ 162.8, 161.4, 159.8, 156.6, 141.1, 136.1, 129.5, 129.2, 121.9, 121.0, 117.4, 114.4, 55.4, 39.9, 29.1, 28.8, 22.2, 13.9; ν<sub>max</sub>/cm<sup>-1</sup> (KBr) 3283, 2929, 1654, 1521, 1343, 1260, 833; mp 139-140 °C; HRMS (EI<sup>+</sup>): *m/z*: calcd for C<sub>20</sub>H<sub>22</sub>N<sub>4</sub>O<sub>7</sub>: 430.1488, Found: 430.1489.

(Z)-N-benzyl-2-((2-chloro-4-nitrophenoxy)imino)-2-(4-methoxyphenyl)acetamide. 5{2,1,4} The crude material was purified by column chromatography (*n*-hexane/EtOAc 8:2) to give the product as light yellow solid (yield 63%). <sup>1</sup>H-NMR (400 MHz, CDCl<sub>3</sub>) δ 8.28 (s, 1H), 8.16 (br d, 1H), 7.76-7.71 (m, 3H), 7.42-7.30 (m, 5H), 6.96 (d, *J*=7.72, 2H), 6.23 (br s, NH), 4.72 (d, *J*=5.52, 2H), 3.87 (s, 3H); <sup>13</sup>C-NMR (100 MHz, DMSO-d<sub>6</sub>) δ 162.6, 161.8, 159.8, 159.2, 142.4, 138.7, 129.5, 128.7, 128.2, 127.5, 126.1, 124.9, 121.9, 119.8, 115.8, 115.1, 55.9, 42.7; ν<sub>max</sub>/cm<sup>-1</sup> (KBr) 3263, 1650, 1512, 1254, 926; mp 149-150 °C; HRMS (EI<sup>+</sup>): *m/z*: calcd for C<sub>22</sub>H<sub>18</sub>ClN<sub>3</sub>O<sub>5</sub>: 439.0935 Found: 439.0939.

(Z)-N-(tert-butyl)-2-((2-chloro-4-nitrophenoxy)imino)-2-(4-methoxyphenyl)acetamide. 5{2,2,4} The crude material was purified by column chromatography (*n*-hexane/EtOAc 9:1) to give the product as amorphous dark-red solid (yield 38%). <sup>1</sup>H-NMR (400 MHz, CDCl<sub>3</sub>) δ 8.29 (br s, 1H), 8.16 (br d, 1H), 7.75-7.72 (m, 3H), 6.95 (d, *J* = 8.76 Hz, 2H), 5.79 (br s, NH), 3.86 (s, 3H), 1.53 (s, 9H); <sup>13</sup>C-NMR (100 MHz, CDCl<sub>3</sub>) δ 162.3, 161.0, 159.3, 158.1, 142.0, 129.1, 125.8, 123.6, 121.7, 120.5, 114.7, 114.4, 55.4, 52.9, 28.7; ν<sub>max</sub>/cm<sup>-1</sup> (KBr) 3566, 1652, 1516, 1338, 1255, 920; HRMS (EI<sup>+</sup>): *m/z*: calcd for C<sub>19</sub>H<sub>20</sub>ClN<sub>3</sub>O<sub>5</sub>: 405.1091, Found: 405.1093.

(Z)-2-((2-chloro-4-nitrophenoxy)imino)-2-(4-methoxyphenyl)-N-pentylacetamide, 5{2,3,4} The crude material was purified by column chromatography (*n*-hexane/EtOAc 8:2) to give the product as yellowish solid (yield 50%). <sup>1</sup>H-NMR (400 MHz, CDCl<sub>3</sub>) δ 8.28 (s, 1H), 8.15 (br d, 1H), 7.75-7.71 (m, 3H), 6.95 (d, *J* = 8.76 Hz, 2H), 5.99 (br s, NH), 3.86 (s, 3H), 3.55-3.50 (m, 2H), 1.69-1.66 (m, 2H), 1.40-1.36 (m, 4H), 0.93-0.90 (m, 3H); <sup>13</sup>C-NMR (100 MHz, CDCl<sub>3</sub>) δ 162.5, 161.8, 159.1, 158.5, 142.3, 129.2, 125.8, 123.7, 121.5, 120.6, 114.8, 114.3, 55.4, 39.8, 29.1, 29.0, 22.3, 13.9; ν<sub>max</sub>/cm<sup>-1</sup> (KBr) 3261, 2958, 1646, 1582, 1335, 1255, 921; mp 124-125 °C; HRMS (EI<sup>+</sup>): *m/z*: calcd for C<sub>20</sub>H<sub>22</sub>ClN<sub>3</sub>O<sub>5</sub>: 419.1248, Found: 419.1248.

(Z)-N-(tert-butyl)-2-(4-methoxyphenyl)-2-(((5-nitropyridin-2-yl)oxy)imino)acetamide, 5{2,2,5} The crude material was purified by column chromatography (*n*-hexane/EtOAc 9:1) to give the product as white solid (yield 22%). <sup>1</sup>H-NMR (400 MHz, CDCl<sub>3</sub>) δ 9.16 (br s, 1H), 8.50 (br d, AA'XX', 1H), 7.76 (d, *J* = 7.76 Hz, 2H), 7.40 (d, *J* = 9.16 Hz, 1H), 6.96 (d, *J* = 7.96 Hz, 2H), 5.65 (br s, NH), 3.86 (s, 3H), 1.53 (s, 9H); <sup>13</sup>C-NMR (100 MHz, DMSO-d<sub>6</sub>) δ 168.1, 162.4, 161.3, 159.3, 145.4, 140.8, 136.2, 129.4, 122.3, 115.1, 108.8, 55.9, 51.9, 28.9; ν<sub>max</sub>/cm<sup>-1</sup> (KBr) 3419, 1613, 1515, 1347, 1258, 927; mp 174-175 °C; HRMS (EI<sup>+</sup>): *m/z*: calcd for C<sub>18</sub>H<sub>20</sub>N<sub>4</sub>O<sub>5</sub>: 372.1434, Found: 372.1439.

(Z)-2-(4-methoxyphenyl)-2-(((5-nitropyridin-2-yl)oxy)imino)-N-pentylacetamide, 5{2,3,5} The crude material was purified by column chromatography (*n*-hexane/EtOAc 9:1) to give the product as sticky dark-red solid (yield 39%). Mixture of E/Z isomers, signals are referred to the main isomer: <sup>1</sup>H-NMR (400 MHz, CDCl<sub>3</sub>) δ 9.16 (br s, 1H), 8.80 (br s, NH), 8.02 (br d, AA'XX', 1H), 7.68 (d, *J* = 8.72 Hz, 1H), 7.51 (d, *J* = 8.64 Hz, 2H), 6.88 (d, *J* = 8.76 Hz, 2H), 3.81 (s, 3H), 3.37-3.34 (m, 2H), 1.65-1.60 (m, 2H), 1.29-1.25 (m, 4H), 0.90-0.84 (m, 3H); <sup>13</sup>C-NMR (100 MHz, CDCl<sub>3</sub>) δ 167.6, 162.6, 161.0, 149.1, 136.9, 133.7, 131.9, 128.0, 123.8, 120.8, 114.1, 55.3, 52.0, 29.7, 28.9, 22.2, 13.9; ν<sub>max</sub>/cm<sup>-1</sup> (KBr) 3473, 3414, 1682, 1616, 1255, 933; HRMS (EI<sup>+</sup>): *m/z*: calcd for C<sub>19</sub>H<sub>22</sub>N<sub>4</sub>O<sub>5</sub>: 386.1590, Found: 386.1587.

(Z)-N-benzyl-2-(4-chlorophenyl)-2((4-nitrophenoxy)imino)acetamide, **5**{3,1,1} The crude material was purified by column chromatography (*n*-hexane/EtOAc 8:2) to give the product as pale yellow solid (yield 55%). <sup>1</sup>H-NMR (400 MHz, CDCl<sub>3</sub>) δ 8.23 (d, *J* = 9.20 Hz, 2H), 7.73 (d, *J* = 8.52 Hz, 2H), 7.44-7.35 (m, 7H), 7.27-7.25 (m, 2H), 6.22 (br t, *NH*), 4.72 (br d, 2H); <sup>13</sup>C-NMR (100 MHz, CDCl<sub>3</sub>) δ 163.0, 161.6, 156.4, 143.0, 138.0, 137.1, 129.3, 128.9, 128.5, 128.0, 127.9, 127.9, 125.7, 114.3, 43.6; *v*<sub>max</sub>/cm<sup>-1</sup> (KBr) 3411, 1654, 1515, 1345, 1220, 929, 850; mp 159-160 °C; HRMS (EI<sup>+</sup>): *m/z*: calcd for C<sub>21</sub>H<sub>16</sub>ClN<sub>3</sub>O<sub>4</sub>: 409.0829, Found: 409.0831.

(Z)-N-(*tert*-butyl)-2-(4-chlorophenyl)-2((4-nitrophenoxy)imino)acetamide, **5**{3,2,1} The crude material was purified by column chromatography (*n*-hexane/EtOAc 9:1) to give the product as yellow solid (yield 53%). <sup>1</sup>H-NMR (400 MHz, CDCl<sub>3</sub>) δ 8.25 (d, *J* = 9.12 Hz, 2H), 7.73 (d, *J* = 8.48 Hz, 2H), 7.44 (d, *J* = 8.44 Hz, 2H), 7.34 (d, *J* = 9.16 Hz, 2H), 5.61 (br s, *NH*), 1.53 (s, 9H); <sup>13</sup>C-NMR (100 MHz, CDCl<sub>3</sub>) δ 163.2, 161.0, 156.6, 142.7, 137.7, 129.2, 128.4, 128.1, 125.6, 114.2, 53.0, 28.7; *v*<sub>max</sub>/cm<sup>-1</sup> (KBr) 3272, 2965, 1651, 1517, 1342, 1237, 917, 841; mp 160-161 °C; HRMS (EI<sup>+</sup>): *m/z*: calcd for C<sub>18</sub>H<sub>18</sub>ClN<sub>3</sub>O<sub>4</sub>: 375.0986, Found: 375.0989.

(Z)- 2-(4-chlorophenyl)-2((4-nitrophenoxy)imino)-N-pentylacetamide, **5**{3,3,1} The crude material was purified by column chromatography (*n*-hexane/EtOAc 9:1) to give the product as yellow solid (yield 43%). <sup>1</sup>H-NMR (400 MHz, CDCl<sub>3</sub>) δ 8.23 (br d, AA'XX', 2H), 7.72 (d, *J* = 8.64 Hz, 2H), 7.42 (d, *J* = 8.60 Hz, 2H), 7.33 (br d, *J* = 9.24 Hz, 2H), 5.94 (br t, *NH*), 3.55-3.50 (m, 2H), 1.68-1.63 (m, 2H), 1.42-1.38 (m, 4H), 0.94-0.91 (m, 3H); <sup>13</sup>C-NMR (100 MHz, CDCl<sub>3</sub>) δ 163.1, 161.6, 156.6, 142.7, 137.7, 129.2, 128.5, 128.1, 125.6, 114.3, 39.6, 29.0, 28.9, 22.2, 13.9; *v*<sub>max</sub>/cm<sup>-1</sup> (KBr) 3301, 2953, 1660, 1508, 1339, 927, 854; mp 106-107 °C; HRMS (EI<sup>+</sup>): *m/z*: calcd for C<sub>19</sub>H<sub>20</sub>ClN<sub>3</sub>O<sub>4</sub>: 389.1142, Found: 389.1141.

(Z)-N-benzyl-2-(4-chlorophenyl)-2((2-nitrophenoxy)imino)acetamide, **5**{3,1,2} The crude material was purified by column chromatography (*n*-hexane/EtOAc 9:1) to give the product as pale yellow solid (yield 42%). <sup>1</sup>H-NMR (400 MHz, CDCl<sub>3</sub>) δ 8.00 (d, *J* = 8.16 Hz, 2H), 7.77-7.72 (m, 3H), 7.63 (br t, 1H), 7.42-7.29 (m, 7H), 7.22-7.18 (m, 1H), 6.80 (br s, *NH*), 4.74 (br d, 2H); <sup>13</sup>C-NMR (100 MHz, CDCl<sub>3</sub>) δ 161.0, 156.5, 152.1, 137.6, 137.0, 134.8, 129.1, 129.0, 128.8, 128.4, 128.1, 127.7, 125.7, 123.1, 117.9, 43.9; *v*<sub>max</sub>/cm<sup>-1</sup> (KBr) 3412, 3248, 1638, 1525, 1337, 1225, 926, 832; mp 145-146 °C; HRMS (EI<sup>+</sup>): *m/z*: calcd for C<sub>21</sub>H<sub>16</sub>ClN<sub>3</sub>O<sub>4</sub>: 409.0829, Found: 409.0832.

(Z)-N-(*tert*-butyl)-2-(4-chlorophenyl)-2((2-nitrophenoxy)imino)acetamide, **5**{3,2,2} The crude material was purified by column chromatography (*n*-hexane/EtOAc 9:1) to give the product as yellow solid (yield 48%). <sup>1</sup>H-NMR (400 MHz, CDCl<sub>3</sub>) δ 7.96 (br d, AA'XX', 1H), 7.74-7.71 (m, 3H), 7.63-7.59 (m, 1H), 7.41-7.39 (m, 2H), 7.21-7.17 (m, 1H), 6.07 (br s, *NH*), 1.53 (s, 9H); <sup>13</sup>C-NMR (100 MHz, CDCl<sub>3</sub>) δ 160.4, 156.5, 152.2, 137.8, 137.4, 134.5, 129.0, 128.7, 128.6, 125.4, 122.8, 118.0, 53.1, 28.5; *v*<sub>max</sub>/cm<sup>-1</sup> (KBr) 3249, 2972, 1634, 1515, 1347, 1228, 915, 739; mp 125-126 °C; HRMS (EI<sup>+</sup>): *m/z*: calcd for C<sub>18</sub>H<sub>18</sub>ClN<sub>3</sub>O<sub>4</sub>: 375.0986, Found: 375.0983.

(Z)- 2-(4-chlorophenyl)-2((2-nitrophenoxy)imino)-N-pentylacetamide, **5**{3,3,2} The crude material was purified by column chromatography (*n*-hexane/EtOAc 9:1) to give the product as brown solid (yield 41%). <sup>1</sup>H-NMR (400 MHz, CDCl<sub>3</sub>) δ 7.99 (d, *J* = 8.20 Hz, 1H), 7.75-7.71 (m, 3H), 7.62 (br t, 1H), 7.40 (d, *J* = 8.20 Hz, 2H), 7.20 (br t, 1H), 6.52 (br s, *NH*), 3.56-3.51 (m, 2H), 1.70-1.67 (m, 2H), 1.37-1.32 (m, 4H), 0.92-0.89 (m, 3H); <sup>13</sup>C-NMR (100 MHz, CDCl<sub>3</sub>) δ 161.0, 156.7, 152.1, 137.7, 137.4, 134.7, 129.0, 128.9, 128.6, 125.6, 123.0, 117.8, 39.9, 29.0, 28.8, 22.2, 13.9; *v*<sub>max</sub>/cm<sup>-1</sup> (KBr) 3255, 2929, 1652, 1521, 1347, 1226, 921, 833; mp 60-61 °C; HRMS (EI<sup>+</sup>): *m/z*: calcd for C<sub>19</sub>H<sub>20</sub>ClN<sub>3</sub>O<sub>4</sub>: 389.1142, Found: 389.1141.

(Z)-N-benzyl-2-(4-chlorophenyl)-2((2,4-dinitrophenoxy)imino)acetamide, **5**{3,1,3} The crude material was purified by column chromatography (*n*-hexane/EtOAc 9:1) to give the product as yellow solid (yield 34%). <sup>1</sup>H-NMR (400 MHz, CDCl<sub>3</sub>) δ 8.92 (br s, 1H), 8.48 (br d, AA'XX', 1H), 8.00 (d, *J* = 9.40 Hz, 1H), 7.75 (d, *J* = 8.52 Hz, 2H), 7.46-7.37 (m, 7H), 6.42 (br s, *NH*), 4.75 (br d, 2H); <sup>13</sup>C-NMR (100 MHz, DMSO-*d*<sub>6</sub>) δ 161.0, 159.8,

155.7, 141.8, 138.2, 137.4, 136.7, 130.2, 129.9, 129.6, 128.9, 128.4, 128.0, 127.6, 122.2, 118.0, 42.9;  $\nu_{\text{max}}/\text{cm}^{-1}$  (KBr) 3236, 1604, 1533, 1342, 835; mp 142-143 °C; HRMS (EI+):  $m/z$ : calcd for  $\text{C}_{21}\text{H}_{15}\text{ClN}_4\text{O}_6$ : 454.0680, Found: 454.0683.

*(Z)-N-(tert-butyl)-2-(4-chlorophenyl)-2-((2,4-dinitrophenoxy)imino)acetamide*, **5**{3,2,3} The crude material was purified by column chromatography (*n*-hexane/EtOAc 9:1) to give the product as yellow solid (yield 46%).  $^1\text{H-NMR}$  (400 MHz,  $\text{CDCl}_3$ )  $\delta$  8.86 (s, 1H), 8.46 (d,  $J = 9.28$  Hz, 1H), 7.96 (d,  $J = 9.32$  Hz, 1H), 7.73 (d,  $J = 8.12$  Hz, 2H), 7.43 (d,  $J = 8.04$  Hz, 2H), 5.93 (br s, NH), 1.53 (s, 9H);  $^{13}\text{C-NMR}$  (100 MHz,  $\text{CDCl}_3$ )  $\delta$  159.7, 158.5, 156.3, 141.5, 138.4, 136.4, 129.3, 129.1, 128.9, 127.7, 121.7, 117.7, 53.5, 28.5;  $\nu_{\text{max}}/\text{cm}^{-1}$  (KBr) 3275, 2972, 1660, 1540, 1344, 1283, 833, 740; mp 118-119 °C; HRMS (EI+):  $m/z$ : calcd for  $\text{C}_{18}\text{H}_{17}\text{ClN}_4\text{O}_6$ : 420.0837, Found: 420.0840.

*(Z)-2-(4-chlorophenyl)-2-((2,4-dinitrophenoxy)imino)-N-pentylacetamide*, **5**{3,3,3} The crude material was purified by column chromatography (*n*-hexane/EtOAc 9:1) to give the product as yellow solid (yield 32%).  $^1\text{H-NMR}$  (400 MHz,  $\text{CDCl}_3$ )  $\delta$  8.90 (br s, 1H), 8.47 (br d, AA'XX', 1H), 7.98 (d,  $J = 9.28$  Hz, 1H), 7.74 (d,  $J = 8.56$  Hz, 2H), 7.44 (d,  $J = 8.52$  Hz, 2H), 6.18 (br s, NH), 3.57-3.52 (m, 2H), 1.70-1.67 (m, 2H), 1.39-1.37 (m, 4H), 0.93-0.90 (m, 3H);  $^{13}\text{C-NMR}$  (100 MHz,  $\text{CDCl}_3$ )  $\delta$  160.6, 158.9, 156.2, 141.5, 138.5, 136.2, 129.3, 129.3, 129.0, 127.4, 121.9, 117.4, 40.0, 29.0, 28.7, 22.2, 13.9;  $\nu_{\text{max}}/\text{cm}^{-1}$  (KBr) 3284, 1652, 1558, 1472, 1344, 834, 739; mp 156-157 °C; HRMS (EI+):  $m/z$ : calcd for  $\text{C}_{19}\text{H}_{19}\text{ClN}_4\text{O}_6$ : 434.0993, Found: 434.0995.

*(Z)-N-benzyl-2-((2-chloro-4-nitrophenoxy)imino)-2-(4-chlorophenyl)acetamide*, **5**{3,1,4} The crude material was purified by column chromatography (*n*-hexane/EtOAc 8:2) to give the product as light yellow solid (yield 63%).  $^1\text{H-NMR}$  (400 MHz,  $\text{CDCl}_3$ )  $\delta$  8.22 (br s, 1H), 8.11 (br d, AA'XX', 1H), 7.69-7.65 (m, 3H), 7.38-7.25 (m, 8H), 4.61 (s, 2H);  $^{13}\text{C-NMR}$  (100 MHz,  $\text{DMSO-d}_6$ )  $\delta$  161.2, 158.9, 158.9, 142.7, 138.4, 137.1, 129.8, 129.4, 128.8, 128.7, 128.2, 127.6, 126.1, 124.9, 119.9, 115.9, 42.8;  $\nu_{\text{max}}/\text{cm}^{-1}$  (KBr) 3353, 3104, 1676, 1523, 1344, 933, 741; mp 165-166 °C; HRMS (EI+):  $m/z$ : calcd for  $\text{C}_{21}\text{H}_{15}\text{Cl}_2\text{N}_3\text{O}_4$ : 443.0440, Found: 443.0441.

*(Z)-N-(tert-butyl)-2-((2-chloro-4-nitrophenoxy)imino)-2-(4-chlorophenyl)acetamide*, **5**{3,2,4} The crude material was purified by column chromatography (*n*-hexane/EtOAc 9:1) to give the product as yellow solid (yield 47%).  $^1\text{H-NMR}$  (400 MHz,  $\text{CDCl}_3$ )  $\delta$  8.30 (s, 1H), 8.18 (d,  $J = 9.04$  Hz, 1H), 7.75-7.72 (m, 3H), 7.43 (d,  $J = 8.20$  Hz, 2H), 5.84 (br s, NH), 1.53 (s, 9H);  $^{13}\text{C-NMR}$  (100 MHz,  $\text{CDCl}_3$ )  $\delta$  160.3, 158.9, 157.3, 142.3, 137.8, 129.1, 128.6, 128.0, 125.8, 123.6, 120.5, 114.7, 53.0, 28.7;  $\nu_{\text{max}}/\text{cm}^{-1}$  (KBr) 3300, 2972, 1652, 1555, 1344, 1233, 930; mp 144-145 °C; HRMS (EI+):  $m/z$ : calcd for  $\text{C}_{18}\text{H}_{17}\text{Cl}_2\text{N}_3\text{O}_4$ : 409.0596, Found: 409.0595.

*(Z)-2-((2-chloro-4-nitrophenoxy)imino)-2-(4-chlorophenyl)-N-pentylacetamide*, **5**{3,3,4} The crude material was purified by column chromatography (*n*-hexane/EtOAc 9:1) to give the product as yellow solid (yield 56%).  $^1\text{H-NMR}$  (400 MHz,  $\text{CDCl}_3$ )  $\delta$  8.29 (br s, 1H), 8.16 (br d, AA'XX', 1H), 7.74-7.69 (m, 3H), 7.42 (d,  $J = 8.56$  Hz, 2H), 6.12 (br s, NH), 3.54-3.49 (m, 2H), 1.69-1.66 (m, 2H), 1.38-1.36 (m, 4H), 0.93-0.90 (m, 3H);  $^{13}\text{C-NMR}$  (100 MHz,  $\text{CDCl}_3$ )  $\delta$  161.1, 158.8, 157.7, 142.4, 138.0, 129.1, 128.6, 127.8, 125.8, 123.6, 120.6, 114.6, 39.8, 31.5, 29.0, 22.2, 13.9;  $\nu_{\text{max}}/\text{cm}^{-1}$  (KBr) 3246, 2929, 1646, 1582, 1343, 928, 834; mp 136-137 °C; HRMS (EI+):  $m/z$ : calcd for  $\text{C}_{19}\text{H}_{19}\text{Cl}_2\text{N}_3\text{O}_4$ : 423.0753, Found: 423.0757.

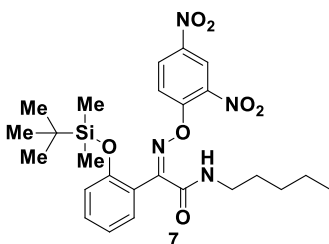
*(Z)-N-(tert-butyl)-2-(4-chlorophenyl)-2-(((4-nitropyridin-2-yl)oxy)imino)acetamide*, **5**{3,2,5} The crude material was purified by column chromatography (*n*-hexane/EtOAc 7:3) to give the product as white solid (yield 42%).  $^1\text{H-NMR}$  (400 MHz,  $\text{CDCl}_3$ )  $\delta$  9.18 (br s, 1H), 8.52 (br d, AA'XX', 1H), 7.76 (d,  $J = 8.56$  Hz, 2H), 7.45-7.39 (m, 3H), 5.70 (br s, NH), 1.53 (s, 9H);  $^{13}\text{C-NMR}$  (100 MHz,  $\text{CDCl}_3$ )  $\delta$  167.8, 160.8, 158.6, 145.4,

141.1, 136.9, 136.3, 129.7, 129.4, 129.1, 109.0, 52.1, 28.8;  $\nu_{\max}/\text{cm}^{-1}$  (KBr) 3414, 3293, 1675, 1577, 1349, 935, 833; mp 193-194 °C; HRMS (EI+):  $m/z$ : calcd for  $\text{C}_{17}\text{H}_{17}\text{ClN}_4\text{O}_4$ : 376.0938, Found: 376.0939.

(*Z*)-2-(4-chlorophenyl)-2-(((5-nitropyridin-2-yl)oxy)imino)-*N*-pentylacetamide, **5**{3,3,5} The crude material was purified by column chromatography (n-hexane/EtOAc 9:1) to give the product as sticky dark-red solid (yield 35%). Mixture of E/Z isomers, signals are referred to the main isomer:  $^1\text{H-NMR}$  (400 MHz,  $\text{CDCl}_3$ )  $\delta$  9.15 (s, 1H), 9.03 (br s, NH), 8.05 (br d, AA'XX', 1H), 7.70 (d,  $J = 8.52$  Hz, 1H), 7.52 (d,  $J = 8.56$  Hz, 2H), 7.34 (d,  $J = 8.60$  Hz, 2H), 3.34-3.30 (m, 2H), 1.65-1.62 (m, 2H), 1.27-1.25 (m, 4H), 0.92-0.85 (m, 3H);  $^{13}\text{C-NMR}$  (100 MHz,  $\text{CDCl}_3$ )  $\delta$  167.2, 160.9, 148.8, 148.0, 144.9, 136.6, 135.1, 133.9, 130.0, 129.0, 127.7, 52.1, 29.7, 28.9, 22.2, 13.9;  $\nu_{\max}/\text{cm}^{-1}$  (KBr) 2932, 1691, 1564, 1345, 1273, 935, 834; HRMS (EI+):  $m/z$ : calcd for  $\text{C}_{18}\text{H}_{19}\text{ClN}_4\text{O}_4$ : 390.1095, Found: 390.1098.

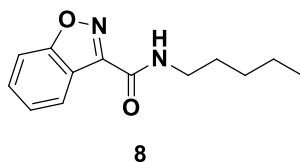
(*Z*)-2-(2-((*tert*-butyldimethylsilyl)oxy)phenyl)-2-((2,4-dinitrophenoxy)imino)-*N*-pentylacetamide, **7**

The crude material was purified by column chromatography (PE/EtOAc 9:1) to give the product as yellow solid (yield 48%).  $^1\text{H-NMR}$  (300 MHz,  $\text{CDCl}_3$ )  $\delta$  8.86 (d,  $J = 2.7$  Hz, 1H), 8.42 (dd,  $J = 6.7, 2.4$  Hz, 1H), 7.99 (d,  $J = 9.5$  Hz, 1H), 7.46 (dd,  $J = 7.65, 1.5$  Hz, 1H), 6.99-6.85 (m, 3H), 3.42-3.38 (m, 2H), 1.67-1.62 (m, 2H), 1.33-1.31 (m, 4H), 0.90 (s, 12H), 0.19 (s, 6H);  $^{13}\text{C-NMR}$  (75 MHz,  $\text{CDCl}_3$ )  $\delta$  159.7, 159.4, 156.5, 154.3, 141.6, 136.1, 132.1, 131.0, 129.5, 122.5, 122.1, 121.3, 119.6, 117.9, 40.3, 29.2, 28.7, 25.8, 22.3, 18.4, 14.0, -4.0;  $m/z$  532 (M+H) $^+$ ;  $\nu_{\max}/\text{cm}^{-1}$  (KBr) 3292, 1607, 1537, 1486, 1260, 914; mp 110.8-111.2°C; HRMS (EI+):  $m/z$ : calcd for  $\text{C}_{25}\text{H}_{34}\text{N}_4\text{O}_7\text{Si}$ : 530.2197, Found: 530.2201.

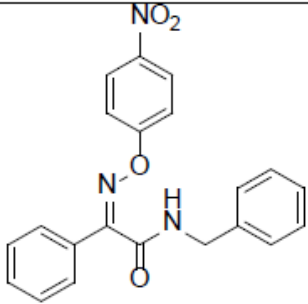
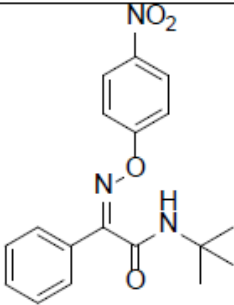
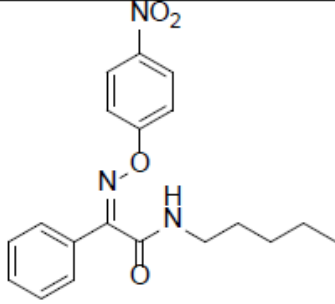
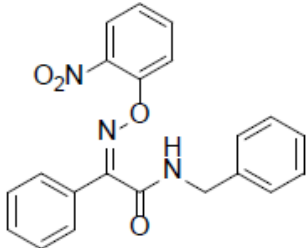
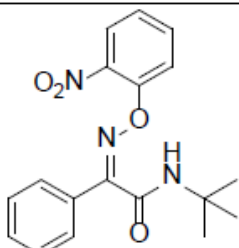


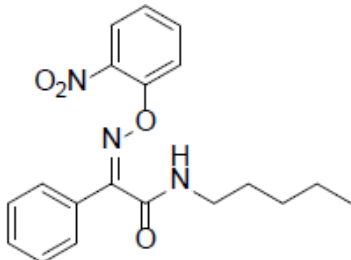
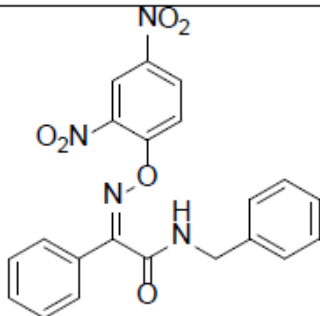
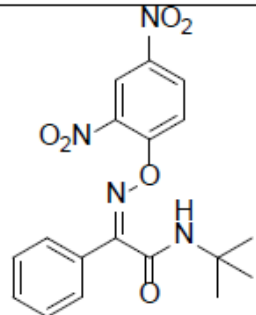
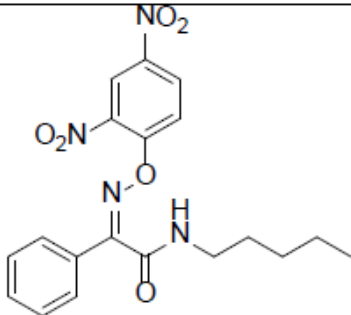
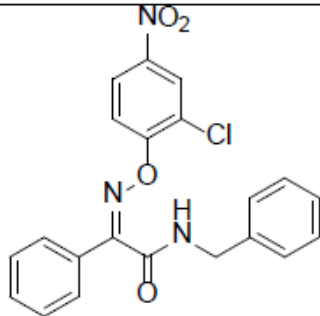
*N*-pentylbenzo[*d*]isoxazole-3-carboxamide, **8**

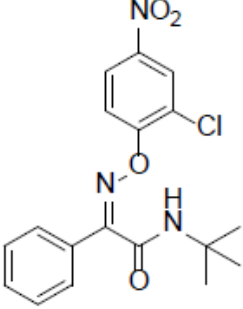
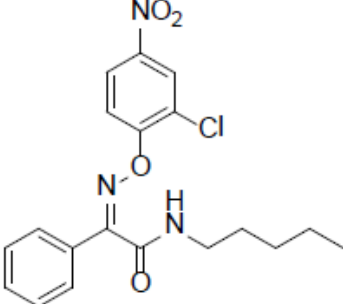
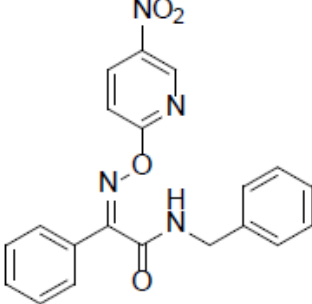
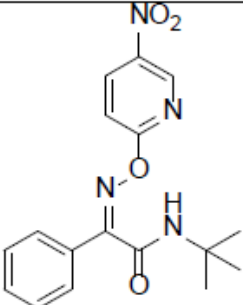
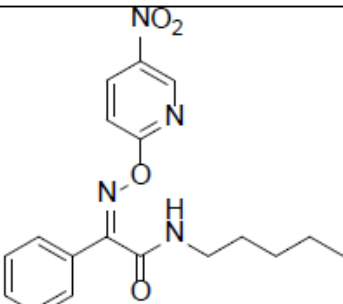
The crude material was purified by column chromatography (PE/EtOAc 9:1) to give the product as yellow amorphous solid (yield quantitative).  $^1\text{H-NMR}$  (300 MHz,  $\text{CDCl}_3$ )  $\delta$  8.26 (d,  $J = 9.30$  Hz, 1H), 7.56 (br d, 2H), 7.36 (m, 1H), 7.08 (br s, NH), 3.49 (m, 2H), 1.65-1.61 (m, 2H), 1.36-1.33 (m, 4H), 0.89-0.87 (m, 3H);  $^{13}\text{C-NMR}$  (75 MHz,  $\text{CDCl}_3$ )  $\delta$  164.15, 159.3, 152.0, 130.4, 124.9, 124.0, 120.0, 109.7, 39.5, 29.2, 29.1, 22.4, 14.0;  $m/z$  233 (M+H) $^+$ ;  $\nu_{\max}/\text{cm}^{-1}$  (KBr) 3271, 1672, 1548, 1254, 913; HRMS (EI+):  $m/z$ : calcd for  $\text{C}_{13}\text{H}_{16}\text{N}_2\text{O}_2$ : 232.1212, Found: 232.1212.



**Table S1.** Aryloxyimino amides synthesized. <sup>§</sup>Yield refers to the purified product. \*Purity refers to the mixture of Z and E isomers.

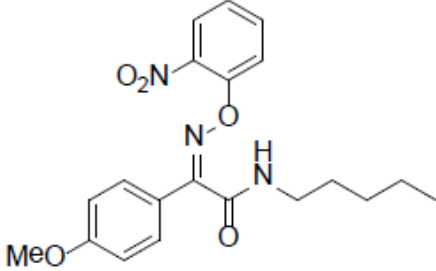
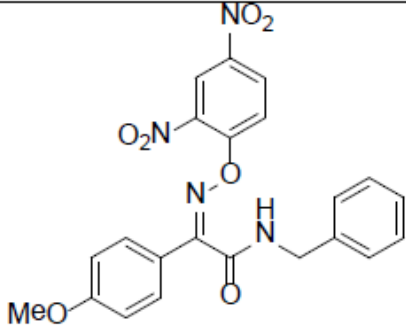
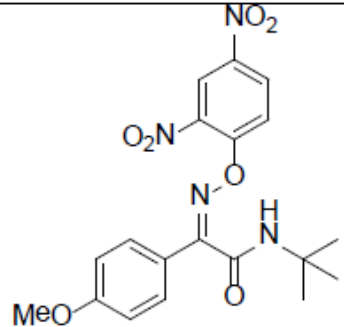
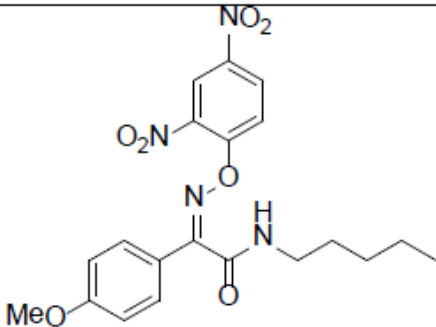
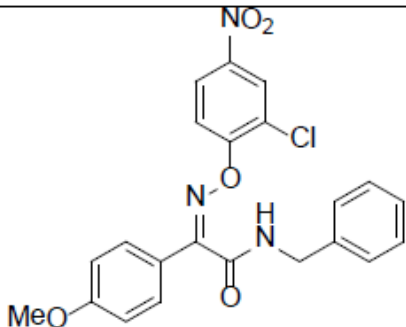
Compound	Structure	Formula weight	Yield <sup>§</sup> (%)	Purity A	Purity B
5{1,1,1}		375.4	33	98.1*	98.1*
5{1,2,1}		341.4	41	99.2*	98.7*
5{1,3,1}		355.4	37	93.0	93.4
5{1,1,2}		375.4	25	97.0*	99.9*
5{1,2,2}		341.4	42	94.8	95.0

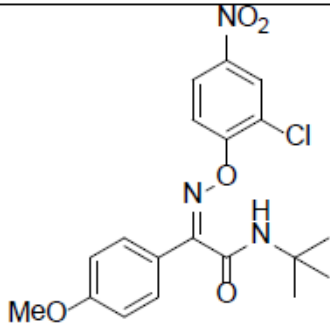
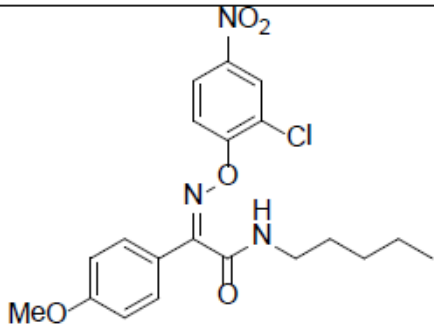
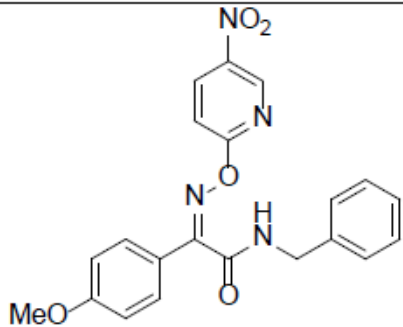
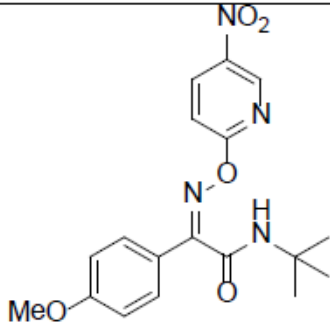
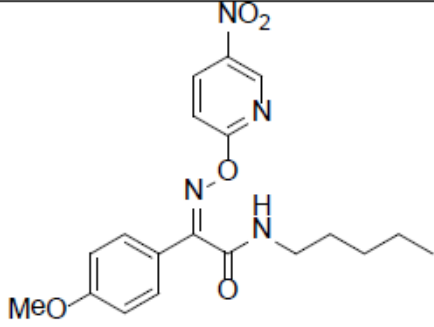
Compound	Structure	Formula weight	Yield <sup>§</sup> (%)	Purity A	Purity B
5{1,3,2}		355.4	51	96.1	96.1
5{1,1,3}		420.4	30	90.3	90.9
5{1,2,3}		386.4	38	90.4	91.1
5{1,3,3}		400.4	32	91.2	92.4
5{1,1,4}		409.8	45	97.9	98.3

Compound	Structure	Formula weight	Yield <sup>§</sup> (%)	Purity A	Purity B
5{1,2,4}		375.8	45	93.9	95.7
5{1,3,4}		389.8	53	95.9	95.3
5{1,1,5}		376.4	-	-	-
5{1,2,5}		342.3	20	93.5	92.5
5{1,3,5}		356.4	33	88.9*	92.4*

Compound	Structure	Formula weight	Yield <sup>§</sup> (%)	Purity A	Purity B
5{2,1,1}		405.4	-	-	-
5{2,2,1}		371.4	33	98.0*	96.0*
5{2,3,1}		385.4	39	95.3*	95.3*
5{2,1,2}		405.4	26	94.1*	92.0*
5{2,2,2}		371.4	49	96.5*	96.5*

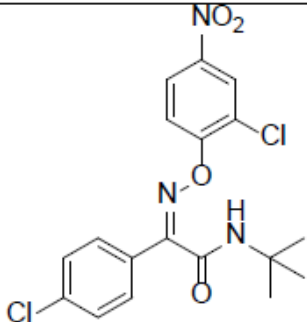
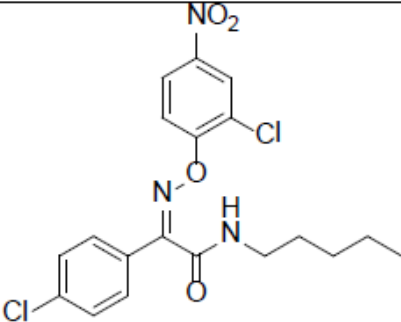
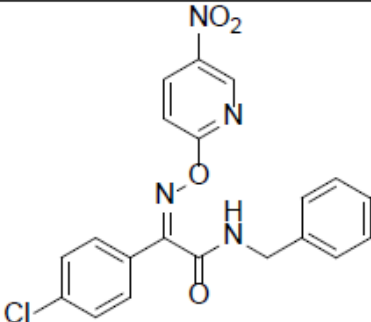
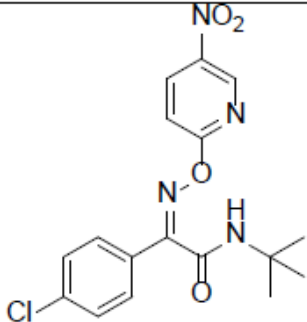
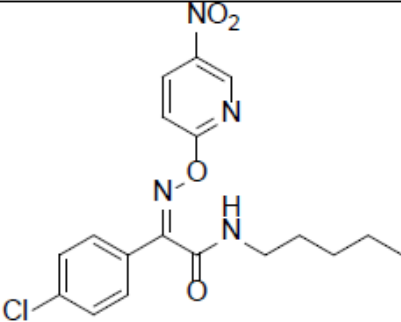


Compound	Structure	Formula weight	Yield <sup>§</sup> (%)	Purity A	Purity B
5{2,3,2}		385.4	45	93.6	95.1
5{2,1,3}		450.4	40	79.8	80.0
5{2,2,3}		416.4	33	83.5	84.6
5{2,3,3}		430.4	40	86.1	85.8
5{2,1,4}		439.6	63	90.9	90.5

Compound	Structure	Formula weight	Yield <sup>§</sup> (%)	Purity A	Purity B
5{2,2,4}		405.8	38	89.6	89.6
5{2,3,4}		419.9	50	91.8	91.4
5{2,1,5}		406.4	-	-	-
5{2,2,5}		372.4	22	85.5	86.4
5{2,3,5}		386.4	39	85.7	90.8

Compound	Structure	Formula weight	Yield <sup>§</sup> (%)	Purity A	Purity B
5{3,1,1}		409.8	55	90.2	89.7
5{3,2,1}		375.8	53	94.6	94.3
5{3,3,1}		389.8	43	95.5	95.6
5{3,1,2}		409.8	42	93.9	95.4
5{3,2,2}		375.8	48	96.6	96.6

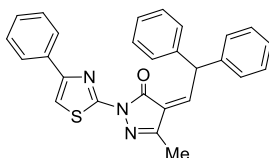
Compound	Structure	Formula weight	Yield <sup>§</sup> (%)	Purity A	Purity B
5{3,3,2}		389.8	41	97.7	97.6
5{3,1,3}		454.8	34	87.2	83.4
5{3,2,3}		420.8	46	93.4	91.7
5{3,3,3}		434.8	32	96.1	95.5
5{3,1,4}		443.8	63	97.1	97.3

Compound	Structure	Formula weight	Yield <sup>§</sup> (%)	Purity A	Purity B
5{3,2,4}		409.8	47	95.3	96.2
5{3,3,4}		423.8	56	96.6	96.5
5{3,1,5}		410.8	-	-	-
5{3,2,5}		376.8	42	96.9	98.5
5{3,3,5}		390.8	35	97.4*	98.5*

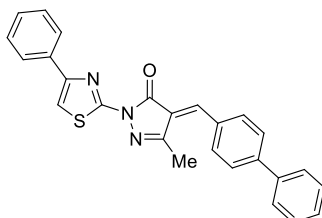
## 4.3 Part III: Synthesis of BAX Direct Activators as Novel Potential Anticancer Agents

**Chemistry.** All reagents and solvents were handled according to material safety data sheet of the supplier and were used as purchased without further purification. Organic solutions were dried over anhydrous sodium sulfate. Evaporation of the solvents was carried out on Büchi Rotavapor R-210 equipped with Büchi V-855 vacuum controller and Büchi V-700 (~5 mbar) and V-710 (~2 mbar) vacuum pumps and on Heidolph Hei-Vap G3B equipped with Vacuubrand PC 3001 vacuum pump (~2 mbar). Column chromatography was performed on glass columns packed with silica gel from Fluka and from Aldrich (70–230 mesh). Silica gel thin layer chromatography (TLC) cards from Fluka and Macherey-Nagel (silica gel precoated aluminum cards with fluorescent indicator visualizable at 254 nm) were used for TLC. Developed plates were visualized by a Spectroline ENF 260C/FE UV apparatus. Melting points (mp) were determined on a Stuart Scientific SMP1 apparatus and on a Stuart Scientific SMP30 apparatus and are uncorrected. Infrared spectra (IR) were run on PerkinElmer SpectrumOne FT-ATR spectrophotometer. Band position and absorption ranges are given in  $\text{cm}^{-1}$ . Mass spectral (MS) and high resolution mass spectral (HRMS) analyses were recorded on AB Sciex API-2000 (MS) and Thermo Fisher Scientific Inc. Orbitrap Exactive (HRMS) spectrometers equipped with an ESI source. Proton ( $^1\text{H}$ , 400.13 MHz) and carbon ( $^{13}\text{C}$ , 100.6 MHz) nuclear magnetic resonance spectra were recorded on a Bruker Avance 400 and a Varian Inova 400 spectrometers in the indicated solvent and corresponding fid files processed by MestreLab Research SL MestreReNova 6.2.1– 769 and Bruker Topspin 3.2 software. Chemical shifts are expressed in  $\delta$  units (ppm) from tetramethylsilane. Elemental analyses of the compounds were found within  $\pm 0.4\%$  of the theoretical values. The purity of tested compounds was found to be  $>95\%$  by high pressure liquid chromatography (HPLC) analysis. The HPLC system used (Thermo Fisher Scientific Inc. Dionex UltiMate 3000) consisted of a SR-3000 solvent rack, a LPG-3400SD quaternary analytical pump, a TCC-3000SD column compartment, a DAD-3000 diode array detector, and an analytical manual injection valve with a 20  $\mu\text{L}$  loop. Samples were dissolved in acetonitrile at 10 mg/mL. HPLC analysis was performed by using a Thermo Fisher Scientific Inc. Acclaim 120 C18 reversed-phase column (5  $\mu\text{m}$ , 4.6 mm  $\times$  250 mm) at  $30 \pm 1^\circ\text{C}$  with an isocratic gradient (acetonitrile:water = 90:10), flow rate of 1.0 mL/min, and signal detector at 254 and 365 nm. Chromatographic data were acquired and processed by Thermo Fisher Scientific Inc. Chromeleon 6.80 software.

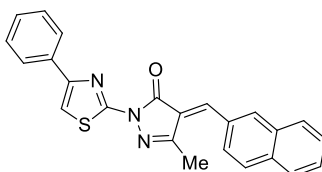
*General Procedure for the Preparation of Compounds 2–5 and 16.* Example: 4-(2,2-Diphenylethylidene)-3-methyl-1-(4-phenylthiazol-2-yl)-1H-1H-pyrazol-5(4H)-one (2). A mixture of 17 (0.21 g, 0.00084 mol), 2,2-diphenylacetaldehyde (0.16 g, 0.15 mL, 0.84 mmol), and piperidine (0.071 g, 0.08 mL, 0.84 mmol) in ethanol (0.5 M) were heated to reflux for 3 h and evaporated. The residue was purified by column chromatography (silica gel, dichloromethane:methanol = 99:1 as eluent) to furnish 2 (0.17 g, 47%), mp  $>220^\circ\text{C}$  with decomposition (from ethanol).  $^1\text{H}$  NMR (DMSO- $d_6$ ):  $\delta$  1.53 (s, 3H), 6.49 (s, 1H), 7.16 (d,  $J = 3.7$  Hz, 2H), 7.22–7.38 (m, 10H), 7.43 (t,  $J = 7.4$  Hz, 2H), 7.72 (s, 1H), 7.96 ppm (d,  $J = 3.8$  Hz, 2H). IR:  $\nu$  1616  $\text{cm}^{-1}$ . Anal. (C<sub>27</sub>H<sub>21</sub>N<sub>3</sub>O<sub>3</sub> (435.54)): C, 74.46; H, 4.86; N, 9.65; S, 7.36. Found: C, 74.44; H, 4.83; N, 9.69; S, 7.34. MS (ESI) calcd for C<sub>27</sub>H<sub>21</sub>N<sub>3</sub>O<sub>3</sub>: 435.1; found (M + H)<sup>+</sup>: 436.1.



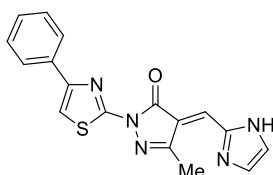
4-([1,1'-Biphenyl]-4-ylmethylene)-3-methyl-1-(4-phenylthiazol-2-yl)-1H-pyrazol-5(4H)-one (3). It was synthesized as 2 starting from 17 and [1,1'-biphenyl]-4-carbaldehyde. Yield 61%, mp >270 °C with decomposition (from ethanol). <sup>1</sup>H NMR (DMSO-d<sub>6</sub>): δ 2.13 (s, 3H), 7.29–7.38 (m, 4H), 7.40–7.48 (m, 5H), 7.58–7.68 (m, 4H), 7.72 (s, 1H), 7.98 (d, J = 3.7 Hz, 2H). IR: ν 1625 cm<sup>-1</sup>. Anal. (C<sub>26</sub>H<sub>19</sub>N<sub>3</sub>O<sub>2</sub> (421.51)): C, 74.08; H, 4.54; N, 9.97; S, 7.61. Found: C, 74.04; H, 4.58; N, 9.92; S, 7.59. MS (ESI) calcd for C<sub>26</sub>H<sub>19</sub>N<sub>3</sub>O<sub>2</sub>: 421.1; found (M + H)<sup>+</sup>: 422.3.



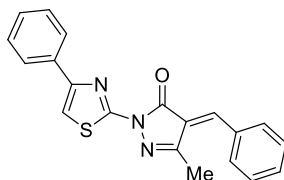
3-Methyl-4-(naphthalen-2-ylmethylene)-1-(4-phenylthiazol-2-yl)-1H-pyrazol-5(4H)-one (4). It was synthesized as 2 starting from 17 and 2-naphthaldehyde. Yield 37%, mp >270 °C with decomposition (from ethanol). <sup>1</sup>H NMR (DMSO-d<sub>6</sub>): δ 2.07 (s, 3H), 7.29–7.38 (m, 1H), 7.39–7.50 (m, 5H), 7.70 (s, 1H), 7.75 (s, 1H), 7.80–7.90 (m, 3H), 7.93–8.03 ppm (m, 3H). IR: ν 1615 cm<sup>-1</sup>. Anal. (C<sub>24</sub>H<sub>17</sub>N<sub>3</sub>O<sub>2</sub> (395.48)): C, 72.89; H, 4.33; N, 10.63; S, 8.11. Found: C, 72.86; H, 4.31; N, 10.59; S, 8.09. MS (ESI) calcd for C<sub>24</sub>H<sub>17</sub>N<sub>3</sub>O<sub>2</sub>: 395.1; found (M + H)<sup>+</sup>: 396.1.



4-((1H-Imidazol-2-yl)methylene)-3-methyl-1-(4-phenylthiazol-2-yl)-1H-pyrazol-5(4H)-one (5). It was synthesized as 2 starting from 17 and 1H-imidazole-2-carbaldehyde. Yield 28%, mp 189–191 °C (from ethanol). <sup>1</sup>H NMR (DMSO-d<sub>6</sub>): δ 1.98 (s, 3H), 7.18 (s, 1H), 7.26–7.48 (m, 5H), 7.62 (d, J = 3.6 Hz, 1H), 7.69 (s, 1H), 7.92 ppm (d, J = 3.8 Hz, 2H). IR: ν 1615 cm<sup>-1</sup>. Anal. (C<sub>17</sub>H<sub>13</sub>N<sub>5</sub>O<sub>2</sub> (335.38)): C, 60.88; H, 3.91; N, 20.88; S, 9.56. Found: C, 60.87; H, 3.90; N, 20.86; S, 9.54. MS (ESI) calcd for C<sub>17</sub>H<sub>13</sub>N<sub>5</sub>O<sub>2</sub>: 335.1; found (M + H)<sup>+</sup>: 336.2.



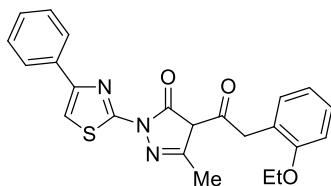
*4-Benzylidene-3-methyl-1-(4-phenylthiazol-2-yl)-1H-pyrazol-5(4H)-one (16)*. It was synthesized as 2 starting from 17 and benzaldehyde. Yield 30%, mp >270 °C with decomposition (from ethanol). <sup>1</sup>H NMR (DMSO-d<sub>6</sub>): δ 2.07 (s, 3H), 7.17–7.23 (m, 1H), 7.24–7.35 (m, 5H), 7.39–7.46 (m, 3H), 7.70 (s, 1H), 7.97 ppm (d, J = 3.7 Hz, 2H). IR: ν 1360, 1495, 1622 cm<sup>-1</sup>. Anal. (C<sub>20</sub>H<sub>15</sub>N<sub>3</sub>O<sub>3</sub> (345.42)): C, 69.54; H, 4.38; N, 12.17; S, 9.28. Found: C, 69.50; H, 4.36; N, 12.17; S, 9.26. MS (ESI) calcd for C<sub>20</sub>H<sub>15</sub>N<sub>3</sub>O<sub>3</sub>: 345.1; found (M + H)<sup>+</sup>: 346.2



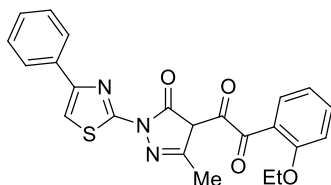
*4-(2-(2-Ethoxyphenyl)acetyl)-3-methyl-1-(4-phenylthiazol-2-yl)-1H-pyrazol-5(4H)-one (6)*. A suspension of potassium tert-butoxide (0.13 g, 1.2 mmol) in anhydrous tetrahydrofuran (15.0 mL) was cooled at -40 °C, and a solution of 17 (0.25 g, 0.97 mmol) in the same solvent (10.0 mL) was added dropwise under Ar stream. The reaction mixture was stirred in the same conditions for 1 h, and a solution of 2-(2-ethoxyphenyl)acetyl chloride (0.31 g, 1.2 mmol) in the same solvent (5.0 mL) was added dropwise. The reaction mixture was stirred at 25 °C for 1 h, diluted with water, and extracted with ethyl acetate. Organic layer was washed with brine, dried, and filtered. Evaporation of the solvent gave a residue that was purified by column chromatography (silica gel, ethyl acetate:n-hexane = 1:1 as eluent) to furnish 6 (0.3 g, 74%), mp 105–110 °C (from ethanol). <sup>1</sup>H NMR (DMSO-d<sub>6</sub>): δ 1.22 (t, J = 6.9 Hz, 3H), 2.25 (s, 3H), 3.97–4.02 (m, 4H), 6.26 (s, 1H), 6.85 (t, J = 7.3 Hz, 1H), 6.99 (d, J = 8.2 Hz, 1H), 7.16 (d, J = 6.4 Hz, 1H), 7.24 (t, J = 8.0 Hz, 1H), 7.40 (t, J = 7.2 Hz, 1H), 7.50 (t, J = 7.8 Hz, 2H), 7.90–7.94 ppm (m, 3H). IR: ν 1780, 1784 cm<sup>-1</sup>. Anal. (C<sub>23</sub>H<sub>21</sub>N<sub>3</sub>O<sub>3</sub>S (419.50)): C, 65.85; H, 5.05; N, 10.02; S, 7.64. Found: C, 65.80; H, 5.02; N, 10.06; S, 7.60. MS (ESI) calcd for C<sub>23</sub>H<sub>21</sub>N<sub>3</sub>O<sub>3</sub>S: 419.1; found (M + H)<sup>+</sup>: 420.0. 2-(2-Ethoxyphenyl)acetyl chloride: A mixture of 2-(2-hydroxyphenyl)acetic acid (2.0 g, 13 mmol) and 37% hydrochloric acid (1.2 mL) in 96 ° ethanol (70.0 mL) was heated to reflux for 3 h, cooled, diluted with water, and extracted with ethyl acetate. The organic layer was washed with brine, dried, and filtered. Removal of the solvent gave ethyl 2-(2-hydroxyphenyl)acetate (2.22 g, 94%), mp 65–67 °C (from petroleum ether), lit. 67–68 °C [154]. A mixture of ethyl 2-(2-hydroxyphenyl)acetate (2.22 g, 12 mmol), anhydrous potassium carbonate (3.69 g, 26 mmol), and iodoethane (4.11 g, 2.1 mL, 26 mmol) in anhydrous N,N-dimethylformamide (10.0 mL) was heated at 50 °C for 12 h. After cooling, the reaction mixture was diluted with water and extracted with ethyl acetate. The organic layer was washed with brine, dried, and filtered. Removal of the solvent gave a residue that was purified by column chromatography (silica gel, ethyl acetate:n-hexane = 3:7 as eluent) to furnish ethyl 2-(2-ethoxyphenyl)acetate (2.22 g, 86%), oil. <sup>1</sup>H NMR (DMSO-d<sub>6</sub>): δ 1.16 (t, J = 7.1 Hz, 3H), 1.27 (t, J = 6.9 Hz, 3H), 3.55 (s, 2H), 3.96–4.07 (m, 4H), 6.86 (t, J = 7.4 Hz, 1H), 6.93 (d, J = 8.1 Hz, 1H), 7.15–7.23 ppm (m, 2H). IR: ν 1733 cm<sup>-1</sup>. A mixture of ethyl 2-(2-ethoxyphenyl)acetate (4.86 g, 23 mmol) in 3N sodium hydroxide/96 ° ethanol (1:1, v/v) (180.0 mL) was heated to reflux for 12 h. After cooling, the reaction mixture was made acidic with 6N hydrogen chloride and extracted with ethyl acetate. The organic layer was washed with brine, dried, and filtered. Removal of the solvent gave 2-(2-ethoxyphenyl)acetic acid (3.50 g, 83%), mp 99–102 °C (from ethanol), lit 103 °C. [155] <sup>1</sup>H NMR (DMSO-d<sub>6</sub>): δ 1.28 (t, J = 6.7 Hz, 3H), 3.48 (s, 2H), 3.98 (q, J = 6.8 Hz, 2H), 6.85 (t, J = 6.9 Hz, 1H), 6.93 (d, J = 8.0 Hz, 1H), 7.14–7.31 (m, 2H), 12.13 ppm (broad s, disappeared on treatment with D<sub>2</sub>O, 1H). IR: ν 1730, 2987 cm<sup>-1</sup>. To a mixture of 2-(2-ethoxyphenyl)acetic acid (0.21 g, 1.2 mol) in anhydrous benzene (9.0 mL) was added thionyl chloride (1.45



g, 0.9 mL, 12 mmol). The reaction mixture was stirred at 25 °C for 1 h and evaporated to give 2-(2-ethoxyphenyl)acetyl chloride that was used without further purification.

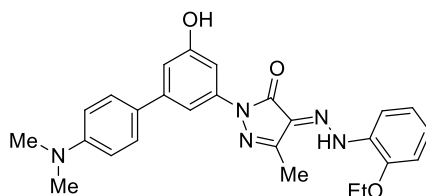


*1-(2-Ethoxyphenyl)-2-(3-methyl-5-oxo-1-(4-phenylthiazol-2-yl)-4,5-dihydro-1H-pyrazol-4-yl)ethane-1,2-dione (7)*. A mixture of 6 (0.25 g, 0.59 mmol), potassium permanganate (0.38 g, 2.4 mmol), and a catalytic amount of 98% sulfuric acid in acetone (10.0 mL) was heated to reflux for 12 h. Removal of the solvent gave a residue that was purified by column chromatography (silica gel, ethyl acetate:nhexane = 3:7 as eluent) to furnish 7 (0.013 g, 5%), mp 108–110 °C (from ethanol). <sup>1</sup>H NMR (DMSO-d<sub>6</sub>): δ 1.22 (t, J = 6.8 Hz, 3H), 2.29(s, 3H), 4.06 (d, J = 6.7 Hz, 2H), 6.39 (s, 1H), 7.12–7.28 (m, 5H), 7.53 (d, J = 7.4 Hz, 2H), 7.74 (m, 1H), 7.86 (s, 1H), 8.19 ppm (d, J = 6.6 Hz, 1H). IR: ν 1215, 2926 cm<sup>-1</sup>. Anal. (C<sub>23</sub>H<sub>19</sub>N<sub>3</sub>O<sub>4</sub>S (433.48)): C, 63.73; H, 4.42; N, 9.69; S, 7.40. Found: C, 63.70; H, 4.39; N, 9.72; S, 7.38. MS (ESI) calcd for C<sub>23</sub>H<sub>19</sub>N<sub>3</sub>O<sub>4</sub>S: 433.1; found (M + H)<sup>+</sup>: 434.4.

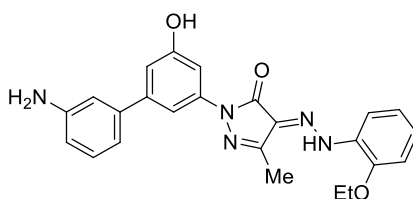


#### General Procedure for the Preparation of Compounds 8, 12, 15, and 22–26.

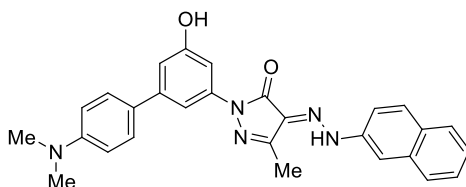
**Example:** *1-(4'-(Dimethylamino)-5-hydroxy-[1,1'-biphenyl]-3-yl)-4-(2-(2-ethoxyphenyl)hydrazono)-3-methyl-1H-pyrazol-5(4H)-one (8)* A mixture of 20 (0.07 g, 0.17 mmol), 2 M sodium carbonate (0.3 mL), and (4-(dimethylamino)phenyl)boronic acid (0.034 g, 0.21 mmol) in tetrahydrofuran (0.6 mL) was degassed for 10 min. Dichloro[1,1'-bis(diphenylphosphino)ferrocene]-palladium(II) (0.0082 g, 0.01 mmol; complex with dichloromethane (1:1), Pd13%) was added, and the reaction mixture was stirred at reflux temperature for 90 min under Ar stream, cooled, diluted with water, and extracted with ethyl acetate. Organic layer was washed with brine, dried, and filtered. Removal of the solvent gave a residue that was purified by column chromatography (silica gel, ethyl acetate:n-hexane = 7:3 as eluent) to furnish 8 (0.010 g, 13%), mp 230–232 °C (from ethanol). <sup>1</sup>H NMR (DMSO-d<sub>6</sub>): δ 1.42 (t, J = 7.1 Hz, 3H), 2.32–2.49 (m, 6H), 2.94 (s, 3H), 4.23 (q, J = 7.1 Hz, 2H), 6.78–6.80 (m, 2H), 7.08 (s, 1H), 7.20 (s, 2H), 7.35 (s, 1H), 7.44–7.46 (d, J = 7.8 Hz, 2H), 7.53–7.70 (m, 3H), 9.71 (broad s, disappeared on treatment with D<sub>2</sub>O, 1H), 13.60 ppm (broad s, disappeared on treatment with D<sub>2</sub>O, 1H). <sup>13</sup>C NMR (DMSO-d<sub>6</sub>): δ 11.97, 15.08, 40.47, 65.12, 103.47, 106.73, 109.75, 113.05, 113.72, 114.72, 122.08, 126.70, 127.49, 128.04, 129.12, 130.59, 139.66, 142.67, 147.58, 148.34, 157.71, 158.55. IR: ν 1656, 2854, 2924 cm<sup>-1</sup>. Anal. (C<sub>26</sub>H<sub>27</sub>N<sub>5</sub>O<sub>3</sub> (457.52)): C, 68.25; H, 5.95; N, 15.31. Found: C, 68.22; H, 5.90; N, 15.29. HRMS (ESI) calcd for C<sub>26</sub>H<sub>27</sub>N<sub>5</sub>O<sub>3</sub>: 457.2114; found (M – H)<sup>-</sup>: 456.2021.



2-(3'-Amino-5-hydroxy-[1,1'-biphenyl]-3-yl)-4-(2-(2-ethoxyphenyl)hydrazono)-5-methyl-2,4-dihydro-3H-pyrazol-3-one(12). It was synthesized as 8 starting from 20 and (3-aminophenyl)-boronic acid. Yield 66%, mp 180–183 °C (from ethanol).  $^1\text{H}$  NMR (DMSO-d<sub>6</sub>):  $\delta$  1.42 (t, J = 7.2 Hz, 3H), 2.31 (s, 3H), 4.21 (q, J = 7.1 Hz, 2H), 5.19 (broad s, disappeared on treatment with D<sub>2</sub>O, 2H), 6.56 (d, J = 6.9 Hz, 1H), 6.70 (d, J = 7.3 Hz, 1H), 6.76–6.80 (m, 2H), 7.03–7.11 (m, 2H), 7.19 (s, 2H), 7.44 (s, 1H), 7.52 (s, 1H), 7.71 (d, J = 8.3 Hz, 1H), 9.75 (broad s, disappeared on treatment with D<sub>2</sub>O, 1H), 13.59 ppm (broad s, disappeared on treatment with D<sub>2</sub>O, 1H). IR:  $\nu$  1693, 2852, 2922, 3271  $\text{cm}^{-1}$ . Anal. (C<sub>24</sub>H<sub>23</sub>N<sub>5</sub>O<sub>3</sub> (429.48)): C, 67.12; H, 5.40; N, 16.31. Found: C, 67.10; H, 5.38; N, 16.29. MS (ESI) calcd for C<sub>23</sub>H<sub>19</sub>N<sub>3</sub>O<sub>4</sub>S: 429.2; found (M + H)<sup>+</sup>: 430.1.

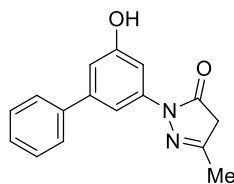


2-(4'-(Dimethylamino)-5-hydroxy-[1,1'-biphenyl]-3-yl)-5-methyl-4-(2-(naphthalen-2-yl)hydrazono)-2,4-dihydro-3H-pyrazol-3-one(15). It was synthesized as 8 starting from 21 and (4-(dimethylamino)phenyl)boronic acid. Yield 18%, mp 221–226 °C (from ethanol).  $^1\text{H}$  NMR (DMSO-d<sub>6</sub>):  $\delta$  2.35 (s, 3H), 2.93 (s, 6H), 3.76–6.81 (m, 3H), 7.29 (s, 1H), 7.38–7.49 (m, 3H), 7.54–7.56 (m, 1H), 7.70 (s, 1H), 7.85–7.93 (m, 3H), 8.00–8.07 (m, 2H), 9.67 (broad s, disappeared on treatment with D<sub>2</sub>O, 1H), 13.59 ppm (broad s, disappeared on treatment with D<sub>2</sub>O, 1H). IR:  $\nu$  1655, 1736, 2852, 2922,  $\text{cm}^{-1}$ . Anal. (C<sub>28</sub>H<sub>25</sub>N<sub>5</sub>O<sub>2</sub> (463.20)): C, 72.55; H, 5.44; N, 15.11. Found: C, 72.53; H, 5.46; N, 15.10. MS (ESI) calcd for C<sub>28</sub>H<sub>25</sub>N<sub>5</sub>O<sub>2</sub>: 463.2; found (M + H)<sup>+</sup>: 463.3.

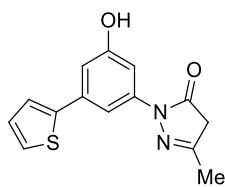


1-(5-Hydroxy-[1,1'-biphenyl]-3-yl)-3-methyl-1H-pyrazol-5(4H)-one (22). It was synthesized as 8 starting from 19 and phenylboronic acid. Yield 60%, mp 160–163 °C (from ethanol).  $^1\text{H}$  NMR (DMSO-d<sub>6</sub>):  $\delta$  2.36 (s,

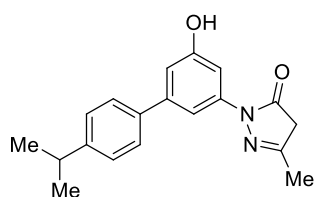
3H), 6.88 (s, 1H), 7.35–7.37 (m, 2H), 7.43–7.46 (m, 3H), 7.60–7.62 (m, 3H), 9.84 (broad s, disappeared on treatment with D<sub>2</sub>O, 1H), 12.12 ppm (broad s, disappeared on treatment with D<sub>2</sub>O, 1H). IR:  $\nu$  1599, 1685, 3063 cm<sup>-1</sup>.



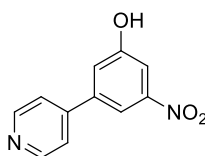
*1-(3-Hydroxy-5-(thiophen-2-yl)phenyl)-3-methyl-1H-pyrazol-5(4H)-one* (23). It was synthesized as 8 starting from 19 and thiophen-2-ylboronic acid. Yield 32%, mp 175–178 °C (from ethanol). <sup>1</sup>H NMR (DMSO-d<sub>6</sub>):  $\delta$  2.10 (s, 3H), 5.37 (s, 1H), 6.87 (s, 1H), 7.12–7.16 (m, 2H), 7.41–7.45 (m, 2H), 7.53 (s, 1H), 9.78 (broad s, disappeared on treatment with D<sub>2</sub>O, 1H), 11.56 ppm (broad s, disappeared on treatment with D<sub>2</sub>O, 1H). IR:  $\nu$  1587, 1679, 3091 cm<sup>-1</sup>.



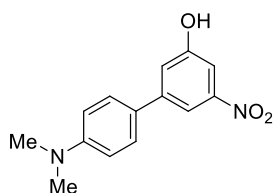
*2-(5-Hydroxy-4'-isopropyl-[1,1'-biphenyl]-3-yl)-5-methyl-2,4-dihydro-3H-pyrazol-3-one* (24). It was synthesized as 8 starting from 19 and (4-isopropylphenyl)boronic acid and was used without further purification.



*3-Nitro-5-(pyridin-4-yl)phenol* (25). It was synthesized as 8 starting from 3-bromo-5-nitrophenol [156] and pyridin-4-ylboronic acid. Yield 14%, mp 200 °C with decomposition (from ethanol). <sup>1</sup>H NMR (DMSO-d<sub>6</sub>):  $\delta$  7.56–7.61 (m, 1H), 7.63–7.64 (m, 1H), 7.74–7.75 (m, 2H), 7.98–8.00 (m, 1H), 8.64–8.67 ppm (m, 2H), 10.76 ppm (broad s, disappeared on treatment with D<sub>2</sub>O, 1H). IR:  $\nu$  2923 cm<sup>-1</sup>.

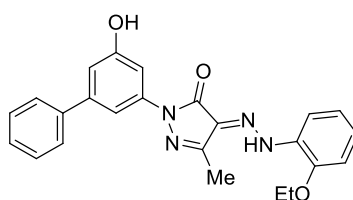


4'-(Dimethylamino)-5-nitro-[1,1'-biphenyl]-3-ol (26). It was synthesized as 8 starting from 1-bromo-3-nitrobenzene and (4-(dimethylamino)phenyl)boronic acid. Yield 25%, mp 130–134 °C (from ethanol). <sup>1</sup>H NMR (DMSO-d<sub>6</sub>): δ 2.95 (s, 6H), 6.80–6.84 (m, 2H), 7.61–7.68 (m, 3H), 8.04–8.07 (m, 2H), 8.33 ppm (m, 1H).

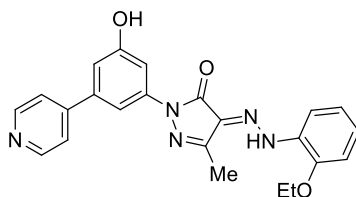


*General Procedure for the Preparation of Compounds 9–11, 13, 14, 20, and 21.*

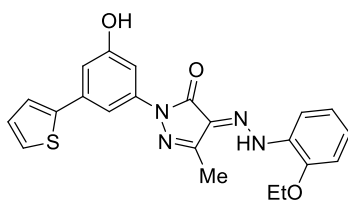
Example: 4-(2-(2-Ethoxyphenyl)-hydrazono)-1-(5-hydroxy-[1,1'-biphenyl]-3-yl)-3-methyl-1H-pyrazol-5(4H)-one (9). A mixture of 22 (0.054 g, 0.000203 mol) and sodium acetate (0.028 g, 0.20 mmol) in 96° ethanol (1.1 mL) was cooled at 0 °C. 2-Ethoxybenzenediazonium chloride (0.02 mmol) was added, and the reaction mixture was stirred at the same temperature for 2 h, diluted with water, and extracted with ethyl acetate. The organic layer was washed with brine, dried, and filtered. Removal of the solvent gave a residue that was purified by column chromatography (silica gel, ethyl acetate:n-hexane = 7:3 as eluent) to furnish 9 (0.070 g, 8%), mp 163–166 °C (from ethanol). <sup>1</sup>H NMR (DMSO-d<sub>6</sub>): δ 1.42 (t, J = 6.9 Hz, 3H), 2.32 (s, 3H), 4.22 (q, J = 7.0 Hz, 2H), 6.86 (s, 1H), 7.06–7.08 (m, 1H), 7.19–7.21 (m, 2H), 7.36–7.38 (m, 1H), 7.47–7.49 (m, 3H), 7.58–7.60 (m, 3H), 7.69–7.71 ppm (m, 1H), 9.84 (broad s, disappeared on treatment with D<sub>2</sub>O, 1H), 13.59 ppm (broad s, disappeared on treatment with D<sub>2</sub>O, 1H). IR: ν 1594, 1663, 2924, 3149 cm<sup>-1</sup>. Anal. (C<sub>24</sub>H<sub>22</sub>N<sub>4</sub>O<sub>3</sub> (414.46)): C, 69.55; H, 5.35; N, 13.52. Found: C, 69.53; H, 5.30; N, 13.54. MS (ESI) calcd for C<sub>24</sub>H<sub>22</sub>N<sub>4</sub>O<sub>3</sub>: 414.2; found (M + H)<sup>+</sup>: 415.1. 2-Ethoxybenzenediazonium chloride: 1-Ethoxy-2-nitrobenzene was synthesized as ethyl 2-(2-ethoxyphenyl)acetate starting from 2-nitrophenol and iodoethane. Yield 90%, yellow oil [157]. A solution of 1-ethoxy-2-nitrobenzene (0.10 g, 0.6 mmol) in methanol (15.0 mL) was treated with hydrogen gas (30psi) in the presence of palladium on carbon (0.01 g) at 25 °C for 2 h, filtered, and evaporated to give 2-ethoxyaniline that was used without further purification. To a cold solution of crude 2-ethoxyaniline (0.05 g, 0.36 mmol) in 37% hydrogen chloride (0.7 mL), a solution of sodium nitrite (0.025 g, 0.36 mmol) in water (0.2 mL) was added dropwise. The reaction mixture was stirred at 0 °C for 20 min to give 2-ethoxybenzenediazonium chloride that was used without further purification.



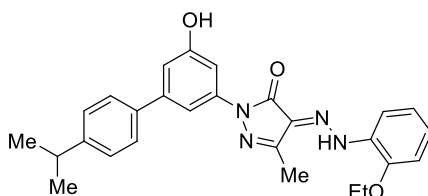
4-(2-(2-Ethoxyphenyl)hydrazono)-1-(3-hydroxy-5-(pyridin-4-yl)-phenyl)-3-methyl-1H-pyrazol-5(4H)-one (10). It was synthesized as 9 starting from 29 and 2-ethoxybenzenediazonium chloride. Yield 36%, slurry. <sup>1</sup>H NMR (DMSO-d<sub>6</sub>): δ 1.43 (t, J = 7.0 Hz, 3H), 2.33 (s, 3H), 4.24 (q, J = 7.0 Hz, 2H), 7.10–7.12 (m, 2H), 7.20–7.22 (m, 2H), 7.71–7.78 (m, 3H), 8.00–8.10 (m, 2H), 8.84–8.86 (m, 2H), 10.22 (broad s, disappeared on treatment with D<sub>2</sub>O, 1H), 13.55 ppm (broad s, disappeared on treatment with D<sub>2</sub>O, 1H). IR: ν 1732, 2583, 2855, 2896 cm<sup>-1</sup>. Anal. (C<sub>23</sub>H<sub>21</sub>N<sub>5</sub>O<sub>3</sub> (415.44)): C, 66.49; H, 5.09; N, 16.86. Found: C, 66.47; H, 5.11; N, 16.84. MS (ESI) calcd for C<sub>23</sub>H<sub>21</sub>N<sub>5</sub>O<sub>3</sub>: 415.2; found (M + H)<sup>+</sup>: 415.9.



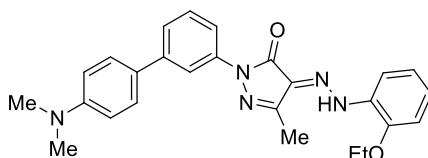
4-(2-(2-Ethoxyphenyl)hydrazono)-1-(3-hydroxy-5-(thiophen-2-yl)phenyl)-3-methyl-1H-pyrazol-5(4H)-one (11). It was synthesized as 9 starting from 23 and 2-ethoxybenzenediazonium chloride. Yield 3%, mp 165–167 °C (from ethanol). <sup>1</sup>H NMR (DMSO-d<sub>6</sub>): δ 1.42 (t, J = 7.0 Hz, 3H), 2.32 (s, 3H), 4.22 (q, J = 7.1 Hz, 2H), 6.90 (s, 1H), 7.08–7.09 (m, 1H), 7.14–7.15 (m, 1H), 7.20–7.22 (m, 2H), 7.42–7.44 (m, 2H), 7.55–7.56 (m, 1H), 7.61–7.63 (m, 1H), 7.69–7.71 (m, 1H), 9.89 (broad s, disappeared on treatment with D<sub>2</sub>O, 1H), 13.59 ppm (broad s, disappeared on treatment with D<sub>2</sub>O, 1H). IR: ν 1661, 1730, 2854, 2923, 2956 cm<sup>-1</sup>. Anal. (C<sub>22</sub>H<sub>20</sub>N<sub>4</sub>O<sub>3</sub>S (420.48)): C, 62.84; H, 4.79; N, 13.32; S, 7.63. Found: C, 62.82; H, 4.78; N, 13.29; S, 7.61. MS (ESI) calcd for C<sub>22</sub>H<sub>20</sub>N<sub>4</sub>O<sub>3</sub>S: 420.1; found (M + H)<sup>+</sup>: 421.0.



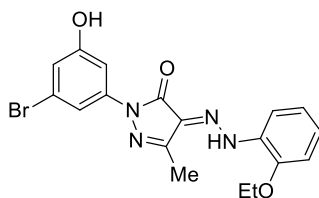
4-(2-(2-Ethoxyphenyl)hydrazono)-1-(5-hydroxy-4'-isopropyl-[1,1'-biphenyl]-3-yl)-3-methyl-1H-pyrazol-5(4H)-one (13). It was synthesized as 9 starting from 24 and 2-ethoxybenzenediazonium chloride. Yield 17%, slurry. <sup>1</sup>H NMR (DMSO-d<sub>6</sub>): δ 1.22 (s, 3H), 1.24 (s, 3H), 1.42 (t, J = 7.0 Hz, 3H), 1.98 (s, 3H), 2.91–2.94 (m, 1H), 4.02 (q, J = 6.2 Hz, 2H), 6.84–6.86 (m, 1H), 7.08–7.10 (m, 1H), 7.19–7.21 (m, 2H), 7.33–7.35 (m, 2H), 7.44–7.46 (m, 1H), 7.50–7.53 (m, 2H), 7.58–7.60 (m, 1H), 7.70–7.72 (m, 1H), 9.79 (broad s, disappeared on treatment with D<sub>2</sub>O, 1H), 13.59 ppm (broad s, disappeared on treatment with D<sub>2</sub>O, 1H). IR: ν 1655, 1728, 2854, 2924, 2958 cm<sup>-1</sup>. Anal. (C<sub>27</sub>H<sub>28</sub>N<sub>4</sub>O<sub>3</sub> (456.54)): C, 71.03; H, 6.18; N, 12.27. Found: C, 71.00; H, 6.16; N, 12.29. MS (ESI) calcd for C<sub>27</sub>H<sub>28</sub>N<sub>4</sub>O<sub>3</sub>: 456.2; found (M + H)<sup>+</sup>: 456.3.



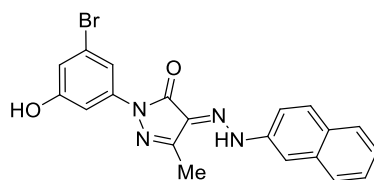
1-(4'-(Dimethylamino)-[1,1'-biphenyl]-3-yl)-4-(2-(2-ethoxyphenyl)hydrazono)-3-methyl-1H-pyrazol-5(4H)-one (14). It was synthesized as 9 starting from 30 and 2-ethoxybenzenediazonium chloride. Yield 47%, 230–232 °C (from ethanol). <sup>1</sup>H NMR (DMFd7): δ 1.67 (t, J = 7.0 Hz, 3H), 2.56 (s, 3H), 3.18 (s, 6H), 4.47 (q, J = 6.9 Hz, 2H), 7.06 (d, J = 8.8 Hz, 2H), 7.28–7.30 (m, 1H), 7.40–7.43 (m, 2H), 7.67–7.69 (m, 2H), 7.76–7.78 (d, J = 8.9 Hz, 2H), 7.96 (d, J = 7.5 Hz, 1H), 8.01–8.13 (m, 1H), 8.41 (s, 1H), 13.98 ppm (broad s, disappeared on treatment with D<sub>2</sub>O, 1H). IR: ν 1652, 1713, 2851, 2922 cm<sup>-1</sup>. Anal. (C<sub>26</sub>H<sub>27</sub>N<sub>5</sub>O<sub>2</sub> (441.52)): C, 70.73; H, 6.16; N, 15.86. Found: C, 70.71; H, 6.14; N, 15.84. MS (ESI) calcd for C<sub>26</sub>H<sub>27</sub>N<sub>5</sub>O<sub>2</sub>: 441.2; found (M + H)<sup>+</sup>: 441.3.



1-(3-Bromo-5-hydroxyphenyl)-4-(2-(2-ethoxyphenyl)hydrazono)-3-methyl-1H-pyrazol-5(4H)-one (20). It was synthesized as 9 starting from 19 and 2-ethoxybenzenediazonium chloride. Yield 48%, mp 215–217 °C (from ethanol). <sup>1</sup>H NMR (DMSO-d<sub>6</sub>): δ 1.43 (t, J = 7.0 Hz, 3H), 2.29 (s, 3H), 4.22 (q, J = 6.9 Hz, 2H), 6.78 (s, 1H), 7.06–7.09 (m, 1H), 7.19–7.21 (m, 2H), 7.45 (s, 1H), 7.55 (s, 1H), 7.69–7.70 (m, 1H), 10.15 (broad s, disappeared on treatment with D<sub>2</sub>O, 1H), 13.50 ppm (broad s, disappeared on treatment with D<sub>2</sub>O, 1H). IR: ν 1661, 2934, 2979, 3121 cm<sup>-1</sup>.

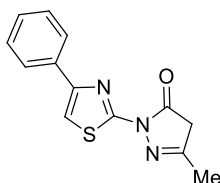


1-(3-Bromo-5-hydroxyphenyl)-3-methyl-4-(2-(naphthalen-2-yl)hydrazono)-1H-pyrazol-5(4H)-one (21). It was synthesized as 9 starting from 19 and naphthalene-2-diazonium chloride. Yield 7%, mp 233–237 °C (from ethanol). <sup>1</sup>H NMR (DMSO-d<sub>6</sub>): δ 1.22 (s, 3H), 6.78 (s, 1H), 7.43–7.47 (m, 2H), 7.52–7.55 (m, 1H), 7.64–7.66 (m, 2H), 7.5–7.87 (m, 1H), 7.90–7.92 (m, 2H), 8.01–8.20 (m, 1H), 8.07 (broad s, disappeared on treatment with D<sub>2</sub>O, 1H), 10.16 ppm (broad s, disappeared on treatment with D<sub>2</sub>O, 1H). IR: ν 1731, 2853, 2922 cm<sup>-1</sup>.

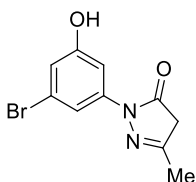


*General Procedure for the Preparation of Compounds 17,19, 29, and 30.*

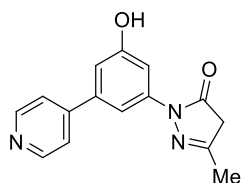
*Example: 3-Methyl-1-(4-phenylthiazol-2-yl)-1Hpyrazol- 5(4H)-one (17).* A solution of 2-hydrazinyl-4-phenylthiazole(0.50 g, 2.6 mmol) and ethyl acetoacetate (0.26 g, 0.3 mL, 2.6 mmol)in glacial acetic acid (5.0 mL) was heated to reflux for 3 h. After evaporation of the solvent, the residue was treated with a saturated aqueous solution of sodium hydrogen carbonate and extracted with ethyl acetate. The organic layer was washed with brine, dried, and filtered. Removal of the solvent gave a residue that was purified by column chromatography (silica gel, ethyl acetate:n-hexane = 2:1 as eluent) to furnish 16 (0.42 g, 62%), mp 188–192 °C (from ethanol), lit. 188–189 °C. [156] .



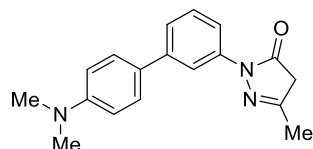
*2-(3-Bromo-5-hydroxyphenyl)-5-methyl-2,4-dihydro-3H-pyrazol-3-one (19).* It was synthesized as 17, starting from 18 and ethyl acetoacetate. Yield 13%, mp 170–172 °C (from ethanol). <sup>1</sup>H NMR (DMSO-d<sub>6</sub>): δ 2.06 (s, 3H), 5.35 (s, 1H), 6.73 (s, 1H), 7.23–7.35 (m, 2H), 10.04 (broad s, disappeared on treatment with D<sub>2</sub>O, 1H), 11.72 ppm (broad s, disappeared on treatment with D<sub>2</sub>O, 1H). IR: ν 1730, 2952, 3160 cm<sup>-1</sup>.



*1-(3-Hydroxy-5-(pyridin-4-yl)phenyl)-3-methyl-1H-pyrazol-5(4H)- one (29).* It was synthesized as 17, starting from 27 and ethyl acetoacetate. Yield 13%, mp 250 °C with decomposition (from ethanol). <sup>1</sup>H NMR (DMSO-d<sub>6</sub>): δ 2.09 (s, 3H), 5.38 (s, 1H), 6.92– 6.95 (m, 1H), 7.30–7.32 (m, 1H), 7.52–7.59 (m, 3H), 8.60–8.62 (m, 2H), 9.89 (broad s, disappeared on treatment with D<sub>2</sub>O, 1H), 11.57 ppm (broad s, disappeared on treatment with D<sub>2</sub>O, 1H). IR: ν 1736, 2854, 2923, 2932 cm<sup>-1</sup>.

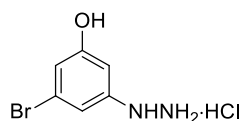


1-(4'-(4-hydroxyphenyl)-[1,1'-biphenyl]-3-yl)-3-methyl-1H-pyrazol-5(4H)-one (30). It was synthesized as 17, starting from 28 and ethyl acetoacetate. Yield 12%, slurry.  $^1\text{H}$  NMR (DMSO- $d_6$ ):  $\delta$  2.12 (s, 3H), 2.94 (s, 6H), 5.43 (s, 1H), 6.80 (d,  $J = 8.8$  Hz, 2H), 7.39–7.41 (m, 2H), 7.49–7.53 (m, 3H), 7.87 (s, 1H), 11.51 ppm (broad s disappeared on treatment with  $\text{D}_2\text{O}$ , 1H). IR:  $\nu$  1715, 2803, 2852, 2921  $\text{cm}^{-1}$ .

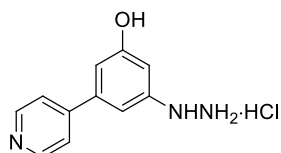


*General Procedure for the Preparation of Compounds 18,27, and 28.*

*Example: 3-Bromo-5-hydrazinylphenol Hydrochloride(18).* A mixture of 3-bromo-5-nitrophenol [158] (1.0 g, 4.6 mmol) and tin(II) chloride dihydrate (5.17 g, 23 mmol) in ethyl acetate (30.0 mL) was heated to reflux for 3 h. After cooling, the reaction mixture was made basic with a saturated aqueous solution of sodium hydrogen carbonate and the resulting suspension filtered. Layers were separated and the organic one washed with brine, dried, and filtered. Removal of the solvent gave 3-amino-5-bromophenol (0.86 g) that was used without further purification. To a cold solution of crude 3-amino-5-bromophenol (0.86 g, 4.5 mmol) in 37% hydrogen chloride (9.4 mL), a solution of sodium nitrite (0.32 g, 4.6 mmol) in water (2.3 mL) was added dropwise. The reaction mixture was stirred at 0 °C for 20 min, and a solution of tin(II) chloride dihydrate (2.30 g, 10 mmol) in 37% hydrogen chloride was added dropwise. The reaction mixture was stirred at the same temperature for additional 20 min and resulting suspension filtered to give 18 (0.93 g) that was used without further purification.

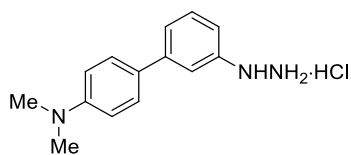


*3-Hydrazinyl-5-(pyridin-4-yl)phenol Hydrochloride (27).* It was synthesized as 18 starting from 25 and was used without further purification.





3'-Hydrazinyl-N,N-dimethyl-[1,1'-biphenyl]-4-amine Hydrochloride (28). It was synthesized as 18 starting from 26 and was used without further purification.



**Peptide Synthesis.**  $N\alpha$ -Fmoc-protected amino acids, Fmoc-Rink Amide-Am resin, O-benzotriazole-N,N,N',N'-tetramethyl-uroniumhexafluorophosphate (HBTU), N,N-diisopropylethylamine (DIEA), triisopropylsilane (TIS), trifluoroacetic acid (TFA), and piperidine were purchased from IRIS Biotech, N-hydroxybenzotriazole (HOBT), N,N-dimethylformamide (DMF), dichloromethane (DCM), and fluorescein-5-isothiocyanate (FITC) from Organics (Morris Plains). For  $N\alpha$ -Fmoc-protected amino acids, the following side chain protecting groups were used: Arg(Pbf), Asn(Trt), Asp(OtBu), Gln(Trt), Trp(Nin-Boc), and Tyr(tBu). Solvents and reagents were reagent grade and used without further purification unless otherwise noted. Peptides were analyzed by analytical HPLC (Shimadzu Prominence HPLC system) equipped with a C18-bounded analytical reverse-phase HPLC column (Phenomenex Luna, 4.6 mm  $\times$  250 mm 5  $\mu$ m) using a gradient elution (10–90% acetonitrile in water (0.1% TFA) over 20 min; flow rate = 1.0 mL/min; diode array UV detector). Peptides were purified by preparative HPLC (Shimadzu HPLC system) equipped with a C18-bounded preparative reverse-phase HPLC column (Phenomenex Kinetex 21.2 mm  $\times$  150 mm 5  $\mu$ m). Molecular weights of compounds were confirmed by ESI-mass spectrometry using an Agilent 6110 quadrupole LC/MS system. Peptide syntheses were performed manually by a stepwise solidphase procedure using 0.1 mmol Rink Amide aminomethylpolystyrene resin (0.48 mmol/g). The linear sequence was synthesized by introducing each amino acid with the following protocols: (1) deprotection of  $N\alpha$ -Fmoc protecting group by the treatment with piperidine (20% in DMF; 1  $\times$  5 min and 1  $\times$  25 min), and (2) coupling reaction using Fmoc-AA (4 equiv) in the presence of HBTU (152 mg, 4 equiv), HOBT (54 mg, 4 equiv), and DIEA (140  $\mu$ L, 8 equiv) in DMF (2 mL) for 2 h at room temperature. The coupling efficiency for each amino acid was determined by the quantitative ninhydrin test and TNBS test. Next, for the peptide BIM-RIF, the  $N\alpha$ -Fmoc of the last amino acid was removed and the free amino group was acetylated with acetic anhydride (96  $\mu$ L, 8 equiv) and DIPEA (174  $\mu$ L, 4 equiv) in DCM (4 mL) for 30 min. For FITC-BIM, once amino hexanoic acid (Ahx) was introduced as spacer, the peptide was fluorescently labeled by mixing the resin with of fluorescein-5-isothiocyanate (FITC) (238 mg, 6 equiv) and DIEA (210  $\mu$ L, 12 equiv) in minimal DMF for 12 h in the dark. Finally, both the peptides were cleaved from the resin by the treatment with TFA/TIS/water (10mL, 90:5:5) for 3 h at room temperature. Then, the resin was filtered and the TFA solution and the peptide was precipitated by adding cold diethyl ether (40 mL) and centrifuged. Crude peptide extracts were then analyzed by analytical reverse-phase HPLC. Analytical separations were conducted in 0.1% TFA with an acetonitrile gradient (10–90%) acetonitrile in water over 20 min, flow rate of 1.0 mL/min) on a Phenomenex C18 column (0.46 mm  $\times$  150 mm 5  $\mu$ m). After analytical analysis, the crude peptide was purified by preparative chromatography in 0.1% TFA with an acetonitrile gradient (10–90% acetonitrile in water over 15 min, flow rate of 15 mL/min) on a Phenomenex Kinetex C18 column (21.2 mm  $\times$  150 mm 5  $\mu$ m).

*Acetylated-BIM (Ac-BIM) (Ac-DMRPEIWIAQELRRIGDEFNAYYARRNH2)*. Purity >95%, tR 16.2 min (analytical HPLC, 10–90% acetonitrile in water (0.1% TFA) over 20 min, flow rate of 1.0 mL/min); molecular formula, C<sub>147</sub>H<sub>225</sub>N<sub>45</sub>O<sub>41</sub>S; calculated mass, 3308.7; found, 1104.4 (M + 3H)/3, 828.4 (M + 4)/4.

*FITC-BIM (FITC-Ahx-EIWIAQELRRIGDEFNAYYARR-NH2)*. Purity >95%, tR 12.3 min (analytical HPLC, 10–90% acetonitrile in water (0.1% TFA) over 20 min, flow rate of 1.0 mL/min); molecular formula, C<sub>152</sub>H<sub>212</sub>N<sub>40</sub>O<sub>40</sub>S; calculated mass, 3269.6; found, 1090.8 (M + 3H)/3.

**Molecular Modeling.** Molecular docking of 1 and 8 into the solution structure of BAX (PDB code: 2K7W) was carried out using the Glide 5.5 program [159]. Maestro 9.0.211 [160] was employed as the graphical user interface, and Figure 11 was rendered by the Chimera software package [161]. The inhibitor structures were first generated through the Maestro sketcher and prepared through the LigPrep module. The target protein was prepared through the Protein Preparation Wizard of the graphical user interface Maestro and the OPLS-2001 force field. Water molecules were removed, hydrogen atoms were added, and minimization was performed until the RMSD of all heavy atoms was within 0.3 Å of the crystallographically determined positions. The binding pocket was identified by placing a 20 Å cube centered on the BIM helix. Molecular docking calculations were performed with the aid of Glide 5.5 in extra-precision (XP) mode, using Glidescore for ligand ranking. For multiple ligand docking experiments, an output maximum of 5000 ligand poses per docking run with a limit of 100 poses for each ligand was adopted.

**Biology. Reagents.** Salt and organic solvents were from Fluka, Sigma-Aldrich (USA), Applichem (Germany), and Carlo Erba (Italy). FITC, Texas Red, and HRP conjugated monoclonal and polyclonal secondary antibodies were from Sigma-Aldrich (USA). The caspase inhibitor peptide NAc-Asp-Glu-Val-Asp-al (Ac-DEVD-CHO) was from Sigma. Escherichia coli produced recombinant N-terminal GSTtagged human BAX (SRP5166), Bcl-2 (SRP0186), and Bcl-XL (SRP0187) were from Sigma.

**Cell Cultures.** HuH7 [81] cells were cultured in DMEM supplemented with 10% FBS. SHSY-5Y [162] were cultured in DMEM/F12 medium supplemented with 10% FBS and nonessential aminoacids. NB4 [70] and Jurkat [163] cells were cultured in RPMI medium supplemented with 10% FBS. Lewis lung carcinoma cells (LLC1), [72] kindly gifted from Prof. Aldo Pinto (Department of Pharmaceutical and Biomedical Sciences, University of Salerno, Italy), were cultured in DMEM containing 10% FBS, penicillin (100 U/mL), and streptomycin (100 µg/mL). MEF cells wild-type (MEF wt), MEF BCL-2 knockout (MEF Bcl2<sup>-/-</sup>), MEF BAD knockout (MEF Bad<sup>-/-</sup>), MEF BAX knockout (MEF BAX<sup>-/-</sup>), MEF BID knockout (MEF Bid<sup>-/-</sup>), MEF BAK knockout (MEF Bak<sup>-/-</sup>), and MEF BAX/BAK double knockout (MEF BAX<sup>-/-</sup>BAK<sup>-/-</sup>) were purchased from ATCC (TCP-2110) and grown in IMDM supplemented with 10% FBS supplemented with nonessential aminoacids and cultivated according manufacturer procedures. All cultures were grown in an atmosphere of 5% CO<sub>2</sub> at 37 °C.

**Primary Antibodies.** Polyclonal AntiBax N20 (Santa Cruz), monoclonal AntiBax 6A7 (Santa Cruz), polyclonal Anti active Casp-3 (Abgene), and polyclonal anti Cyt-C (Santa Cruz).

**Buffers.** Buffer B: 20 mM Tris HCl pH 7.4, NaCl 150 mM, protease inhibitors. Buffer D: 100 mM potassium phosphate pH 6.7, 7.5 mM MgCl<sub>2</sub>, 250 mM sucrose, digitonin 40 µg/mL. Buffer E: 20 mM Hepes KOH pH 7.4, 150 mM NaCl. Buffer F: 3.7% formaldehyde in PBS pH 7.4. Buffer G: 0.1 M glycine in PBS. Buffer H: 20 mM Hepes KOH pH 7.4, 120 mM sucrose. Buffer S: 1% SDS in Buffer B. Buffer L: 1% Triton X-100 in Buffer B. Buffer T: 0.1% Triton in PBS pH 7.4.

**Fluorescence Polarization Binding Assay.** FITC-BIM direct binding curves to GST-BAX, BCL-2, and BCL-XL were generated by incubation of the fluorescent peptide (50 nM) with the indicated dilution of

recombinant purified proteins in buffer E. Fluorescent polarization was measured before and after the addition of Acetylated- BIM (50  $\mu$ M). FITC-BIM specific binding was calculated subtracting nonspecific binding (measured in the presence of Acetylated-BIM) from total binding (measured in the absence of acetylated-BIM). EC50 was calculated by fitting direct total binding data by nonlinear regression analysis of dose–response curve using Prism software (GraphPad). Ki was calculated by fitting direct specific binding data by nonlinear regression analysis of competitive binding curves. Fluorescent polarization was measured with an Envision station (PerkinElmer) using the following setting (excitation filter, FITC-FP- 480 (code: 104) (X480; CWL = 480 nm; BW = 30 nm; Tmin = 70%); emission filter (P), FITC FP P-pol 535 (code: 209) (M535p; CWL = 535 nm; BW = 40 nm; Tmin = 80%); emission filter (S) FITC FP S-pol 535 (code: 208) (M535s; CWL = 535 nm; BW = 40 nm; Tmin = 80%) and the mirror modules FP 431 used by top. For competition assays, serial dilution of the candidate compounds were obtained by dilution in buffer E supplemented with 50 nM FITC-BIM. After 5 min, recombinant proteins were added to the mixture at 1  $\mu$ M concentration. Fluorescence polarization was measured after 30 min of incubation. Measurements were done in triplicates, and pKi were calculated fitting the values by nonlinear regression analysis of competitive binding curves using Prism software (GraphPad). All the best-fit values reported in Table 1 had SE <10% (the curve fitting for competitive binding of compound 3 to BAX has SE <15%, the one of compound 15 for Bcl-2 has SE <16%).

*Assessment of Apoptosis Rate.* Mother stocks of compounds dissolved in DMSO (30 mM) were diluted in complete culture medium. Cells were treated with the diluted compounds for the indicated time. After treatment, cells were fixed in buffer F and apoptosis rate was measured by evaluation of nuclear fragmentation (visualized by DAPI staining), positivity to antiactive caspase 3 antibody, and blebbing of cell membrane. Percent of cells in apoptosis was calculated by counting cells from 20 random fields. Measurements were done in triplicate, and EC50 were calculated fitting the values by nonlinear regression analysis of competitive binding curves using Prism software (GraphPad). All the best-fit values reported in Table 1 had SE <10%.

*Immunofluorescence.* HuH7 cells growing on glass coverslips were fixed in buffer F for 30 min. Formaldehyde was quenched by incubating the coverslips for 30 min in buffer G. Cells were permeabilized in buffer T for 10 min at 25 °C to then be incubated with primary and secondary antibody diluted in PBS for 1 h and 30 min, respectively. The following dilutions were used: polyclonal anti- Bax 1:50, antiactive Casp-3 1:500, DAPI 1:400, and anti Cyt-C 1:200. Immunofluorescence images were taken by a Leica DFC320 video camera (Leica, Milan, Italy) connected to a Leica DMRB microscope equipped with a 100 $\times$  objective, and the ImageJ Software (National Institutes of Health, Bethesda, MD) was used for analysis.

*MitoTracker Staining and Measurement.* Cells were incubated for 30 min at 37 °C in complete medium supplemented with MitoTracker Red CMXRos (Invitrogen) at the final concentration of 200 nM. After the incubation, cells were washed twice in fresh medium and then lysed in absolute DMSO. The absorbance of the probe was read at 570 nM in a spectrophotometer. For microscope visualization of stained cells, cells were fixed in buffer F and processed as described above.

*Mice.* Female C57BL/6J mice (6 wks) were purchased from Harlan Laboratories (Milan, Italy) and housed at the Department of Pharmacy, University of Naples, Italy. Before the experiments, the mice were acclimated for 1 week and were fed with standard chow diet and water ad libitum. All animal experiments were performed under protocols that followed the Italian and European Community Council for Animal Care (DL no. 116/92).

*Animal Experiments.* Subconfluent LLC1 cells were harvested and passed through a 40  $\mu$ m cell strainer, washed 3 times in PBS, resuspended in PBS, and inoculated at 3  $\times$  10<sup>5</sup> cells in 7 week old mice through the

tail vein (day 0). After 14 days, mice were randomly divided into two groups: control and 8 1 mg/kg (n = 6 and n = 8, respectively). For the treatment, 8 was first dissolved in DMSO and then suspended in sterile water (1% DMSO final concentration). 8 (1 mg/kg) was administered once a day by ip injection from day 14 to 17. The control group received 1% DMSO (2  $\mu$ L) daily. At day 18, mice were euthanized, the thorax was opened, and the lungs were perfused with phosphate-buffered saline (PBS), pH 7.4, via the pulmonary artery to remove blood. The entire tumor-bearing lung was used and examined as described below. Drug toxicity indexes such as weight loss, ruffled fur, behavior change, and feeding patterns were continuously observed during the whole treatment.

*Splenocyte Preparation.* C57BL/6J mice were euthanized as already described. After excision, spleen was sliced into pieces and passed through a strainer using the plunger end of a syringe. Cell suspension was centrifuged for 5 min at 1600 rpm and cell pellet resuspended in prewarmed complete culture medium with the treatment with compounds starting immediately.

*Organic Extraction of Tissue.* First, 100  $\mu$ g of protein lysates were supplemented with 9 volumes of cold acetone and incubated for 2 h at  $-20^{\circ}\text{C}$ . Proteins were then pelleted by centrifuging the samples at 14000 rpm at  $4^{\circ}\text{C}$ . The absorbance spectrum of the organic extracts (1 mL in volume using quartz cuvettes) was recorded in the wavelength range between 220 and 800 nm and compared with the absorbance spectra of 8 10  $\mu$ M in water, acetone, or extraction buffer (acetone:water = 9:1) as indicated.

*Histological Analysis.* Right lung lobes were fixed in 10% buffered formalin for 24–48 h. The fixed lobes were cut in two transverse portions, paraffin-embedded, and sectioned at 7  $\mu$ m. Haematoxylin and eosin staining was performed and used to measure the tumor burden. Tumor lesions and lung area were analyzed by using 20 serial sections per lobe. The results were expressed as the ratio of the tumor lesions area compared with the total lung area. Images were taken by a Leica DFC320 video camera (Leica, Milan, Italy) connected to a Leica DMRB microscope, and the ImageJ Software (National Institutes of Health, Bethesda, MD) was used for analysis.

*Mitochondria Isolation.* Cells or lung tissue were incubated in buffer D for 30 min. After lysis, cell debris and permeabilized cells were spun down for 30 min at 3000g ( $4^{\circ}\text{C}$ ). Mitochondrial fractions were obtained centrifuging the supernatant for 30 min at 14000g. Mitochondrial pellet was lysed in B-buffer 1% Triton for 1 h at  $4^{\circ}\text{C}$ .

*Processing of the Tissues.* Lung tissues were disrupted in buffer H in a Teflon Douce. The tissue homogenate was supplemented with 1% Triton and incubated for 1 h on ice. Cell debris and unbroken cells were sedimented by spinning down the homogenate for 1 h at 14000g. The supernatant containing the protein extracts was quantitated by Biorad (Pierce) using BSA as standard. Equal amounts of protein were processed further and stored at  $-80^{\circ}\text{C}$  after having been snap frozen in liquid nitrogen.

*Immunoprecipitation.* Lysates were immunoprecipitated with 6A7 anti-BAX mouse monoclonal antibody overnight at  $4^{\circ}\text{C}$  (25  $\mu$ L of antibody per mL of lysate) and with protein-A sepharose for 45 min followed by four washes in buffer L. After the last wash, beads were resuspended in 20  $\mu$ L of buffer L before Western blot processing.

*Western Blotting.* Samples were diluted in 20 mM Tris HCl (pH 6.8), 50 mM DTT, 1% SDS, 5% glycerol, and bromophenol blue to then be boiled for 10 min at  $95^{\circ}\text{C}$ . Samples were loaded on a 12.5% SDS PAGE gel. Run was performed at 100 V at  $25^{\circ}\text{C}$ . After the run, proteins were transferred on nitrocellulose filter (Schleicher-Schuel) at 80 V for 1 h at  $4^{\circ}\text{C}$ . Filters were blocked for 2 h at  $25^{\circ}\text{C}$  in PBS supplemented with 3% nonfat dry milk (Biorad) for 2 h at  $25^{\circ}\text{C}$  and incubated with primary and secondary antibody diluted in PBS

supplemented with 0.3% nonfat dry milk in PBS. ECL reaction was performed using the Lumi Light ECL kit (Roche) according manufacturer procedures.

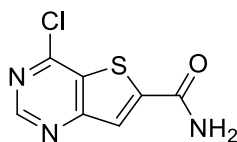
## 4.4 Part IV: Synthesis of Sirt6 Inhibitors

**Chemistry:** Commercially available solvents and reagents were used without further purification. Organic solutions were dried over anhydrous sodium sulfate. Evaporation of the solvents was carried out on Büchi Rotavapor R-210 equipped with Büchi V-855 vacuum controller and Büchi V-700 (~ 5 mbar). Column chromatography was performed on glass columns packed with silica gel from Fluka and from Aldrich (70–230 mesh). Silica gel thin layer chromatography (TLC) cards from Fluka and Macherey-Nagel (silica gel precoated aluminum cards with fluorescent indicator visualizable at 254 nm) were used for TLC. Developed plates were visualized by a Spectroline ENF 260C/FE UV apparatus. Melting points (mp) were determined on a Stuart Scientific SMP1 apparatus and on a Stuart Scientific SMP30 apparatus and are uncorrected. Mass spectral (MS) and high resolution mass spectral (HRMS) analyses were recorded on AB Sciex API-2000 (MS) and Thermo Fisher Scientific Inc. Orbitrap Exactive (HRMS) spectrometers equipped with an ESI source. Proton ( $^1\text{H}$ , 400.13 MHz) and carbon ( $^{13}\text{C}$ , 100.6 MHz) nuclear magnetic resonance spectra were recorded on a Bruker Avance 400 and a Varian Inova 400 spectrometers in the indicated solvent and corresponding fid files processed by MestreLab Research SL MestreReNova 6.2.1– 769 and Bruker Topspin 3.2 software. Chemical shifts are expressed in  $\delta$  units (ppm) from tetramethylsilane. Elemental analyses of the compounds were found within  $\pm 0.4\%$  of the theoretical values.

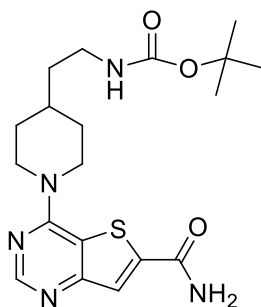
*Methyl- 4-oxo-3,4-dihydrothieno[3,2-d]pyrimidine-6-carboxylate* : A mixture of dimethyl-3-aminothiophene-2,5-dicarboxylate (1 equiv), formamidinium acetate salt (4 equiv) and 2-methoxyethanol dry (0.6 M) under  $\text{N}_2$  was stirred at reflux  $130^\circ\text{C}$  for 60 min. The addition of formamidinium acetate salt (4 equiv) was repeated and then the mixture was heated for overnight. Then the reaction was cooled to room temperature, was diluted with water and  $\text{NaHCO}_3$  solution and extracted with EtOAc. Organic phase was washed with water, brine and dried. To obtain the methyl-3H thieno[3,2-d]pyrimidin-4-one-6-carboxylate as a yellow solid without purification Yield 73%. NMR ( $\text{DMSO-d}_6$ )  $\delta$  8.24 (s, 1H), 8.01 (s, 1H), 3.92 (s, 3H). MS (ESI) calcd for  $\text{C}_8\text{H}_6\text{N}_2\text{O}_3\text{S}$ ; 210.0; found (M + H) $^+$ : 211.0.

*4-oxo-3,4-dihydrothieno[3,2-d]pyrimidine-6-carboxylic acid* : A suspension of methyl- 4-oxo-3,4-dihydrothieno[3,2-d]pyrimidine-6-carboxylate,  $\text{LiOH}\cdot\text{H}_2\text{O}$  (5 equiv) in 2-propanol (0.25 M) and water (0.40 M) was stirred at  $75^\circ\text{C}$  for 1h. Then the reaction was cooled and diluted with water and EtOAc. The two phases were separated and the aqueous phase was acidified with HCl 1M at pH 1 and the precipitate was filtered and washed with water to obtain a white solid. Yield 75%. NMR ( $\text{DMSO-d}_6$ )  $\delta$  12.80 (br s, 1H), 9.16 (s, 1H), 8.27 (s, 1H). MS (ESI) calcd for  $\text{C}_7\text{H}_4\text{N}_2\text{O}_3\text{S}$ ; 196.1; found (M + H) $^+$ : 197.1

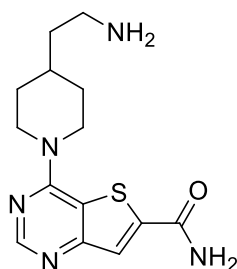
*4-chlorothieno[3,2-d]pyrimidine-6-carboxamide*: A solution of 4-oxo-3,4-dihydrothieno[3,2-d]pyrimidine-6-carboxylic acid in  $\text{SO}_2\text{Cl}$  (0.17 M) and DMF (33 M) was stirred at  $80^\circ\text{C}$  for 2h. Then the reaction was concentrated to dryness. The crude acid chloride was dissolved in a solution of  $\text{NH}_4\text{OH}$  28-30% basis (1 M) in EtOAc (0.35 M) was added to chloride in ice bath and then the reaction was stirred at room temperature for 2h under  $\text{N}_2$ . The mixture was diluted with water and extracted with EtOAc. Organic phase was dried and concentrated to give the 4-chlorothieno[3,2-d]pyrimidine-6-carboxamide as a yellow solid without purification. Yield 75%.  $^1\text{H}$  NMR ( $\text{DMSO-d}_6$ )  $\delta$  9.11 (s, 1H), 8.62 (br s, 1H), 8.35 (s, 1H), 8.15 (br s, 1H).  $^{13}\text{C}$  NMR ( $\text{DMSO-d}_6$ )  $\delta$  161.53, 161.21, 154.75 (CH), 154.13, 150.77, 131.47, 124.80 (CH). MS (ESI) calcd for  $\text{C}_7\text{H}_4\text{ClN}_3\text{OS}$ ; 213.6; found (M + H) $^+$ : 214.0



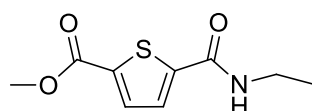
*tert-Butyl (2-(1-(6-Carbamoylthieno[3,2-d]pyrimidin-4-yl)-piperidin-4-yl)ethyl)carbamate*: A solution of 4-chlorothieno[3,2-d]pyrimidine-6-carboxamide, *tert*-butyl(2-(piperidin-4-yl)ethyl)carbamate (1 equiv) and DIEA (1 equiv) in CH<sub>3</sub>CN (0,076 M) was heated at reflux for 2h. The reaction mixture was cooled at room temperature and concentrated to dryness. The residue was suspended in MeOH (0,608 M) and water (0,06 M) was added. The mixture was sonicated and the precipitate was filtered, washed with water and dried under vacuum to obtain *tert*-butyl(2-(1-(6-carbamoylthieno[3,2-d]pyrimidin-4-yl)piperidin-4-yl)ethyl)carbamate as white solid. Yield 80%. NMR (DMSO-*d*<sub>6</sub>) δ 8.48 (s, 1H), 8.40 (br s, 1H), 8.03 (s, 1H), 7.87 (br s, 1H), 6.81 (t, 1H), 4.69 (d, 2H), 3.16 (t, 2H), 2.976 (q, 2H), 1.83 (d, 2H), 1.66 (br, 1H), 1.37 (s, 9H), 1.34 (m, 2H), 1.16 (m, 2H). MS (ESI) calcd for C<sub>19</sub>H<sub>27</sub>N<sub>5</sub>O<sub>3</sub>S, 405.5; found, 406.5.



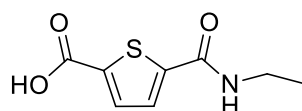
*4-(4-(2-Aminoethyl)piperidin-1-yl)thieno[3,2-d]pyrimidine-6-carboxamide*: To a solution of *tert*-butyl(2-(1-(6-carbamoylthieno[3,2-d]pyrimidin-4-yl)piperidin-4-yl)ethyl)carbamate in CH<sub>2</sub>Cl<sub>2</sub> (0,05 M) was added trifluoroacetic acid (0,207 M). The reaction was stirred at room temperature for overnight, concentrated to dryness and chased with CH<sub>2</sub>Cl<sub>2</sub>. To obtain 4-(4-(2-Aminoethyl)piperidin-1-yl)thieno[3,2-d]pyrimidine-6-carboxamide as the trifluoroacetic salt, white solid. Yield 100%. <sup>1</sup>H NMR (DMSO-*d*<sub>6</sub>) δ 8.72 (s, 1H), 8.62 (br s, 1H), 8.08 (s, 1H), 8.03 (br s, 1H), 7.75 (br s, 3H), 4.80 (d, J=4.79 Hz, 2H), 3.37 (t, J=3.36 Hz, 2H), 2.89 (m, 2H), 1.93 (d, J=1.92 Hz, 2H), 1.81 (s, 1H), 1.51 (m, 2H), 1.28 (m, 2H). MS (ESI) calcd for C<sub>14</sub>H<sub>19</sub>N<sub>5</sub>OS, 305.1; found, 306.1.



*Methyl 5-(Ethylcarbamoyl)thiophene-2-carboxylate*: To a solution of 5-(methoxycarbonyl)thiophene-2-carboxylic acid, EDCI.HCl (1,1 equiv), HOBT (1,1 equiv) in DMF (0,268 M) was added DIEA (2,5 equiv). The reaction was stirred for 15 min at room temperature, and then ethylamine hydrochloride (1 equiv) was added as a solid. The reaction was stirred at room temperature for overnight. The reaction was diluted with water and extracted with EtOAc. Organic phase was washed with brine, dried and concentrated. The crude was purified by column (7Pe\3 EtOAc) to give 5-(ethylcarbamoyl)thiophene-2-carboxylate as a yellow solid. Yield 63%. <sup>1</sup>H NMR (DMSO-d6) δ 8.76 (t, 1H), 7.76 (d, J=7.74 Hz, 1H), 7.48 (d, J=7.46 Hz, 1H), 3.93 (s, 3H), 3.51 (m, 2H), 1.30 (t, J=1.28 Hz, 3H). MS (ESI) calcd for C<sub>9</sub>H<sub>11</sub>NO<sub>3</sub>S, 213.1; found, 214.1.

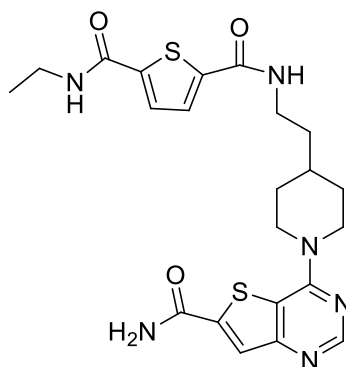


*5-(Ethylcarbamoyl)thiophene-2-carboxylic Acid*: To a solution of methyl 5-(ethylcarbamoyl)thiophene-2-carboxylate in THF (0,25M) was added a solution of LiOH.H<sub>2</sub>O (2 equiv) in water (0,5 M). The reaction was stirred at room temperature for 48h, concentrated to dryness. The residue was diluted with water and EtOAc. The two phases were separated and the aqueous phase was acidified with HCl 1M at pH 1 and extracted with EtOAc. Organic phase was washed with brine, dried and concentrated. To obtain 5-(ethylcarbamoyl)thiophene-2-carboxylic acid as a white solid. Yield 80%. <sup>1</sup>H NMR (DMSO-d6) δ 13.40 (s, 1H), 8.71 (t, J=8.69 Hz, 1H), 7.71 (d, J=7.70 Hz, 1H), 7.68 (d, J=7.67 Hz, 1H), 3.26 (m, 2H), 1.12 (t, J=1.10 Hz, 3H). MS (ESI) calcd for C<sub>8</sub>H<sub>9</sub>NO<sub>3</sub>S, 199.0; found, 200.0.

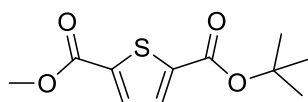


*N<sup>2</sup>-(2-(1-(6-Carbamoylthieno[3,2-d]pyrimidin-4-yl)piperidin-4-yl)-ethyl)-N<sup>5</sup>-ethylthiophene-2,5-dicarboxamide*: To a solution of 5-(ethylcarbamoyl)thiophene-2-carboxylic acid, HATU (1,2 equiv) and DIEA (4 equiv) in DMF (0,2 M) was stirred at room temperature for 10 min. Then 4-(4-(2-aminoethyl)piperidin-1-yl)-thieno[3,2-d]pyrimidine-6-carboxamide (0,80 equiv) was added and the reaction was stirred overnight. The mixture was diluted with water and extracted with EtOAc. Organic phase was washed with NaHCO<sub>3</sub> sol, brine, dried and concentrated. The crude was purified by column (93 DCM\0,7 MeOH) to give the N<sup>2</sup>-(2-(1-(6-carbamoylthieno[3,2-d]pyrimidin-4-yl)piperidin-4-yl)-ethyl)-N<sup>5</sup>-ethylthiophene-2,5-dicarboxamide as a white solid. Yield 50%. <sup>1</sup>H NMR (DMSO-d6) δ 8.67 (s, 1H), 8.56–8.62 (m, 3H), 8.06 (s, 1H), 8.00 (br, 1H), 7.68 (m, 2H), 4.76 (m, 2H), 3.21–3.37 (m, 6H), 1.95 (m, 2H), 1.76 (m, 1H), 1.49 (m, 2H), 1.25 (m, 2H), 1.11 (t, J=1.09 Hz, 3H). MS (ESI) calcd for C<sub>22</sub>H<sub>27</sub>N<sub>6</sub>O<sub>3</sub>S<sub>2</sub>, 486.1; found, 487.1.

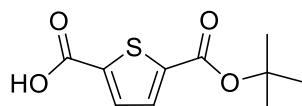




*2-tert-butyl 5-methyl thiophene-2,5-dicarboxylate* : A solution of 5-(methoxycarbonyl)thiophene-2-carboxylic acid , (Boc)<sub>2</sub>O (2,20 equiv), DMAP (0,200 equiv ) in THF (0,54 M) was stirred for overnight at room temperature. The reaction was concentrated , was diluted with NaHCO<sub>3</sub> sol and extracted with EtOAc. Organic phase was dried and concentrated. The crude was purified by column (99Pe\0,1 EtOAc) to give 2-tert-butyl 5-methyl thiophene-2,5-dicarboxylate as a white solid. Yield 72%. <sup>1</sup>H NMR (DMSO-d<sub>6</sub>) δ 7.74 (d, J=7.73 Hz, 1H), 7.68 (d, J=7.67 Hz, 1H), 3.94 (d, J=3.93 Hz, 3H), 1.60 (s, 9H). MS (ESI) calcd for C<sub>11</sub>H<sub>14</sub>O<sub>4</sub>S, 242.0; found 243.0

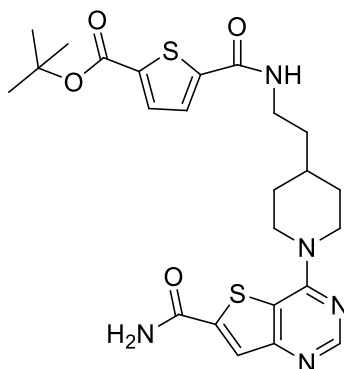


*5-(tert-butoxycarbonyl)thiophene-2-carboxylic acid*: To a solution of 2-tert-butyl 5-methyl thiophene-2,5-dicarboxylate in THF(0,25M) was added a solution of LiOH.H<sub>2</sub>O(2 eq) in water(0,5M). The reaction was stirred at room temperature for 48h, concentrated to dryness. The residue was diluted with water and EtOAc. The two phases were separated and the aqueous phase was acidified with HCl 1M at pH 1 and extracted with EtOAc. Organic phase was washed with brine, dried and concentrated. To give the 5-(tert-butoxycarbonyl)thiophene-2-carboxylic acid as a white solid 80%. <sup>1</sup>H NMR (DMSO-d<sub>6</sub>) δ 13.20 (s, 1H), 7.74 (d, J=7.73 Hz, 1H), 7.69 (d, J=7.68 Hz, 1H), 1.60 (s, 9H). MS (ESI) calcd for C<sub>10</sub>H<sub>12</sub>O<sub>4</sub>S, 228.0; found , 229.0

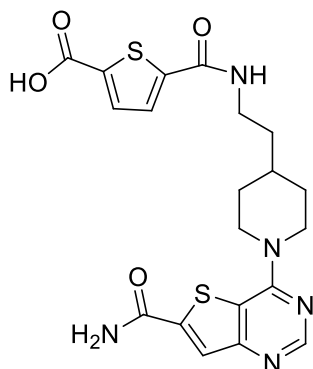


To a solution of 5-(tert-butoxycarbonyl)thiophene-2-carboxylic acid, HATU (1,2eq) and DIEA(5eq) in DMF(0,2M) was stirred at rt for 10 min . Then 4-(4-(2-aminoethyl)piperidin-1-yl)-thieno[3,2-d]pyrimidine-6-carboxamide tfa salt(1eq) was added and the reaction was stirred overnight. The mixture was diluted with water and extracted with EtOAc(x3). Organic phase was washed with NaHCO<sub>3</sub> sol, brine(x6) , dried and concentrated. The crude was purified by colonm(97 DCM\0,3MeOH) to give the 5-ter-butyl((2-(1-(6-carbamoyl)thieno[3,2-d]pyrimidin-4-yl)piperidin-4-yl))ethyl)carbamoyl)thiophene-2-carboxylate as a white

solid. Yield 30%.  $^1\text{H}$  NMR (DMSO- $d_6$ )  $\delta$  8.46 (s, 1H), 7.90 (s, 1H), 7.68 (d,  $J=7.67$  Hz, 1H), 7.64 (d,  $J=7.63$  Hz, 1H), 3.48 (t,  $J=3.47$  Hz, 2H), 3.27 (t,  $J=3.25$  Hz, 2H), 1.99 (m, 2H), 1.83 (m, 1H), 1.64 (m, 2H), 1.60 (s, 9H), 1.35 (m, 2H). MS (ESI) calcd for  $\text{C}_{24}\text{H}_{29}\text{N}_5\text{O}_4\text{S}_2$ , 515.1; found, 516.1

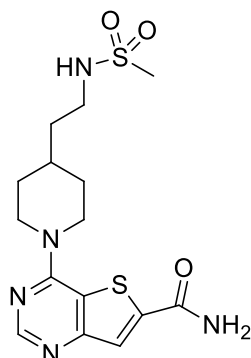


5-((2-(1-(6-carbamoylthieno[3,2-d]pyrimidin-4-yl)piperidin-4-yl)ethyl)carbamoyl)thiophene-2-carboxylic acid : A solution of 5-ter-butyl((2-(1-(6-carbamoyl)thieno[3,2-d]pyrimidin-4-yl)piperidin-4-yl)ethyl)carbamoyl)thiophene-2-carboxylate in 1:1 TFA\DCM (2,5ml) was stirred overnight. The mixture was concentrated and azeotrope with DCM, triturated with the mixture of diethyl ether/ pentane for 20 min and dried. To obtain a solid orange. Yield 70%.  $^1\text{H}$  NMR (DMSO- $d_6$ )  $\delta$  8.72 (m, 1H), 8.66 (s, 1H), 8.55 (br, 1H), 8.05 (s, 1H), 7.99 (br, 1H), 7.74 (d,  $J=7.73$  Hz, 1H), 7.70 (d,  $J=7.69$  Hz, 1H), 4.76 (m, 2H), 3.28-3.42 (m, 4H), 1.95 (m, 2H), 1.75 (m, 1H), 1.50 (m, 2H), 1.20 (m, 3H). MS (ESI) calcd for  $\text{C}_{20}\text{H}_{22}\text{N}_5\text{O}_4\text{S}_2$ , 459.1; found, 460.1

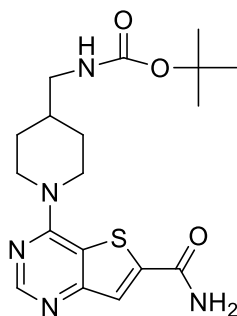


4-(4-(2-(methylsulfonylamido)ethyl)piperidin-1-yl)thieno[3,2-d]pyrimidine-6-carboxamide: To a mixture of 4-(4-(2-aminoethyl)piperidin-1-yl)-thieno[3,2-d]pyrimidine-6-carboxamide and trimethylamine (0,506 M) in pyridine (0,050 M) was added methansulfonyl chloride (1,10 equiv) at  $0^\circ\text{C}$  under  $\text{N}_2$ . The mixture was stirred at room temperature overnight, quenched with ammonia hydroxide 5N and concentrated in vacuo. The residue was neutralized to pH-7 using  $\text{Na}_2\text{CO}_3$  sol and extracted with DCM. Organic phase was washed with brine, dried and concentrated. The crude was purified by column (93DCM\0,7MeOH) to give the 4-(4-(2-(methylsulfonylamido)ethyl)piperidin-1-yl)thieno[3,2-d]pyrimidine-6-carboxamide as orange solid. Yield 30%.  $^1\text{H}$  NMR (DMSO- $d_6$ )  $\delta$  8.49 (s, 1H), 8.40 (br, 1H), 8.03 (s, 1H), 7.87 (br, 1H), 6.95 (t, 1H), 4.70 (m, 2H),

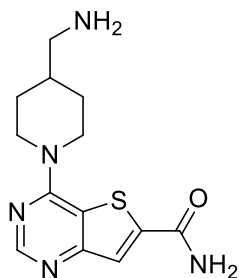
3.18 (m, 2H), 2.99 (q, 2H), 2.89 (s, 3H), 1.7-1.9 (m, 3H), 1.42 (q, 2H), 1.18 (m, 2H). MS (ESI) calcd for  $C_{15}H_{21}N_5O_3S_2$ , 383.1; found, 384.1



*tert-Butyl ((1-(6-Carbamoylthieno[3,2-d]pyrimidin-4-yl)-piperidin-4-yl)methyl)carbamate*: A solution of 4-chlorothieno[3,2-d]pyrimidine-6-carboxamide, *tert*-butyl (piperidin-4-ylmethyl)carbamate (1 equiv) and DIEA (1 equiv) in  $CH_3CN$  (0,076 M) was heated at reflux for 2h. The reaction mixture was cooled at room temperature and concentrated to dryness. The residue was suspended in  $MeOH$  (0,608 M) and water (0,06 M) was added. The mixture was sonicated and the precipitate was filtered, washed with water and dried under vacuum to obtain *tert*-butyl(2-(1-(6-carbamoylthieno[3,2-d]pyrimidin-4-yl)piperidin-4-yl)ethyl)carbamate as white solid. Yield 80%. NMR ( $DMSO-d_6$ )  $\delta$  8.49 (s, 1H), 8.41 (br s, 1H), 8.04 (s, 1H), 7.88 (br s, 1H), 6.92 (t, 1H), 4.67 (d, 2H), 3.18 (t, 2H), 2.85 (q, 2H), 1.77 (d, 2H), 1.66 (br, 1H), 1.38 (s, 9H), 1.15 (m, 2H). MS (ESI) calcd for  $C_{19}H_{27}N_5O_3S$ , 405.5; found, 406.5.



*4-(4-(Aminomethyl)piperidin-1-yl)thieno[3,2-d]pyrimidine-6-carboxamide*: To a solution of *tert*-butyl ((1-(6-carbamoylthieno[3,2-d]pyrimidin-4-yl)piperidin-4-yl)methyl)carbamate in CH<sub>2</sub>Cl<sub>2</sub> (0,05 M) was added trifluoroacetic acid (0,207 M). The reaction was stirred at room temperature for overnight, concentrated to dryness and chased with CH<sub>2</sub>Cl<sub>2</sub>. To obtain 4-(4-(2-Aminoethyl)piperidin-1-yl)thieno[3,2-d]pyrimidine-6-carboxamide as the trifluoroacetic salt, white solid. Yield 100%. <sup>1</sup>H NMR (DMSO-d<sub>6</sub>) δ 8.72 (s, 1H), 8.62 (br s, 1H), 8.08 (s, 1H), 8.03 (br s, 1H), 7.75 (br s, 3H), 4.80 (d, J=4.79 Hz, 2H), 3.37 (t, J=3.36 Hz, 2H), 2.89 (m, 2H), 1.81 (s, 1H), 1.51 (m, 2H), 1.28 (m, 2H). MS (ESI) calcd for C<sub>14</sub>H<sub>19</sub>N<sub>5</sub>OS, 305.1; found, 306.1.



## Chapter 5 – Conclusions

In summary, new anticancer drugs have been designed and developed by application of new synthetic strategies.

In the first chapter, the identification of novel electrophilic partners have helped develop the new isocyanide mediated MCRs. Specifically, new methodology to prepare structurally diverse aryl  $\alpha$ -ketoamide amides has been demonstrated. It is important to highlight that the entire sequence of reactions is realized under mild reaction conditions avoiding the use of expensive coupling agents and using simple and easily available starting materials ((Z)-arylchlorooximes and  $\alpha$ -isocyanoacetamides). This method is complementary to those previously reported for the synthesis of alkyl  $\alpha$ -ketoamide amides [164]. This new protocol can find application in the synthesis of tailored aryl  $\alpha$ -ketoamide amides given their importance in both organic and medicinal chemistry. As a continuous of this study, a solution phase parallel synthesis method have been reported to obtain stable  $\alpha$ -aryloxyiminoamide derivatives. It is an application of Passerini-Smiles reaction which is realized under basic condition using (Z)-chlorooximes, isocyanides and electron-deficient phenols. This parallel synthesis method allows to produce easily and rapidly  $\alpha$ -aryloxyiminoamides and they can be applied in organic and medicinal chemistry.

In the second chapter, a structure-based lead optimization and biological evaluation of BAX direct activators have been reported. Optimization of BAX direct activators has been already shown to be challenging [63]. In this work it was showed that **1** optimization can successfully lead to new hits with improved affinity for BAX. However, minimal changes in the chemical structure of the hits can drastically change their selectivity, affecting their affinity for other BCL-2 family members. In MEF cells, whatever the main target is, the event of binding leads always to apoptosis. However, in tumor cells, a severe unbalancing between proapoptotic and antiapoptotic proteins exists, with the latter being overexpressed in almost every tumor. Thus, ligands with low selectivity can be sequestered by antiapoptotic proteins that, ultimately, buffer them, inhibiting the activation of proapoptotic proteins. As a result of this first round of **1** optimization, it was here presented **8**. In vitro affinity of **8** for BAX is only slightly higher than **1**. On the contrary, it shows lower affinity for BCL-2 and BCL-XL than **1**. Its selectivity manifests in MEF BAX<sup>-/-</sup> knockout cells that, differently from many other tested MEF knockout clones, are insensitive to **8** treatments. In cultured tumor cells, it induces MOMP with an EC<sub>50</sub> of 700 nM, **1** order of magnitude lower than the one measured for **1**. As such, it is the most active, low molecular weight, direct activator of BAX reported in the published literature. SAR data here developed clearly suggest that the phenyl-thiazol moiety can be replaceable by other aromatic groups and that the activity is increased by a terminal positive charged group that, according to a theoretical binding mode, would interact with negatively charged BAX residues. **8** is able to induce BAX activation and translocation to mitochondria, MOMP, and consequent release of cyt-c in all the tumor cell line tested. Moreover, **8** seems to be rather selective for cancer cells (HuH7, NB4, SHSY-5Y, and LLC1) and immortalized cells (MEF), leaving unperturbed apoptosis rate in healthy resting cells (healthy splenocytes). The in vivo efficiency of **8** in tumor mass reduction together with the absence of gross toxicity, although just 4 days of treatment was applied, would suggest that BAX direct activators may really represent a novel promising class of anticancer agents rather than venoms.

Moreover, it was attempted a molecular screening campaign toward pharmacological chaperones rescuing Fz4-FEVR folding with the ultimate goal to identify small organic wild-type (WT) Fz4 (Fz4-WT) modulators. It

is reported molecules able to work as folding chaperones by measuring their potency in restoring Fz4-FEVR folding and localization at the PM. In this context it was identified three pharmacological chaperones of Fz4-FEVR that are indeed Fz4-WT ligands and act as Wnt- $\beta$ -catenin inhibitors, proving the validity of the new screening strategy. One of these hits, namely FzM1, exerts its modulatory activity by inducing conformational changes in Fz4-WT that ultimately allow it to inhibit  $\beta$ -catenin nuclear transport and antagonize the Wnt pathway. The Fz4 modulators here described represent what are to our knowledge the first organic molecules addressing this still-undruggable receptor. Here, the novelty of the screening approach, the step of the Wnt- $\beta$ -catenin cascade targeted by our new compounds together with their mechanism of action suggest new avenues for development of inhibitors of the Wnt- $\beta$ -catenin pathway and for drug discovery.

In the third chapter, the ability of small molecules to bind and inhibit SIRT6 has been explored and experimented for the first time in the literature. According to *in vitro* tests, this work has identified N<sup>2</sup>-(2-(1-(6-Carbamoylthieno[3,2-d]pyrimidin-4-yl)piperidin-4-yl)-ethyl)-N<sup>5</sup>-ethylthiophene-2,5 dicarboxamide (the so called compound 1) which shows a perceivable SIRT6 inhibition activity. Compound 1, which finds applications in cancer treatment, may represent the starting point for further structure lead optimization and structure-activity relationship studies.

# Bibliography

- [1] I. G. Book, "Heterocyclic Compounds. Available online: <http://goldbook.iupac.org/H02798.html>," [Online].
- [2] A. Gomtsyan, "Heterocycles in drugs and drug discovery.," *Chem. Heterocycl. Compd.*, vol. 48, pp. 7-10, 2012.
- [3] M. G. G. L. R. S. B. S. P. S. D. M. H. C. A. B. M. M. M. D. R. S. L. M. D. S. S. B. E. N. M. S. S.F Generoso, "Pharmacological folding chaperones act as allosteric ligands of Frizzled4," *Nature Chemical Biology*, vol. 11, no. 4, pp. 280-6, 2015.
- [4] R. V. A. O. a. M. d. Greef, *Synthesis*, pp. 1471-1499, 2003.
- [5] A. D. R. G. A. D. d. I. S. Palacios F., *J.M. Curr. Org. Chem.*, vol. 13, pp. 810-, 2009.
- [6] A. Hantzsch, *Justus Liebigs Ann. Chem.*, vol. 1, p. 215, 1882.
- [7] A. Hantzsch, *Ber. Dtsch Chem. Ges.*, vol. 23, p. 1474, 1890.
- [8] P. Biginelli, *Ber. Dtsch. Chem. Ges.*, vol. 24, p. 1317–1319 and 2962–2967., 1891.
- [9] M. Passerini, *Gazz. Chim. Ital.*, vol. 51, p. 126, 1921.
- [10] D. J. R. a. M. Yus, *Angew. Chem., Int. Ed.*, vol. 44, pp. 1602-1634, 2005.
- [11] A. Gautier, *Ann. Chim (Paris)*, vol. 17, p. 218, 1869.
- [12] L. W., *Justus Liebigs Ann. Chem.*, vol. 112, p. 316, 1859.
- [13] G. A., *Justus Liebigs Ann. Chem.*, vol. 146, p. 119, 1869.
- [14] H. A, W. *Justus Liebigs Ann. Chem.*, vol. 144, p. 114, 1867.

- [15] B. K. W. B. P. U. Fehlhammer W. P., *Chem.Ber.* , vol. 118, pp. 2220-2234, 1985.
- [16] I. U. A. Dömling, "Multicomponent Reactions with Isocyanides," *Angew.Chem.Int.Ed*, vol. 39, pp. 3168-3210, 2000.
- [17] O. Mumm., *Ber. Dtsch. Chem. Ges.*, vol. 43, p. 887, 1910.
- [18] W. M. R. Huisgen, *Tetrahedron Lett.*, vol. 17, pp. 583-586, 1961.
- [19] R. M. S. G. G. C. T. T. Pirali, *Org. Lett.*, vol. 13, p. 3734-3737, 2011.
- [20] M. A. P. Vita Finzi, *Tetrahedron Lett.*, vol. 6, pp. 4645-4646, 1965.
- [21] A. Hegarty, *Acc. Chem. Res.* , vol. 13, pp. 448-454, 1980.
- [22] L. M. L. R. G. Leandri, *Boll. Sci. Fac. Chim. Ind. Bologna*, vol. 15, pp. 57-62, 1957.
- [23] P. J. G. Z. H. B. J.-. Z. X. Sun, *Org. Lett.*, vol. 3, pp. 877-880, 2001.
- [24] V. M. H. C. S. D. M. U. G. E. N. G. T. M. Giustiniano, *J.Org.Chem.* , vol. 79, no. 13, pp. 6006-6014, 2014.
- [25] K. C. S. B. Liu and R. Howe, *J.Org.Chem.* , vol. 45, pp. 3916-3918, 1980.
- [26] B. B. F. T. Y. A. Dömling A., *J. Comb. Chem.* , vol. 8, pp. 872-880., 2006.
- [27] Z. J. Housseman C., *Synlett* , pp. 1777-1779., 2006.
- [28] S. X. N. L. D. J. ., Z. R. Quan N., *Synlett* , pp. 1028-1032, 2011.
- [29] L. El Kaïm, M. Gizolme and L. Grimaud, "O-Arylative Passerini reactions.," *Org. Lett.*, vol. 8, pp. 5021-5023, 2006.
- [30] E. Martinand-Lurin, A. Dos Santos, L. El Kaïm, L. Grimaud and P. Retailleau, "Double Smiles rearrangement of Passerini adducts towards benzoxazinones.," *Chem. Commun.* , vol. 50, pp. 2214-2217, 2014.



- [31] N. J. Hrib, J. G. Jurcak, K. L. Burgher, P. G. Conway, H. B. Hartman, L. L. Kerman, J. E. Roehr and A. T. Woods, "Benzisoxazole- and benzisothiazole-3-carboxamides as potential atypical antipsychotic agents.," *J. Med. Chem.*, vol. 37, pp. 2308-2314, 1994.
- [32] W. E. Truce and D. C. Hampton, "Butyllithium-induced rearrangement of methyl methylnaphthyl," *J. Org. Chem.*, vol. 28, pp. 2276-2279, 1963.
- [33] L. El Kaïm, L. Grimaud and J. Oble, "Phenol Ugi-Smiles systems: strategies for the multicomponent N-arylation of primary amines with isocyanides, aldehydes, and phenols," *Angew. Chem., Int.*, vol. 44, pp. 7961-7964, 2005.
- [34] S. M. C. Group, "<http://www.symech.it/> MCRcombiS," MCR Combinatorial Stoichiometry (MCRcombiS), 2007-2014. [Online].
- [35] N. J. Hrib, J. G. Jurcak, K. L. Burgher, P. G. Conway, H. B. Hartman, L. L. Kerman, J. E. Roehr and A. T. Woods, "Benzisoxazole- and benzisothiazole-3-carboxamides as potential atypical antipsychotic agents.," *J. Med. Chem.*, vol. 37, p. 2308-2314, 1994.
- [36] K. Narasaka and M. Kitamura, "Amination with oximes.," *Eur. J. Org. Chem.*, pp. 4505-4519, 2005.
- [37] S. Elmore, "Apoptosis: A Review of Programmed Cell Death," *Toxicol Pathol.*, vol. 35, no. 4, pp. 495-516, 2007.
- [38] M. Hengartner, "The biochemistry of apoptosis," *Nature*, vol. 407, p. 770-776, 2000.
- [39] M. Y. L. L. X. W. C.Y. Du, "Smac, a mitochondrial protein that promotes cytochrome c- dependent caspase activation by eliminating IAP inhibition," *Cell*, vol. 102, pp. 33-42, 2000.
- [40] S. S. D. E. S. W. C. S. L. C. S. T. E. A. C. H. R. L. Joza N, "Essential role of the mitochondrial apoptosis-inducing factor in programmed cell death.," *Nature*, vol. 410, pp. 549-554, 2001.
- [41] D. E. R. L. S. K. Z. N. L. M. C. P. F. K. Susin SA, "Two distinct pathways leading to nuclear apoptosis.," *J Exp Med*, vol. 192, pp. 571-580, 2000.
- [42] L. X. W. X. Li LY, "Endonuclease G is an apoptotic DNase when released from mitochondria," *Nature*, vol. 412, pp. 95-99, 2001.

- [43] S. H. Y. H. O. K. I. A. N. S. Enari M, "A caspase-activated DNase that degrades DNA during apoptosis, and its inhibitor ICAD.," *Nature* , vol. 391, pp. 43-50, 1998.
- [44] L. F. J. Y. P. N. C. C. Y. Tsujimoto, "Cloning of the chromosome breakpoint of neoplastic B cells with the t(14;18) chromosome translocation.," *Science* , vol. 226, pp. 1097-1099, 1984.
- [45] a. A. J. Cory S, "The Bcl-2 family : Regulators of the cellular life or death switch," *Nat. Rev. Cancer*, vol. 2, pp. 647-656, 2002.
- [46] H. C. H. V. N. Z. I. M. Z. X. B. L. D. H. D. J. R. G. K. C. Brenner, "Bcl-2 and Bax regulate the channel activity of the mitochondrial adenine nucleotide translocator.," *Oncogene*, vol. 19, pp. 329-336, 2000.
- [47] S. P. Z.X. Chen, "Bcl-2 induces pro-oxidant state by engaging mitochondrial respiration in tumor cells.," *Cell Death Differ.* , vol. 14, pp. 1617-1627, 2007.
- [48] G. T. ., S. P. C. B. I R. Indran a, "Recent advances in apoptosis, mitochondria and drug resistance in cancer cells," *Biochimica et Biophysica Acta* , vol. 1807, pp. 735-745, 2011.
- [49] L. Z. D. Z. G. H. J. J. D. B. M.Y. Vyssokikh, "Bax releases cytochrome c preferentially from a complex between porin and adenine nucleotide translocator Hexokinase activity suppresses this effect," *Mol Biol Rep* , vol. 29, pp. 93-96, 2002.
- [50] C. B. N. Z. J. J. S. S. H. V. M. Z. X. S. M. J. R. G. K. I. Marzo, "Bax and adenine nucleotide translocator cooperate in the mitochondrial control of apoptosis.," *Science*, vol. 281, pp. 2027-2031, 1998.
- [51] J. Z. J. J. L. B. C. T. S. K. E. Yang, "Bad a heterodimeric partner for Bcl-XL and Bcl-2, displaces Bax and promotes cell death.," *Cell*, vol. 80, pp. 285-291, 1995.
- [52] C. M, G. Moore Vdel, M. Nishino, G. Wei, S. Korsmeyer and S. a. L. A. Armstrong, "Mitochondria primed by death signals determine cellular addiction to antiapoptotic BCL-2 family members.," *Cancer Cell*, vol. 9, pp. 351-365, 2006.
- [53] W. R. S. J. C. M. Weiss LM, "Molecular analysis of the t(14;18) chromosomal translocation in malignant lymphomas.," *N Engl. J Med*, vol. 317, pp. 1185-1189, 1987.
- [54] H. J. D. K. P. N. C. J. L. D. e. a. Rao PH, "Chromosomal and gene amplification in diffuse large B-cell lymphoma.," *Blood*, vol. 92, p. 234-240, 1998.

- [55] D. D. A. A. S. E. R. J. Hanada M, "bcl-2 gene hypomethylation and high-level expression in B-cell chronic lymphocytic leukemia," *Blood*, vol. 82, p. 1820–1828, 1993.
- [56] C. G. F. M. I. M. F. M. S. M. Cimmino A, "miR-15 and miR-16 induce apoptosis by targeting BCL2.," *Proc Natl Acad Sci USA*, vol. 102, p. 13944–13949, 2005.
- [57] Y. H. I. Y. L. Y. S. H. R. J. e. a. Rampino N, "Somatic frameshift mutations in the BAX gene in colon cancers of the microsatellite mutator phenotype," *Science*, vol. 275, p. 967–969., 1997.
- [58] P. I. S. A. R. J. Kitada S, "Dysregulation of apoptosis genes in hematopoietic malignancies.," *Oncogene*, vol. 21, p. 3459–74., 2002.
- [59] B. W. H. M. H. C. Greenblatt MS, "Mutations in the p53 tumor suppressor gene: clues to cancer etiology and molecular pathogenesis," *Cancer Res*, vol. 54, pp. 4855-4878, 1994.
- [60] C. N. T. K. D. C. P. S. M. a. L. A. Deng J., "BH3 profiling identifies three distinct classes of apoptotic blocks to predict response to ABT-737 and conventional chemotherapeutic agents.," *Cancer Cell*, vol. 12, pp. 171-185, 2007.
- [61] R. J. Miyashita T, "Bcl-2 oncoprotein blocks chemotherapy-induced apoptosis in a human leukemia cell lines.," *Blood*, vol. 81, pp. 151-157, 1993.
- [62] M. Suzuki, R. J. Youle and N. Tjandra, "Structure of BAX: coregulation of dimer formation and intracellular localization," *Cell*, vol. 103, p. 645–654, 2000.
- [63] E. Gavathiotis, M. Suzuki, M. L. Davis, K. Pitter, G. H. Bird, S. G. Katz, H. C. Tu, H. Kim, E. H. Cheng, N. Tjandra and L. D. Walensky, "BAX activation is initiated at a novel interaction site.," *Nature*, vol. 455, p. 1076–1081., 2008.
- [64] E. Gavathiotis, D. E. Reyna, J. A. Bellairs, E. S. Leshchiner and L. D. Walensky, "Direct and selective small-molecule activation of proapoptotic BAX," *Nature Chem. Biol*, vol. 8, pp. 639-645, 2012.
- [65] R. A. Friesner, J. L. Banks, R. B. Murphy, T. A. J. J. Halgren, D. T. Mainz, M. P. Repasky, E. H. Knoll, M. Shelley, J. K. Perry, D. E. Shaw, P. Francis and P. S. Shenkin, "Glide: A new approach for rapid, accurate docking and scoring. 1. Method and assessment of docking accuracy," *J. Med. Chem*, vol. 47, p. 1739–1749., 2004.
- [66] R. A. Friesner, R. B. Murphy, M. P. Repasky, L. L. Frye, J. R. Greenwood, T. A. Halgren, P. C.

Sanschagrín and D. T. Mainz, "Extra precision Glide: docking and scoring incorporating a model of hydrophobic enclosure for protein–ligand complexes," *J. Med. Chem.*, vol. 49, p. 6177–6196., 2006 .

- [67] M. García-Calvo, E. P. Peterson, B. Leitinger, R. Ruel, D. W. Nicholson and N. A. Thornberry, "Inhibition of human caspases by peptide-based and macromolecular inhibitors," *J. Biol. Chem.*, vol. 273, p. 32608–32613., 1998.
- [68] L. Cam, A. Boucquey, A. Coulomb-L'Hermine, A. Weber and P. Horellou, "Gene transfer of constitutively active caspase-3 induces apoptosis in a human hepatoma cell line.," *J. Gene Med.*, vol. 7, pp. 30-38, 2005.
- [69] S. Varadarajan, M. Vogler, M. Butterworth, D. Dinsdale, L. D. Walensky and G. M. Cohen, "Evaluation and critical assessment of putative MCL-1 inhibitors," *Cell Death Differ.*, vol. 20, p. 1475–1484, 2013.
- [70] M. Lanotte, V. Martin-Thouvenin, S. Najman, P. Balerini, F. Valensi and R. Berger, "NB4, a maturation inducible cell line with t(15;17) marker isolated from a human acute promyelocytic leukemia (M3).," *Blood*, vol. 77, pp. 1080-1086, 1991.
- [71] A. A. Ovejera, R. K. Johnson and A. Goldin, "Growth characteristics and chemotherapeutic response of intravenously implanted Lewis lung carcinoma.," *Cancer Chemother. Rep.*, vol. 5, pp. 111-125, 1975.
- [72] P. Brodt, "Characterization of two highly metastatic variants of Lewis lung carcinoma with different organ specificities," *Cancer Res.*, vol. 46, pp. 2442-2448, 1986.
- [73] T. Giraldi, G. Sava, R. Cuman, C. Nisi and L. Tassiani, "Selectivity of the antimetastatic and cytotoxic effects of 1-p-(3,3-dimethyl-1-triazeno)benzoic acid potassium salt, (±)-1,2-di(3,5-dioxopiperazin-1-yl)propane, and cyclophosphamide in mice bearing Lewis lung carcinoma," *Cancer Res.*, vol. 41, pp. 2524-2528, 1981.
- [74] S. W. Tait and D. R. Green, "Mitochondria and cell death: outer membrane permeabilization and beyond," *Nature Rev. Mol. Cell Biol.*, vol. 11, pp. 621-632, 2012.
- [75] G. Schulte, "The class Frizzled receptors," *Pharmacol. Rev.*, vol. 62, p. 632–667, 2010.
- [76] Y. e. a. Wang, "Norrin/Frizzled4 signaling in retinal vascular development and blood brain barrier plasticity," *Cell*, vol. 151, pp. 1332-1344, 2012.
- [77] H. e. a. Wong, "Structural basis of the recognition of the dishevelled DEP domain in the Wnt signaling

pathway," *Nat. Struct. Biol.* , vol. 7, pp. 1178-1184, 2000.

- [78] J. e. a. Robitaille, "Mutant frizzled-4 disrupts retinal angiogenesis in familial exudative vitreoretinopathy," *Nat. Genet.* , vol. 32, pp. 326-330, 2002.
- [79] J. R. R. & M. T. Malaterre, "Wnt-Frizzled signaling and the many paths to neural development and adult brain homeostasis.," *Front. Biosci.* , vol. 12, pp. 492-506, 2007.
- [80] X. e. a. Jin, "Frizzled 4 regulates stemness and invasiveness of migrating glioma cells established by serial intracranial transplantation," *Cancer Res.*, vol. 71, p. 3066–3075 , 2011.
- [81] V. Lemma, M. D'Agostino, M. G. Caporaso, M. Mallardo, G. Oliviero, M. Stornaiuolo and S. Bonatti, "A disorder-to-order structural transition in the COOH-tail of Fz4 determines misfolding of the L501fsX533-Fz4 mutant.," *Sci. Rep.*, vol. 3, p. 2659, 2013.
- [82] M. e. a. D'Agostino, "The cytosolic chaperone  $\alpha$ -crystallin B rescues folding and compartmentalization of misfolded multispans transmembrane proteins.," *J. Cell Sci.* , vol. 126, pp. 4160-4172, 2013.
- [83] K. e. a. Varga, "Enhanced cell surface stability of rescued  $\Delta$ F508 cystic fibrosis transmembrane conductance regulator by pharmacological chaperones," *Biochem. J.* , vol. 410, pp. 555-564, 2008.
- [84] R. e. a. Ekkebus, "On terminal alkynes that can react with active-site cysteine nucleophiles in proteases," *J. Am. Chem. Soc.* , vol. 135, pp. 2867-2870, 2013.
- [85] D. e. a. Tauriello, "Wnt/ $\beta$ -catenin signaling requires interaction of the Dishevelled DEP domain and C terminus with a discontinuous motif in Frizzled.," *Proc. Natl. Acad. Sci.*, vol. 109, pp. E812-E820, 2012.
- [86] B. & H. X. MacDonald, "Frizzled and LRP5/6 receptors for Wnt/ $\beta$ -catenin signaling.," *Cold Spring Harb. Perspect. Biol.* , vol. 4, p. a007880, 2012.
- [87] H. e. a. Jung, "Deubiquitination of Dishevelled by Usp14 is required for Wnt signaling," *Oncogenesis* , Vols. 2, E64, pp. 1-11, 2013.
- [88] A. & K. S. Voronkov, "Wnt/ $\beta$ -catenin signaling and small molecule inhibitors.," *Curr. Pharm. Des.* , vol. 19, pp. 634-664, 2013.
- [89] M. M. R. F. A. P. O. & G. C. Maher, " $\beta$ -Catenin phosphorylated at serine 45 is spatially uncoupled from  $\beta$ -catenin phosphorylated in the GSK3 domain: implications for signaling," *PLoS ONE* , vol. 5, p.

- [90] A. e. a. Gurney, "Wnt pathway inhibition via the targeting of Frizzled receptors results in decreased growth and tumorigenicity of human tumors.," *Proc. Natl. Acad. Sci. USA*, vol. 109, pp. 11717-11722, 2012.
- [91] J. S. J. N. H. J. B. & H. I. Rine, "A suppressor of mating-type locus mutations in *Saccharomyces cerevisiae*: evidence for and identification of cryptic mating-type loci.," *Genetics* , vol. 93, pp. 877-901, 1979.
- [92] O. M. Aparicio, B. L. Billington and D. E. Gottschling, *Cell*, vol. 66, p. 1279–1287., 1991.
- [93] M. Braunstein, A. B. Rose, S. G. Holmes, C. D. Allis and J. R. Broach, *Genes Dev.* , vol. 7, pp. 592-604, 1993.
- [94] R. A. Frye, *Biochem. Biophys. Res. Commun.*, vol. 273, pp. 793-798, 2000.
- [95] C. A. M. K. L. G. S. Imai, "Transcriptional silencing and longevity protein Sir2 is an NAD-dependent histone deacetylase.," *Nature* , vol. 403, pp. 795-800, 2000.
- [96] M. S. Finnin, J. R. Donigian and N. P. Pavletich, *Nat. Struct. Mol Biol.* , vol. 8, pp. 621-625, 2001.
- [97] A. A. Sauve, I. Celic, J. Avalos, H. Deng, J. D. Boeke and V. L. Schramm, *Biochemistry* , vol. 40, pp. 15456-15463, 2001.
- [98] S.-i. Imai and L. 2. 3. 2. Guarente, *Trends Pharmacol. Sci.*, vol. 31, pp. 212-220, 2010.
- [99] B. a. G. L., "The sir2 family of protein deacetylases.," *Annu. Rev. Biochem.* , vol. 73, pp. 417-435, 2004.
- [100] B. J. M. B. L. B. M. T. D. J. M. a. V. E. North, *Mol. Cell* , vol. 11, pp. 437-444, 2003.
- [101] A. D.-R. K. Y. W. B. D. S. E. M. C. J. T. M. B. A. H. A. e. a. Hebert, "Calorie restriction and SIRT3 trigger global reprogramming of the mitochondrial protein acetylome.," *Mol. Cell* , vol. 49, pp. 186-199, 2013.
- [102] G. G. N. S. A. d. B. V. D. M. K. T. N. F. F. B. G. V. B. e. a. Laurent, "SIRT4 coordinates the balance between lipid synthesis and catabolism by repressing malonyl CoA decarboxylase," *Mol. Cell* , vol. 50,

p. 686–698., 2013.

- [103] M. M. R. H. K. F. K. C. D. A. V. D. Y. G. K. M. B. G. Haigis, "SIRT4 inhibits glutamate dehydrogenase and opposes the effects of calorie restriction in pancreatic beta cells.," *Cell*, vol. 126, p. 941–954., 2006.
- [104] J. Z. Y. S. X. Y. J. K. S. J. H. K. J. W. J. K. J. B. e. a. Du, "Sirt5 is a NAD-dependent protein lysine demalonylase and desuccinylase," *Science*, vol. 334, pp. 806-809, 2011.
- [105] M. a. S. C. Gertz, "Function and regulation of the mitochondrial sirtuin isoform Sirt5 in Mammalia.," *Biochim. Biophys. Acta*, vol. 1804, pp. 1658-1665, 2010.
- [106] R. e. a. Ferrari, "Epigenetic reprogramming by adenovirus e1a.," *Science*, vol. 321, pp. 1086-1088, 2008.
- [107] H. Jiang, S. Khan, Y. Wang, G. Charron, B. He, C. Sebastian, J. Du, R. Kim, E. Ge, R. Mostoslavsky, H. Hang, Q. Hao and H. Lin, "SIRT6 regulates TNF- secretion through hydrolysis of long-chain fatty acyl lysine.," *Nature*, vol. 496, no. 7443, pp. 110-3, 2013.
- [108] E. e. a. Michishita, "Evolutionarily conserved and nonconserved cellular localizations and functions of human SIRT proteins.," *Mol.Biol. Cell*, vol. 16, no. 10, pp. 4623-4635, 2005.
- [109] E. Michishita, R. McCord, E. Berber, M. Kioi, H. Padilla-Nash, M. Damian, P. Cheung, R. Kusumoto, T. Kawahara and Barrett, "SIRT6 is a histone H3 lysine 9 deacetylase that modulates telomeric chromatin.," *Nature*, vol. 452, no. 7186, pp. 492-6, 2008.
- [110] B. Yang, B. Zwaans, M. Eckersdorff and D. Lombard, "The sirtuin SIRT6 deacetylates H3 K56Ac in vivo to promote genomic stability.," *Cell Cycle*, vol. 8, no. 16, pp. 2662-3, 2009.
- [111] R. Gil, S. Barth, Y. Kanfi and H. Y. Cohen, *Nucleic Acids Res*, vol. 41, p. 8537–8545, 2013.
- [112] E. Michishita, R. A. McCord, L. D. Boxer, M. F. Barber, T. Hong, O. Gozani and K. F. Chua, *Cell Cycle*, vol. 8, pp. 2664-2666, 2009.
- [113] L. e. a. Chen, "WRN, the protein deficient in Werner syndrome, plays a critical structural role in optimizing DNA repair.," *Aging Cell*, vol. 2, p. 191–199, 2003.
- [114] A. a. C. S. Multani, "WRN at telomeres: implications for aging and cancer.," *J. Cell Sci.*, vol. 120, pp. 713-721, 2007.

- [115] Z. e. a. Mao, "SIRT6 promotes DNA repair under stress by activating PARP1.," *Science*, vol. 332, pp. 1443-1446, 2011 .
- [116] A. e. a. Kaidi, "Human SIRT6 promotes DNA end resection through CtIP deacetylation.," *Science*, vol. 329, pp. 1348-1353, 2010.
- [117] A. e. a. Sartori, "Human CtIP promotes DNA end resection.," *Nature* , vol. 450, pp. 509-514, 2007.
- [118] L. e. a. Chen, "Cell cycle-dependent complex formation of BRCA1.CtIP.MRN is important for DNA double-strand break repair.," *J. Biol. Chem.* , vol. 283, pp. 7713-7720, 2008.
- [119] S. a. B. J. Jackson, "The DNA-damage response in human biology and disease.," *Nature*, vol. 461, pp. 1071-1078, 2009.
- [120] R. e. a. McCord, "SIRT6 stabilizes DNA-dependent protein kinase at chromatin for DNA double-strand break repair.," *Aging (Albany NY)* , vol. 1, pp. 109-121, 2009.
- [121] D. e. a. Toiber, "SIRT6 recruits SNF2H to DNA break sites,preventing genomic instability through chromatin remodeling," *Mol.Cell*, vol. 51, p. 454-468, 2013.
- [122] L. e. a. Zhong, "The histone deacetylase Sirt6 regulates glucose homeostasis via Hif1alpha. *Cell*," *Cell*, vol. 140, pp. 280-293, 2010.
- [123] P. e. a. Puigserver, "Insulin-regulated hepatic gluconeogenesis through FOXO1-PGC-1alpha interaction.," *Nature*, vol. 423, pp. 550-555, 2003.
- [124] H. e. a. Kim, "Hepatic-specific disruption of SIRT6 in mice results in fatty liver formation due to enhanced glycolysis and triglyceride synthesis. .," *Cell Metab.*, vol. 12, pp. 224-236, 2010.
- [125] R. e. a. Tao, "FoxO3 transcription factor and Sirt6 deacetylase regulate low density lipoprotein (LDL)-cholesterol homeostasis via control of the proprotein convertase subtilisin/kexin type 9 (Pcsk9) gene expression.," *J. Biol. Chem.* , vol. 288, p. 29252-29259, 2013.
- [126] R. e. a. Tao, "Hepatic SREBP-2 and cholesterol biosynthesis are regulated by FoxO3 and Sirt6.," *J. Lipid Res.*, vol. 54, p. 2745-2753, 2013.
- [127] S. e. a. Elhanati, "Multiple regulatory layers of SREBP1/2 by SIRT6.," *Cell Rep.*, vol. 4, pp. 905-912,



2013.

- [128] H. e. a. Jiang, "SIRT6 regulates TNF-alpha secretion through hydrolysis of long-chain fatty acyl lysine.," *Nature*, vol. 496, pp. 110-113, 2013.
- [129] T. e. a. Kawahara, "SIRT6 links histone H3 lysine 9 deacetylation to NF-kappaB-dependent gene expression and organismal life span," *Cell*, vol. 136, pp. 62-74, 2009.
- [130] N. e. a. Sundaresan, "The sirtuin SIRT6 blocks IGF-Akt signaling and development of cardiac hypertrophy by targeting c-Jun.," *Nat. Med.*, vol. 18, pp. 1643-1650, 2012.
- [131] C. a. V. H. M. Metallo, "Understanding metabolic regulation and its influence on cell physiology," *Mol.Cell.*, vol. 49, p. 388-398, 2013.
- [132] O. e. a. Warburg, "The metabolism of tumors in the body.," *J. Gen.Physiol.*, vol. 8, pp. 519-530, 1927.
- [133] L. Zhong, A. D'Urso, D. Toiber, C. Sebastian, R. Henry, D. Vadysirisack, A. Guimaraes, B. Marinelli and J. Wikstrom, "The histone deacetylase Sirt6 regulates glucose homeostasis via Hif1alpha.," *Cell*, vol. 140, no. 2, pp. 280-93, 2010.
- [134] D. Hanahan and R. Weinberg, "Hallmarks of cancer: the next generation," *Cell*, vol. 144, no. 5, pp. 646-74, 2011.
- [135] C. Sebastián, B. Zwaans, D. Silberman, M. Gymrek, A. Goren, L. Zhong, O. Ram, J. Truelove and A. Guimaraes, "The histone deacetylase SIRT6 is a tumor suppressor that controls cancer metabolism.," *Cell*, vol. 151, no. 6, pp. 1185-99, 2012.
- [136] E. Varfolomeev and A. Ashkenazi, "Tumor necrosis factor: an apoptosis JuNKie?," *Cell*, vol. 116, no. 4, pp. 491-7, 2004.
- [137] L. Wang, F. Du and X. Wang, "TNF-alpha induces two distinct caspase-8 activation pathways," *Cell*, vol. 133, no. 4, pp. 693-703, 2008.
- [138] C. Pham, C. Bubici, F. Zazzeroni, S. Papa, J. Jones, K. Alvarez, S. Jayawardena, E. De Smaele, R. Cong, C. Beaumont, TortiF.M., S. Torti and G. Franzoso, "Ferritin heavy chain upregulation by NF-kappaB inhibits TNFalpha-induced apoptosis by suppressing reactive oxygen species," *Cell*, vol. 119, no. 4, pp. 529-42, 2004.

- [139] L. Chang, H. Kamata, G. Solinas, J. Luo, S. Maeda, V. K., Y. Liu and M. Karin, "The E3 ubiquitin ligase itch couples JNK activation to TNF $\alpha$ -induced cell death by inducing cFLIP(L) turnover.," *Cell*, vol. 124, no. 3, pp. 601-13, 2006.
- [140] J. S. S. D. E. C. L. P. J. B. C.B. Brachmann, "The SIR2 gene family, conserved from bacteria to humans, functions in silencing, cell cycle progression, and chromosome stability.," *Genes. Dev.*, vol. 9, p. 2888–2902., 1995.
- [141] J. D. N. P. M.S. Finnin, "Structure of the histone deacetylase SIRT2.," *Nat. Struct. Biol.* , vol. 8, pp. 621-625, 2001.
- [142] J. L. R. S. R. X. J. Min, "Crystal structure of a SIR2 homolog-NAD complex.," *Cell* , vol. 105, pp. 269-279, 2001.
- [143] R. H. X. C. R. M. K. Zhao, "Structural basis for nicotinamide cleavage and ADP-ribose transfer by NAD(+)-dependent Sir2 histone/protein deacetylases.," *Proc. Natl. Acad. Sci. U. S. A.* , vol. 101, p. 8563–8568., 2004.
- [144] J. A. K. S. C. W. K.G. Hoff, "Insights into the sirtuin mechanism from ternary complexes containing NAD+ and acetylated peptide.," *Structure* , vol. 14, p. 1231–1240., 2006.
- [145] K. H. D. F. A. D. O. Z. V. S. W. C. W. W.F. Hawse, "Structural insights into intermediate steps in the Sir2 deacetylation reaction.," *Structure*, vol. 16, p. 1368–1377., 2008.
- [146] K. B. C. W. J.L. Avalos, "Mechanism of sirtuin inhibition by nicotinamide: altering the NAD(+) cosubstrate specificity of a Sir2 enzyme," *Mol. Cell.* , vol. 17, pp. 855-868, 2005.
- [147] I. C. S. M. M. C. J. B. C. W. J.L. Avalos, "Structure of a Sir2 enzyme bound to an acetylated p53 peptide.," *Mol. Cell.*, vol. 10, p. 523–535., 2002.
- [148] K. B. J. A. S. M. X. Z. C. W. M.S. Cosgrove, "The structural basis of sirtuin substrate affinity.," *Biochemistry* , vol. 45, pp. 7511-7521, 2006.
- [149] L. W. W. J. Y. P. H. C. J. M. C. D. H. C. W. J. E. J. M. R. M. J. C. W. C. H. a. P. R. B. Jin, "Crystal Structures of Human SIRT3 Displaying Substrate-induced Conformational Changes," *J. Biol. Chem.*, vol. 284, p. 24394–24405, 2009.
- [150] J. L. F. M. K. D. A. D. A. M. E. a. J. M. D. P. W. Pan, "Structure and Biochemical Functions of SIRT6,"

- [151] G. E. C. C. B. e. a. J.S. Disch, "Discovery of Thieno[3,2-d]pyrimidine-6-carboxamides as Potent Inhibitors of SIRT1, SIRT2, and SIRT3," *J Med. Chem.*, vol. 56, pp. 3666-3679, 2013.
- [152] J. H. X. Z. H. L. B. He, "Thiomyrystoyl peptides as cell-permeable Sirt6 inhibitors," *Org. Biomol. Chem.*, vol. 12, pp. 7498-7502, 2014.
- [153] K. Liu, B. Shelton and R. Howe, "A particularly convenient preparation of benzohydroximinoyl chlorides (nitrile oxide precursors)," *J.Org.Chem*, vol. 45, pp. 3916-3918, 1980.
- [154] P. C. Lv, Z.-P. Xiao, R.-Q. Fang, H.-Q. Li, H.-L. Zhu and C.-H. Liu, "Synthesis, characterization and structure-activity relationship analysis of novel depsides as potential antibacterials," *Eur. J. Med Chem.*, vol. 44, pp. 1779-1787, 2009.
- [155] R. Pschorr and F. M. S. V. Zeidler, "Synthesis of the 3,4 Dimethoxy-8-ethoxyphenanthrene Obtained in the Degradation of Thebenine," *Justus Liebig's Ann. Chem.*, vol. 373, pp. 75-79, 1910.
- [156] C. A. Brooks, M. Cheung, H. S. Eidam, R. M. Fox, M. Hilfker, E. S. Manas and G. Ye, "4-Quinolincarboxamide derivatives as TRPV4 antagonists and their preparation and use for the treatment of diseases". Patent PCT Int. Appl. WO 2011119704 A1, September 29, 2011.
- [157] S. Bondock, H. El-Azap, E.-E. M. Kandeel and M. A. Metwally, "Eco-friendly solvent-free synthesis of thiazolopyrazole derivatives," *Monatsh. Chem.*, vol. 139, pp. 1329-1335, 2008.
- [158] T. Weidlich, M. Pokorny, Z. Padelkova and A. Ruzicka, "Aryl ethyl ethers prepared by ethylation using diethyl carbonate," *Green Chem.Lett. Rev. 2007, 1, 53-59.*, vol. 1, pp. 53-59, 2007.
- [159] T. Weidlich, M. Pokorny, Z. Padelkova and Ruzicka, "Aryl ethyl ethers prepared by ethylation using diethyl carbonate," *Green Chem. Lett. Rev.*, vol. 1, pp. 53-59, 2007.
- [160] L. Schrödinger, "Glide, version 5.5," New York, 2009.
- [161] E. F. Pettersen, T. D. Goddard, C. C. Huang, G. S. Couch, D. M. Greenblatt, E. C. Meng and T. E. Ferrin, "UCSF Chimera—a visualization system for exploratory research and analysis," *J. Comput. Chem.*, vol. 25, pp. 1605-1612, 2004.
- [162] J. L. Biedler, S. Roffler-Tarlov, M. Schachner and L. S. Freedman, "Multiple neurotransmitter synthesis

by human neuroblastoma cell lines and clones," *Cancer Res.*, vol. 38, pp. 3751-3757, 1978.

- [163] A. Weiss, R. L. Wiskocil and J. D. Stobo, "The role of T3 surface molecules in the activation of human T cells: a two-stimulus requirement for IL-2 production reflects events occurring at a pre translational level.," *J. Immunol.*, vol. 133, pp. 123-128, 1984.
- [164] R. Mossetti, T. Pirali, G. C. Tron and Zhu, "Efficient synthesis of alpha-ketoamides via 2-acyl-5-aminooxazoles by reacting acyl chlorides and alpha-isocyanoacetamides.," *J. Org. Lett.*, vol. 12, pp. 820-3, 2010.
- [165] D. A. Fruman and C. Rommel, "PI3K and cancer: lessons.," *Nature Rev. Drug Discovery*, vol. 13, p. 140-156., 2014.
- [166] T. N. C. a. A. Letai, "Mimicking the BH3 domain to kill cancer cells.," *Oncogene*, vol. 27, pp. S149-S157, 2009.
- [167] F. S., "Tumor resistance to apoptosis," *Int. J. Cancer*, Vols. 511-515, p. 124, 2009.
- [168] G. D. Tait S.W.G., "Mitochondria and cell death: outer membrane permeabilization and beyond," *Nature Rew*, vol. 11, pp. 621-630, 2010.
- [169] M. Kaeberlein, M. McVey and L. Guarente, *Genes Dev.*, vol. 13, p. 2570-2580., 1999.
- [170] J. N. A. Y. I. S. C. D. S. F. S. A. G. L. a. G. W. Luo, "Negative control of p53 by Sir2alpha promotes cell survival under stress.," *Cell*, vol. 107, pp. 137-148, 2001.
- [171] F. H. J. E. R. C. S. K. M. D. J. D. R. F. R. A. M. M. W. Yeung, "Modulation of NF-kappaB-dependent transcription and cell survival by the SIRT1 deacetylase.," *EMBO J.*, vol. 23, p. 2369-2380., 2004.
- [172] A. e. a. Brunet, "Stress-dependent regulation of FOXO transcription factors by the SIRT1 deacetylase.," *Science*, vol. 303, pp. 2011-2015, 2004.
- [173] J. L. Feldman, J. Baeza and J. M. Denu, *J. Biol. Chem.*, vol. 288, p. 31350-31356., 2013.
- [174] H. S. Kim, C. Xiao, R. H. Wang, T. Lahusen, X. Xu, A. Vassilopoulos, G. Vazquez-Ortiz, W. I. Jeong, O. Park, S. H. Ki, B. Gao and C. X. Deng, *Cell Metab.*, vol. 12, pp. 224-236, 2010.

- [175] C. Sebastian, B. M. Zwaans, D. M. Silberman, M. Gymrek, A. Goren, L. Zhong, O. Ram, J. Truelove, A. R. Guimaraes, D. Toiber, C. Cosentino, J. K. Greenson, A. I. MacDonald, L. F. McGlynn, J. Edwards, S. Giacosa, E. Guccione and Weisslede, *Cell*, vol. 151, pp. 1185-1199, 2012.
- [176] T. L. Kawahara, E. Michishita, A. S. Adler, M. Damian, E. Berber, M. Lin, R. A. McCord, K. C. Ongaiqui, L. D. Boxer, H. Y. Chang and K. F. Chua, *Cell*, vol. 136, pp. 62-74, 2009.
- [177] N. R. Sundaresan, P. Vasudevan, L. Zhong, G. Kim, SamantS., V. Parekh, V. B. Pillai, P. V. Ravindra, M. Gupta, JeevanandamV., J. M. Cunningham, C. X. Deng, D. B. Lombard, MostoslavskyR. and M. P. Gupta, *Nat. Med.*, vol. 18, p. 1643–1650., 2012.
- [178] R. Tao, X. Xiong, R. A. DePinho, C. X. Deng and X. C. Dong, *J. Lipid Res.*, vol. 54, pp. 2745-2753, 2013.
- [179] R. Mostoslavsky, "DNA repair; insulin signaling and sirtuins: at the crossroads between cancer and aging.," *Front Biosci.*, vol. 13, pp. 6966-90, 2008.
- [180] A. Adler, T. Kawahara, E. Segal and H. Chang, "Reversal of aging by NFkappaB blockade," *Cell Cycle*, 2008, 7(5), 556-9, vol. 7, no. 5, pp. 556-9, 2008.
- [181] C. Das, M. Lucia, K. Hansen and J. Tyler, "CBP/p300-mediated acetylation of histone H3 on lysine 56," *Nature*, vol. 459, no. 7243, pp. 113-7., 2009.
- [182] D. Toiber, F. Erdel, K. Bouazoune, D. Silberman, L. Zhong, P. Mulligan, C. Sebastian, C. Cosentino, B. Martinez-Pastor, S. Giacosa, A. D'Urso, A. Näär, R. Kingston, K. Rippe and MoMostoslavsky, "SIRT6 recruits SNF2H to sites of DNA breaks; preventing genomic instability through chromatin remodeling," *Mol.Cell.*, vol. 51, no. 4, pp. 454-68, 2013.
- [183] C. e. a. Sebastian, "The histone deacetylase SIRT6 is a tumor suppressor that controls cancer metabolism.," *Cell*, vol. 151, pp. 1185-1199, 2012.
- [184] A. L. C. B. L. B. M.G. Rossmann, "Evolutionary and structural relationships among dehydrogenases.," in *Academic Press*, New York, 1975, pp. Vol. XI, 3rd edition.
- [185] J. B. C. W. J.L. Avalos, "Structural basis for the mechanism and regulation of Sir2 enzymes.," *Mol. Cell.*, vol. 13, pp. 639-648, 2004.
- [186] M. R.-R. P. H. K. T. H. T. L. A. P. E. J. a. M. L.-K. Piia Kokkonen, "Peptides and Pseudopeptides as SIRT6 Deacetylation Inhibitors," *ACS Med. Chem. Lett.*, p. 969–974, 2012.

- [187] G. A. B. I. G. L. D. P. M. E. S. G. F. C. B. A. B. S. D. R. A. N. A. Parenti MD1, "Discovery of novel and selective SIRT6 inhibitors," *J Med Chem.*, vol. 57, no. 11, pp. 4796-804, 2014.
- [188] T. Oltersdorf, S. W. Elmore, A. R. Shoemaker and R. a. Armstrong, "An inhibitor of Bcl-2 family proteins induces regression of solid tumours," *Nature*, vol. 435, pp. 677-681, 2005.
- [189] C. Tse, A. R. Shoemaker, J. Adickes, M. G. Anderson and J. e. a. Chen, "ABT-263: a potent and orally bioavailable Bcl-2 family inhibitor," *Cancer Res.*, vol. 68, p. 3421-3428., 2008.
- [190] A. J. Souers, J. D. Levenson, E. R. Boghaert, S. L. Ackler and e. all, "ABT-199, a potent and selective BCL-2 inhibitor, achieves antitumor activity while sparing platelets," *Nature Med.*, vol. 19, p. 202-208., 2013.
- [191] S. a. V. H. M. Lunt, "Aerobic glycolysis: meeting the metabolic requirements of cell proliferation," *Annu. Rev. Cell Dev. Biol*, vol. 27, p. 441-464., 2011.
- [192] G. L. Nakagawa T, "Sirtuins at a glance," *J Cell Sci*, vol. 124, pp. 833-8, 2011.
- [193] M. E. H. T. e. a. McCord RA, "SIRT6 stabilizes DNA-dependent protein kinase at chromatin for DNA double-strand break repair.," *Aging (Albany NY)*, vol. 1, pp. 109-21, 2009.
- [194] G. G. M. F. M. A. Allavena P, "Chemokines in cancer related inflammation," *Exp Cell Res*, vol. 317, pp. 664-73., 2011.
- [195] M. D. P. A. G. A. B. I. B. A. D. R. a. A. N. S. Bruzzone, "Rejuvenating Sirtuins: The Rise of a New Family of Cancer Drug Targets," *Current Pharmaceutical Design*, vol. 19, pp. 614-623, 2013.
- [196] C. A. G. M. e. a. Cea M, "New Insights into the Treatment of Multiple Myeloma with Histone Deacetylase Inhibitors.," *Curr Pharm Des*, vol. 19, no. 4, pp. 734-44, 2013.
- [197] L. J. S. R. X. R. Min J, "Crystal structure of a SIR2 homolog-NAD complex," *Cell*, vol. 105, pp. 269-79, 2001.
- [198] J. e. a. Robitaille, "Mutant frizzled-4 disrupts retinal angiogenesis in familial exudative vitreoretinopathy.," *Nat. Genet.*, vol. 32, pp. 326-330, 2002.
- [199] C. Bodur and H. Basaga, "Bcl-2 inhibitors: emerging drugs in cancer therapy.," *Curr. Med. Chem.*, vol.

